INFORMATION TO USERS

This manuscript has been reproduced from the microfilm master. UMI films the text directly from the original or copy submitted. Thus, some thesis and dissertation copies are in typewriter face, while others may be from any type of computer printer.

The quality of this reproduction is dependent upon the quality of the copy submitted. Broken or indistinct print, colored or poor quality illustrations and photographs, print bleedthrough, substandard margins, and improper alignment can adversely affect reproduction.

In the unlikely event that the author did not send UMI a complete manuscript and there are missing pages, these will be noted. Also, if unauthorized copyright material had to be removed, a note will indicate the deletion.

Oversize materials (e.g., maps, drawings, charts) are reproduced by sectioning the original, beginning at the upper left-hand corner and continuing from left to right in equal sections with small overlaps.

ProQuest Information and Learning
300 North Zeeb Road, Ann Arbor, MI 48106-1346 USA
800-521-0600

UMI®

SIMULATION OF A SIMULATED MOVING BED REACTOR FOR HYDROCARBON ISOMERIZATION

BY

Mohammad Aminuddin

A Thesis Presented to the

DEANSHIP OF GRADUATE STUDIES

KING FAHD UNIVERSITY OF PETROLEUM & MINERALS

DHAHRAN, SAUDI ARABIA

In Partial Fulfillment of the
Requirements for the Degree of

MASTER OF SCIENCE

In

CHEMICAL ENGINEERING

January, 2003

UMI Number: 1411741

UMI®

UMI Microform 1411741
Copyright 2003 by ProQuest Information and Learning Company.
All rights reserved. This microform edition is protected against
unauthorized copying under Title 17, United States Code.

ProQuest Information and Learning Company
300 North Zeeb Road
P.O. Box 1346
Ann Arbor, MI 48106-1346

King Fahd University of Petroleum & Minerals

DHAHRAN 31261, SAUDI ARABIA

DEANSHIP OF GRADUATE STUDIES

This thesis, written by

Mohammad Aminuddin

under the direction of his Thesis Advisor and approved by his Thesis Committee, has been presented to and accepted by the Dean of Graduate Studies, in partial fulfillment of the requirements for the degree of

MASTER OF SCIENCE IN CHEMICAL ENGINEERING

Thesis Committee

Dr. Kevin F. Loughlin
(Chairman)

Dr. Ashraf I. Fatehi
(Member)

Dr. Habib D. Zughbi
(Member)

Prof. Mohamed B. Amin
(Department Chairman)

Prof. Osama A. Jannadi
(Dean of Graduate Studies)

18/1/2003
Date

This Thesis is dedicated to

my Parents *and*

my Baby Brother

who made it all worthwhile

ACKNOWLEDGMENT

Acknowledgment is due to the King Fahd University of Petroleum & Minerals for supporting this research.

I wish to express my appreciation to Dr Kevin Loughlin who served as my thesis advisor. I also wish to thank the other members of my thesis committee Dr Ashraf Fatehi and Dr Habib Zughbi. Thanks to the chemical engineering chairman Dr Mohamed Amin as well.

I would also like to acknowledge Mr Mohammad Ba-Shammakh for his efforts in translating the Abstract.

CONTENTS

LIST OF TABLES viii
LIST OF FIGURES ix
ABSTRACT (English) xv
ABSTRACT (Arabic) xvi

CHAPTER 1 INTRODUCTION 1

1.1 OBJECTIVES OF THE PRESENT RESEARCH 6

CHAPTER 2 LITERATURE SURVEY & BACKGROUND 7

2.1 TOTAL ISOMERIZATION PROCESS 7
2.2 PRESSURE SWING ADSORPTION REACTOR (PSAR) 9
2.3 SIMULATED MOVING BED 11
2.4 CHROMATOGRAPHIC REACTORS 14
2.4a Countercurrent Moving Bed Chromatographic Reactor 15
2.4b Simulated Moving Bed Reactor 17
2.5 BASIC CONCEPTS 30
2.5a Adsorption Equilibrium Isotherms 31
2.5b Kinetics of Sorption 32
2.5c Interparticle and Intraparticle Mass Transport 32
2.5d Reaction Mechanism 36
2.5e Kinetic Model 39
2.5f Unsteady State Catalysis 42
2.5g Unsteady State Reactor Modeling 44
NOMENCLATURE 49

CHAPTER 3 MODELING AND SIMULATION OF THE BASE CASE 52

3.1 MODEL ASSUMPTIONS 52

3.2 MODEL EQUATIONS 54
3.2.1 Adsorbent Bed 54
3.2.2 Catalyst Bed 57
3.2.2a Pseudo-Homogeneous Model 57
3.2.2b Heterogeneous Model 59
3.3 NORMALIZED EQUATIONS 64
3.3.1 Adsorbent Bed 64
3.3.2 Catalyst Bed 67
3.3.2a Pseudo-Homogeneous Model 67
3.3.2b Heterogeneous Model 68
3.4 NUMERICAL SOLUTION 73
3.5 PARAMETERS ESTIMATIONS 73
3.6 MODEL SENSITIVITY ANALYSIS 75
3.7 RESULTS AND DISCUSSION 85
3.7a Adsorbent Bed 85
3.7b Catalyst Bed 104
3.7c Integrated Reactor-Adsorber 111
NOMENCLATURE 121

CHAPTER 4 THE SIMULATED MOVING BED REACTOR FOR HYDROCARBON ISOMERIZATION 125

4.1 MODEL EQUATIONS 127
4.1a Regeneration Section 127
4.1b Reaction Section 128
4.1c Adsorption Section 132
4.2 RESULTS AND DISCUSSION 136
4.2a Isothermal Operation 136
4.2b Adiabatic Operation 149
4.2c Non-Isothermal Non-Adiabatic Operation 155
NOMENCLATURE 210

CHAPTER 5 THE ULTIMATE SANDWICH REACTOR 216

5.1 MODEL EQUATIONS 220
5.2 RESULTS AND DISCUSSION 221
NOMENCLATURE 233

CHAPTER 6 CONCLUSIONS & RECOMMENDATIONS **234**

6.1 SUMMARY OF CONCLUSIONS 234
6.2 RECOMMENDATIONS FOR FUTURE WORK 237

REFERENCES **239**

Appendix A Derivations **246**

A.1 DERIVATION OF THE LUMPED MODEL 246
A.2 DERIVATION OF THE OVERALL EFFECTIVENESS FACTOR (Ω) 247
A.3 MATERIAL & ENERGY BALANCES AT THE MIXING POINT 250
A.4 EVALUATION OF AVERAGE TEMPERATURE OF A STREAM 255

Appendix B Numerical Solution **261**

B.1 ADSORBENT BED 261
B.2 CATALYST BED 263
B.2a Pseudo-Homogeneous Model 263
B.2b Heterogeneous Model 265

Appendix C Simulation Code **270**

C.1 MAIN PROGRAM 270
C.2 ODE FILE 287
C.2a Ode File for Adsorbent Bed 288
C.2b Ode File for Catalyst Bed 290

LIST OF TABLES

Table		Page
2.1	Summary of Various Systems Studied Using SMBR	28
3.1	Data for the Base-Case System	74
3.2	Parametric Values for the Model Sensitivity Analysis @ 15 bar	76
3.3	Parametric Values for the Solution of Breakthrough Curves @ 15 bar	86
3.4	Parametric Values for Fixed Bed Simulations @ 15 bar (Figures 3.12 to 3.22)	92
3.5	Parametric Values for Adiabatic Reactor Simulations @ 15 bar	107
3.6	Parametric Values for Integrated Reactor-Adsorber Simulations @ 15 bar (Figures 3.27 to 3.30)	114
4.1	Cases for Isothermal and Adiabatic SMBR Simulations	137
4.2	Parametric Values for Isothermal SMBR Simulations (Cases 1, 2, 3 & 6)	138
4.3	Parametric Values for Isothermal SMBR Simulations (Case 4)	139
4.4	Parametric Values for Isothermal SMBR Simulations (Case 5)	140
4.5	Switch Times for Isothermal and Adiabatic SMBR Simulations	142
4.6	Parametric Values for Adiabatic SMBR Simulations (Case 7)	150
4.7	Cases for Thermal Swing SMBR Simulations	157
4.8	Parametric Values for Thermal Swing SMBR Simulations (Cases 8, 9, 10, 11, 12 & 22)	158
4.9	Parametric Values for Thermal Swing SMBR Simulations (Case 13)	160
4.10	Parametric Values for Thermal Swing SMBR Simulations (Case 14)	162
4.11	Parametric Values for Thermal Swing SMBR Simulations (Case 15)	164
4.12	Parametric Values for Thermal Swing SMBR Simulations (Case 16)	166
4.13	Parametric Values for Thermal Swing SMBR Simulations (Case 17)	168
4.14	Parametric Values for Thermal Swing SMBR Simulations (Case 18)	170
4.15	Parametric Values for Thermal Swing SMBR Simulations (Case 19)	172
4.16	Parametric Values for Thermal Swing SMBR Simulations (Case 20)	174
4.17	Parametric Values for Thermal Swing SMBR Simulations (Case 21)	176
4.18	Switch Times for Thermal Swing SMBR Simulations	178

LIST OF FIGURES

Figure		Page
2.1	Block-Flow Diagram for the Total Isomerization Process	8
2.2	Flow Diagram for the Combined Isomerization Reactor/Adsorber Process	10
2.3	Four-Section True Countercurrent Unit	12
2.4	True Countercurrent Moving Bed Chromatographic Reactor	16
2.5	Single Column SMBR. Feed and product ports move in the same direction as carrier.	19
2.6	Multi-Column SMBR. There is no flow through the dashed lines.	21
2.7	Five-Column Reactor Configuration	22
2.8	SMBR for Oxidative Coupling of Methane	23
2.9	Adiabatic SMBR for Methanol Synthesis	25
2.10	Isothermal SMBR for Methanol Synthesis	26
2.11	Resistances to Mass Transfer in a Zeolite Molecular Sieve	33
3.1	Effect of Dispersion Coefficient on Breakthrough Curve for $N = 8$. Parametric values are in Table 3.2.	77
3.2	Breakthrough Curves for Varying Number of Nodes. Parametric values are in Table 3.2.	79
3.3	Effect of Mass Transfer Coefficient on Breakthrough Curve. Parametric values are in Table 3.2.	80
3.4	Effect of Thermal Conductivity on Breakthrough Curve. Parametric values are in Table 3.2	81
3.5	Effect of Thermal Conductivity on Exit Temperature. Parametric values are in Table 3.2.	82
3.6	Effect of Wall Heat Transfer Coefficient on Breakthrough Curve. Parametric values are in Table 3.2.	83

3.7 Effect of Wall Heat Transfer Coefficient on Exit Temperature. Parametric values are in Table 3.2. 84
3.8 Effect of Operating Temperature on Breakthrough Curve. Parametric values are in Table 3.3. 87
3.9 Effect of Feed Flow Rate and Feed Concentration on Breakthrough Curve. Parametric values are in Table 3.3. 88
3.10 Effect of Feed Flow Rate and Column Length on Breakthrough Curve. Parametric values are in Table 3.3. 89
3.11 Effect of Column Diameter on Breakthrough Curve. Parametric values are in Table 3.3. 91
3.12 Effect of Temperature on Desorption Curve. Parametric values are in Table 3.4. 93
3.13 Exit Temperature during Non-Adiabatic Adsorption and Desorption Steps. Parametric values are in Table 3.4. 95
3.14 Effect of Regeneration Temperature on Adsorbed Phase Concentration Profiles. Parametric values are in Table 3.4. 96
3.15 Concentration Profiles of *n*-Pentane at Various Times during the Non-Adiabatic Adsorption Step. Parametric values are in Table 3.4. 98
3.16 Concentration Profiles of Isopentane at Various Times during the Non-Adiabatic Adsorption Step. Parametric values are in Table 3.4. 99
3.17 Adsorbed Phase Concentration Profiles at Various Times during the Non-Adiabatic Adsorption Step. Parametric values are in Table 3.4. 100
3.18 Fluid Flow Rate Profiles at Various Times during the Non-Adiabatic Adsorption Step. Parametric values are in Table 3.4. 101
3.19 Temperature Profiles at Various Times during the Non-Adiabatic Adsorption Step. Parametric values are in Table 3.4. 102
3.20 Temperature Profiles at Various Times during the Adiabatic Adsorption Step. Parametric values are in Table 3.4. 103

3.21 Adsorbed Phase Concentration Profiles at Various Times during the Regeneration Step @ 430 K in Forward Direction. Parametric values are in Table 3.4 105
3.22 Adsorbed Phase Concentration Profiles at Various Times during the Regeneration Step @ 430 K in Reverse Direction. Parametric values are in Table 3.4 106
3.23 Breakthrough Curves for the Three Reactor Models. Parametric values are in Table 3.5. 108
3.24 Effect of Column Length on Steady State Conversion for the Three Reactor Models (Results Overlap). Parametric values are in Table 3.5 109
3.25 Effect of Feed Temperature on Steady State Conversion for the Three Reactor Models (Results Overlap). Parametric values are in Table 3.5. 110
3.26 Effect of Feed Composition on Steady State Conversion for the Three Reactor Models (Results Overlap). Parametric values are in Table 3.5. 112
3.27 Adsorption and Desorption Curves for *n*-/iso- Pentanes in an Integrated Reactor-Adsorber Arrangement. Parametric values are in Table 3.6. 116
3.28 Concentration Profiles of *n*-/iso- Pentanes in an Integrated Reactor-Adsorber Arrangement @ 174.5 min. Parametric values are in Table 3.6. 117
3.29 Adsorbed Phase Concentration Profiles of *n*-/iso- Pentanes in an Integrated Reactor-Adsorber Arrangement @ 174.5 min. Parametric values are in Table 3.6 118
3.30 Temperature Profile in an Integrated Reactor-Adsorber Arrangement @ 174.5 min. Parametric values are in Table 3.6. 120
4.1 SMBR in Operation 126
4.2 SMBR with Reverse Flow Regeneration 134
4.3 Effect of Number of Regeneration Beds on Product Purity (Cases 1, 2 & 3) 143
4.4 Cyclic Steady State Adsorbed Phase Concentration Profiles in the Regeneration Section at the Start and End of Switching Period (Case 3, Run 1) 144

4.5 Effect of Temperature on Product Purity (Cases 2, 4 & 5) 146
4.6 Effect of Temperature on Single Pass Conversion (Cases 2, 4 & 5) 147
4.7 Effect of Bed Rotation on Product Purity (Cases 2 & 6) 148
4.8 Effect of Adiabatic Operation on Product Purity (Cases 2 & 7) 153
4.9 Cyclic Steady State Temperature Profiles during Adiabatic Operation at the End of Switching Period (Case 7, Run 1) 154
4.10 Effect of Number of Beds on Product Purity (Cases 8, 9 & 10) 179
4.11 Effect of Using Various Reactor Models on Product Purity (Cases 9, 11 & 12) 180
4.12 Effect of Using Various Reactor Models on Single Pass Conversion (Cases 9, 11 & 12) 181
4.13 Effect of Reaction Section Length on Product Purity (Cases 9, 13 & 14) 183
4.14 Effect of Reaction Section Length on Single Pass Conversion (Cases 9, 13 & 14) 184
4.15 Cyclic Steady State Concentration Profiles of *n*-/iso- Pentanes just after Switching Flows (Case 9, Run 1) 185
4.16 Cyclic Steady State Concentration Profiles of *n*-/iso- Pentanes at Half-time Between Switching Flows (Case 9, Run 1) 186
4.17 Cyclic Steady State Concentration Profiles of *n*-/iso- Pentanes just before Switching Flows (Case 9, Run 1) 187
4.18 Cyclic Steady State Adsorbed Phase Concentration Profiles just after Switching Flows (Case 9, Run 1) 189
4.19 Cyclic Steady State Adsorbed Phase Concentration Profiles at Half-time Between Switching Flows (Case 9, Run 1) 190
4.20 Cyclic Steady State Adsorbed Phase Concentration Profiles just before Switching Flows (Case 9, Run 1) 191
4.21 Cyclic Steady State Temperature Profile just after Switching Flows (Case 9, Run 1) 193

4.22 Cyclic Steady State Temperature Profile at Half-time Between Switching Flows (Case 9, Run 1) 194
4.23 Cyclic Steady State Temperature Profile just before Switching Flows (Case 9, Run 1) 195
4.24 Effect of Temperature Difference between Adsorption and Regeneration Sections on Product Purity (Cases 9, 15 & 16) 197
4.25 Effect of Temperature on Product Purity While Maintaining the Temperature Difference Constant (Cases 15 & 17) 198
4.26 Effect of Inlet Flow Rates and Reaction Section Length on Product Purity (Cases 9, 18 & 19) 199
4.27 Effect of Inlet Flow Rates and Reaction Section Length on Single Pass Conversion (Cases 9, 18 & 19) 201
4.28 Effect of Fresh Feed Temperature on Product Purity (Cases 9, 20 & 21) 202
4.29 Effect of Fresh Feed Temperature on Single Pass Conversion (Cases 9, 20 & 21) 203
4.30 Effect of Bed Rotation on Product Purity (Cases 9 & 22) 205
4.31 Effect of Switch Time on Product Purity (Case 9, Run 1) 207
4.32 Approach to Cyclic Steady State for Mean Exit Concentration of Isopentane and Mean Exit Temperature (Case 9, Run 1) 208
4.33 Approach to Cyclic Steady State for Purity and Overall Conversion (Case 9, Run 1) 209
5.1 Industrial Sandwich Reactor 217
5.2 Simulation of Sandwich Reactor 219
5.3 Purity Obtained by a Sandwich Reactor 222
5.4 Cyclic Steady State Concentration Profiles of *n*-/iso- Pentanes just after Reversing Flow 223
5.5 Cyclic Steady State Concentration Profiles of *n*-/iso- Pentanes at Half-time Between Reversing Flow 224

5.6 Cyclic Steady State Concentration Profiles of *n*-/iso- Pentanes just before Reversing Flow 225
5.7 Cyclic Steady State Adsorbed Phase Concentration Profiles just after Reversing Flow 227
5.8 Cyclic Steady State Adsorbed Phase Concentration Profiles at Half-time Between Reversing Flow 228
5.9 Cyclic Steady State Adsorbed Phase Concentration Profiles just before Reversing Flow 229
5.10 Cyclic Steady State Temperature Profile just after Reversing Flow 230
5.11 Cyclic Steady State Temperature Profile at Half-time Between Reversing Flow 231
5.12 Cyclic Steady State Temperature Profile just before Reversing Flow 232

ABSTRACT

NAME OF STUDENT	Mohammad Aminuddin
TITLE OF STUDY	Simulation of a Simulated Moving Bed Reactor for Hydrocarbon Isomerization
MAJOR FIELD	Chemical Engineering
DATE OF DEGREE	January 2003

A process for isomerizing *n*-pentane in a Simulated Moving Bed Reactor (SMBR) is proposed. It consists of a catalyst bed (Pd/Y-zeolite) and several adsorbent beds (5A zeolite) for separating and recycling the unconverted reactant, as the reaction is equilibrium limited. The objective is to obtain >99% purity of the product isopentane.

A mathematical model is developed that relaxes most simplified assumptions such as equilibrium theory, plug flow and constant velocity. Twenty-two cases are studied involving variation of operating conditions. Isothermal and adiabatic simulations do not give the desired results. Constant wall temperatures are thus applied over the adsorbers to produce a thermal swing and achieve the desired purity. The equilibrium limited conversion is about 60% which increases to >99% because of the recycle stream.

The performance does not improve significantly by increasing hydrogen purge rate in modest amounts or using more beds in regeneration section. The model is robust to small variations in fresh feed temperature and flow rate. Maximum purity exists for every run at an optimum switch time. Reverse flow regeneration yields 100% purity.

Both pseudo-homogeneous and heterogeneous reactor models are developed. They differ significantly in their dynamic performance but give similar results once attaining steady state and when incorporated in the SMBR.

A sandwich reactor is also simulated that consists of a catalyst bed sandwiched between the adsorbent beds. It also yields the ideal performance of 100% purity.

ملخص الرسالة

الاســـــم : محمد أمين الدين

عنوان الرسالة : محاكاة لمفاعل ذو صفيحة متحركة من أجل الأيسرومرية للهيدروكربونات

التخصـــص : هندسة كيميائية

تاريخ الرسالة : يناير 2003 م

البحث يعرض ويحاكي الأيسرومرية للبنتين الطبيعي في مفاعل ذو صحيفة متحركة والذي يحتوي على محفز (Pd/Y-Zeolite) وصفائح ممتصة (5A Zeolite) من أجل فصل وإعادة المواد المتفاعلة الغير ملتقية كما أن التفاعل هو محدود بالتوازن. إن الهدف هو الحصول على نقاء بنسبة تزيد عن 99% من الناتج من الأيسوبنتين.

نموذج رياضي تم تطويره ليحل أكثر الافتراضات السهلة مثل نظرية التوازن، التدفق الكتلي والسرعة الثابتة. اثنان وعشرون حالة تمت دراستها التي تحتوي على تفاوت واختلاف في حالات التشغيل. المحاكاة ذات درجة الحرارة الثابتة والادياباتية لا تعطي النتائج المتوقعة. درجة حرارة الجدار الثابتة طبقت على صفائح الامتصاص للحصول على النقاء المطلوب، التحول التوازني المحدود هو بحدود 60% الذي يزيد إلى أكثر من 99% بسبب التيار المعاد، الأداء لم يتحسن بزيادة الهيدروجين أو بواسطة استخدام أكثر صفائح في القسم، النموذج هو قوي للاختلاف البسيط في درجة حرارة التيار الداخل، التيار المعكوس المعاد يعطي نسبة 100% نقاء.

المفاعل المتجانس الكاذب أو الغير متجانس تم تطويره، وهما يختلفان في الأداء الديناميكي لكن يعطيان نفس النتائج. المفاعل السندويش الذي هو عبارة عن صفيحة محفزة بين صفيحتين ممتصة تمت محاكاته وأعطى نسبة أداء لدرجة 100% نقاء.

درجة الماجستير في العلوم

جامعة الملك فهد للبترول و المعادن

الظهران, المملكة العربية السعودية

يناير 2003 م

CHAPTER 1

INTRODUCTION

The isomerization of *n*-paraffins to high-octane number branched isomers is a method of upgrading naphtha to improve their utility as motor fuel components. For example, the unleaded research octane number (RON) for isopentane is 93 compared with 62 for *n*-pentane. As the isomerization reaction of *n*-paraffins to isoparaffins is equilibrium limited, it is necessary to recycle the unconverted reactants to the reactor. The separation of *n*-paraffins/isoparaffins can be done by using molecular sieves such as 5A zeolite exchanged with calcium, zeolites R or T, or the natural zeolites chabazite or erionite [3]. The 5A zeolite excludes branched paraffins because of the steric effects and adsorbs linear n-C_5 and n-C_6. A well-known isomerization process using molecular sieves for the vapor phase separation of unconverted *n*-paraffins is the total isomerization process (TIP) [23].

Adsorption-based separations exhibit two advantages with respect to distillation. Firstly, isomers with very close boiling points can be separated easily, such as the Parex process [7] where *p*-xylene is separated from a mixture of alkylaromatic C_8 fraction. Secondly, a feed stream constituted of many components can be fractionated based on molecular properties other than differences in boiling points. Examples are given by the separation of paraffins from olefins in the Olex process [58], based on the presence of the

unsaturated double bond, and the separation of linear paraffins from branched and cyclic ones in the Molex process, based on steric factors [6].

One of the first industrial adsorption processes based on 5A zeolites was the separation of *n*-paraffins/isoparaffins developed by Union Carbide for the octane improvement of gasoline pools [71]. The extensive work in adsorption allows us to consider several processes to perform the *n*-paraffins/isoparaffins separation on a scientific basis. Industrial processes include pressure swing adsorption (PSA), temperature swing adsorption (TSA), simulated moving bed (SMB), and purge stripping and displacement processes.

In conventional chemical reaction processes, the conversion is often limited by chemical equilibrium. The Total Isomerization Process [23] continuously separates the unconverted normals from the product and recycles them back to the reactor in order to achieve total conversion. The simulated moving bed reactor is also developed for a similar purpose.

Paraffin isomerization requires a stable catalyst with high activity to take advantages of the higher equilibrium conversions to branched products at lower temperatures [32]. Selectivity is another important property for the catalyst where the undesired reaction is the cracking of alkanes [4].

Different isomerization catalyst systems have been developed, and a good summary of them is presented by Fujimoto *et al.* [20]. The catalyst systems can be classified into three groups: Friedel-Craft, bifunctional, and solid superacid catalysts. The first group, that is the Friedel-Craft catalyst, is out of use today because of its low

selectivity, poor structure stability, and strong corrosivity. The bifunctional catalysts, with a hydrogenation-dehydrogenation function (e.g., Pt or Pd) and an acid function (zeolites) are now used for the hydrocarbon isomerization process. The solid superacid catalysts such as sulfated zirconia are still under study. They are shown to comprise the positive properties of the other two groups of catalysts.

Spivey and Bryant [68] studied experimentally the hydroisomerization of n-C_5/n-C_6 mixtures on 0.5 wt% Pt/H-mordenite and 0.5 wt% Pd/H-faujasite catalysts. They showed that mordenite is more active than faujasite. However, mordenite suffers from a high rate of deactivation [55,56]. Thus, faujasite is chosen as the catalyst for the present study.

Having identified the catalyst, faujasite, and the adsorbent, 5A zeolite, Al-Juhani [1] modified the Total Isomerization Process by combining the reactor and the adsorber in a single vessel. The present study is concerned with the hydroisomerization of hydrocarbons in a similar reactor, but with the separation of effluent mixture through a Simulated Moving Bed (SMB), thus the name Simulated Moving Bed Reactor (SMBR).

Fresh feed of normal/iso- pentanes is added to the reaction section of SMBR and the effluent stream passed on to the adsorption section where the unconverted n-pentane is retained and the product, isopentane, is eluted. Before the reactant breaks through the raffinate stream, supply to the adsorbent bed is cut off and diverted to the next bed in series. The previous bed now undergoes regeneration with a hydrogen purge and the desorbed n-pentane recycled back to the catalyst bed. Modeling of SMBR is thus a modeling of fixed beds connected in series.

The first and simplest approach of modeling is by the equilibrium theory, which is based on the assumption that local equilibrium always exists between the bulk and solid phases and hence mass transfer resistance is negligible. An advantage of this approach is that it allows for analytical solution of the governing mass balance equation. However, the predictions by the equilibrium model are not accurate for real systems where the mass transfer resistance is considerable.

Dynamic modeling, the other approach, allows for mass transfer resistance in the system, but the governing equations can be solved only by numerical methods. Chihara and Suzuki [10] developed a dynamic model based on the assumption that the velocity is constant along the column. Constant velocity models are most useful for liquid systems or gaseous purification systems where the adsorbable components exist in the feed in trace amount. However, for bulk gas separation, where the change in flow rate due to adsorption-desorption is significant, this assumption is clearly inappropriate. Later on, Ruthven and Raghavan [59] developed a variable velocity model.

The first isothermal full solution model, which includes the dispersion term in the mass balance equation and allows for variable velocity during adsorption-desorption steps is the one published by Shin and Knaebel [63]. Limited studies have been published for developing the nonisothermal full solution model.

SMBR is a periodic reactor with the boundary conditions across the beds changing continuously so that at best it can reach a cyclic steady state. In order to determine this state, cycles are repeated until minor differences are noticed in concentration profiles between two consecutive switching. This is called the successive

substitution method, and used by most authors because of its simplicity, although in some cases the computation time is high.

Most dynamic models developed so far have been solved numerically by either finite difference or orthogonal collocation techniques. The latter method is computationally much superior to the former [59]. For the previous studies, all computer simulation codes were developed in FORTRAN language. However, MATLAB is used for the simulation of SMBR in this study, as the application of orthogonal collocation on PDEs requires a set of matrices, which can be handled by the latter much more easily. Moreover, the output can be directly visualized and does not need any other graphical software. The ODE solver `ode15s` is a relatively new subroutine available in MATLAB that uses the Numerical Differentiation Formulas (NDF) and has proven to be much more efficient than the subroutines based upon the traditional Backward Differentiation Formula (BDF) [61].

1.1 OBJECTIVES OF THE PRESENT RESEARCH

The objectives of this research work are:

1) To develop and establish nonisothermal models which describe Simulated Moving Bed Reactor (SMBR) and Sandwich Reactor, for isomerizing *n*-pentane to its branched isomer. The models are to be full solution models, that is, the most simplified assumptions shall be relaxed.

2) To solve the models numerically using orthogonal collocation technique and to generate computer simulation codes in MATLAB using the subroutine `ode15s`.

3) To predict the breakthrough curves for fixed-bed adsorber and reactor, and to study the effect of operating and design parameters on them.

4) To simulate the SMBR process. The catalyst is Pd/Y-zeolite and the adsorbent is 5A zeolite. The operating temperature is in the range of 430 K to 573 K. Pressure is held constant at 15 bar.

5) To achieve >99% purity of the product isopentane using the SMBR by varying the operating and design parameters.

6) To simulate the sandwich reactor in order to achieve >99% product purity.

CHAPTER 2

LITERATURE SURVEY & BACKGROUND

2.1 TOTAL ISOMERIZATION PROCESS

The total isomerization process (TIP) for improving octane rating of certain hydrocarbon fractions, especially mixed feedstocks containing normal and iso- pentanes and hexanes, involves an initial catalytic reaction which must be conducted in the presence of hydrogen to protect the catalyst, and a separation procedure that employs molecular sieve adsorbers [23] (Figure 2.1). The adsorbers employ a hydrogen-containing purge gas stream to desorb normals and a recycle system to return desorbed normals and purge gas to the isomerization reactor.

The adsorbers are operated in a cycle that involves the following steps: (1) pressurization, (2) adsorption, (3) blowdown, and (4) desorption. The product (isomers) leaves the system in the adsorption step. Since four adsorbers are employed, a continuous product stream is obtained.

The hydrogen in the recycled purge gas supplies sufficient partial pressure in the reactor, which is required to prevent the deleterious effect of coking on catalyst life. By virtue of the recycle, the process will eventually totally isomerize all normal pentanes and hexanes in the feed.

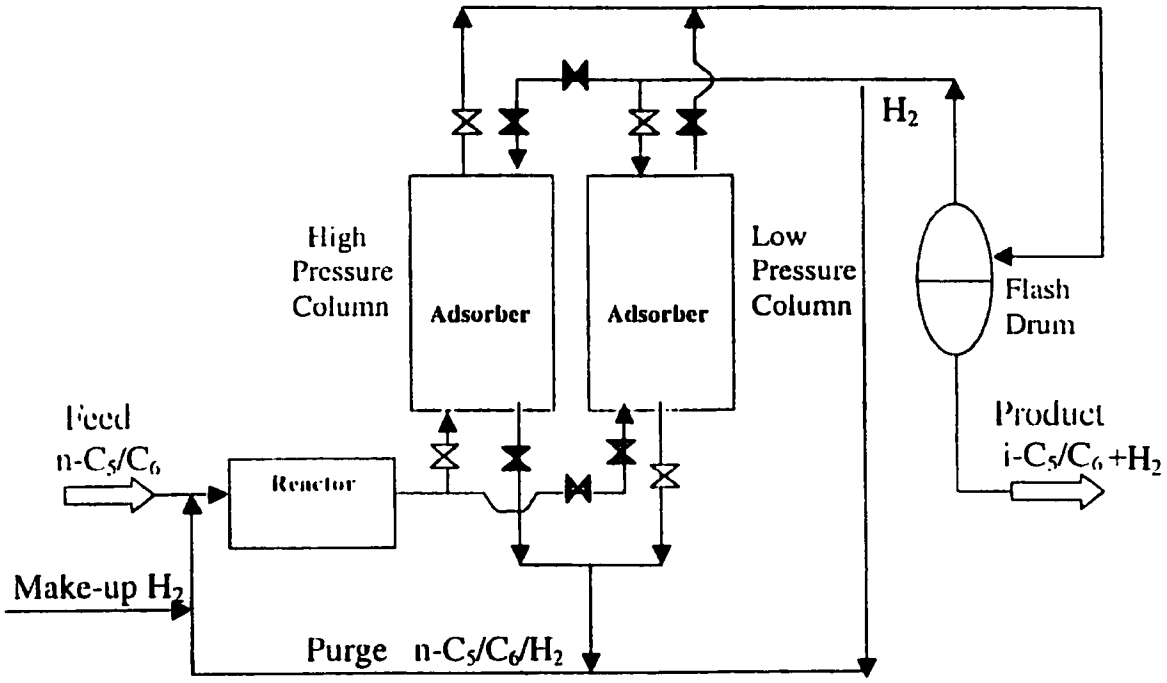

Figure 2.1. Block-Flow Diagram for the Total Isomerization Process

2.2 PRESSURE SWING ADSORPTION REACTOR (PSAR)

Al-Juhani [1] proposed a novel process for isomerizing *n*-pentane to its branched isomer in a combined reactor/pressure swing adsorption unit (Figure 2.2). The unit was packed with two separate layers containing a catalyst (Pd/Y-zeolite) and an adsorbent (5A zeolite). The objective was to combine reaction with separation in one unit so that a significant cost saving in ancillary equipment may be achieved.

A mathematical model linking the catalyst layer and the adsorbent layer was developed. The model was general because it relaxed most simplified assumptions used in modeling pressure swing adsorption systems such as equilibrium theory, plug flow, constant velocity and frozen solid approximation. The frozen solid approximation assumes that no adsorption takes place in the pressurization step and no desorption occurs in the blowdown step. However, a substantial amount of normals was adsorbed in the pressurization step and similarly a significant amount was desorbed in the blowdown step because of which the frozen solid approximation had to be relaxed [1]. The model was used to simulate a PSAR cycle with a configuration similar to the simple Skarstrom cycle [67]. Under the new configuration, the blowdown stream had a considerable amount of isomers and could be considered as part of the product.

It should be noted, however, that only two adsorbers were used. Thus, the product stream in this case was not continuous. Moreover, although the adsorption/reaction step was conducted at high pressures (15-20 bar), desorption/reaction step was conducted at a much lower pressure (2 bar), which can have a deteriorating effect on the catalyst.

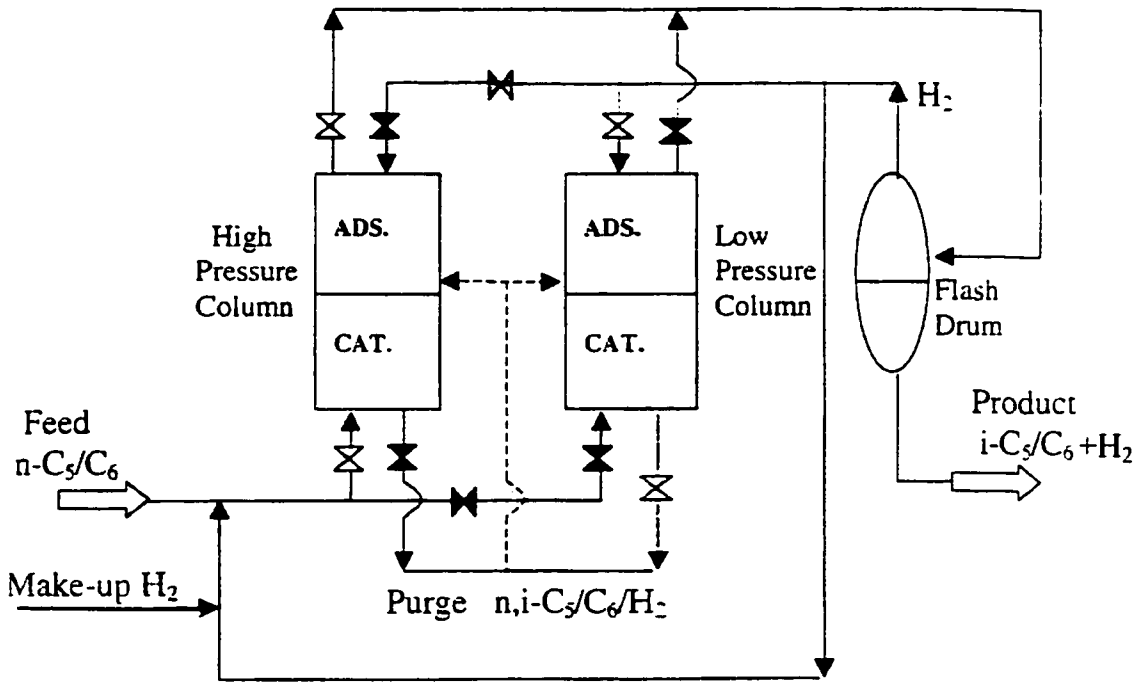

Figure 2.2. Flow Diagram for the Combined Isomerization Reactor/Adsorber Process

2.3 SIMULATED MOVING BED

Large-scale adsorptive separations based on simulated moving bed (SMB) technology [60] have been widely applied to mixtures of hydrocarbons since the development of the Sorbex process by UOP [5,28]. This technique exploits the principle of displacement chromatography; hence, in addition to a suitable adsorbent, an appropriate desorbent is also needed.

Mazzoti *et al.* [39] studied the separation of various mixtures of C_5-C_6 paraffin fraction. The separation was carried out in a six-bed vapor phase SMB pilot plant operated at 448 K and 350 kPa, using *n*-heptane as desorbent and 5A zeolite as adsorbent.

In principle, adsorptive separations are most conveniently operated in a continuous true countercurrent unit (TCC) where the solid and the fluid phases move countercurrently [58] (Figure 2.3). There are two inlet streams, that is, the mixture to be separated and the desorbent makeup. The two outlet streams are the extract, where the most adsorbable components (*A*) are preferentially collected, and the raffinate, which contains the least adsorbable species (*B*). Each of the four sections plays a specific role in the separation process. Sections 2 and 3 perform the fractionation, by conveying the strong components downward toward the extract outlet and the weak components upward toward the raffinate outlet. Section 1 regenerates the adsorbent by desorbing *A*, thus enabling the recycle of clean adsorbent. Section 4, on the other hand, regenerates the desorbent by adsorbing *B*. In other words, section 4 removes *B* from the fluid stream which makes the recycling of desorbent to section 1 possible [70].

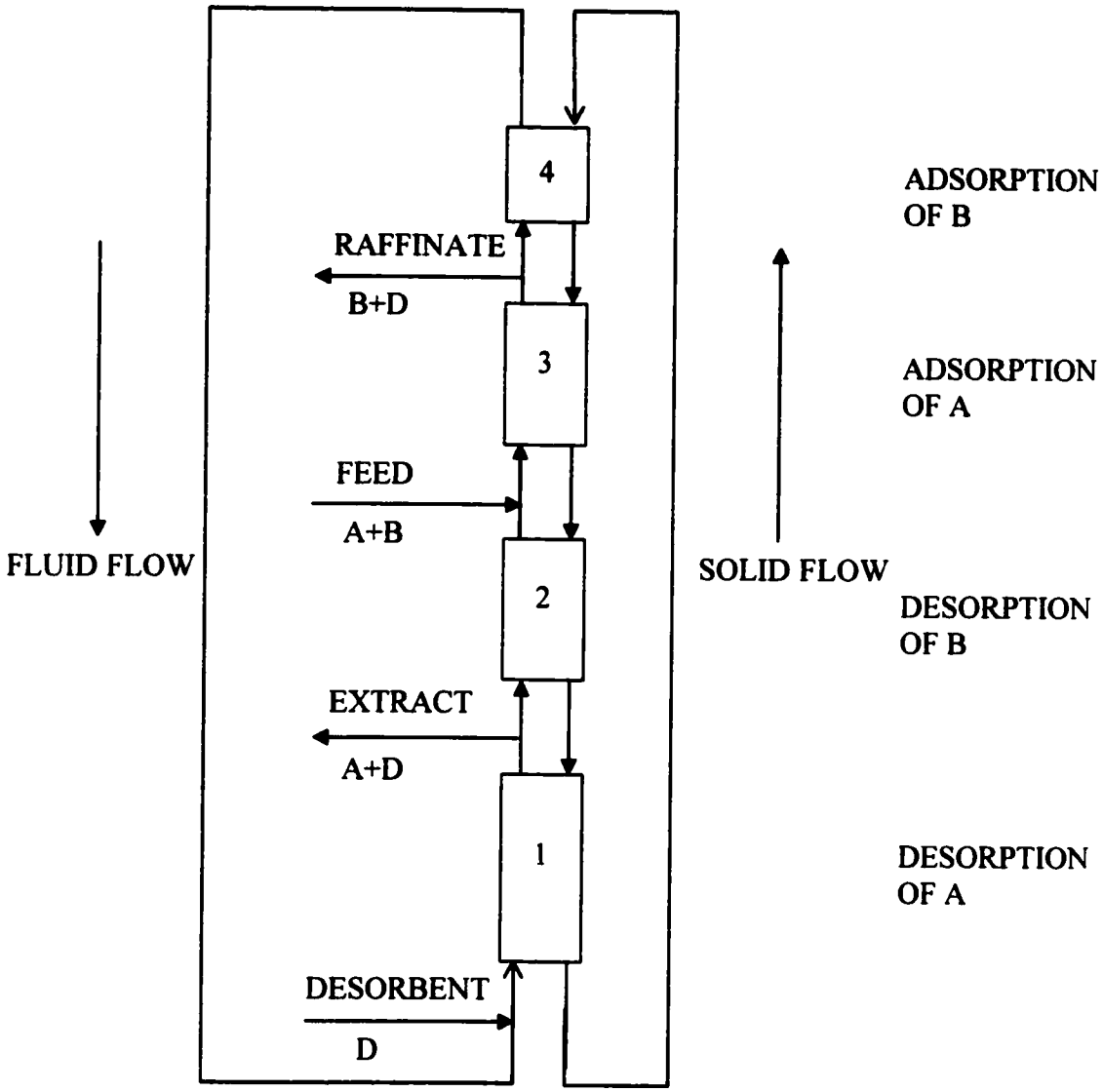

Figure 2.3. Four-Section True Countercurrent Unit

However, purging is used to regenerate the adsorbent bed in this study instead of displacement chromatography. Neither the purge (H_2) nor the isomer (*B*) adsorb over the adsorbent (zeolite 5A) so that they cannot be separated inside the TCC unit. Thus it becomes necessary to have an open loop for hydrocarbon separation by collecting all of the outlet stream from section 3 as raffinate and removing section 4 all together. Section 2 is used for desorbing the less adsorbable component so that it also becomes redundant for this system. Hence the separation of normal and iso- paraffins can be performed using just sections 1 and 3 provided that purging is used as a means for regenerating the adsorbent bed instead of displacement chromatography.

The practical problems related to the actual movement of the solid phase can be overcome via simulating this countercurrent contact by moving the fluid phase and the column in a fixed bed unit known as the simulated moving bed. The continuous column movement is simulated by a discrete movement obtained by shifting the feed and withdrawal nodes at discrete time along the column axis in the same direction of the fluid flow. In order to closely mimic the countercurrent apparatus the sections of the separation unit are divided into several ports or subsections. Each one of these is constituted of a fixed bed which is fed with the fluid stream leaving the previous subsection after addition or withdrawal of an external stream when required. A typical sorbex process contains 4-3-3-2 beds arranged in the four sections respectively. Section 1 normally contains the highest number of beds indicating that the regeneration of adsorbent bed takes the largest time.

The two unit configurations are related by a set of geometric and kinematic equivalence relationships which state that:

1) the relative velocity of the two phases must be the same whether the adsorbent beds are fixed or not;

2) the solid velocity in the TCC unit corresponds in the SMB configuration to the average velocity given by the ratio between the bed length, L, and the switch time, τ_s (which is the time period between two successive port switches), that is,

$$u_s = L/\tau_s \tag{2.1}$$

3) the section length in the TCC unit, L_j, is equal to the bed length times the number of beds per section in the SMB configuration, that is,

$$L_j = Ln_j \tag{2.2}$$

2.4 CHROMATOGRAPHIC REACTORS

Traditional chromatographic reactors are fixed beds with mixed catalyst and adsorbent as the solid phase. The reactant is introduced at one end of the reactor in the fluid phase along with a carrier. As the reactant moves along the reactor, some of it reacts to form products. The success of this reactor depends on selective adsorption. The difference in affinity for the solid phase between the reactants and products must be sufficient to give good separation. The more strongly adsorbed reactants will be held up by the adsorbent in the solid phase while the products are swept away with the fluid phase and separation is achieved. The major problem with these chromatographic reactors is that they are batch processes.

2.4a Countercurrent Moving Bed Chromatographic Reactor

In order to get continuous operation and product elution, the countercurrent moving bed chromatographic reactor (CMCR) (Figure 2.4) is used [11]. In this reactor, the solid phase is again mixed catalyst and adsorbent, but now is introduced at the top of the column and moves down. The fluid phase is introduced at the bottom of the column and moves up. The reactant is fed either in the bottom or in the middle of the column. For appropriate parameter values, the more strongly adsorbed reactants can be made to move down the column while the less strongly adsorbed products are eluted from the top of the column with the fluid phase. The product stream should be essentially free from reactants and almost all of the reactants will react before leaving the bottom of the column with the solid phase.

The majority of research to date on the CMCR has been concerned with the development of mathematical models. Viswanathan and Aris [78,79] were first to develop such a model. An irreversible, first order, solid catalyzed reaction with instantaneous adsorption and bottom fed reactants was studied. The model predicted complete conversion and pure product in a finite length of reactor. Similar conversions and purities were predicted using other model modifications [11,46,47,72-74,76] which use various combinations of linear or Langmuir adsorption isotherms, reversible reactions, side fed reactors and dispersionless or dispersion included models.

Only a few experimental studies have been reported on the CMCR. The first [75], a study on the oxidation of CO over Al_2O_3, verified model predictions of simultaneous reaction and separation and agreed with species concentration profiles for low gas to

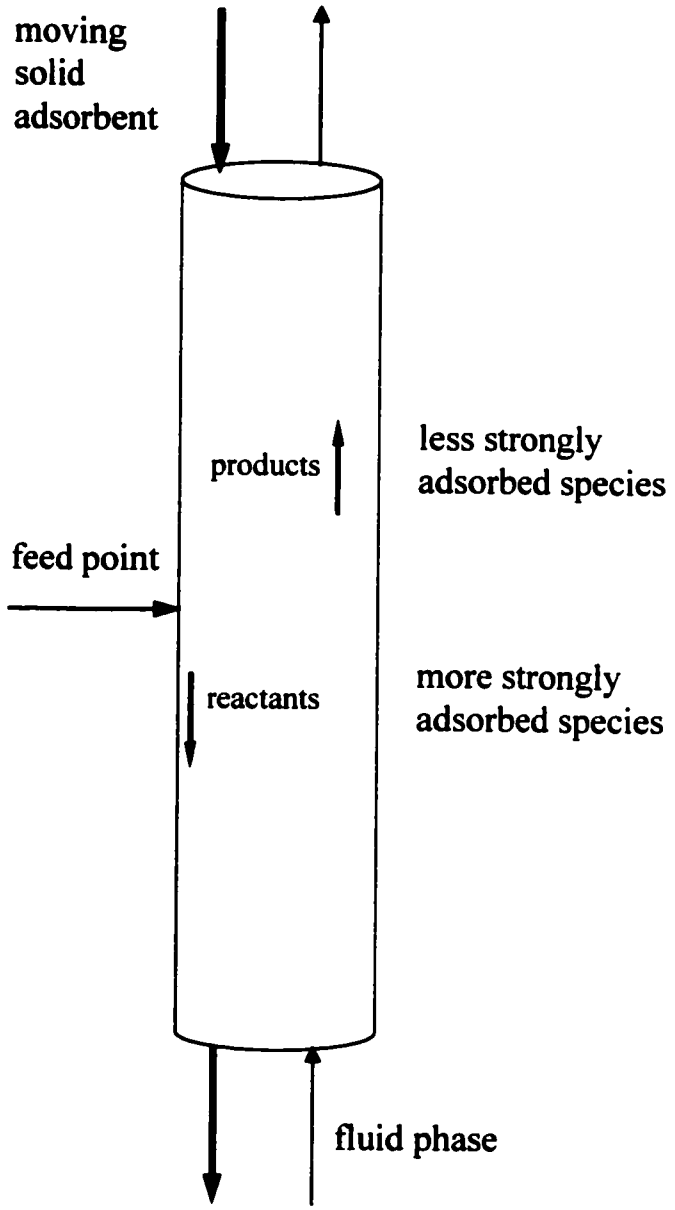

Figure 2.4. True Countercurrent Moving Bed Chromatographic Reactor

solid flow ratios (a linear isotherm model). The other reaction investigated is the catalytic hydrogenation of mesitylene to trimethylcyclohexane [47]. Fish *et al.* [14] describe design and construction of a CMCR. This group reports conversions much greater than equilibrium with high product purity [15] in the CMCR.

One major drawback to the CMCR is that of solids handling. Problems such as channeling, abrasion, attrition and fines removal can be avoided by simulating the countercurrent flow. This leads to single column [51] or multi-column simulated moving bed reactor (SMBR) [50]. Besides avoidance of solid handling problems, other advantages gained by the SMBR over the CMCR are reduction of adsorbent inventory by elimination of the recycle stream and top and bottom holding vessels, and minimizing catalyst cost for solid catalyzed reactions. In addition, the absence of bed expansion, which occurs in the CMCR, would allow a smaller reactor volume for the SMBR.

2.4b Simulated Moving Bed Reactor

The simulated moving bed reactor (SMBR) is a novel catalytic reactor design that allows equilibrium limited and low conversion reactions to proceed to near completion in theory. Experimental implementation of this reactor scheme has resulted in great improvements in product purity and yield when compared to the same reactions carried out in conventional reactors. This reactor configuration takes advantage of: (1) *reaction chromatography* for increased conversion and product purity due to separation of products from reactants; (2) *countercurrency* for continuous operation and throughput; and (3) *simulation of countercurrency* to avoid solid handling problems.

In the single column configuration (Figure 2.5), rather than moving the solid phase countercurrent to the fluid phase, the reactant feed point is moved along a fixed bed in the same direction as fluid flow, but at a slower speed. This configuration is similar to early Sorbex simulated countercurrent separation processes [6,7,58]. Now, in the frame of reference of the feed point, the fluid phase is moving forward and the solid phase backwards. For properly chosen parameters, the products and reactants move forward and backward relative to the feed point rather than up and down the column.

If the feed point were to move continuously along the bed, this would exactly simulate the CMCR. In practice, there are feed point inlets and product removal outlets spaced evenly along the column. Because of these discrete feed points, the product profile for the SMBR will be approximately a step function, with dead times and periods of high product concentration, rather than the constant product concentration of the CMCR. Higher sections in SMBR will give output profiles that more closely approximate the CMCR, although this does not mean that it will necessarily yield better performance. The feed point location adjustment (analogous to the solid phase velocity) is determined by the switching time, the time interval between switching the feed from inlet to inlet. Thus, the SMBR is a periodic reactor.

Ray *et al.* [51] used a similar single column SMBR to study the hydrogenation of 1,3,5-trimethylbenzene. The reaction occurs over Pt whereas the selective adsorption for separation occurs over Al_2O_3. It was shown that reaction and separation can be achieved simultaneously and that the yield of the reversible reaction can be improved greatly.

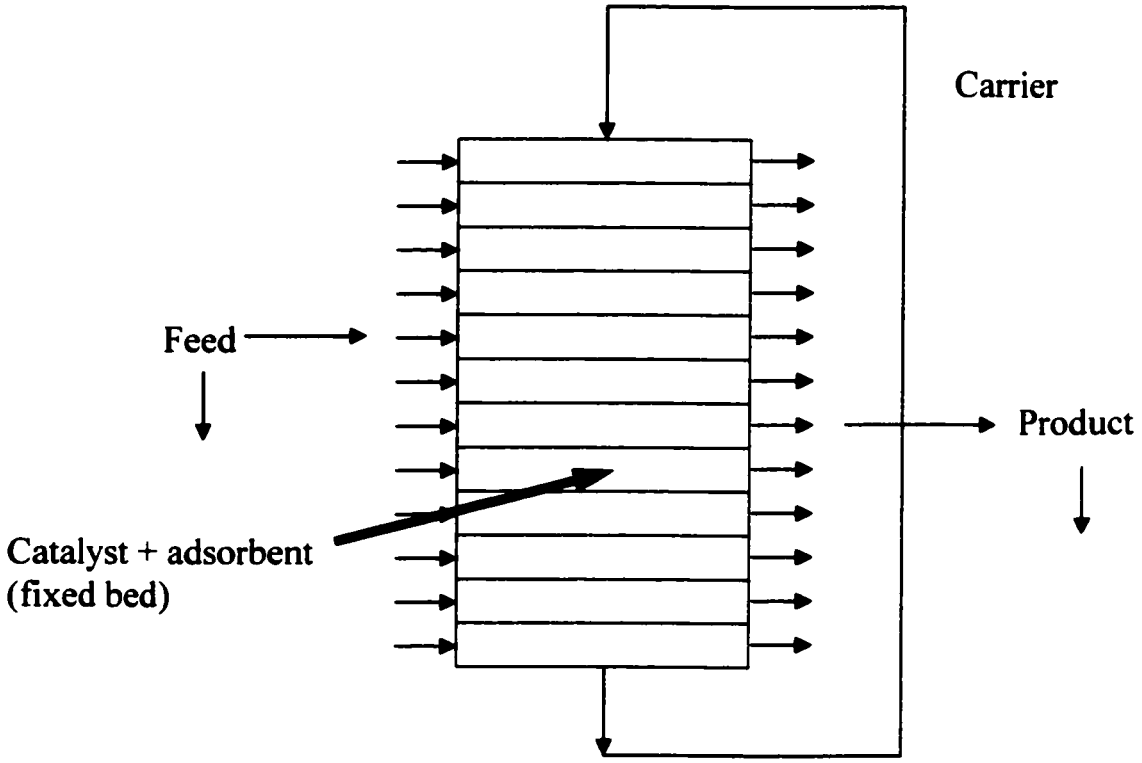

Figure 2.5. Single Column SMBR. Feed and product ports move in the same direction as carrier.

It was found that a multiple column configuration of the SMBR is more convenient for laboratory investigations [50]. If the single column SMBR is divided at the feed points into several smaller columns with inlet and outlet ports between columns, one arrives at the multi-column SMBR (Figure 2.6).

A multi-column SMBR was modeled and experimentally tested using equilibrium limited mesitylene hydrogenation reaction [50]. This reaction was shown to proceed to near completion in both theory and experiment, when carried out in a similar SMBR design (Figure 2.7). The reactor is divided into two distinct sections. In the first two-column section, feed and carrier gas are introduced, and the product (1,3,5-trimethylcyclohexane) is completely collected, while in the other, a make-up carrier is introduced to purge unconsumed reactant. A granular mixture (60/80 mesh) of 90% cross-linked polystyrene adsorbent (Chromosorb 106) was used with 10% Pt/Al_2O_3 catalyst in these columns.

Tonkovich and Carr [77] applied the SMBR to the oxidative coupling reaction of methane. A four-section experimental apparatus (Figure 2.8), each section containing a reaction column and two separation columns, was used to quickly separate the reactants and products using the principles of simulated countercurrent flow, the adsorbent being activated charcoal. The catalyst and adsorbent were placed in series to separately control their respective temperatures. Microreactor trials with a samarium oxide (Sm_2O_3) catalyst gave yields between 2% and 10% whereas yields as high as 50% were observed with the same catalyst and run conditions in the SMBR.

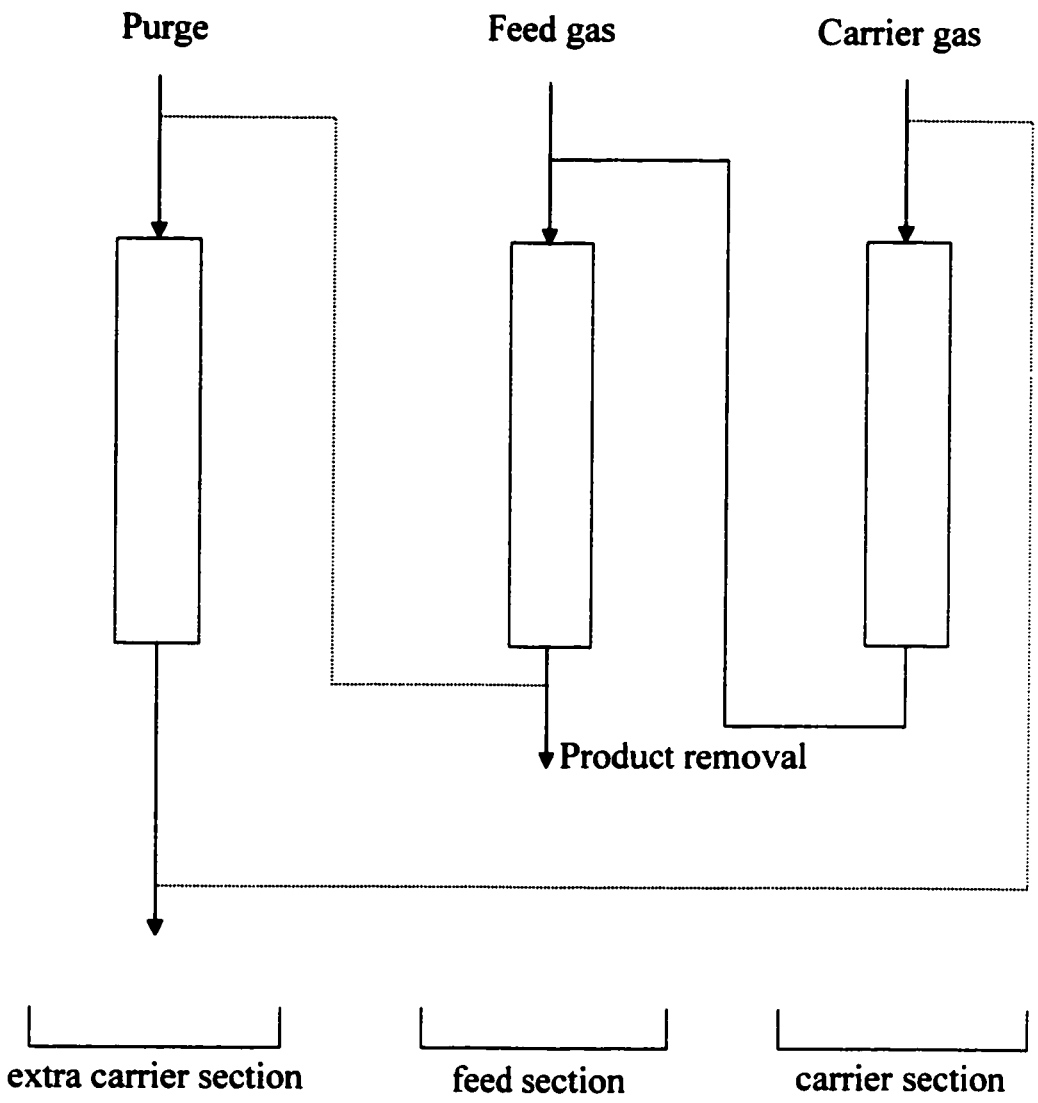

Figure 2.6. Multi-Column SMBR. There is no flow through the dashed lines.

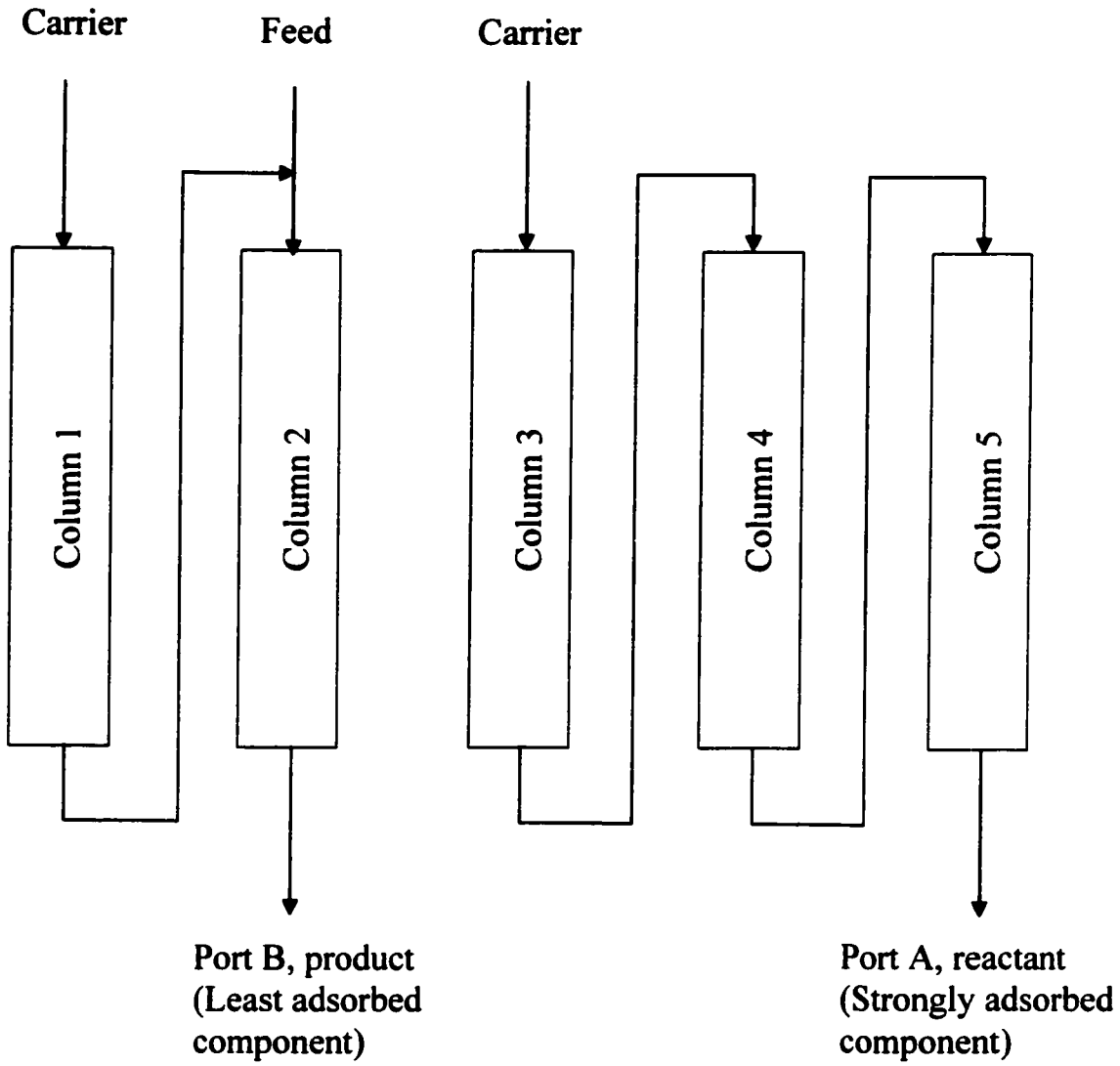

Figure 2.7. Five-Column Reactor Configuration

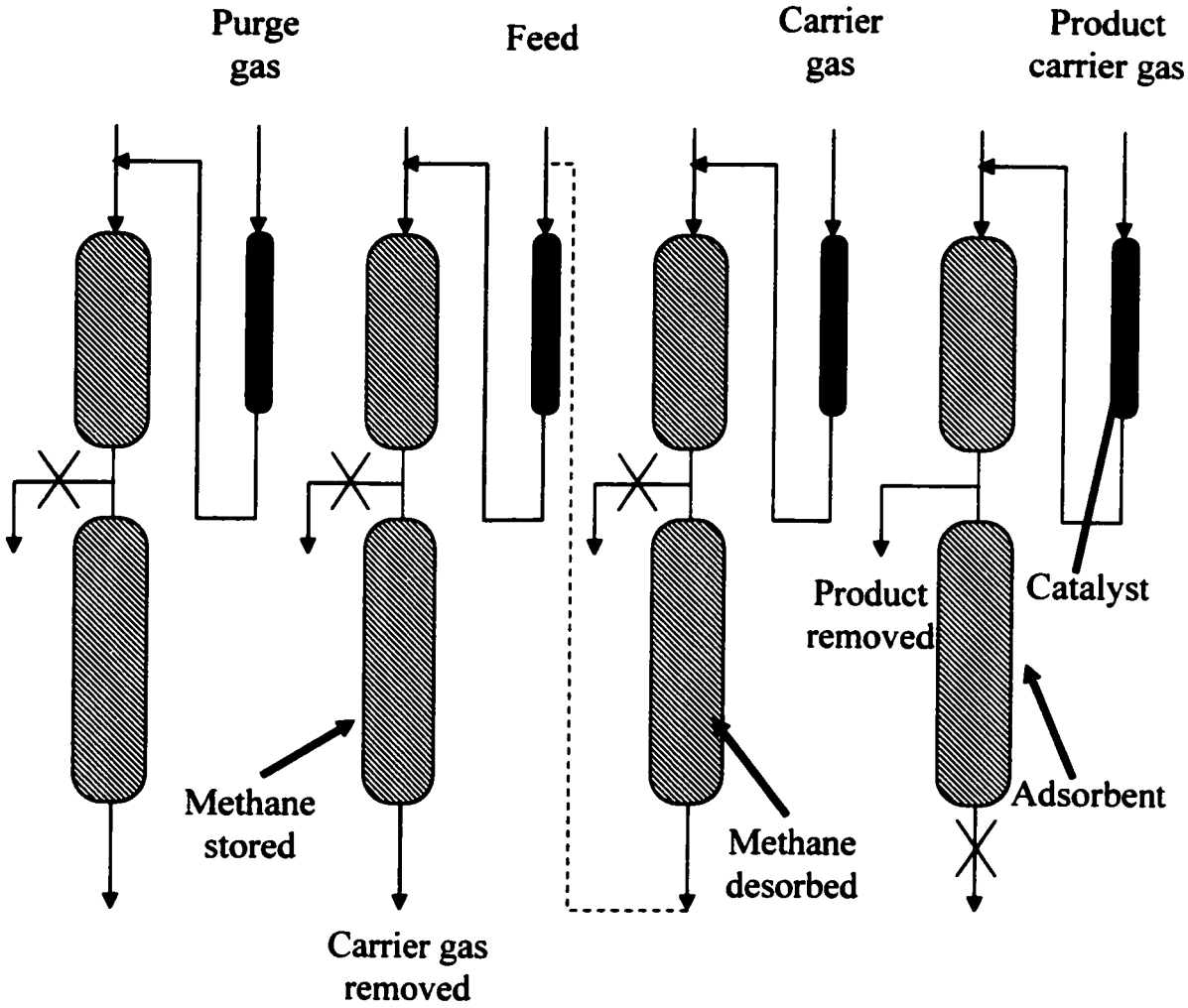

Figure 2.8. SMBR for Oxidative Coupling of Methane

During the operation of the SMBR, the unconverted reactant (methane) is stored in the separation column of the current feed section. Prior to methane breakthrough, the feed is switched to the next section. The carrier gas enters the section behind the feed, where it desorbs the reactants stored from the previous cycle. This stream is then added to the make-up feed and sent to the reaction column in the feed section. To prevent further decomposition, the products (ethane and ethylene) are rapidly removed from the reaction conditions in the low-temperature separation column of the feed section. A pure product stream is removed from the first of the two separation columns connected in series in each section with the aid of a separate carrier gas stream. Product removal occurs two sections behind the feed section.

Kruglov [33] studied the synthesis of methanol from syngas using two different configurations of simulated moving bed reactor. In the first, operating under adiabatic conditions, the fixed bed consists of a catalyst and a selective product adsorbent mixed together (Figure 2.9). In the other one, operating isothermally, the catalyst and adsorbent are alternately packed in beds containing catalyst or adsorbent and only adsorber sections participate in a discrete countercurrent movement (Figure 2.10). The reaction takes place over a $Cu/ZnO/Al_2O_3$ catalyst and adsorption of methanol occurs onto a silica-alumina adsorbent.

Gaseous reactants (CO and H_2) are introduced into a section in the feed position. They sequentially pass through fixed beds in the reaction zone (the three right-hand sections in Figure 2.9) with methanol forming on the catalyst surface. Having formed, it is bound by adsorbent, allowing the reaction to achieve higher conversion. The

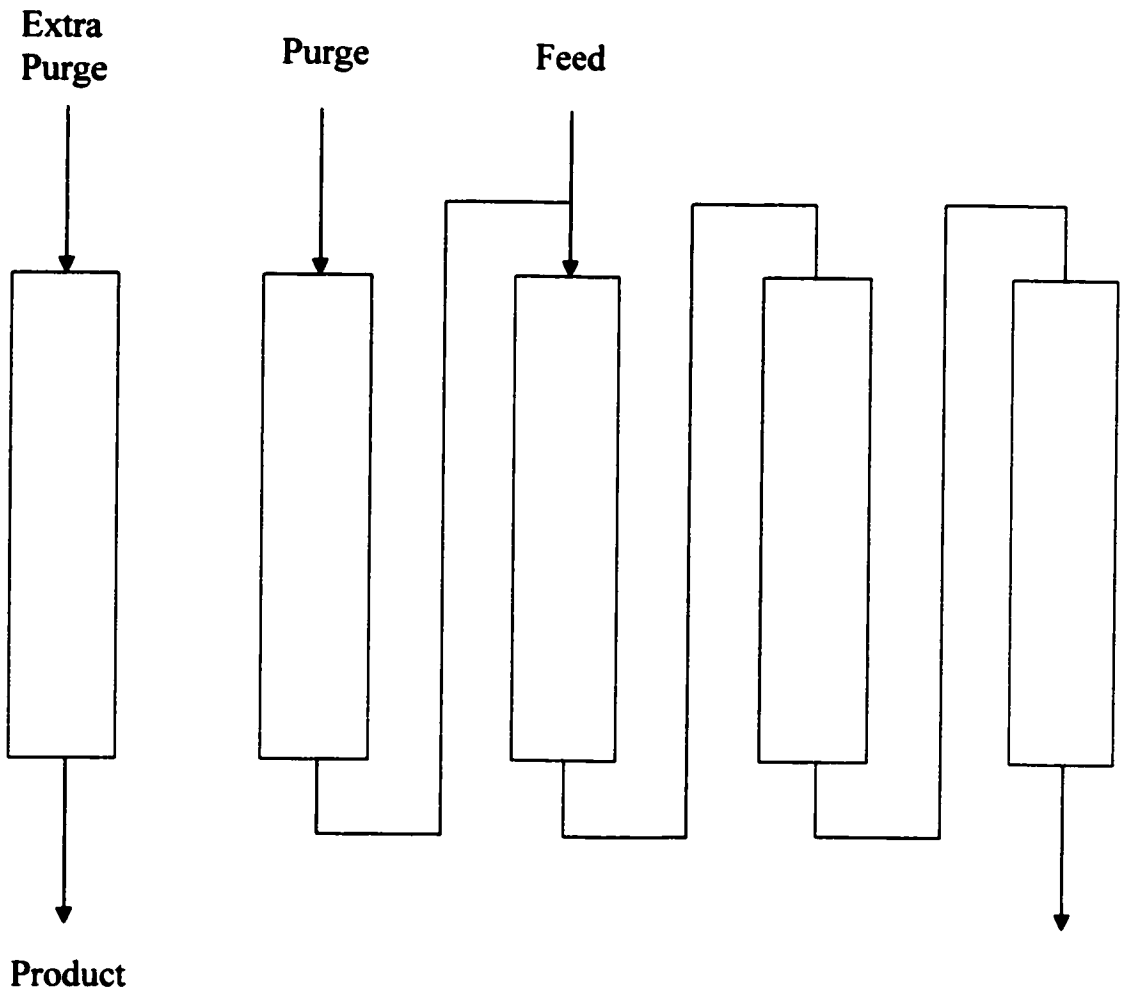

Figure 2.9. Adiabatic SMBR for Methanol Synthesis

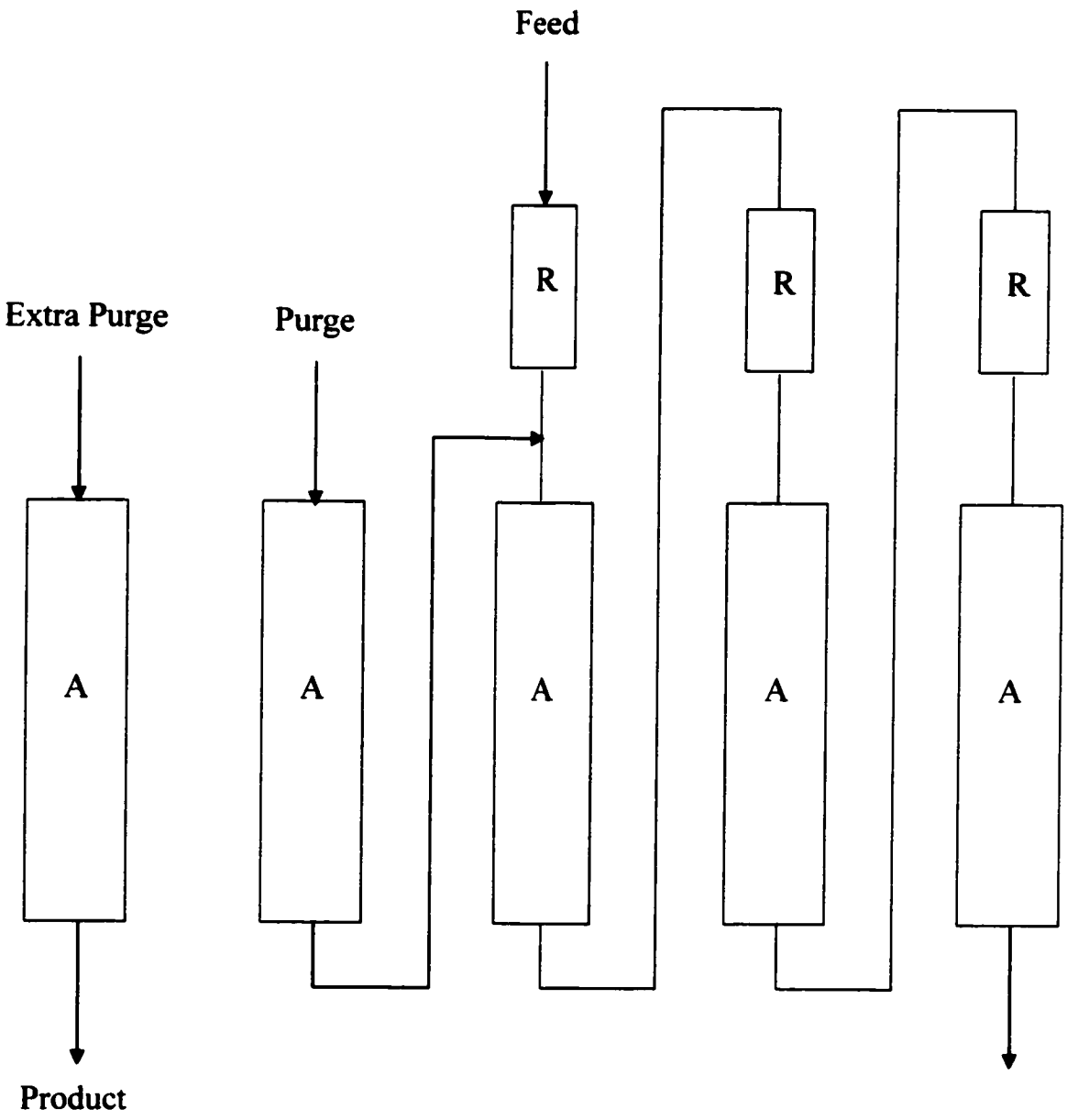

Figure 2.10. Isothermal SMBR for Methanol Synthesis

unconverted reactants leave the reactor. The section in the feed position contains unconverted reactants in the gas phase and, clearly, a stripping section (second section from the left) is necessary before the product is desorbed in the left most section to obtain high enough or complete conversion.

Besides the differences mentioned above for the second type of SMBR, the outgoing stream from stripping section is passed over the adsorbent rather than the catalyst in the feed section (Figure 2.10). This is done to avoid a capacity drop in the first catalyst fixed bed caused by the presence of methanol in the flow outgoing from stripping section. This type of SMBR cannot be operated adiabatically because the heat released due to chemical reaction cannot be withdrawn any longer by means of recirculated solids, as the reactor sections remain stationary with respect to inlet and outlet locations of the gas stream. Both of these configurations gave very high carbon monoxide conversions (>97%). A summary of the various systems studied over the simulated moving bed reactor is presented in Table 2.1.

In the oxidative coupling of methane, the products (ethane and ethylene) are the more strongly adsorbed species [77]. So is the case in the synthesis of methanol [33] because of which the alternate sequence of reactors and adsorbers is possible (Figures 2.8 & 2.10). However, in this study, the adsorbent (5A zeolite) only adsorbs the reactants (normal paraffins) and not the products (branched paraffins) because of the steric effect. If the outlet stream were allowed to pass through the remaining reactor-adsorber sequence, the products would undergo reverse reaction. Therefore, such a system does

Table 2.1. Summary of Various Systems Studied Using SMBR

1977	Zabransky & Anderson [84]	Alkylation process
1983	Hashimoto *et al.* [24]	Production of high-fructose corn syrup
1994	Kruglov [33]	Synthesis of methanol from syngas
1994	Tonkovich & Carr [77]	Oxidative coupling of methane
1995	Ray & Carr [52]	Hydrogenation of 1,3,5-trimethylbenzene
1996	Funk *et al.* [21]	Hydrolysis of esters
1996	Kawase *et al.* [30]	Production of β-phenethyl acetate from acetic acid and β-phenethyl alcohol
1996	Mazzotti *et al.* [40]	Esterification of acetic acid with ethanol
1996	Shieh & Barker [62]	Hydrolysis of lactose
1999	Fricke *et al.* [17]	Effect of process parameters on SMBR performance
1999	Kawase *et al.* [31]	Production of Bisphenol A
1999	Migliorini *et al.* [42]	Development of a design strategy for SMBRs
2001	Azevedo & Rodrigues [2]	Inversion of sucrose by enzymatic action
2001	Huang & Carr [27]	Design and performance of the SMBR
2001	Lode *et al.* [37]	Synthesis of methyl acetate

not seem applicable for the hydrocarbon isomerization. Kruglov [33] also raised such concerns in the synthesis of methanol.

The alternating reactor-adsorber sequence is also possible when two products are formed in a reversible reaction:

$$A \leftrightarrow B + C$$

The conversion is maximum when the adsorption equilibrium constant K_A for reactant A is intermediate between those of the products B and C. The products are separated from each other because of the different K values thus inhibiting the reverse reaction. However if the reactant A is either the best or the worst adsorbable component, good separation does not enhance reactor performance because then both products move in the same direction relative to A and the reverse reaction is not significantly suppressed.

Meurer *et al.* [41] showed that a homogeneous mixture of adsorbent and catalyst in a batch chromatographic reactor gave a higher conversion for the above system as compared to a heterogeneous reactor consisting of alternately packed catalyst and adsorbent beds. However using just two catalyst and two adsorbent beds in the heterogeneous reactor greatly increases the conversion as compared to a conventional reactor. In theory, a heterogeneous reactor with an infinite partition operates similar to the homogeneous reactor.

An example in which the reactant gets strongly adsorbed in an SMBR is the hydrogenation of mesitylene to trimethylcyclohexane (Figure 2.7) [51,52]. The catalyst and adsorbent are mixed homogeneously in this case. In modeling the system, no

distinction is made between the adsorbed phase concentration over the catalyst and that over the adsorbent. In fact, the following reaction scheme is followed:

$$A(g) \leftrightarrow A_{ads} \leftrightarrow B_{ads} \leftrightarrow B(g)$$

Similar reaction occurs over the Pd/Y-zeolite catalyst in *n*-paraffin isomerization. However, a distinction needs to be made between adsorption over the catalyst and that over the adsorbent because the catalyst can adsorb both the reactant and the product whereas the adsorbent (5A zeolite) can only adsorb the reactant. Meurer *et al.* [41] proposed separate model equations for catalyst and adsorbent phases in a homogeneously mixed solid.

It is, nevertheless, inappropriate to mix homogeneously the adsorbent and catalyst for hydrocarbon isomerization because the isopentane would undergo reverse reaction in the latter part of the vessel where the reactant has not yet reached. In light of the above discussion, only one reactor should be used in series with a cascade of simulated moving beds, the extract stream (containing the desorbed reactant) being recycled back to the same reactor. Huang and Carr [27] studied a hypothetical SMBR containing just one reactor and several adsorbent beds.

2.5 BASIC CONCEPTS

Modeling of SMBR is actually a process of linking up several models for sub-processes in the system. The model should essentially consider physical equilibrium models, mass transfer and reaction kinetics. Reviews of these concepts are presented here.

2.5a Adsorption Equilibrium Isotherms

Adsorption equilibria are described by isotherms, a relationship between adsorbed and bulk phase concentrations at constant temperatures. Sorption isotherms in zeolites generally follow type I in IUPAC classification, which can be represented by the Langmuir equation [35]:

$$K_{ads} = \frac{1}{P_i}\frac{\theta}{1-\theta} \tag{2.3}$$

where $\theta = q/q_{\max}$ is the degree of filling of sites and $q_{\max}$ is the maximum concentration of adsorbate at the saturation of the adsorbent. Silva and Rodrigues [65] deduced a reasonable value for 5A zeolite saturation with *n*-pentane as 4 molecules/cavity, corresponding to $13\mathrm{g}_{n\text{-C5}}/100\mathrm{g}_{\mathrm{ads}}$. If the Langmuir equation were valid, a plot of $\theta/P_i(1-\theta)$ against θ would give a straight line parallel to the θ axis. However, they showed that it did not represent the experimental data well.

More recently, Nitta *et al.* [44] developed an adsorption equilibrium isotherm, which is similar to the Langmuir one. They assumed localized adsorption in which the adsorbed molecule occupies a certain number of active sites, *n*. The isotherm expression is, neglecting the interaction term between adsorbed molecules in the original model:

$$K_{ads} = \frac{1}{P_i}\frac{\theta}{(1-\theta)^n} \tag{2.4}$$

The value of *n* is 5 for *n*-pentane because plots of $\theta/P_i(1-\theta)^5$ against θ are all straight lines [65].

2.5b Kinetics of Sorption

In bidisperse porous adsorbents such as zeolite pellets (Figure 2.11), there are two or more diffusion mechanisms: the macropore diffusion with time constant $D_p/R_p^2(1+K)$ and the micropore diffusion with time constant D_c/r_c^2. It is important to carry out experiments in pellets with different sizes but with the same crystal size (different R_p, same r_c) or pellets with the same size but with different crystals (same R_p, different r_c). If macropore diffusion is controlling, time constants for diffusion should depend directly on pellet size and should be insensitive to crystal size changes. If micropore diffusion controls, the reverse is true. Silva and Rodrigues [65] concluded that at low loadings of the adsorbent, mass transfer in the pellet was dominated by macropore diffusion for their particular system.

2.5c Interparticle and Intraparticle Mass Transport

In modeling the fluid particle system, three different phases need to be identified: the fluid-bulk phase, the pore fluid phase, and the solid phase. The first two are connected by mass transfer through the external film. Once the adsorbable molecule has reached the particle surface, it diffuses with simultaneous adsorption through the pore fluid phase within the particle. This process can be described by a material balance of the generic adsorbable component A, in a spherical adsorbent particle:

$$\varepsilon_p \frac{\partial c_{pA}}{\partial t} = \varepsilon_p \frac{D_p}{r^2}\frac{\partial}{\partial r}\left[r^2 \frac{\partial c_{pA}}{\partial r}\right] - \frac{\partial q_A}{\partial t}\rho_s\left(1-\varepsilon_p\right) \tag{2.5}$$

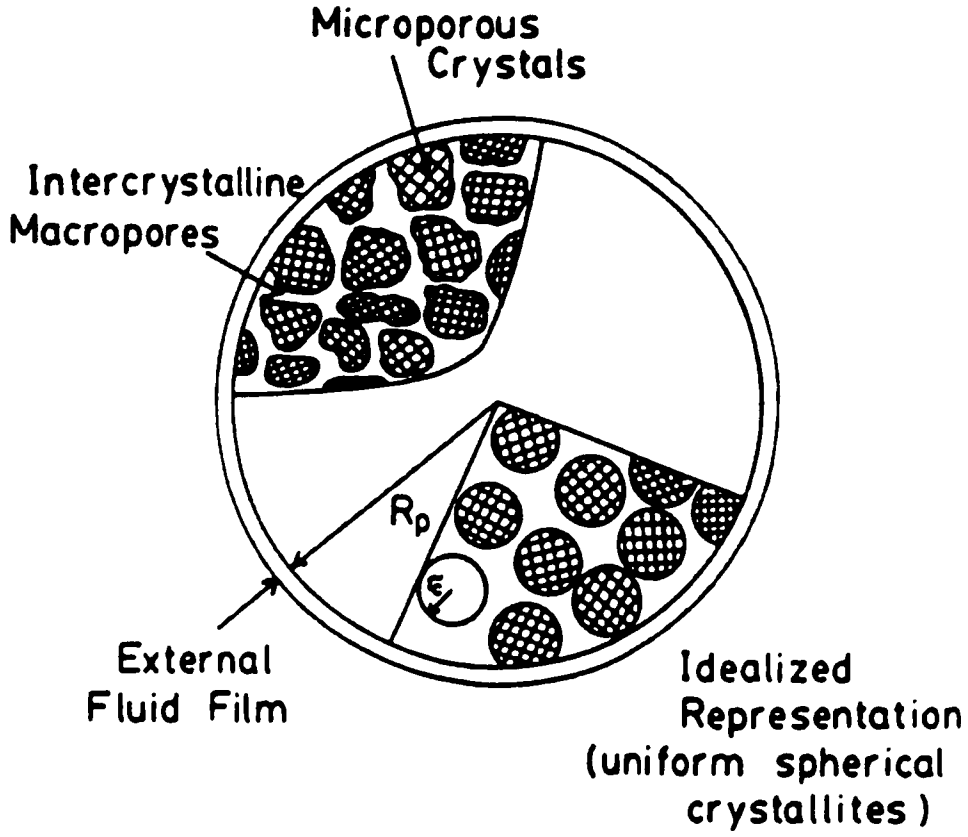

Figure 2.11. Resistances to Mass Transfer in a Zeolite Molecular Sieve

with the boundary conditions

$$\frac{\partial c_{pA}}{\partial r} = 0; \qquad r = 0 \tag{2.6a}$$

$$\varepsilon_p D_p \frac{\partial c_{pA}}{\partial r} = k_e\left(c_A - c_{pA}\right); \qquad r = R_p \tag{2.6b}$$

and the initial condition $c_{pA} = 0$ at $t = 0$. The evaluation of q_A, which is assumed to be in equilibrium with c_{pA} throughout the particle, is performed by means of an adsorption isotherm (such as equation 2.4). Different modifications of this model can be obtained whenever the diffusion in the particle is not represented by normal diffusion in the pore fluid phase (pore-diffusion), as in equation 2.5, but by diffusion in the solid phase (solid-diffusion) or in the pore surface (surface-diffusion). All of these models have been reported in detail by Liapis and Rippin [36].

In order to simplify subsequent calculations, Morbidelli *et al.* [43] applied a lumping procedure to equation 2.5. Integrating both sides of this equation in the particle volume, they obtained:

$$\varepsilon_p \frac{\mathrm{d}\langle c_A\rangle}{\mathrm{d}t} = k_e \frac{3}{R_p}\left[c_A - c_{pA}\left(R_p\right)\right] - \frac{\mathrm{d}\langle q_A\rangle}{\mathrm{d}t}\rho_s\left(1-\varepsilon_p\right) \tag{2.7}$$

where $\langle c_A\rangle$ and $\langle q_A\rangle$ are the volume average values of the concentration in the pore fluid and in the solid phase, respectively. The details of the integration are shown in Appendix A.1. Using the linear driving force approximation:

$$k_e\left(c_A - c_{pA}\left(R_p\right)\right) = K_{gl}\left(c_A - \langle c_A\rangle\right) \tag{2.8}$$

where K_{gl} is the global mass transfer coefficient, which can be evaluated from the external and internal mass transfer coefficients, k_e and k_i, respectively:

$$\frac{1}{K_{gl}} = \frac{1}{k_e} + \frac{1}{\varepsilon_p k_i} \tag{2.9}$$

Two problems arise from this procedure. The first is the evaluation of the term $\langle q_A \rangle$. The approximation generally used is:

$$\langle q_A \rangle \equiv \frac{1}{V_p} \int f(c_{pA}) \mathrm{d}V_p = f(\langle c_A \rangle) \tag{2.10}$$

where $f(c_{pA})$ indicates the adsorption isotherm. Equation 2.10 is correct for linear adsorption isotherms but involves some approximation for nonlinear isotherms. The second difficulty lies with the evaluation of the internal mass transfer coefficient, k_i. It is defined by the relationship [43]:

$$k_i = \frac{D_p \left. \frac{\partial c_{pA}}{\partial r} \right|_{r=R_p}}{\left(c_{pA}(R_p) - \langle c_A \rangle \right)} \tag{2.11}$$

The exact value of k_i is thus time dependent and requires solution of the complete problem (equations 2.5 and 2.6). Normally a time average value of k_i proposed by Glueckauf [22] is used:

$$k_i = 5 \frac{D_p}{R_p} \tag{2.12}$$

Morbidelli *et al.* [43] point out the approximations involved in the lumping procedure. Equation 2.12 has been derived for the pure diffusion problem, which is without reaction, while here we assume equilibrium between the solid and the pore fluid

phases, which is infinite adsorption rate. Rate of reaction is known to play an important role on the value of k_i. Namely, the presence of the consumption of the component in the particle, due either to a chemical reaction or to an adsorption reaction process, increases the concentration gradient at the particle surface and thus the value of k_i through equation 2.11.

Combining equations 2.7 and 2.8, Silva and Rodrigues [66] neglected the accumulation of mass in the gas phase relative to the solid phase to arrive at the following equation for a lumped particle system controlled by macropore diffusion in a fixed bed:

$$\rho_a \frac{\partial \langle q_A \rangle}{\partial t} = a_p K_{gl} \left(c_A - \langle c_A \rangle \right) \tag{2.13}$$

The relationship between the solid density (ρ_s) of the crystal, the apparent density (ρ_a) of the pellet and the bulk density (ρ_b) of the bed through the particle porosity (ε_p) and the bed void fraction (ε) is as follows:

$$(1 - \varepsilon_p)\rho_s = \rho_a \tag{2.14a}$$

$$(1 - \varepsilon)\rho_a = \rho_b \tag{2.14b}$$

It is worth noting that Silva and Rodrigues [66] used cylindrical pellets in their experiments so that the specific area (a_p) in equation 2.13 is no longer $3/R_p$.

2.5d Reaction Mechanism

Hosten and Froment [26] studied the kinetics of *n*-pentane isomerization on a dual function Pt/Al_2O_3 reforming catalyst, carried out in the presence of hydrogen. This reaction involves a three-step sequence consisting of dehydrogenation, isomerization, and

hydrogenation. The dehydrogenation and hydrogenation steps occur on platinum sites, represented by l; and the isomerization step occurs on the acidic alumina sites, represented by σ. Each of these steps involves adsorption, surface reaction, and desorption. At steady state all of the individual reactions in the following mechanism are at equilibrium except the surface reaction in the isomerization step, which is assumed rate limiting:

Dehydrogenation:

$$A + l \leftrightarrow Al \qquad K_1 = c_{Al}/P_A \cdot c_l$$
$$Al + l \leftrightarrow Ml + H_2l \qquad K_2 = c_{Ml} \cdot c_{H_2l}/c_{Al} \cdot c_l$$
$$H_2l \leftrightarrow H_2 + l \qquad K_3 = P_{H_2} \cdot c_l/c_{H_2l}$$
$$Ml \leftrightarrow M + l \qquad K_4 = P_M \cdot c_l/c_{Ml}$$

Isomerization:

$$M + \sigma \leftrightarrow M\sigma \qquad K_5 = c_{M\sigma}/P_M \cdot c_\sigma$$
$$M\sigma \leftrightarrow N\sigma \qquad K_6 = (c_{N\sigma})_{eq}/(c_{M\sigma})_{eq}$$
$$N\sigma \leftrightarrow N + \sigma \qquad K_7 = P_N \cdot c_\sigma/c_{N\sigma}$$

Hydrogenation:

$$N + l \leftrightarrow Nl \qquad K_8 = c_{Nl}/P_N \cdot c_l$$
$$H_2 + l \leftrightarrow H_2l \qquad K_9 = c_{H_2l}/P_{H_2} \cdot c_l$$
$$Nl + H_2l \leftrightarrow Bl + l \qquad K_{10} = c_{Bl} \cdot c_l/c_{Nl} \cdot c_{H_2l}$$
$$Bl \leftrightarrow B + l \qquad K_{11} = P_B \cdot c_l/c_{Bl}$$

According to the above reaction scheme, *n*-pentane dehydrogenates on the metal site to form *n*-pentene, which undergoes isomerization reaction over the acid site to form isopentene. Hydrogenation of the iso-olefin takes place over the metal site to form the product isopentane.

The overall reaction rate is given by:

$$r = \frac{kK_5\left(P_M - \frac{P_N}{K_5K_6K_7}\right)}{1 + K_5P_M + \frac{1}{K_7}P_N} \tag{2.15}$$

Under steady state conditions, *n*-pentene is in equilibrium with *n*-pentane/hydrogen and isopentene with isopentane/hydrogen. When the equilibrium relations are used, the partial pressures of the pentenes can be expressed in terms of the partial pressures of the pentanes and hydrogen, leading to:

$$r = \frac{kK_5K_D\left(P_A - \frac{P_B}{K}\right)}{P_{H_2} + K_5K_DP_A + \frac{1}{K_7K_H}P_B} \tag{2.16}$$

where $K_D = K_1K_2K_3K_4$ is the equilibrium constant for dehydrogenation, and $K_H = K_8K_9K_{10}K_{11}$ is the equilibrium constant for hydrogenation. The equilibrium reaction rate constant (K) for the overall reaction is determined from thermodynamic data and is related to the change in Gibbs free energy [16]. This equation type is often termed Langmuir-Hinshelwood or Hougen-Watson rate equation.

In this study, 0.5 wt% Pd/H-faujasite type Y catalyst is used because catalyst deactivation is assumed negligible when modeling the process. Weisz [82] proposed the following mechanism for hydroisomerization of *n*-paraffins on bifunctional catalysts:

$$n-C_5 \xleftrightarrow{-H_2} n-\text{pentene} \xleftrightarrow{+H^+} n-C_5^+ \leftrightarrow i-C_5^+ \xleftrightarrow{-H^+} \text{isopentene} \xleftrightarrow{+H_2} i-C_5$$

Under this mechanism, olefin is formed at the metallic site by dehydrogenation of the normal paraffin feed and is then adsorbed at an acidic site to form a carbonium ion, *n*-

C_5^+, which undergoes skeletal rearrangement. The resulting isocarbonium ion, i-C_5^+, is converted to an iso-olefin, which is then hydrogenated at the metallic site and desorbed. Different authors have proved that the skeletal isomerization of the reactive intermediate (that is, the carbonium ion) is the rate-controlling step [4,68,80]. Spivey and Bryant [68] adopted the latter mechanism while determining the rate law.

2.5e Kinetic Model

As noted earlier the general Langmuir-Hinshelwood model describing reactions of gases on solid catalysts is given by:

$$\text{rate} = \frac{[\text{kinetic term}][\text{potential term}]}{[\text{adsorption term}]} \tag{2.17}$$

The kinetic term includes the true surface reaction rate constant as well as constants characterizing the surface of the catalyst and in some cases adsorption constants. The potential term for the first-order elementary reaction $A \leftrightarrow B$ has the form $P_A - P_B/K$. The adsorption term has the form $(1+\sum K_i P_i)^n$, where n is the number of active catalyst sites involved in the reaction, usually 1 or 2. The exact form of the adsorption term may change depending on the rate-limiting step for a given reaction.

Spivey and Bryant [68] assumed a first order reversible rate of reaction for the hydroisomerization of n-pentane into iso-pentane, with the isomerization step being the rate-limiting step:

$$-r_A = k(c_A - c_B/K) \tag{2.18}$$

Here, the rate constant (k) is a lumped term including both the adsorption term and the effectiveness factor (Ω).

Assuming that Langmuir adsorption isotherms may be applied to the model, the first-order rate constant may be expressed as:

$$k = \bar{k} \Big/ \left[1 + \sum K_i P_i\right]^n \tag{2.19}$$

where

$$\bar{k} = k_0 \lambda \prod_i K_i \tag{2.20}$$

If the adsorption constants for the normal and iso- pentanes are approximately equal, equation 2.19 may be rewritten as:

$$k^{-1/n} = \bar{k}^{-1/n} \left[1 + P_t \frac{\tilde{R} K_{H_2} + K_{HC}}{1 + \tilde{R}}\right] \tag{2.21}$$

Statistical analysis revealed the isomerization of the reactive intermediate to be rate controlling and that the reaction follows a dual-site mechanism ($n = 2$) [68]. It should be noted, however, that Fogler [16] and Hosten and Froment [26] reported a single-site mechanism for the isomerization of the reactive intermediate, that is, $n = 1$.

Spivey and Bryant [68] reported values of reaction rate constant, k, at various pressures for hydrogen/hydrocarbon mole ratio ($\tilde{R}$) of 10/1. Equation 2.21 could be used to correct the k value for the present study, which employs a mole ratio of 2.5/1 instead. The value of $\bar{k}$ is thus required which can be easily determined by extrapolating the $k^{-1/n}$-P_t plot to zero pressure (P_t). In fact, it approximately equals 1 cm^3/g-s at 514 K by

this method. However, it should be kept in mind that the system does not follow equation 2.21 at low hydrogen partial pressures because coking takes place then.

The value of K_{HC}, the adsorption equilibrium constant for pentanes, is also required before equation 2.21 could be used. If the properties of the adsorbent (5A zeolite) and the catalyst (Y-zeolite) are assumed the same, one may be tempted to use the value of K_{ads} in equation 2.4 for K_{HC}. A close examination reveals some discrepancies. It was already pointed out that an adsorbed molecule occupies five active sites on a 5A zeolite [65] whereas just two acid sites for reaction on a faujasite [68]. The dilemma may be resolved by realizing that the hydrocarbons undergo physisorption in the former case [58] whereas they undergo chemisorption in the latter case [16].

Faujasite, like 5A zeolite, is a bidisperse porous particle containing both macropores and micropores. The micropores are about the size of the molecules themselves. The hydrocarbons diffusing through them immediately come under the electrostatic forces of the solid and are thus considered to be in the adsorbed phase [29], which is physisorption. The molecules shall further have to chemisorb over the metal and acid sites to undergo the isomerization reaction. So even though if the physical parameters such as K_{ads} and n in equation 2.4 are assumed the same for both the zeolites, K_{HC} still needs to be determined in order to correct the reaction rate constant k.

Voorhies and Bryant [80] yet report that the rate constant is a function of the total pressure (P_t) and not of the individual partial pressures. This finding is consistent with equation 2.19 only if the adsorption equilibrium constants for hydrogen, normal pentane and isopentane are approximately equal.

In this case:

$$k = \frac{\bar{k}}{\left(1+\sum K_i P_i\right)^n} = \frac{\bar{k}}{\left(1+K_0 \sum P_i\right)^n} = \frac{\bar{k}}{\left(1+K_0 P_t\right)^n} \tag{2.22}$$

Thus, the rate constant is assumed to be independent of the hydrogen/hydrocarbon ratio in the present study.

2.5f Unsteady State Catalysis

The rate expression 2.16 assumes that the reactive intermediates in the rate-limiting step are in equilibrium with their gas phase counterparts. This is the case for steady state conditions only. For unsteady state situations, no such explicit expression in terms of gas phase concentrations is possible [18]. However, the catalyst state can be considered as quasi-steady with respect to that of the reaction medium, that is a kinetic reaction model obtained under steady state conditions is applied [9,19].

Spivey and Bryant [68] used the rate expression 2.18 to model a fixed bed reactor under steady state conditions. The expression incorporates bulk gas phase concentrations that are in equilibrium with the solid phase. This requires use of the overall effectiveness factor (Ω). If the expression utilized the concentration at the catalyst surface instead, the internal effectiveness factor (η) would have been used. The effectiveness factors are defined as:

$$\eta = \frac{\text{actual overall rate of reaction}}{\text{rate of reaction that would result if entire interior surface were exposed to the external pellet surface conditions, } c_{pA}^{s}} \tag{2.23}$$

$$\Omega = \frac{\text{actual overall rate of reaction}}{\text{rate of reaction that would result if entire surface were exposed to the bulk concentration, } c_A} \tag{2.24}$$

Since SMBR operates under unsteady state conditions, the bulk gas phase concentration cannot be assumed to be in equilibrium with the solid phase and thus the rate law needs to be modified. It seems more appropriate to use the macropore concentration instead, as it is assumed to be in equilibrium with the adsorbed phase concentration even at unsteady state conditions. So if somehow the overall effectiveness factor could be extracted from the lumped rate constant k, the following expression could be used:

$$-r_A = k'\left(\langle c_A \rangle - \frac{\langle c_B \rangle}{K}\right) \tag{2.25a}$$

where $k' = \dfrac{k}{\Omega}$ (2.25b)

Moreover, the term $-r_A$ is the average rate of reaction over the catalyst particle:

$$\begin{aligned} -r_A &= \frac{1}{V_p}\int k'\left(c_{pA} - \frac{c_{pB}}{K}\right)\mathrm{d}V_p \\ &= k'\left(\langle c_A \rangle - \frac{\langle c_B \rangle}{K}\right) \end{aligned} \tag{2.26}$$

The above treatment assumes that the adsorption term $(1+\sum K_i P_i)^2$ in the rate constant k is not affected by mass transfer limitations in and around the catalyst. This is a reasonable assumption taking into account the results obtained by Voorhies and Bryant [80]. Fogler [16] neglects the adsorption term altogether while deriving expressions for the effectiveness factors because it anyhow approaches one at high temperatures.

Furthermore, it was found that the overall effectiveness factor was very close to unity so that the rate constant k does not need to be corrected. Details of the calculations are shown in Appendix A.2. The rate law thus takes the following form for modeling the SMBR:

$$-r_A = k\left(\langle c_A \rangle - \frac{\langle c_B \rangle}{K}\right) \tag{2.27}$$

2.5g Unsteady State Reactor Modeling

Froment [18] classifies the modeling of transient behavior of reactors into two broad categories: pseudo-homogeneous and heterogeneous models. An isothermal pseudo-homogeneous model is:

$$D_L \frac{\partial^2 c_A}{\partial z^2} - u\frac{\partial c_A}{\partial z} + \left(\frac{1-\varepsilon}{\varepsilon}\right)\rho_a r_A = \frac{\partial c_A}{\partial t} \tag{2.28}$$

with the boundary conditions

$$-D_L \frac{\partial c_A}{\partial z} = u\left(c_{Af} - c_A\right); \qquad z = 0 \tag{2.29a}$$

$$\frac{\partial c_A}{\partial z} = 0; \qquad z = L \tag{2.29b}$$

and the initial condition $c_A = c_{A0}$ at $t = 0$. A similar pseudo-homogeneous model was used by Al-Juhani [1] in the modeling of the pressure swing adsorption-reactor.

For very rapid reactions with an important heat effect, it may be essential to distinguish between conditions in the fluid and on the catalyst surface or even inside the

catalyst so that a heterogeneous model should then be used [19]. An isothermal one-dimensional heterogeneous model is given below:

Gas phase:

$$\frac{\partial c_A}{\partial t} = -u\frac{\partial c_A}{\partial z} - \left(\frac{1-\varepsilon}{\varepsilon}\right)a_p k_e\left(c_A - c_{pA}^s\right) \tag{2.30}$$

Solid phase:

$$\varepsilon_p \frac{\partial c_{pA}}{\partial t} = a_p k_e\left(c_A - c_{pA}^s\right) + \eta\rho_a r_A \tag{2.31}$$

with the boundary condition $c_A = c_{Af}$ at $z = 0$ and the initial condition $c_A = c_{pA} = c_{A0}$ at $t = 0$.

The model accounts for resistance to mass transfer between the gas and the solid phase and to mass transfer inside the catalyst. It, however, does not account for the axial dispersion. The effectiveness factor η has to be obtained from the integration, in each grid point in the z-direction and for each time, of the following equation:

$$\varepsilon_p \frac{D_p}{r^2}\frac{\mathrm{d}}{\mathrm{d}r}\left[r^2\frac{\mathrm{d}c_{pA}}{\mathrm{d}r}\right] + \rho_a r_A\left(c_{pA}\right) = 0 \tag{2.32}$$

Spherical geometry is assumed in the above equation.

The boundary conditions are:

$$\frac{\mathrm{d}c_{pA}}{\mathrm{d}r} = 0; \qquad r = 0 \tag{2.33a}$$

$$\varepsilon_p D_p \frac{\mathrm{d}c_{pA}}{\mathrm{d}r} = k_e\left(c_A - c_{pA}\right); \qquad r = R_p \tag{2.33b}$$

Froment and Bischoff [19] on the other extreme simplify the solid phase balance by assuming the macropore concentration all over the particle to be equal to the surface concentration (c_{pA}^{s}) so that the effectiveness factor (η) equals unity:

$$\varepsilon_p \frac{\partial c_{pA}^{s}}{\partial t} = a_p k_e \left(c_A - c_{pA}^{s}\right) + \rho_a r_A \tag{2.34}$$

The former heterogeneous model (equations 2.30 to 2.33) is too complicated as it even takes into consideration the intraparticle gradients whereas the latter (equation 2.30 in conjunction with equation 2.34) is too simplistic as it assumes the entire particle to have the same surface concentration. In this study, however, a lumping procedure is applied in order to avoid the complexities involved with the former model and the errors associated with the latter.

The lumped model for a catalyst bed similar to the previously derived model for the adsorbent bed is as follows:

$$\varepsilon_p \frac{\partial \langle c_A \rangle}{\partial t} = a_p K_{gl} \left(c_A - \langle c_A \rangle\right) - \rho_a \frac{\partial \langle q_A \rangle}{\partial t} + \rho_a r_A \left(\langle c_A \rangle\right) \tag{2.35}$$

The solid phase models (equations 2.31 and 2.34) take into consideration the accumulation in the macropores but not in the solid phase. It is thus assumed that whatever amount of species adsorbs into the solid reacts, that is the catalyst is at a quasi-steady state, an assumption used to derive the rate law. Applying the same assumption to the lumped model, equation 2.35 becomes:

$$\varepsilon_p \frac{\partial \langle c_A \rangle}{\partial t} = a_p K_{gl} \left(c_A - \langle c_A \rangle\right) + \rho_a r_A \left(\langle c_A \rangle\right) \tag{2.36}$$

where the rate law is given in equation 2.27.

In order to be consistent with model equation 2.13 of 5A zeolite adsorbent, accumulation in the solid phase shall be taken into consideration in this study whereas accumulation in macropores shall be neglected. The lumped model (equation 2.35) then takes the form:

$$\rho_a \frac{\partial \langle q_A \rangle}{\partial t} = a_p K_{gl}\left(c_A - \langle c_A \rangle\right) + \rho_a r_A\left(\langle c_A \rangle\right) \tag{2.37}$$

This model takes into account the fact that not all of the reactant that enters the catalyst micropores reacts. Only the amount that further chemisorbs over the reactive sites contributes to the reaction rate term.

Calculation of the intrapore mass transfer resistance revealed that significant configurational diffusion resistance, which occurs when the pore diameter approaches the diameter of the diffusing molecule, could be expected in the faujasite catalyst [69]. In order to study this effect, catalysts of varying pore sizes are needed. Studies on similar catalysts carried out by Bryant [8] and Hopper [25] examined the effect of catalyst particle size on the observed rate constant. No variation was observed over a tenfold change in particle size, indicating constant intra-particle diffusion resistance that need not be included in examining the hydroisomerization. Voorhies and Bryant [80] raised concerns that this in no way means that the micropore diffusion resistance is not significant. However, they could not systematically investigate diffusion inside these micropores due to the lack of crystals with different particle size ranges.

The catalyst particles cannot be used in their original crushed form when incorporated in a fixed bed reactor. Otherwise, the pressure drop across the packed bed shall be very high. They need to be pelletized to the size of the adsorbent pellets. Since

micropore diffusion in 5A zeolite is not the controlling mechanism and because the size of micropores in faujasite catalyst is even greater, it can be safely assumed that micropore diffusion will also not offer major resistance inside the catalyst pellet. Thus, macropore concentration shall be in equilibrium with the adsorbed phase concentration by an adsorption equilibrium model that needs to be determined for the type Y faujasite. However in this study the same Nitta *et al.* [44] model shall be used for the catalyst as well. Although the two phases are at equilibrium, the use of the rate law (equation 2.27) in the lumped model (equation 2.37) is still an approximation because the solid phase concentration is at an unsteady state. Meurer *et al.* [41] developed a catalyst phase model similar to equation 2.37. However, they incorporated the bulk phase concentrations in the rate law instead.

NOMENCLATURE

a_p	specific area of adsorbent or catalyst [m^{-1}]
c_{Af}	concentration of component A in the feed [mol/m^3]
c_{A0}	initial concentration of component A [mol/m^3]
c_i	concentration of species i in bulk phase [mol/m^3]
c_{il}	adsorbed phase concentration of species i over platinum surface [mol/kg]
c_l	concentration of vacant sites over platinum surface [mol/kg]
c_{pi}	concentration of component i in macropores [mol/m^3]
c_σ	concentration of vacant acidic sites [mol/kg]
$c_{i\sigma}$	adsorbed phase concentration of species i over acidic surface [mol/kg]
$\langle c_i \rangle$	average concentration of sorbate i in macropores [mol/m^3]
D_c	micropore diffusivity [m^2/s]
D_L	axial mass dispersion coefficient [m^2/s]
D_p	macropore diffusivity [m^2/s]
H	Henry's law coefficient [kg/kg.Pa]
H_{ad}	dimensionless Henry's law coefficient [$= \rho_s RTH / M_w$]
k	forward reaction rate constant for rate limiting step or general reaction rate constant for the rate law (2.18) [m^3/kg cat. s]
k_e	external mass-transfer coefficient [m/s]
k_i	internal mass-transfer coefficient [m/s]
k_0	surface reaction rate constant
k'	general reaction rate constant after extracting Ω [m^3/kg cat. s]
$\bar{k}$	general surface reaction rate term [m^3/kg cat. s]
K	equilibrium reaction rate constant [-] or capacity factor [$= (1-\varepsilon_p) H_{ad} / \varepsilon_p$]
K_{ads}	adsorption equilibrium constant in Nitta *et al.* model [Pa^{-1}]
K_{gl}	global mass-transfer coefficient [m/s]
K_i	adsorption equilibrium constant for component i [Pa^{-1}]
K_y	equilibrium rate constant for reaction y

K_0	mean adsorption equilibrium constant for hydrogen, *n*-pentane and isopentane [Pa^{-1}]
L	length of column [m]
L_j	length of section *j* in true countercurrent unit [m]
M_w	molecular mass of sorbate [kg/mol]
n	coefficient of Nitta *et al.* isotherm [-] or number of acid sites involved in reaction
n_j	number of beds in section *j*
P_i	partial pressure of sorbate *i* [Pa]
P_t	total pressure [Pa]
q	adsorbed phase concentration [mol/kg]
q_A	adsorbed phase concentration of component *A* [mol/kg]
q_{max}	maximum adsorbed-phase concentration [mol/kg]
$\langle q_A \rangle$	average adsorbed-phase concentration of component *A* [mol/kg]
r	radial coordinate [m] or rate of reaction of *n*-pentane [mol/kg cat. s]
$-r_A$	rate of reaction of component *A* [mol/kg cat. s]
r_c	crystal radius [m]
R	ideal gas law constant [J/mol.K]
R_p	pellet radius [m]
$\widetilde{R}$	hydrogen/hydrocarbon mole ratio [-]
t	time [s]
T	temperature [K]
u	interstitial velocity [m/s]
u_s	solid velocity in true countercurrent unit [m/s]
V_p	pellet volume [m^3]
z	axial coordinate of column [m]

Greek Letters

ε	bed void fraction [-]
ε_p	pellet porosity [-]
η	internal effectiveness factor [-]
λ	surface concentration of active sites
θ	fractional coverage of adsorbent [-]
ρ_a	apparent density of adsorbent or catalyst [kg/m^3]
ρ_b	bulk density of adsorbent bed [kg/m^3]
ρ_s	solid density of adsorbent crystals [kg/m^3]
τ_s	switch time [s]
Ω	overall effectiveness factor [-]

Subscripts

A	*n*-pentane
B	isopentane
HC	hydrocarbons
M	*n*-pentene
N	isopentene

Superscript

s	surface conditions

CHAPTER 3

MODELING AND SIMULATION OF THE BASE CASE

The Simulated Moving Bed Reactor (SMBR) consists of several beds connected in series. Thus, in order to get an in-depth knowledge of the process, a single adsorbent bed is first considered. A fixed bed unsteady-state reactor is also studied using both the pseudo-homogeneous and the heterogeneous models. Later, an integrated reactor-adsorber system is simulated to examine the combined effect of both, which is an intermediate step between simulating the fixed beds individually and the entire SMBR process. The feed to the system consists of normal and iso- pentanes together with hydrogen.

3.1 MODEL ASSUMPTIONS

The following assumptions are made in modeling the SMBR:

1) The gas is ideal. Although the operating pressure is maintained at 15 bar, the compressibility factor turns out to be close to unity using the Redlich-Kwong equation of state. This is because the operating temperature is high and so is the hydrogen content of the feed.

2) The frictional pressure drop through the beds is neglected as the ΔP calculated via Ergun equation is negligibly small.

3) The main resistances to mass transfer are external fluid film resistance and macropore diffusion in series [65], which can be combined in a global resistance according to a lumped model [43].

4) The adsorption equilibrium is described by the Nitta *et al.* [44] model.

5) Variation in fluid velocity along the bed is accounted for.

6) The flow pattern is described by the axial dispersed plug flow model.

7) The boundary conditions for the energy balance are written assuming the heat-mass transfer analogy for a dispersed plug flow system.

8) The temperature dependency of adsorption equilibrium constant follows a vant Hoff equation: $K_{ads} = K_0 \exp[(-\Delta H_{ads})/RT]$.

9) Intraparticle temperature gradients are neglected, as the effective thermal conductivity of commercial adsorbents is relatively high [58,83].

10) Thermal equilibrium exists between the fluid and the solid particles. If similarity between heat and mass transfer is assumed the calculated difference in temperature between solid and gas is small showing that the effect of heat transfer resistance is minor [58].

11) The temperature dependence of the gas and solid properties is neglected.

12) The thermal capacitance of the wall is neglected. This introduces error in the adiabatic operation.

13) The heat of reaction is neglected [55-57,68].

14) Heat effects due to sorption process over the catalyst are neglected in the heterogeneous model because of reaction stoichiometry. At steady state, the

number of moles of *n*-pentane adsorbed is equal to the number of moles of isopentane desorbed. Therefore, the energy released by adsorption is compensated by the energy consumed due to desorption. This, of course, introduces some error in the dynamic model.

15) The rate law derived under steady state conditions, $-r_A = k\left(\langle c_A \rangle - \langle c_B \rangle / K\right)$, is used in the unsteady state heterogeneous reactor model. Moreover in the derivation of the rate law, isomerization of the reactive intermediate ($n-C_5^+$) is assumed to be the rate-controlling step.

16) Physical properties of type Y faujasite and 5A zeolite are assumed the same.

17) Deactivation of the catalyst is negligible. This is the case when partial pressure of hydrogen is sufficiently high.

18) Hydrocracking products are negligible [12].

3.2 MODEL EQUATIONS

The model equations for fluid and solid phase balances of *n*-pentane (*A*), isopentane (*B*) and inert hydrogen (*I*) in the adsorber and reactor are as follows.

3.2.1 Adsorbent Bed

The fluid phase material balance for *n*-pentane while realizing that it only is adsorbed over zeolite 5A is:

$$\varepsilon \frac{\partial}{\partial t}(c_T y_A) = \varepsilon D_L \frac{\partial}{\partial z}\left(c_T \frac{\partial y_A}{\partial z}\right) - \frac{\partial}{\partial z}(F y_A) - (1-\varepsilon)\rho_a \frac{\partial \langle q_A \rangle}{\partial t} \tag{3.1a}$$

The Danckwert's boundary conditions are:

$$-\varepsilon D_L c_T \frac{\partial y_A}{\partial z} = F\left(y_{Af} - y_A\right) \qquad z = 0 \qquad (3.1b)$$

$$\frac{\partial y_A}{\partial z} = 0 \qquad z = L_1 \qquad (3.1c)$$

The material balance for isopentane is:

$$\varepsilon \frac{\partial}{\partial t}\left(c_T y_B\right) = \varepsilon D_L \frac{\partial}{\partial z}\left(c_T \frac{\partial y_B}{\partial z}\right) - \frac{\partial}{\partial z}\left(F y_B\right) \qquad (3.2a)$$

The Danckwert's boundary conditions are:

$$-\varepsilon D_L c_T \frac{\partial y_B}{\partial z} = F\left(y_{Bf} - y_B\right) \qquad z = 0 \qquad (3.2b)$$

$$\frac{\partial y_B}{\partial z} = 0 \qquad z = L_1 \qquad (3.2c)$$

The material balance for the inert hydrogen is:

$$\varepsilon \frac{\partial}{\partial t}\left(c_T y_I\right) = \varepsilon D_L \frac{\partial}{\partial z}\left(c_T \frac{\partial y_I}{\partial z}\right) - \frac{\partial}{\partial z}\left(F y_I\right) \qquad (3.3a)$$

The Danckwert's boundary conditions are:

$$-\varepsilon D_L c_T \frac{\partial y_I}{\partial z} = F\left(y_{If} - y_I\right) \qquad z = 0 \qquad (3.3b)$$

$$\frac{\partial y_I}{\partial z} = 0 \qquad z = L_1 \qquad (3.3c)$$

The overall fluid phase material balance is obtained by summing equations 3.1a, 3.2a and 3.3a.

$$\varepsilon \frac{\partial c_T}{\partial t} + \frac{\partial F}{\partial z} + (1-\varepsilon)\rho_a \frac{\partial \langle q_A \rangle}{\partial t} = 0 \qquad (3.4a)$$

The boundary condition for flow rate F is:

$$F = F_f \qquad z = 0 \tag{3.4b}$$

The material balance for inert hydrogen (equation 3.3) has become redundant with the introduction of the overall material balance and is thus discarded. The adsorbed phase material balance for n-pentane is:

$$\rho_a \frac{\partial \langle q_A \rangle}{\partial t} = a_p K_{gl} c_T \left(y_A - \langle y_A \rangle \right) \tag{3.5}$$

The macropore concentration is calculated using the following adsorption equilibrium isotherm model proposed by Nitta *et al.* [44]:

$$\langle y_A \rangle P = \frac{1}{K_{ads}(T)} \frac{\theta_A}{(1-\theta_A)^5} \tag{3.6a}$$

where K_{ads} is the adsorption equilibrium constant:

$$K_{ads}(T) = K_0 \exp\left(-\Delta H_{ads} / RT \right) \tag{3.6b}$$

The energy balance is:

$$\begin{aligned} \left(\varepsilon C_{pg} c_T + (1-\varepsilon) C_{ps} \rho_a \right) \frac{\partial T}{\partial t} &= K_L \frac{\partial^2 T}{\partial z^2} - C_{pg} F \frac{\partial T}{\partial z} \\ &\quad + (-\Delta H_{ads})(1-\varepsilon) \rho_a \frac{\partial \langle q_A \rangle}{\partial t} - a_c h_w (T - T_w) \end{aligned} \tag{3.7a}$$

where a_c is the specific area of the column:

$$a_c = 4 / d_c \tag{3.7b}$$

The Danckwert's boundary conditions are:

$$-K_L \frac{\partial T}{\partial z} = C_{pg} F(T_f - T) \qquad z = 0 \qquad (3.7c)$$

$$\frac{\partial T}{\partial z} = 0 \qquad z = L_1 \qquad (3.7d)$$

For initially clean adsorbent and gas phases with temperature equal to that at the entrance, the initial conditions are:

$$y_A(z, t = 0) = 0 \qquad (3.8a)$$

$$y_B(z, t = 0) = 0 \qquad (3.8b)$$

$$\langle q_A \rangle (z, t = 0) = 0 \qquad (3.8c)$$

$$T(z, t = 0) = T_f \qquad (3.8d)$$

3.2.2 Catalyst Bed

The unsteady state reactor modeling is divided into two broad categories, namely the pseudo-homogeneous model and the heterogeneous model.

3.2.2a Pseudo-Homogeneous Model

The pseudo-homogeneous model assumes the catalyst bed to be at steady state at all times so that only the fluid phase balance needs to be considered. The material balance for *n*-pentane is:

$$\varepsilon \frac{\partial}{\partial t}(c_T y_A) = \varepsilon D_L \frac{\partial}{\partial z}\left(c_T \frac{\partial y_A}{\partial z}\right) - \frac{\partial}{\partial z}(F y_A) - (1 - \varepsilon)\rho_a k c_T \left(y_A - \frac{y_B}{K}\right) \qquad (3.9a)$$

The Danckwert's boundary conditions are:

$$-\varepsilon D_L c_T \frac{\partial y_A}{\partial z} = F\left(y_{Af} - y_A\right) \qquad z = 0 \qquad (3.9b)$$

$$\frac{\partial y_A}{\partial z} = 0 \qquad z = L_2 \qquad (3.9c)$$

The material balance for isopentane is:

$$\varepsilon \frac{\partial}{\partial t}\left(c_T y_B\right) = \varepsilon D_L \frac{\partial}{\partial z}\left(c_T \frac{\partial y_B}{\partial z}\right) - \frac{\partial}{\partial z}\left(F y_B\right) + \left(1-\varepsilon\right)\rho_a k c_T\left(y_A - \frac{y_B}{K}\right) \qquad (3.10a)$$

The Danckwert's boundary conditions are:

$$-\varepsilon D_L c_T \frac{\partial y_B}{\partial z} = F\left(y_{Bf} - y_B\right) \qquad z = 0 \qquad (3.10b)$$

$$\frac{\partial y_B}{\partial z} = 0 \qquad z = L_2 \qquad (3.10c)$$

The material balance for the inert hydrogen is:

$$\varepsilon \frac{\partial}{\partial t}\left(c_T y_I\right) = \varepsilon D_L \frac{\partial}{\partial z}\left(c_T \frac{\partial y_I}{\partial z}\right) - \frac{\partial}{\partial z}\left(F y_I\right) \qquad (3.11a)$$

The Danckwert's boundary conditions are:

$$-\varepsilon D_L c_T \frac{\partial y_I}{\partial z} = F\left(y_{If} - y_I\right) \qquad z = 0 \qquad (3.11b)$$

$$\frac{\partial y_I}{\partial z} = 0 \qquad z = L_2 \qquad (3.11c)$$

The overall material balance is obtained by summing equations 3.9a, 3.10a and 3.11a:

$$\varepsilon \frac{\partial c_T}{\partial t} + \frac{\partial F}{\partial z} = 0 \qquad (3.12a)$$

The boundary condition for flow rate F is:

$$F = F_f \qquad z = 0 \tag{3.12b}$$

The material balance for inert hydrogen (equation 3.11) has become redundant with the introduction of the overall material balance and is thus discarded.

The energy balance for pseudo-homogeneous model of the adiabatic reactor is:

$$\varepsilon C_{pg} c_T \frac{\partial T}{\partial t} = K_L \frac{\partial^2 T}{\partial z^2} - C_{pg} F \frac{\partial T}{\partial z} \tag{3.13a}$$

The Danckwert's boundary conditions are:

$$-K_L \frac{\partial T}{\partial z} = C_{pg} F (T_f - T) \qquad z = 0 \tag{3.13b}$$

$$\frac{\partial T}{\partial z} = 0 \qquad z = L_2 \tag{3.13c}$$

For initially clean gas with temperature equal to that at the entrance, the initial conditions are:

$$y_A(z, t = 0) = 0 \tag{3.14a}$$

$$y_B(z, t = 0) = 0 \tag{3.14b}$$

$$T(z, t = 0) = T_f \tag{3.14c}$$

3.2.2b Heterogeneous Model

The heterogeneous model takes into account the changes that take place both in the fluid phase and that over the catalyst.

The fluid phase material balance for *n*-pentane is:

$$\varepsilon \frac{\partial}{\partial t}(c_T y_A) = \varepsilon D_L \frac{\partial}{\partial z}\left(c_T \frac{\partial y_A}{\partial z}\right) - \frac{\partial}{\partial z}(F y_A) - (1-\varepsilon) a_p K_{gl} c_T (y_A - \langle y_A \rangle) \tag{3.15a}$$

The Danckwert's boundary conditions are:

$$-\varepsilon D_L c_T \frac{\partial y_A}{\partial z} = F(y_{Af} - y_A) \qquad z = 0 \tag{3.15b}$$

$$\frac{\partial y_A}{\partial z} = 0 \qquad z = L_2 \tag{3.15c}$$

The fluid phase material balance for isopentane while noting that it also is adsorbed over the catalyst is:

$$\varepsilon \frac{\partial}{\partial t}(c_T y_B) = \varepsilon D_L \frac{\partial}{\partial z}\left(c_T \frac{\partial y_B}{\partial z}\right) - \frac{\partial}{\partial z}(F y_B) - (1-\varepsilon) a_p K_{gl} c_T (y_B - \langle y_B \rangle) \tag{3.16a}$$

The Danckwert's boundary conditions are:

$$-\varepsilon D_L c_T \frac{\partial y_B}{\partial z} = F(y_{Bf} - y_B) \qquad z = 0 \tag{3.16b}$$

$$\frac{\partial y_B}{\partial z} = 0 \qquad z = L_2 \tag{3.16c}$$

The material balance for the inert hydrogen is:

$$\varepsilon \frac{\partial}{\partial t}(c_T y_I) = \varepsilon D_L \frac{\partial}{\partial z}\left(c_T \frac{\partial y_I}{\partial z}\right) - \frac{\partial}{\partial z}(F y_I) \tag{3.17a}$$

The Danckwert's boundary conditions are:

$$-\varepsilon D_L c_T \frac{\partial y_I}{\partial z} = F(y_{If} - y_I) \qquad z = 0 \tag{3.17b}$$

$$\frac{\partial y_I}{\partial z} = 0 \qquad z = L_2 \tag{3.17c}$$

The overall fluid phase material balance is obtained by summing equations 3.15a, 3.16a and 3.17a:

$$\varepsilon \frac{\partial c_T}{\partial t} + \frac{\partial F}{\partial z} + (1-\varepsilon) a_p K_{gl} c_T \left(y_A - \langle y_A \rangle + y_B - \langle y_B \rangle \right) = 0 \tag{3.18a}$$

The boundary condition for flow rate F is:

$$F = F_f \qquad z = 0 \tag{3.18b}$$

The material balance for inert hydrogen (equation 3.17) has become redundant with the introduction of the overall material balance and is thus discarded.

For initially clean gas phase, the initial conditions are:

$$y_A(z, t=0) = 0 \tag{3.19a}$$

$$y_B(z, t=0) = 0 \tag{3.19b}$$

In order to model the solid phase, two approaches may be followed thus leading to two different sets of equations. The first one, which is often used in the literature, assumes that whatever reactant adsorbs onto the catalyst is reacted. The material balance for *n*-pentane over the catalyst thus becomes:

$$\varepsilon_p c_T \frac{\partial \langle y_A \rangle}{\partial t} = a_p K_{gl} c_T \left(y_A - \langle y_A \rangle \right) - \rho_a k c_T \left(\langle y_A \rangle - \frac{\langle y_B \rangle}{K} \right) \tag{3.20}$$

The material balance for isopentane over the catalyst is:

$$\varepsilon_p c_T \frac{\partial \langle y_B \rangle}{\partial t} = a_p K_{gl} c_T \left(y_B - \langle y_B \rangle \right) + \rho_a k c_T \left(\langle y_A \rangle - \frac{\langle y_B \rangle}{K} \right) \tag{3.21}$$

For initially clean catalyst, the initial conditions are:

$$\langle y_A \rangle (z, t=0) = 0 \tag{3.22a}$$

$$\langle y_B \rangle (z, t = 0) = 0 \tag{3.22b}$$

The second approach is developed in this study to be consistent with the adsorbent bed model, which is also a bidisperse system. In this approach, the accumulation in the micropores is taken into account so that not all of the reactant that adsorbs onto the catalyst reacts.

The adsorbed phase material balance for *n*-pentane is:

$$\rho_a \frac{\partial \langle q_A \rangle}{\partial t} = a_p K_{gl} c_T \left(y_A - \langle y_A \rangle \right) - \rho_a k c_T \left(\langle y_A \rangle - \frac{\langle y_B \rangle}{K} \right) \tag{3.23}$$

The adsorbed phase material balance for isopentane is:

$$\rho_a \frac{\partial \langle q_B \rangle}{\partial t} = a_p K_{gl} c_T \left(y_B - \langle y_B \rangle \right) + \rho_a k c_T \left(\langle y_A \rangle - \frac{\langle y_B \rangle}{K} \right) \tag{3.24}$$

The macropore concentration of *n*-pentane is calculated using the Nitta *et al.* [44] model for multicomponent system:

$$\langle y_A \rangle P = \frac{1}{K_{ads}(T)} \frac{\theta_A}{(1 - \theta_A - \theta_B)^5} \tag{3.25}$$

Similarly, the macropore concentration of isopentane is:

$$\langle y_B \rangle P = \frac{1}{K_{ads}(T)} \frac{\theta_B}{(1 - \theta_A - \theta_B)^5} \tag{3.26}$$

where K_{ads}, the adsorption equilibrium constant, is evaluated as:

$$K_{ads}(T) = K_0 \exp\left(-\Delta H_{ads} / RT \right) \tag{3.27}$$

For initially clean catalyst, the initial conditions are:

$$\langle q_A \rangle (z, t = 0) = 0 \tag{3.28a}$$

$$\langle q_B \rangle (z, t = 0) = 0 \tag{3.28b}$$

The energy balance for heterogeneous model of the adiabatic reactor is:

$$\left(\varepsilon C_{pg} c_T + (1-\varepsilon) C_{ps} \rho_a\right) \frac{\partial T}{\partial t} = K_L \frac{\partial^2 T}{\partial z^2} - C_{pg} F \frac{\partial T}{\partial z} \tag{3.29a}$$

The Danckwert's boundary conditions are:

$$-K_L \frac{\partial T}{\partial z} = C_{pg} F (T_f - T) \qquad z = 0 \tag{3.29b}$$

$$\frac{\partial T}{\partial z} = 0 \qquad z = L_2 \tag{3.29c}$$

For initial temperature of the system equal to that of the gas at entrance:

$$T(z, t = 0) = T_f \tag{3.30}$$

The pressure drop in the beds is negligible. Moreover, the total concentration (c_T) is assumed to depend upon the average temperature only so that it remains uniform inside the vessel. Thus, it is a function of time and not of the axial position (z). The variation of molar flux (F) along the axis is neglected in energy balance to avoid an implicit solution. The heat capacity of gas is assumed constant at the reference composition. These assumptions were also made by Silva and Rodrigues [66] for modeling a similar system but were relaxed by Kruglov [33] in the methanol synthesis study.

3.3 NORMALIZED EQUATIONS

The above set of equations is written in normalized form using the following dimensionless variables:

$$x_j = \frac{z}{L_j} \qquad j = 1,2 \qquad \tau = \frac{tu_{ref}}{L_1} \qquad \overline{F} = \frac{F}{F_{ref}}$$

$$Q_i = \frac{\langle q_i \rangle}{q_{A,ref}} \qquad i = A,B \qquad C_T = \frac{c_T}{c_{T,ref}} \qquad \overline{T} = \frac{T - T_{ref}}{T_{ref}}$$

where $u_{ref} = \dfrac{F_{ref}}{\varepsilon c_{T,ref}}$ is the interstitial velocity and $q_{A,ref}$ is the solid phase concentration of *n*-pentane in equilibrium with the gas phase concentration $y_{A,ref}$ at a pressure of 15 bar and temperature T_{ref}. It is calculated using the Nitta *et al.* [44] isotherm model:

$$y_{A,ref} P = \frac{1}{K_{ads}(T_{ref})} \frac{(q_{A,ref}/q_{\max})}{\left[1 - (q_{A,ref}/q_{\max})\right]^5} \tag{3.31}$$

The parameters of the fresh feed stream are considered the reference parameters for the simulations performed in this chapter.

3.3.1 Adsorbent Bed

The fluid phase material balances for components *A* and *B* are:

$$\frac{\partial y_A}{\partial \tau} = \frac{1}{Pe_1}\frac{\partial^2 y_A}{\partial x_1^2} - \frac{1}{C_T}\frac{\partial}{\partial x_1}(\overline{F} y_A) - \frac{y_A}{C_T}\frac{\partial C_T}{\partial \tau} - \frac{1}{C_T}\zeta_m \frac{\partial Q_A}{\partial \tau} \tag{3.32a}$$

$$-\frac{1}{Pe_1}\frac{\partial y_A}{\partial x_1} = \frac{\overline{F}}{C_T}(y_{Af} - y_A) \qquad x_1 = 0 \tag{3.32b}$$

$$\frac{\partial y_A}{\partial x_1} = 0 \qquad x_1 = 1 \tag{3.32c}$$

$$\frac{\partial y_B}{\partial \tau} = \frac{1}{Pe_1}\frac{\partial^2 y_B}{\partial x_1^2} - \frac{1}{C_T}\frac{\partial}{\partial x_1}\left(\overline{F} y_B\right) - \frac{y_B}{C_T}\frac{\partial C_T}{\partial \tau} \tag{3.33a}$$

$$-\frac{1}{Pe_1}\frac{\partial y_B}{\partial x_1} = \frac{\overline{F}}{C_T}\left(y_{Bf} - y_B\right) \qquad x_1 = 0 \tag{3.33b}$$

$$\frac{\partial y_B}{\partial x_1} = 0 \qquad x_1 = 1 \tag{3.33c}$$

The overall fluid phase material balance is:

$$\frac{\partial C_T}{\partial \tau} + \frac{\partial \overline{F}}{\partial x_1} + \zeta_m \frac{\partial Q_A}{\partial \tau} = 0 \tag{3.34a}$$

$$\overline{F} = \overline{F}_f \qquad x_1 = 0 \tag{3.34b}$$

The adsorbed phase balance for component A is:

$$\zeta_m \frac{\partial Q_A}{\partial \tau} = N_f C_T \left(y_A - \langle y_A \rangle\right) \tag{3.35}$$

The macropore concentration of component A is calculated by:

$$\langle y_A \rangle P = \frac{1}{K_{ads}\left(\overline{T}\right)} \frac{\theta_{ref} Q_A}{\left(1 - \theta_{ref} Q_A\right)^5} \tag{3.36a}$$

$$K_{ads}\left(\overline{T}\right) = K_0 \exp\left(\frac{\gamma_f}{\overline{T} + 1}\right) \tag{3.36b}$$

The energy balance is:

$$\frac{\partial \overline{T}}{\partial \tau} = \frac{1}{Pe_{H1}(C_T + \zeta_H)} \frac{\partial^2 \overline{T}}{\partial x_1^2} - \frac{\overline{F}}{(C_T + \zeta_H)} \frac{\partial \overline{T}}{\partial x_1} + \frac{B\zeta_H}{(C_T + \zeta_H)} \frac{\partial Q_A}{\partial \tau} - \frac{N_w}{(C_T + \zeta_H)} (\overline{T} - \overline{T}_w) \tag{3.37a}$$

$$-\frac{1}{Pe_{H1}} \frac{\partial \overline{T}}{\partial x_1} = \overline{F}(\overline{T}_f - \overline{T}) \qquad x_1 = 0 \tag{3.37b}$$

$$\frac{\partial \overline{T}}{\partial x_1} = 0 \qquad x_1 = 1 \tag{3.37c}$$

The initial conditions are:

$$y_A(x_1, \tau = 0) = 0 \tag{3.38a}$$

$$y_B(x_1, \tau = 0) = 0 \tag{3.38b}$$

$$Q_A(x_1, \tau = 0) = 0 \tag{3.38c}$$

$$\overline{T}(x_1, \tau = 0) = \overline{T}_f \tag{3.38d}$$

3.3.2 Catalyst Bed

The normalized equations for both the pseudo-homogeneous and heterogeneous models are shown below.

3.3.2a Pseudo-Homogeneous Model

The material balances for components A and B are:

$$\frac{\partial y_A}{\partial \tau} = \frac{1}{\upsilon \cdot Pe_2}\frac{\partial^2 y_A}{\partial x_2^2} - \frac{1}{\upsilon \cdot C_T}\frac{\partial}{\partial x_2}\left(\overline{F} y_A\right) - \frac{y_A}{C_T}\frac{\partial C_T}{\partial \tau} - Da \exp\left(\gamma_r \frac{\overline{T}}{\overline{T}+1}\right)\left(y_A - \frac{y_B}{K}\right) \tag{3.39a}$$

$$-\frac{1}{Pe_2}\frac{\partial y_A}{\partial x_2} = \frac{\overline{F}}{C_T}\left(y_{Af} - y_A\right) \qquad x_2 = 0 \tag{3.39b}$$

$$\frac{\partial y_A}{\partial x_2} = 0 \qquad x_2 = 1 \tag{3.39c}$$

$$\frac{\partial y_B}{\partial \tau} = \frac{1}{\upsilon \cdot Pe_2}\frac{\partial^2 y_B}{\partial x_2^2} - \frac{1}{\upsilon \cdot C_T}\frac{\partial}{\partial x_2}\left(\overline{F} y_B\right) - \frac{y_B}{C_T}\frac{\partial C_T}{\partial \tau} + Da \exp\left(\gamma_r \frac{\overline{T}}{\overline{T}+1}\right)\left(y_A - \frac{y_B}{K}\right) \tag{3.40a}$$

$$-\frac{1}{Pe_2}\frac{\partial y_B}{\partial x_2} = \frac{\overline{F}}{C_T}\left(y_{Bf} - y_B\right) \qquad x_2 = 0 \tag{3.40b}$$

$$\frac{\partial y_B}{\partial x_2} = 0 \qquad x_2 = 1 \tag{3.40c}$$

The overall material balance is:

$$\frac{\partial C_T}{\partial \tau} + \frac{1}{\upsilon}\frac{\partial \overline{F}}{\partial x_2} = 0 \tag{3.41a}$$

$$\overline{F} = \overline{F}_f \qquad x_2 = 0 \tag{3.41b}$$

The energy balance for the pseudo-homogeneous model is:

$$\frac{\partial \overline{T}}{\partial \tau} = \frac{1}{\upsilon \cdot C_T \cdot Pe_{H2}}\frac{\partial^2 \overline{T}}{\partial x_2^2} - \frac{\overline{F}}{\upsilon \cdot C_T}\frac{\partial \overline{T}}{\partial x_2} \tag{3.42a}$$

$$-\frac{1}{Pe_{H2}}\frac{\partial \overline{T}}{\partial x_2} = \overline{F}\left(\overline{T}_f - \overline{T}\right) \qquad x_2 = 0 \tag{3.42b}$$

$$\frac{\partial \overline{T}}{\partial x_2} = 0 \qquad x_2 = 1 \tag{3.42c}$$

The initial conditions are:

$$y_A(x_2, \tau = 0) = 0 \tag{3.43a}$$

$$y_B(x_2, \tau = 0) = 0 \tag{3.43b}$$

$$\overline{T}(x_2, \tau = 0) = \overline{T}_f \tag{3.43c}$$

3.3.2b Heterogeneous Model

The fluid phase material balances for components A and B are:

$$\frac{\partial y_A}{\partial \tau} = \frac{1}{\upsilon \cdot Pe_2}\frac{\partial^2 y_A}{\partial x_2^2} - \frac{1}{\upsilon \cdot C_T}\frac{\partial}{\partial x_2}\left(\overline{F} y_A\right) - \frac{y_A}{C_T}\frac{\partial C_T}{\partial \tau} - N_f\left(y_A - \langle y_A \rangle\right) \tag{3.44a}$$

$$-\frac{1}{Pe_2}\frac{\partial y_A}{\partial x_2} = \frac{\overline{F}}{C_T}\left(y_{Af} - y_A\right) \qquad x_2 = 0 \tag{3.44b}$$

$$\frac{\partial y_A}{\partial x_2} = 0 \qquad x_2 = 1 \tag{3.44c}$$

$$\frac{\partial y_B}{\partial \tau} = \frac{1}{\upsilon \cdot Pe_2}\frac{\partial^2 y_B}{\partial x_2^2} - \frac{1}{\upsilon \cdot C_T}\frac{\partial}{\partial x_2}\left(\overline{F} y_B\right) - \frac{y_B}{C_T}\frac{\partial C_T}{\partial \tau} - N_f\left(y_B - \langle y_B \rangle\right) \tag{3.45a}$$

$$-\frac{1}{Pe_2}\frac{\partial y_B}{\partial x_2} = \frac{\overline{F}}{C_T}\left(y_{Bf} - y_B\right) \qquad x_2 = 0 \tag{3.45b}$$

$$\frac{\partial y_B}{\partial x_2} = 0 \qquad x_2 = 1 \tag{3.45c}$$

The overall material balance is:

$$\frac{\partial C_T}{\partial \tau} + \frac{1}{\upsilon}\frac{\partial \overline{F}}{\partial x_2} + N_f C_T\left(y_A - \langle y_A \rangle + y_B - \langle y_B \rangle\right) = 0 \tag{3.46a}$$

$$\overline{F} = \overline{F}_f \qquad x_2 = 0 \tag{3.46b}$$

The initial conditions for fluid phase concentrations are:

$$y_A\left(x_2, \tau = 0\right) = 0 \tag{3.47a}$$

$$y_B\left(x_2, \tau = 0\right) = 0 \tag{3.47b}$$

The material balances of components A and B over the catalyst while assuming no accumulation in the micropores are:

$$\sigma \frac{\partial \langle y_A \rangle}{\partial \tau} = N_f\left(y_A - \langle y_A \rangle\right) - Da \exp\left(\gamma_r \frac{\overline{T}}{\overline{T}+1}\right)\left(\langle y_A \rangle - \frac{\langle y_B \rangle}{K}\right) \tag{3.48}$$

$$\sigma \frac{\partial \langle y_B \rangle}{\partial \tau} = N_f\left(y_B - \langle y_B \rangle\right) + Da \exp\left(\gamma_r \frac{\overline{T}}{\overline{T}+1}\right)\left(\langle y_A \rangle - \frac{\langle y_B \rangle}{K}\right) \tag{3.49}$$

The initial conditions over the catalyst then become:

$$\langle y_A \rangle (x_2, \tau = 0) = 0 \tag{3.50a}$$

$$\langle y_B \rangle (x_2, \tau = 0) = 0 \tag{3.50b}$$

The adsorbed phase material balances of components A and B while considering the micropore accumulation are:

$$\zeta_m \frac{\partial Q_A}{\partial \tau} = N_f C_T \left(y_A - \langle y_A \rangle \right) - C_T Da \exp\left(\gamma_r \frac{\overline{T}}{\overline{T}+1} \right) \left(\langle y_A \rangle - \frac{\langle y_B \rangle}{K} \right) \tag{3.51}$$

$$\zeta_m \frac{\partial Q_B}{\partial \tau} = N_f C_T \left(y_B - \langle y_B \rangle \right) + C_T Da \exp\left(\gamma_r \frac{\overline{T}}{\overline{T}+1} \right) \left(\langle y_A \rangle - \frac{\langle y_B \rangle}{K} \right) \tag{3.52}$$

The macropore concentrations of components A and B are calculated by:

$$\langle y_A \rangle P = \frac{1}{K_{ads}(\overline{T})} \frac{\theta_{ref} Q_A}{\left(1 - \theta_{ref} Q_A - \theta_{ref} Q_B\right)^5} \tag{3.53}$$

$$\langle y_B \rangle P = \frac{1}{K_{ads}(\overline{T})} \frac{\theta_{ref} Q_B}{\left(1 - \theta_{ref} Q_A - \theta_{ref} Q_B\right)^5} \tag{3.54}$$

and K_{ads}, the adsorption equilibrium constant, is evaluated as:

$$K_{ads}(\overline{T}) = K_0 \exp\left(\frac{\gamma_f}{\overline{T}+1} \right) \tag{3.55}$$

The initial conditions in the adsorbed phase then become:

$$Q_A (x_2, \tau = 0) = 0 \tag{3.56a}$$

$$Q_B (x_2, \tau = 0) = 0 \tag{3.56b}$$

The energy balance for the heterogeneous model is:

$$\frac{\partial \overline{T}}{\partial \tau} = \frac{1}{\upsilon \cdot Pe_{H2} \cdot (C_T + \zeta_H)} \frac{\partial^2 \overline{T}}{\partial x_2^2} - \frac{\overline{F}}{\upsilon \cdot (C_T + \zeta_H)} \frac{\partial \overline{T}}{\partial x_2} \tag{3.57a}$$

$$-\frac{1}{Pe_{H2}} \frac{\partial \overline{T}}{\partial x_2} = \overline{F}\left(\overline{T}_f - \overline{T}\right) \qquad x_2 = 0 \tag{3.57b}$$

$$\frac{\partial \overline{T}}{\partial x_2} = 0 \qquad x_2 = 1 \tag{3.57c}$$

The initial reactor temperature is:

$$\overline{T}(x_2, \tau = 0) = \overline{T}_f \tag{3.58}$$

In the above equations, dependency of the forward reaction rate constant (k) upon temperature is Arrhenius:

$$k = A_{app} \exp\left(\frac{-E_{app}}{RT}\right) \tag{3.59}$$

The three reactor models developed so far are labeled as follows:

Pseudo-Homogeneous:	Model *A*
Heterogeneous (Macropore Accumulation):	Model *B*
Heterogeneous (Micropore Accumulation):	Model *C*

Unless otherwise stated, reactor model *C* is used for simulation purposes in this study.

In the normalized equations above, dimensionless groups are defined as follows:

Damkohler number: $$Da = \frac{1-\varepsilon}{\varepsilon} \rho_a \frac{k_{ref} L_1}{u_{ref}}$$

Mass Peclet number: $$Pe_j = \frac{u_{ref} L_j}{D_L}$$

Thermal Peclet number: $$Pe_{Hj} = \frac{C_{pg} F_{ref} L_j}{K_L}$$

Mass capacity factor: $$\zeta_m = \frac{1-\varepsilon}{\varepsilon} \frac{\rho_a q_{A,ref}}{c_{T,ref}}$$

Thermal capacity factor: $$\zeta_H = \frac{1-\varepsilon}{\varepsilon} \frac{\rho_a C_{ps}}{c_{T,ref} C_{pg}}$$

Number of film mass-transfer units: $$N_f = \frac{1-\varepsilon}{\varepsilon} \frac{a_p K_{gl} L_1}{u_{ref}}$$

Number of wall heat-transfer units: $$N_w = \frac{a_c h_w L_1}{C_{pg} F_{ref}}$$

Adiabatic temperature rise: $$B = \frac{(-\Delta H_{ads}) q_{A,ref}}{C_{ps} T_{ref}}$$

Dimensionless heat of adsorption: $$\gamma_f = \frac{(-\Delta H_{ads})}{R T_{ref}}$$

Dimensionless activation energy: $$\gamma_r = \frac{E_{app}}{R T_{ref}}$$

Nonlinearity parameter of isotherm: $$\theta_{ref} = \frac{q_{A,ref}}{q_{\max}}$$

Macropore porosity per unit bed porosity: $$\sigma = \frac{(1-\varepsilon)\varepsilon_p}{\varepsilon}$$

Length ratio: $$\upsilon = \frac{L_2}{L_1}$$

3.4 NUMERICAL SOLUTION

The model equations 3.32 through 3.58 are solved by applying the orthogonal collocation technique to the spatial coordinate (Appendix B). The set of coupled partial differential equations reduces to a set of ordinary differential/algebraic equations. The collocation points are given by the zeros of Jacobi polynomials $P_N^{(\alpha,\beta)}(x)=0$ [54], with $\alpha=\beta=0$, also known as the shifted Legendre polynomials [49]. Twenty collocation points are needed. The resulting system is solved using a subroutine `ode15s` available in MATLAB, which uses Numerical Differentiation Formula [61] and an adaptive time step size. The average temperature over the spatial coordinate, which is needed to calculate the total gas concentration, is determined using the Gauss-Jacobi quadrature weights.

3.5 PARAMETERS ESTIMATIONS

The column characteristics, adsorbent and catalyst properties, and adsorption and reaction parameters are summarized in Table 3.1. Adsorption data is obtained from Silva and Rodrigues [66] whereas that of reaction from Spivey and Bryant [68]. Since the catalyst particles must be pelletized to the size of the adsorbent pellets, the dimensions of the catalyst are assumed equal to that of the adsorbent. Moreover, the physical properties such as the adsorption equilibrium isotherm are not known for the Pd/faujasite used. Thus, in the heterogeneous model of the reactor, these parameters are also assumed equal to that of the adsorbent.

The axial mass dispersion coefficient (D_L) is calculated by:

$$D_L = 0.7D_m + 0.5d_p u \tag{3.60}$$

Table 3.1. Data for the Base-Case System

System: n-C_5/i-C_5/H_2			
Column Characteristics			
• L	=	20	cm
• d_c	=	3.35	cm
Adsorbent Properties			
• ρ_a	=	1.13	g/cm^3
• ε	=	0.32	
• ε_p	=	0.35	
• d_p	=	1.6	mm
• a_p	=	28.3	cm^{-1}
• C_{ps}	=	0.9	J/g.K
Catalyst Properties			
• ρ_b	=	0.66	g/cm^3
Adsorption Equilibrium Isotherm Parameters			
• $-\Delta H_{ads}$	=	13.2	kcal/mol
• n	=	5	
• q_{max}	=	1.8	mmol$_{n\text{-}C5}$/g$_{ads}$
• K_0	=	2.01×10^{-5}	bar^{-1}
Chemical Reaction Parameters			
• k	=	0.046	cm^3/g.s @ 514 K
• E_{app}	=	37	kcal/mol
• K		(in equation 3.64)	

As mentioned in Chapter 2 the global mass transfer coefficient (K_{gl}) can be evaluated from the external and internal mass transfer coefficients:

$$\frac{1}{K_{gl}} = \frac{1}{k_e} + \frac{1}{\varepsilon_p k_i} \tag{3.61}$$

Moreover, the internal mass transfer coefficient (k_i) can be calculated according to the lumped model proposed by Glueckauf [22]:

$$k_i = 5\frac{D_p}{R_p} \tag{3.62}$$

The external mass transfer coefficient (k_e) is estimated with the correlation of Wakao and Funazkri [81]:

$$Sh = 2.0 + 1.1 Re^{0.6} Sc^{0.33} \tag{3.63}$$

The values of effective axial bed thermal conductivity (K_L) and the overall heat transfer coefficient (h_w) are obtained from Silva and Rodrigues [66]. The reaction equilibrium constant (K) is determined from the correlation obtained by Pines *et al.* [48]:

$$R \ln K = \frac{1861}{T} - 1.299 \tag{3.64}$$

3.6 MODEL SENSITIVITY ANALYSIS

It is important to identify the parameters to which the model is most sensitive. Thus, breakthrough curves are determined for various parameters listed in Table 3.2. The number of nodes required for a stable solution depends upon the operating parameters. As seen in Figure 3.1, the lower Peclet number curve is stable using just eight nodes whereas the larger Peclet number curve, which represents typical parameters used in this study, is

Table 3.2. Parametric Values for the Model Sensitivity Analysis @ 15 bar

Parameters	**Figure 3.1**	**Figure 3.2**	**Figure 3.3**	**Figures 3.4 & 3.5**	**Figures 3.6 & 3.7**
Varying parameter	D_L	No. of nodes	K_{gl}	K_L	h_w
$y_{Af} = y_{Bf}$	0.125	0.125	0.125	0.125	0.125
F_f (mol/m^2.s)	0.20	0.20	0.20	0.20	0.20
$T_f = T_w$ (K)	430	430	430	430	430
D_L (cm^2/s)	0.45*, 0.045	0.045	0.045	0.045	0.045
K_{gl} (cm/s)	0.31	0.31	0.31, 3.1*	0.31	0.31
K_L (W/m.K)	0.35	0.35	0.35	0.35, 0.035*	0.35
C_{pg} (J/mol.K)	63.0	63.0	63.0	63.0	63.0
h_w (W/m^2.K)	15	15	15	15	1.5*, 15, 150*
Pe	6.62*, 66.2	66.2	66.2	66.2	66.2
Pe_H	7.20	7.20	7.20	7.20, 72.0*	7.20
ζ_m	6.97	6.97	6.97	6.97	6.97
ζ_H	81.8	81.8	81.8	81.8	81.8
N_f	2516	2516	2516, 25160*	2516	2516
N_w	28.4	28.4	28.4	28.4	2.84*, 28.4, 284*
B	0.174	0.174	0.174	0.174	0.174
γ_f	15.5	15.5	15.5	15.5	15.5
θ_{ref}	0.677	0.677	0.677	0.677	0.677

*Note: Parameters marked with asterisks do not correspond to the operating conditions.

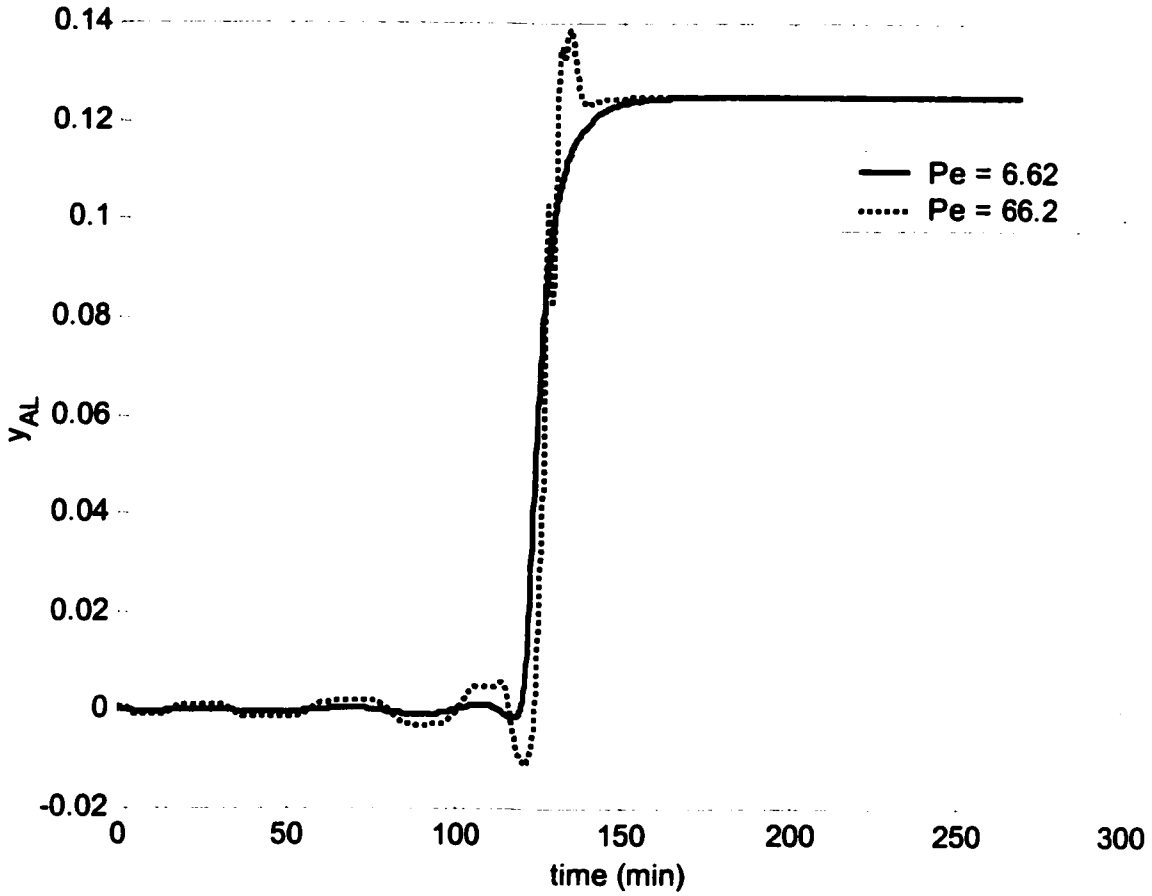

Figure 3.1. Effect of Dispersion Coefficient on Breakthrough Curve for N = 8. Parametric values are in Table 3.2.

not stable at all. However, when the number of nodes is increased to 18, the solution becomes stable once again (Figure 3.2). Thus higher the Peclet number, greater is the number of nodes required to achieve stability. Moreover, there is virtually no difference between the curves simulated at 18 and 20 nodes. Thus, 20 nodes are used for simulation purposes from this point onwards.

The breakthrough curve does not seem to be sensitive to changes in the global mass transfer coefficient even when it is increased tenfold (Figure 3.3). It is also not sensitive to changes in the effective thermal conductivity of the bed (Figure 3.4). However, the exit temperature is very sensitive (Figure 3.5). When thermal conductivity is large (corresponding to low Pe_H), the temperature curve is broad because of high thermal dispersion and the maximum value reached is low. Nevertheless, this study is more concerned with the purity obtained by SMBR rather than its heat effects so that one needs to concentrate on the breakthrough curves instead of the temperature profiles.

The curves are, however, sensitive to wall heat transfer coefficient (Figures 3.6 & 3.7). A large value makes the process almost isothermal, as the heat of adsorption is effectively removed by the wall temperature hence leading to a sharp breakthrough curve and very low rise in temperature. Conversely, a low value makes it nearly adiabatic. Moreover, the breakthrough time reduces, as the heat released lowers the equilibrium capacity of adsorbent. This points to the necessity to determine the exact value of heat transfer coefficient. Anyhow, the operating conditions used in this study are similar to those used elsewhere [66]. Thus, the value of wall heat transfer coefficient stated in the literature is used in SMBR simulations rather than determining ones own.

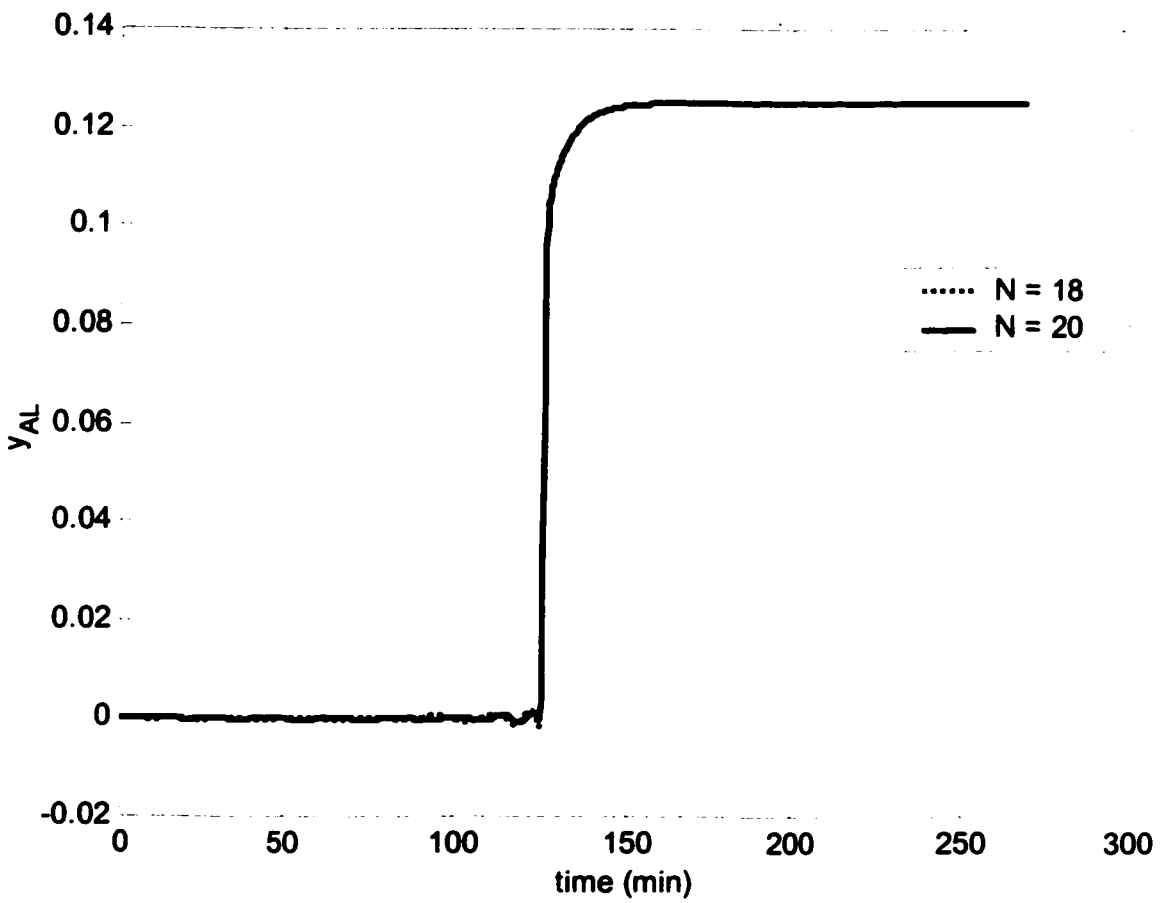

Figure 3.2. Breakthrough Curves for Varying Number of Nodes. Parametric values are in Table 3.2.

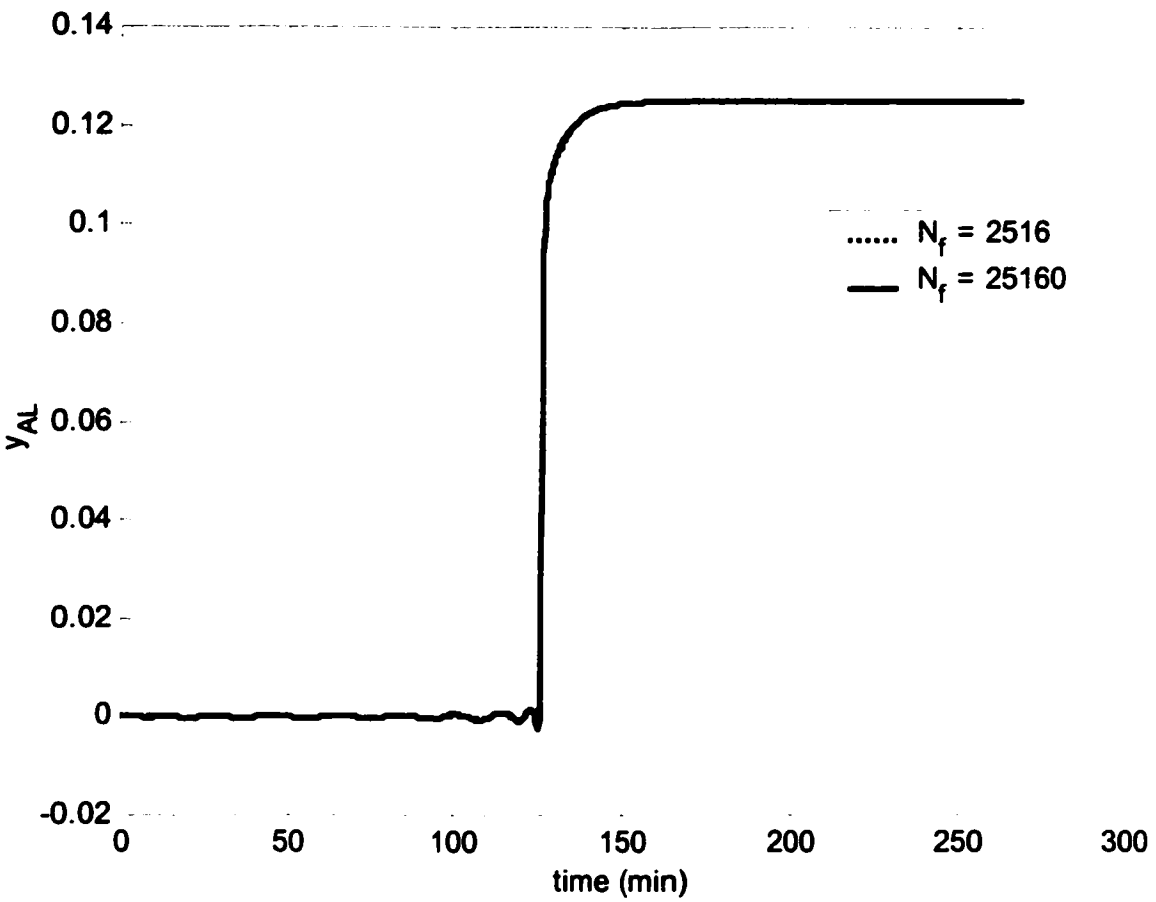

Figure 3.3. Effect of Mass Transfer Coefficient on Breakthrough Curve. Parametric values are in Table 3.2.

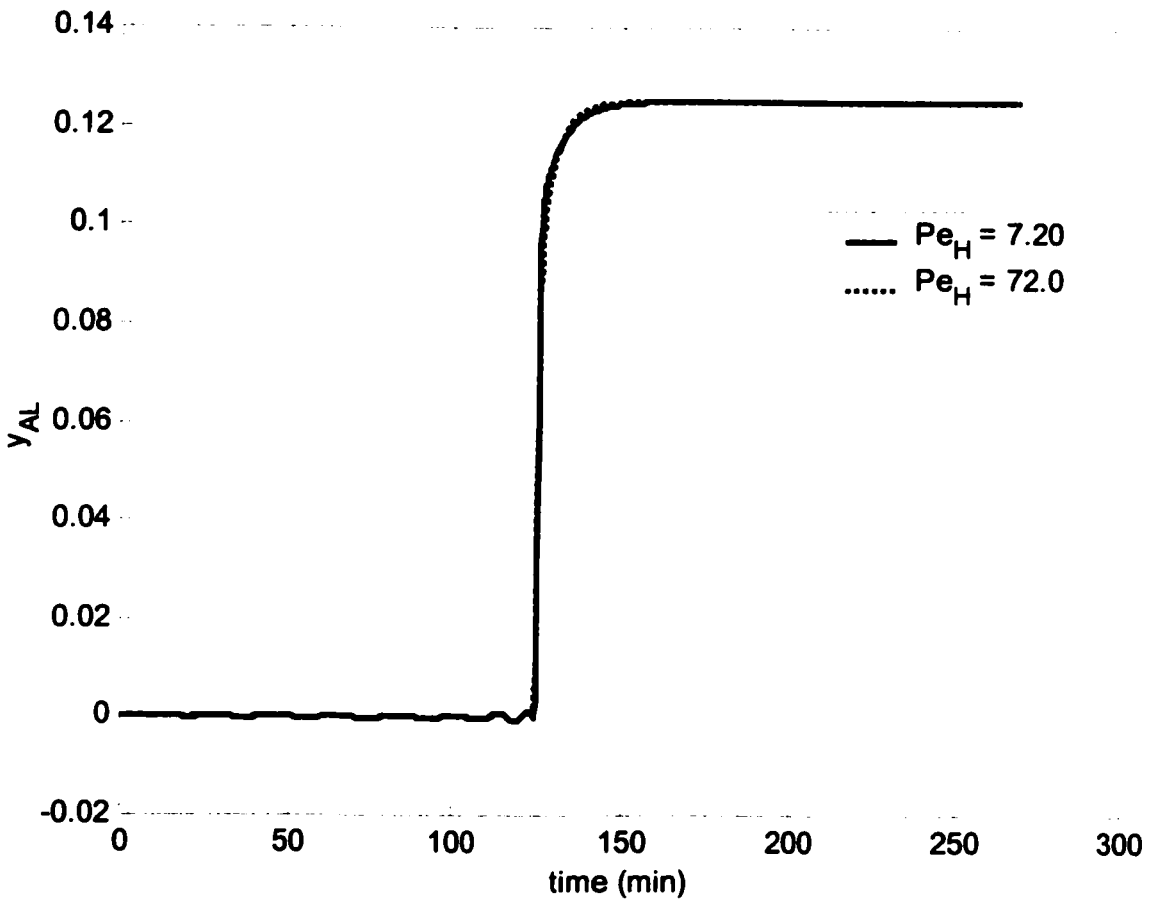

Figure 3.4. Effect of Thermal Conductivity on Breakthrough Curve. Parametric values are in Table 3.2.

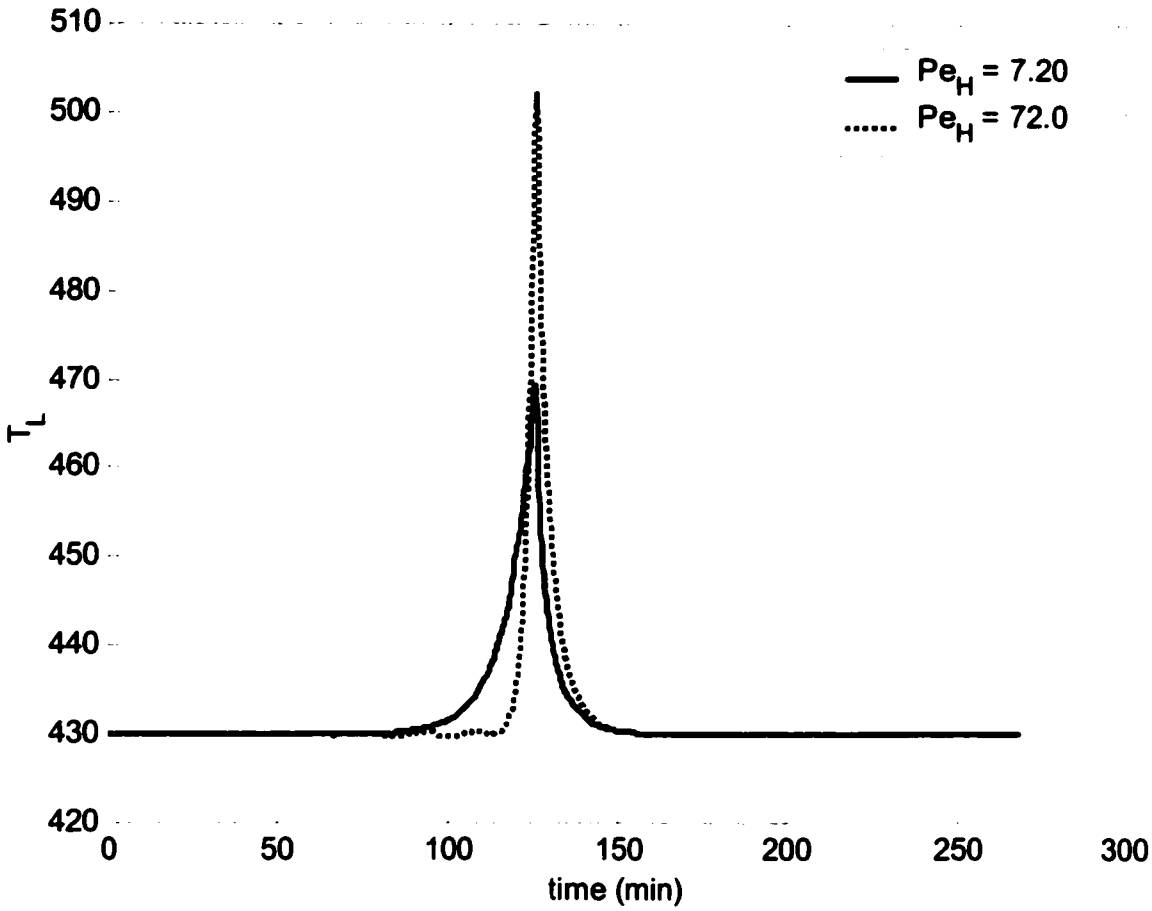

Figure 3.5. Effect of Thermal Conductivity on Exit Temperature. Parametric values are in Table 3.2.

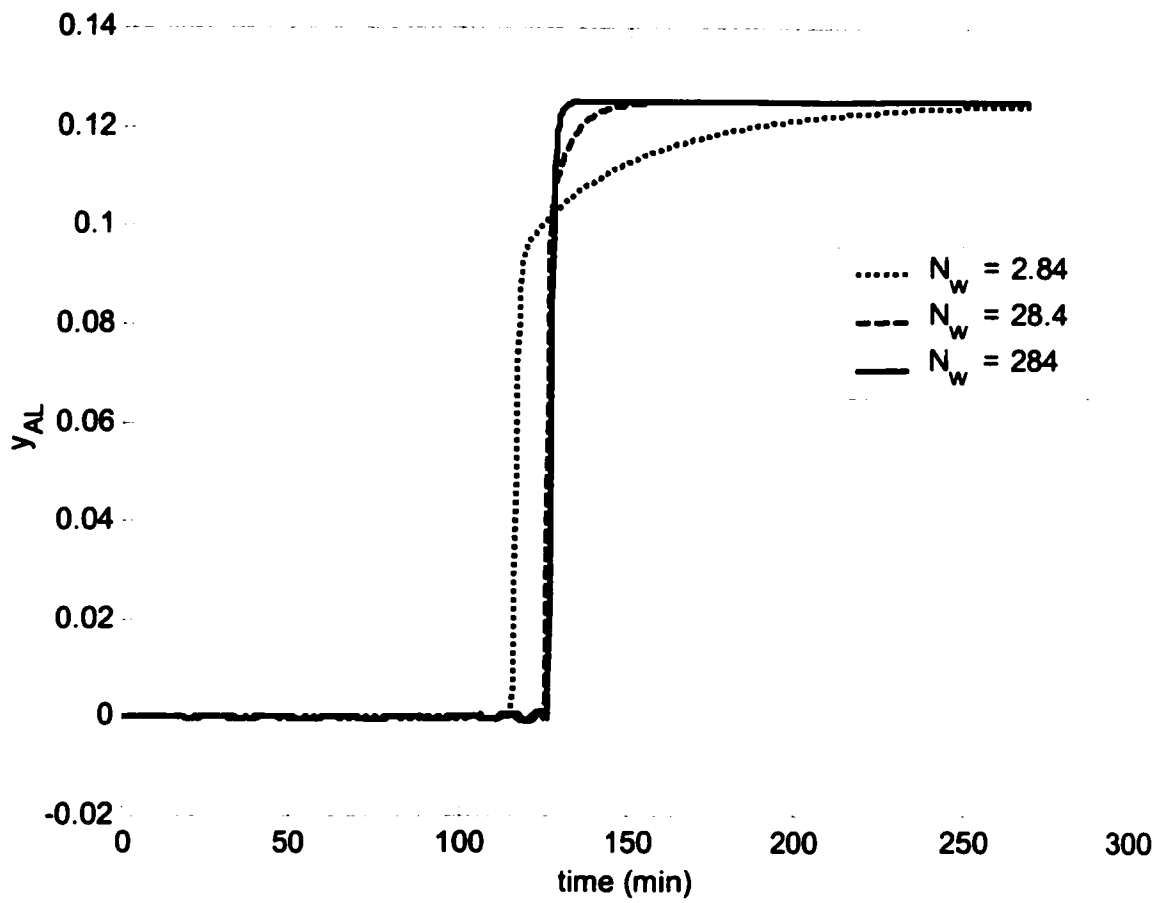

Figure 3.6. Effect of Wall Heat Transfer Coefficient on Breakthrough Curve. Parametric values are in Table 3.2.

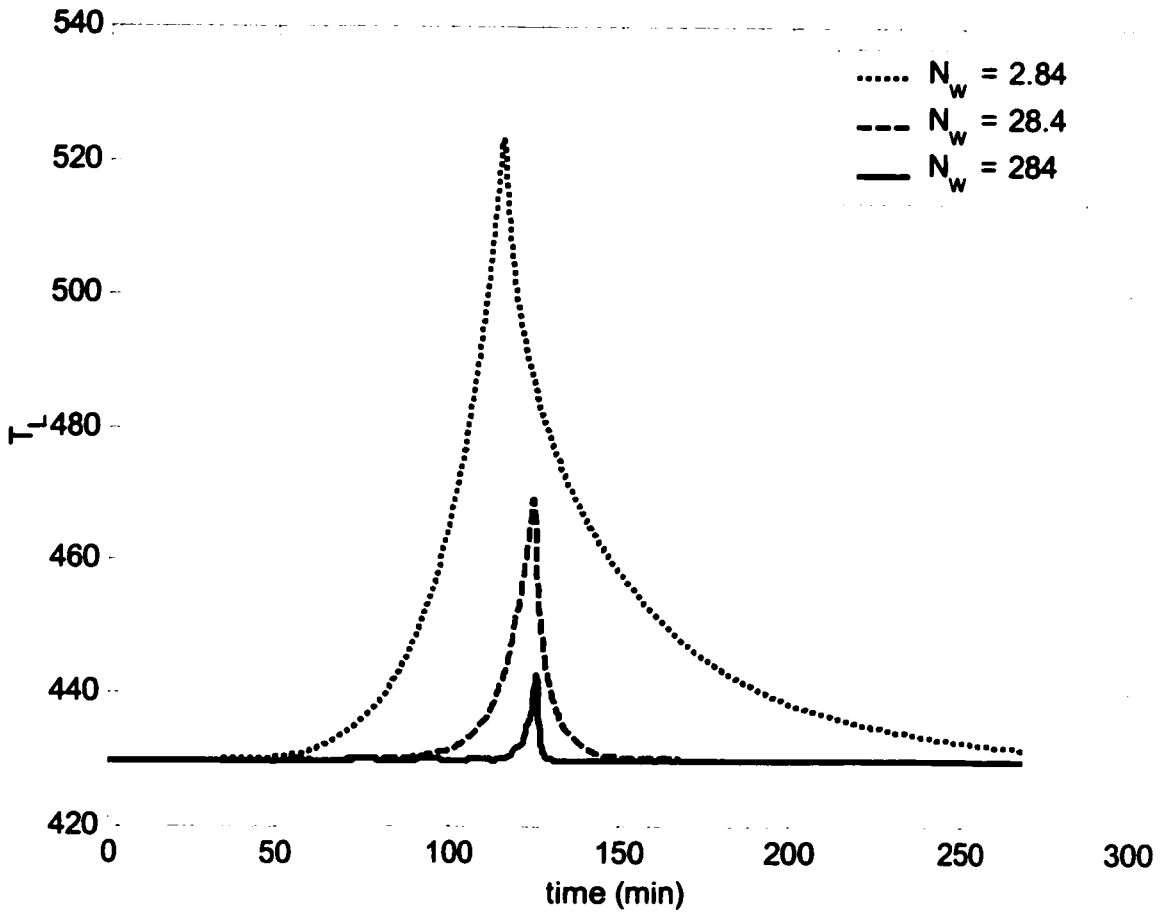

Figure 3.7. Effect of Wall Heat Transfer Coefficient on Exit Temperature. Parametric values are in Table 3.2.

3.7 RESULTS AND DISCUSSION

3.7a Adsorbent Bed

It is instructive to first study a single adsorbent bed before incorporating the model in the complicated SMBR simulations. This is because the effect of operating parameters on the model can be studied easily by observing the breakthrough curves, which is not possible in an SMBR, as feed to the adsorbent bed is switched to the next one in series before breakthrough is achieved. The effects of temperature, sorbate concentration in feed, flow rate and vessel dimensions are studied, and the parameters listed in Table 3.3.

The effect of temperature on adsorption breakthrough curves is demonstrated in Figure 3.8. Earlier breakthrough is achieved at higher temperatures because the adsorption equilibrium constant (K_{ads}) reduces with increasing temperature, thus lowering the equilibrium capacity of the bed.

The *n*-pentane breaks through the bed earlier if the flow rate of sorbate, $F_{Af} = F_f \cdot y_{Af}$, is higher (Figure 3.9). However, the breakthrough time also depends upon the sorbate concentration in the feed, as the equilibrium capacity of adsorbent is larger at higher partial pressures.

If feed concentration of sorbate is constant, exactly the same breakthrough curve is obtained by changing both the feed flow rate (F_f) and the adsorber length (L) with the same magnitude (Figure 3.10). Thus, the ratio of these two quantities is more important. In fact, the quantity $\tau_R = \dfrac{L}{u_f} = \dfrac{L\varepsilon c_{Tf}}{F_f}$ should be used as the characteristic value, which

Table 3.3. Parametric Values for the Solution of Breakthrough Curves @ 15 bar

Parameters	**Figure 3.8**	**Figure 3.9**		**Figure 3.10**		**Figure 3.11**
Varying parameter	T	F_f, y_{Af}		F_f, L		d_c
y_{Af} (y_{If} = 0.75)	0.125	0.125	0.0625	0.125		0.125
F_f (mol/m^2.s)	0.20	0.20, 0.10	0.40, 0.20	0.40	0.20	0.20
$T_f = T_w$ (K)	540, 430	430	430	430	430	430
L (cm)	20	20	20	20, 40	10, 20	20
d_c (cm)	3.35	3.35	3.35	3.35	3.35	0.335, 3.35, 33.5
D_L (cm^2/s)	0.064, 0.045	0.045, 0.039	0.057, 0.045	0.057	0.045	0.045
K_{gl} (cm/s)	0.44, 0.31	0.31, 0.30	0.32, 0.31	0.32	0.31	0.31
K_L (W/m.K)	0.35	0.35	0.35	0.35	0.35	0.35
C_{pg} (J/mol.K)	70.7, 63.0	63.0	63.0	63.0	63.0	63.0
h_w (W/m^2.K)	15	15	15	15	15	15
Pe	58.5, 66.2	66.2, 38.1	104.7, 66.2	104.7, 209.3	33.1, 66.2	66.2
Pe_H	8.08, 7.20	7.20, 3.60	14.4, 7.20	14.4, 28.8	3.60, 7.20	7.20
ζ_m	5.73, 6.97	6.97	6.53	6.97	6.97	6.97
ζ_H	91.5, 81.8	81.8	81.8	81.8	81.8	81.8
N_f	2857, 2516	2516, 4883	1309, 2516	1309, 2619	1258, 2516	2516
N_w	25.4, 28.4	28.4, 56.9	14.2, 28.4	14.2, 28.4	14.2, 28.4	284, 28.4, 2.84
B	0.091, 0.174	0.174	0.163	0.174	0.174	0.174
γ_f	12.3, 15.5	15.5	15.5	15.5	15.5	15.5
θ_{ref}	0.443, 0.677	0.677	0.634	0.677	0.677	0.677

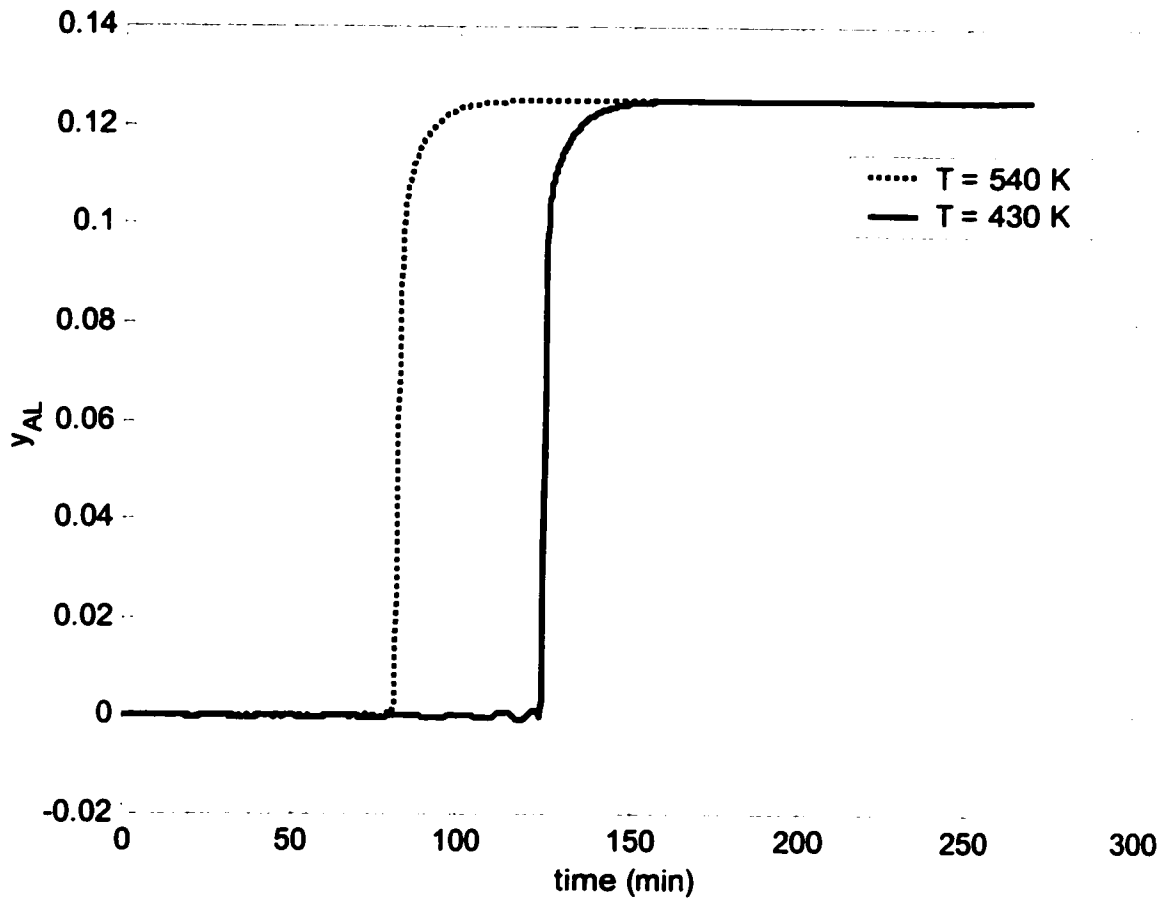

Figure 3.8. Effect of Operating Temperature on Breakthrough Curve. Parametric values are in Table 3.3.

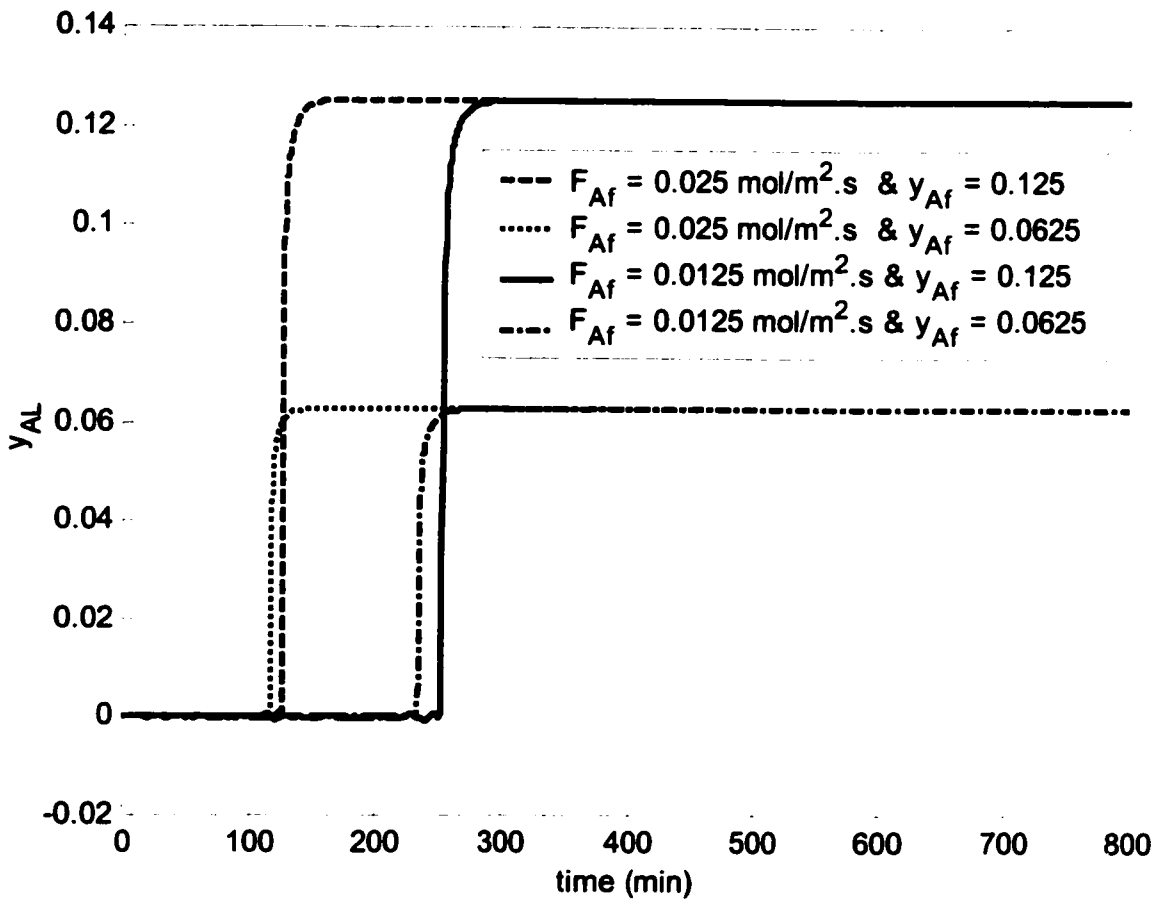

Figure 3.9. Effect of Feed Flow Rate and Feed Concentration on Breakthrough Curve. Parametric values are in Table 3.3.

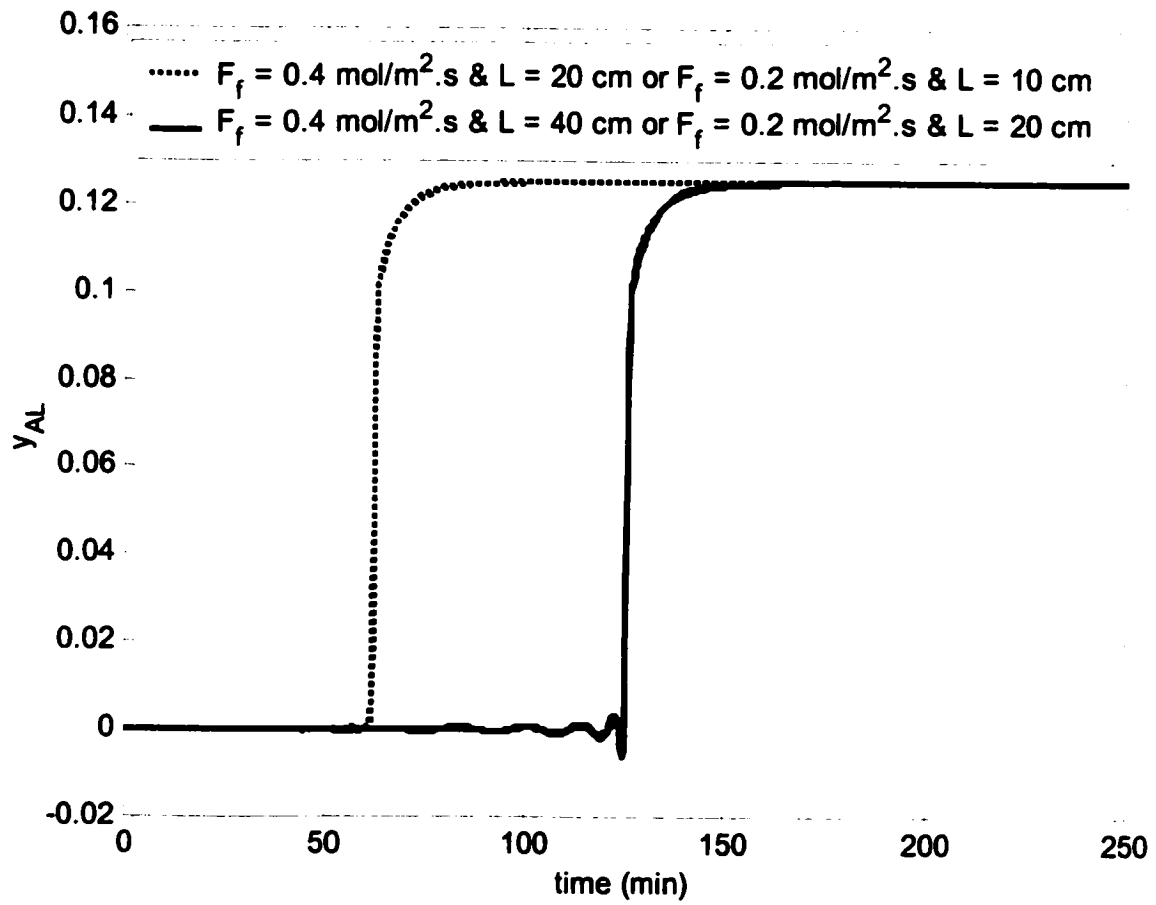

Figure 3.10. Effect of Feed Flow Rate and Column Length on Breakthrough Curve. Parametric values are in Table 3.3.

is essentially the residence time of gas at steady state, i.e. when breakthrough is reached. Actually, this is the parameter used to normalize the time variable (t). Earlier breakthrough is achieved at lower τ_R.

Column diameter (d_c) plays a role in the adsorbent bed simulations when the system is non-isothermal. Heat is released during adsorption and the efficiency of its removal depends upon the column diameter (Figure 3.11). Smaller diameters tend towards isothermal operations because the specific area of column is high. On the other hand, typically large diameters tend towards adiabatic operations. It is, however, unrealistic to use such extreme values of diameter for a fixed length of adsorber. Actually, the ratio L/d_c is essential as this is the quantity that appears in the dimensionless group N_w. Thus, when the adsorber is scaled up to an industrial level, it should give a similar performance if the quantities τ_R and L/d_c are held constant.

Having studied the effects of various parameters on fixed bed adsorption, it is also informative to study the regeneration process because the SMBR incorporates both of these. So far, all of the fixed bed simulations were non-isothermal and non-adiabatic with the wall temperature set equal to that of the feed. The advantages of low diameter and high heat transfer coefficient were used to avoid unwanted rise in temperature. Parametric values for the remaining fixed bed simulations are in Table 3.4.

The adsorption breakthrough curve followed by desorption curves at two different temperatures are shown in Figure 3.12. Adsorption process is carried for 268.5 min before the hydrocarbon supply is cut off and only pure hydrogen purge is allowed to pass through. When the regeneration is performed at the same temperature as that of the

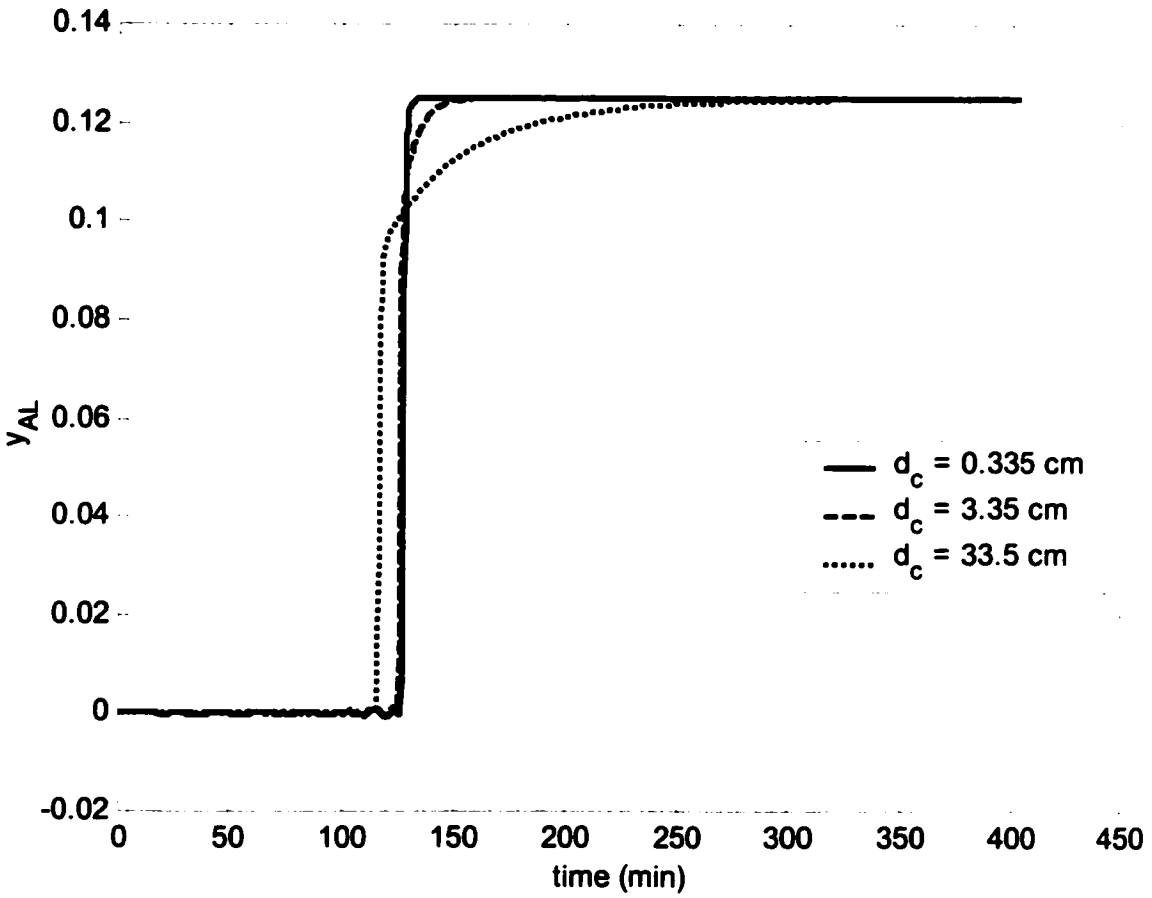

Figure 3.11. Effect of Column Diameter on Breakthrough Curve. Parametric values are in Table 3.3.

Table 3.4. Parametric Values for Fixed Bed Simulations @ 15 bar (Figures 3.12 to 3.22)

Parameters	Adsorption		Desorption (Non-Adiabatic)	
	Adiabatic	Non-Adiabatic	@ T = 430 K	@ T = 540 K
$y_{Af} = y_{Bf}$	0.125	0.125	0	0
F_f (mol/m^2.s)	0.20	0.20	0.15	0.15
T_f	430	430	430	540
T_w (K)	-	430	430	540
D_L (cm^2/s)	0.045	0.045	0.045	0.064
K_{gl} (cm/s)	0.31	0.31	0.31	0.44
K_L (W/m.K)	0.35	0.35	0.35	0.35
C_{pg} (J/mol.K)	63.0	63.0	63.0	70.7
h_w (W/m^2.K)	0	15	15	15
Pe	66.2	66.2	66.2	46.6
Pe_H	7.20	7.20	7.20	8.08
ζ_m	6.97	6.97	6.97	6.97
ζ_H	81.8	81.8	81.8	72.9
N_f	2516	2516	2516	3553
N_w	0	28.4	28.4	25.4
B	0.174	0.174	0.174	0.174
γ_f	15.5	15.5	15.5	15.5
θ_{ref}	0.677	0.677	0.677	0.677

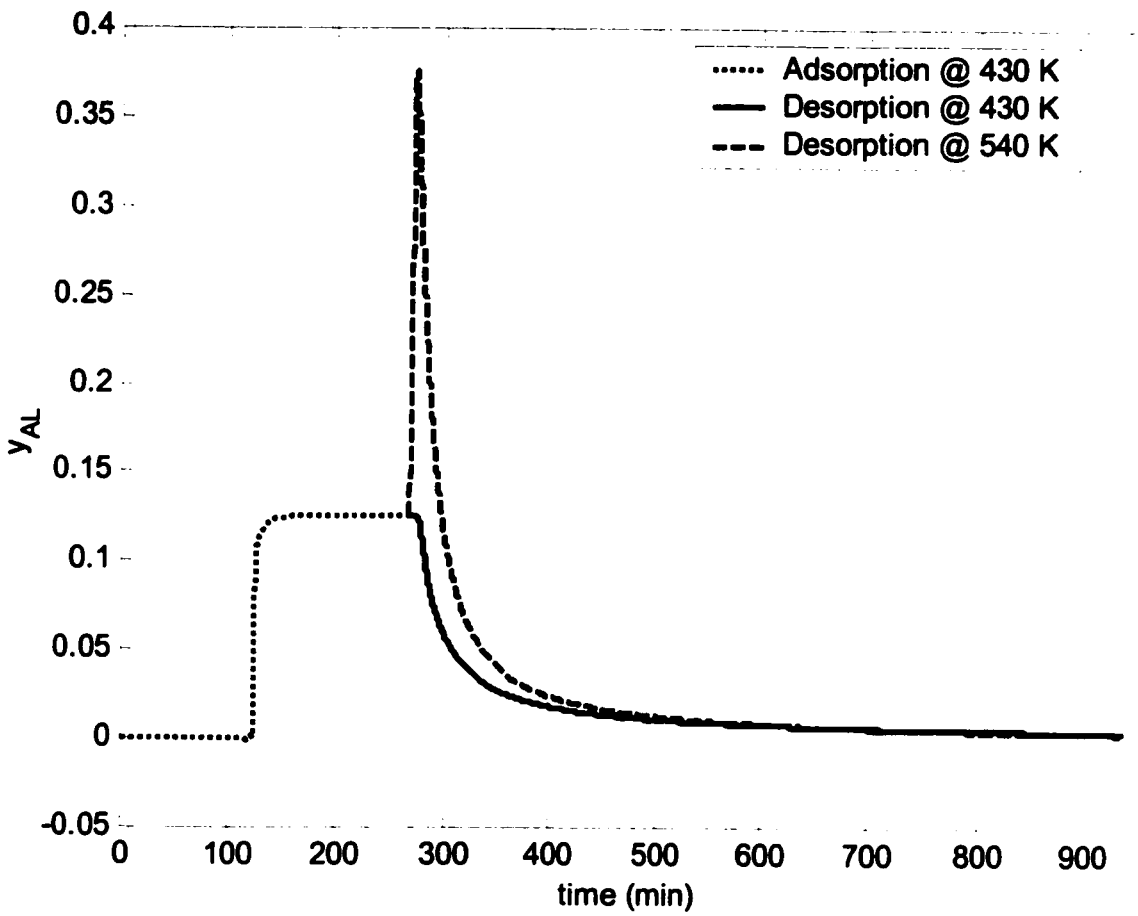

Figure 3.12. Effect of Temperature on Desorption Curve. Parametric values are in Table 3.4.

adsorption step, a smooth curve is obtained with peak tailing. However, when it is done at a higher temperature, a sudden shoot in exit concentration is first observed. The abrupt rise is not because of any numerical instability. It can be explained by observing Figure 3.13.

The first rise in outlet temperature occurs at breakthrough, i.e. when the adsorption front reaches the bed exit. Since regeneration is a slower process, the temperature drop is compensated by the constant wall temperature. However, when the desorption is performed at the higher temperature, immediate increase in exit temperature is observed because the high heat transfer coefficient makes possible fast heat transfer from wall to the system. The higher temperature of purge alone would not have been sufficient to increase the temperature of the bed effectively. The instantaneous temperature increase rapidly desorbs *n*-pentane thus producing the shoot in exit concentration.

The explanation is further reinforced by studying the adsorbed phase concentration profiles in Figure 3.14. Much less desorption takes place after 10 minutes of operation at the lower temperature but a significant amount desorbs at the higher temperature, even from the bed exit. Moreover, the bed is almost clean at the end of the regeneration process when the higher temperature is used.

The sharp nature of breakthrough curves thus far studied is because of the highly favorable isotherm of *n*-pentane at the partial pressures used. The peak tailing, in contrast, for desorption curves occurs because of the dispersed nature of the desorption front.

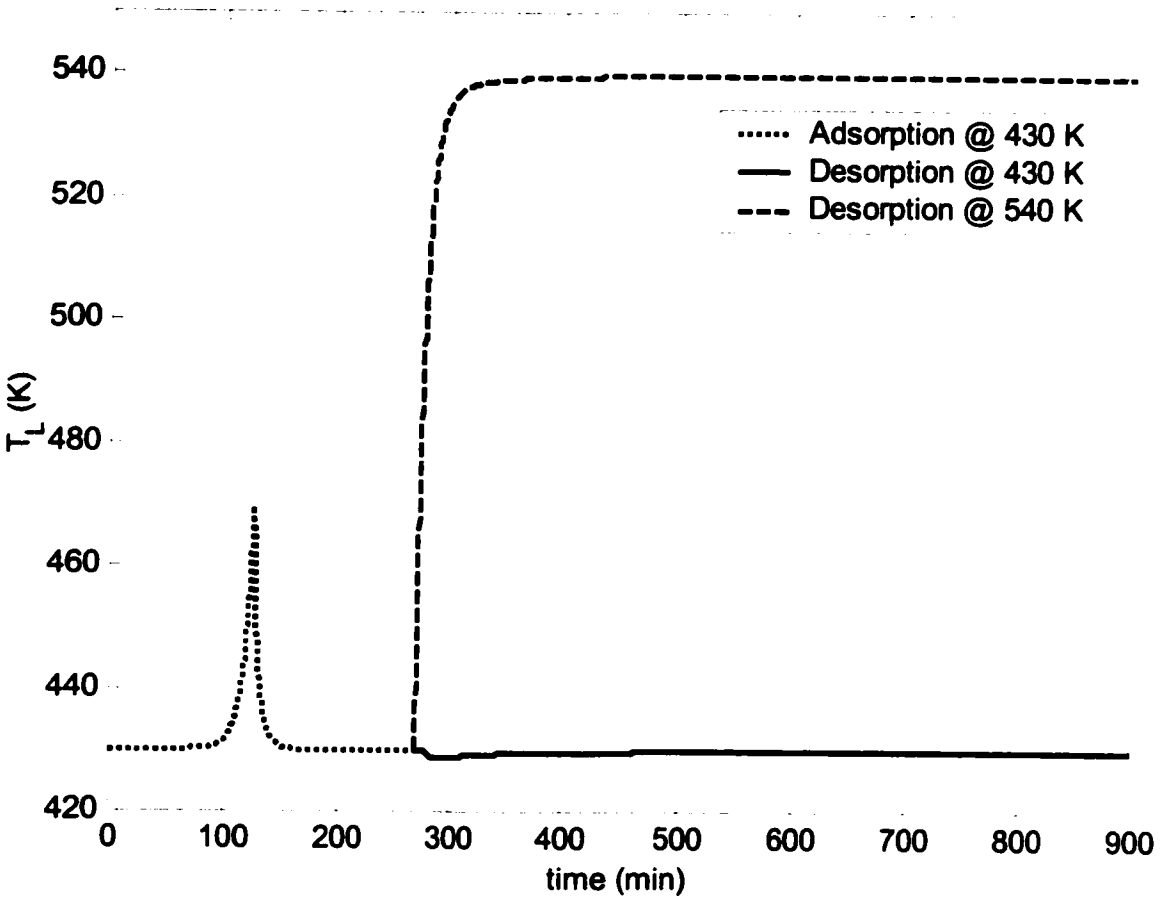

Figure 3.13. Exit Temperature during Non-Adiabatic Adsorption and Desorption Steps. Parametric values are in Table 3.4.

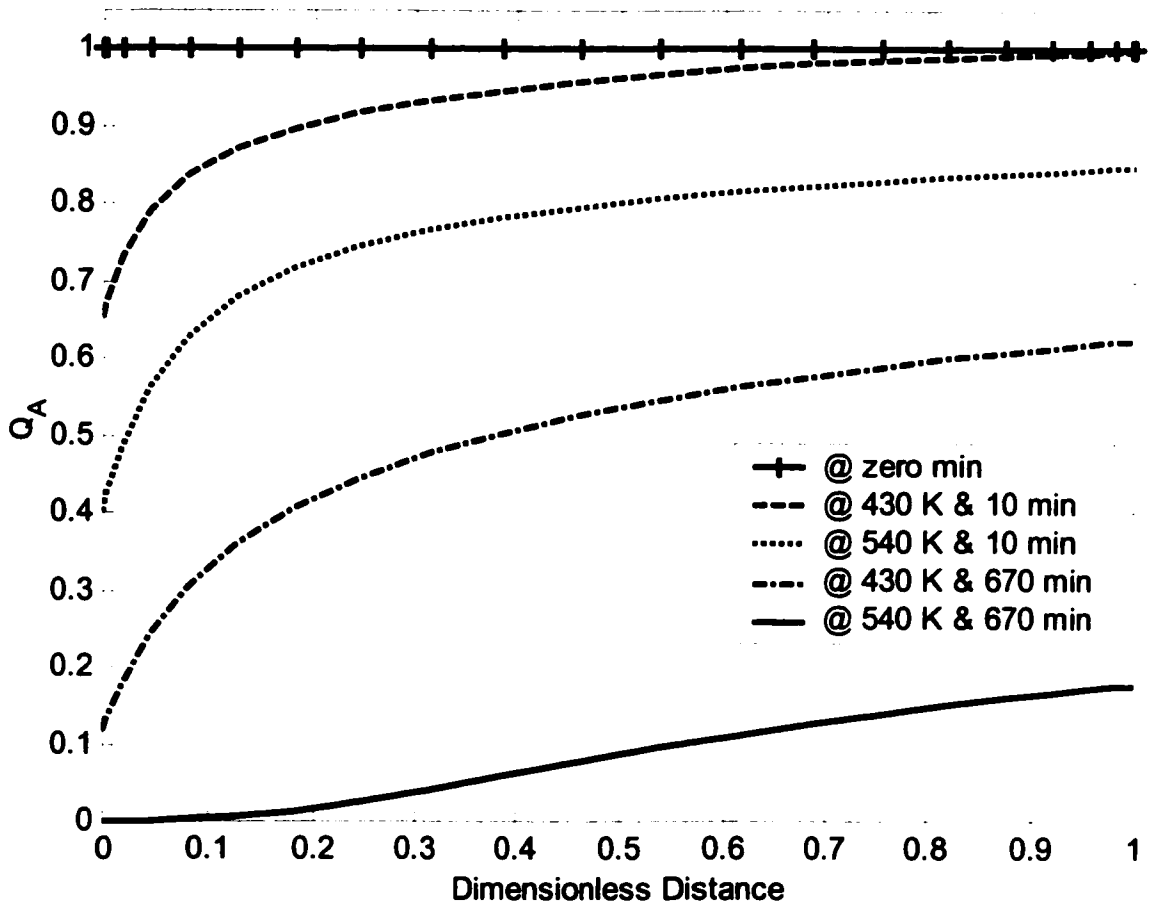

Figure 3.14. Effect of Regeneration Temperature on Adsorbed Phase Concentration Profiles. Parametric values are in Table 3.4.

The gas phase concentration profiles during the adsorption step are shown in Figures 3.15 and 3.16. As expected, the mole fraction of isopentane rises at the point where *n*-pentane adsorbs. The isopentane mole fraction at the bed exit prior to *n*-pentane breakthrough can be calculated by a material balance. In fact, it equals $y_{Bf}/(y_{Bf}+y_{If})$ $=0.143$ which is approximately the same value predicted by the simulation code. Moreover, once the adsorption front exits the bed, the concentration profiles become uniform throughout. The steep nature of adsorption front is because of the favorable adsorption isotherm. In effect, sorbate concentration drops to zero as soon as it encounters the clean portion of the adsorbent. The sharp slope causes oscillation in the profiles along the bed, which can be avoided by concentrating the collocation points at the adsorption front. However, in this study the oscillations are filtered off instead by using curve fitting. Furthermore, any negative value in the final output is forced to become zero.

The adsorbed phase concentration profiles (Figure 3.17) and fluid flow rate profiles (Figure 3.18) follow the same pattern as that of gas phase *n*-pentane. The change in normalized flow rate at the adsorption front is clearly noticeable which drops by 0.125, i.e. the mole fraction of *n*-pentane in the feed, to 0.875. Moreover, the oscillations before the adsorption front cause the flow rate to exceed unity.

The temperature front (Figure 3.19) travels with the same velocity of the adsorption front until it breaks through the adsorber. Temperature profiles for the adiabatic operation, on the other hand, are shown in Figure 3.20. In this case, the temperature keeps on increasing as the front travels along the column. This is because hot

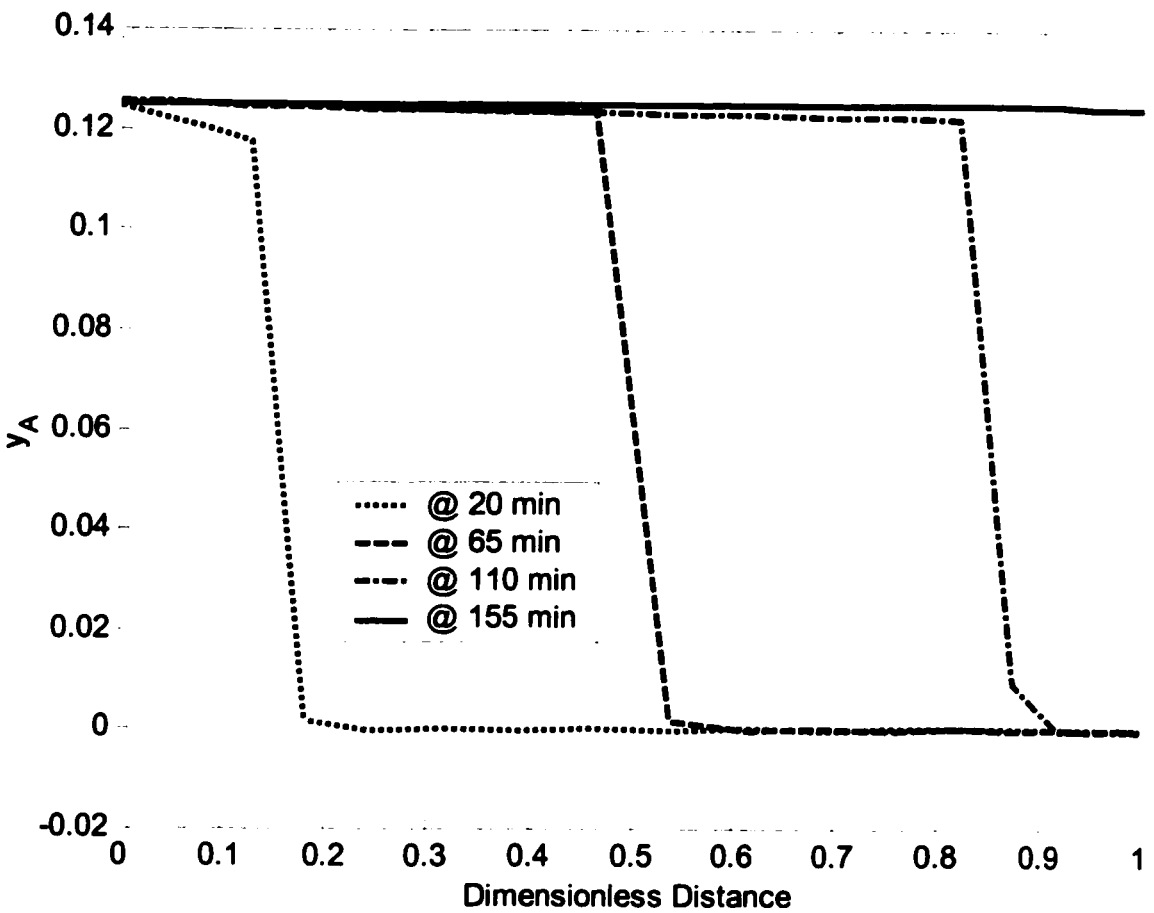

Figure 3.15. Concentration Profiles of *n*-Pentane at Various Times during the Non-Adiabatic Adsorption Step. Parametric values are in Table 3.4.

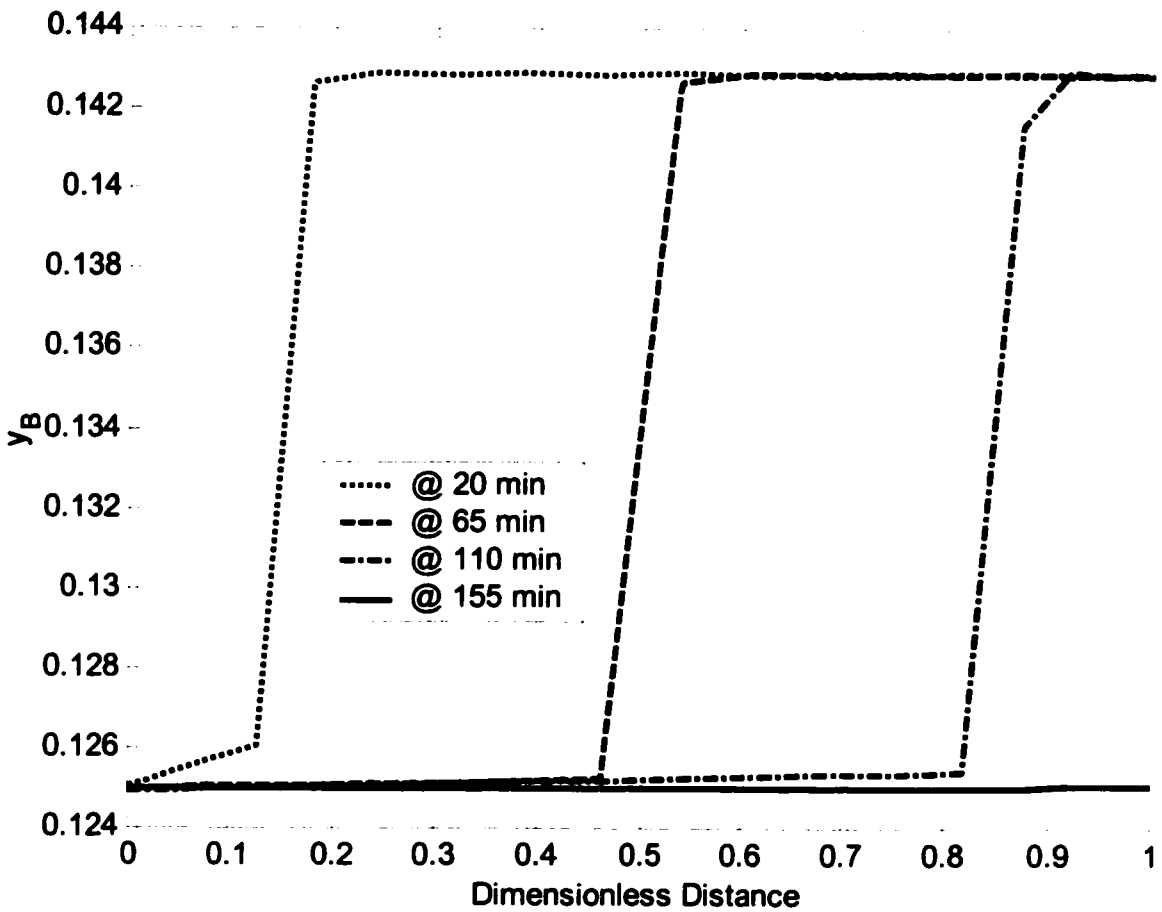

Figure 3.16. Concentration Profiles of Isopentane at Various Times during the Non-Adiabatic Adsorption Step. Parametric values are in Table 3.4.

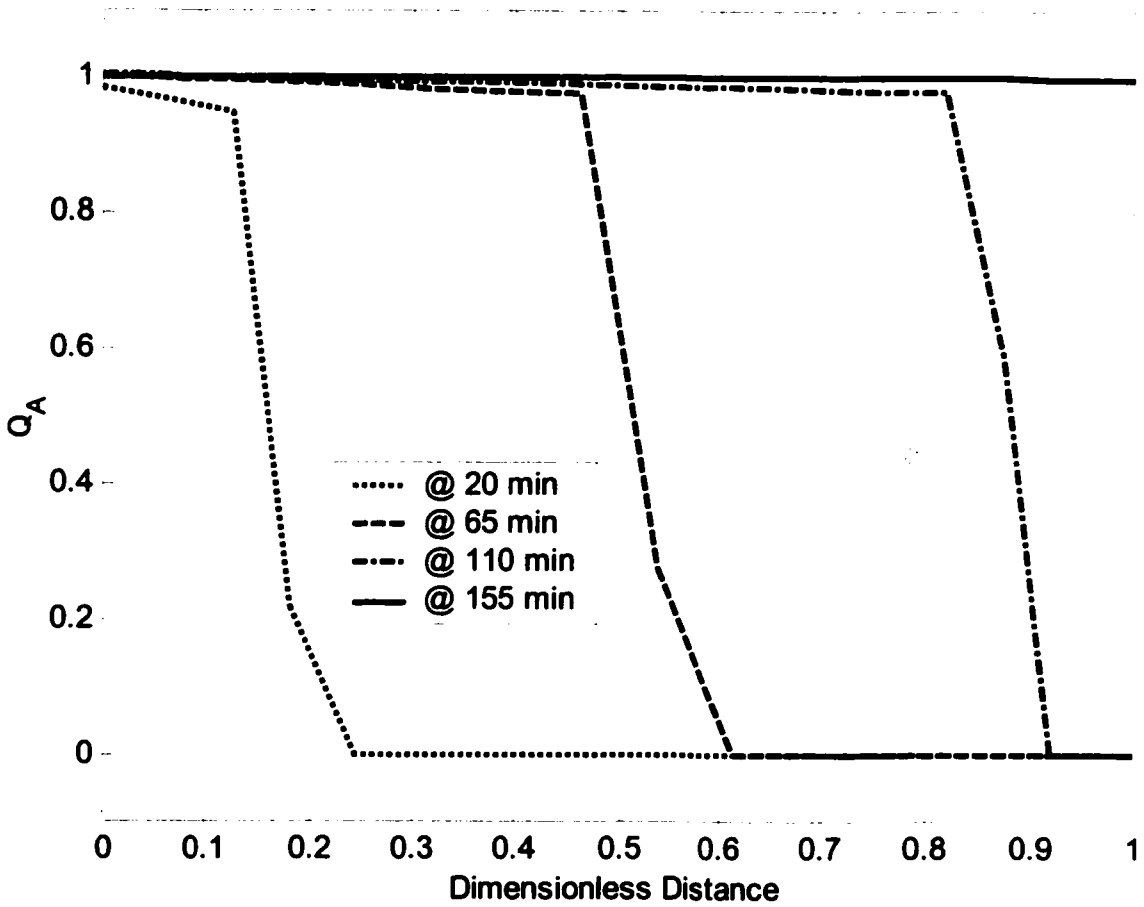

Figure 3.17. Adsorbed Phase Concentration Profiles at Various Times during the Non-Adiabatic Adsorption Step. Parametric values are in Table 3.4.

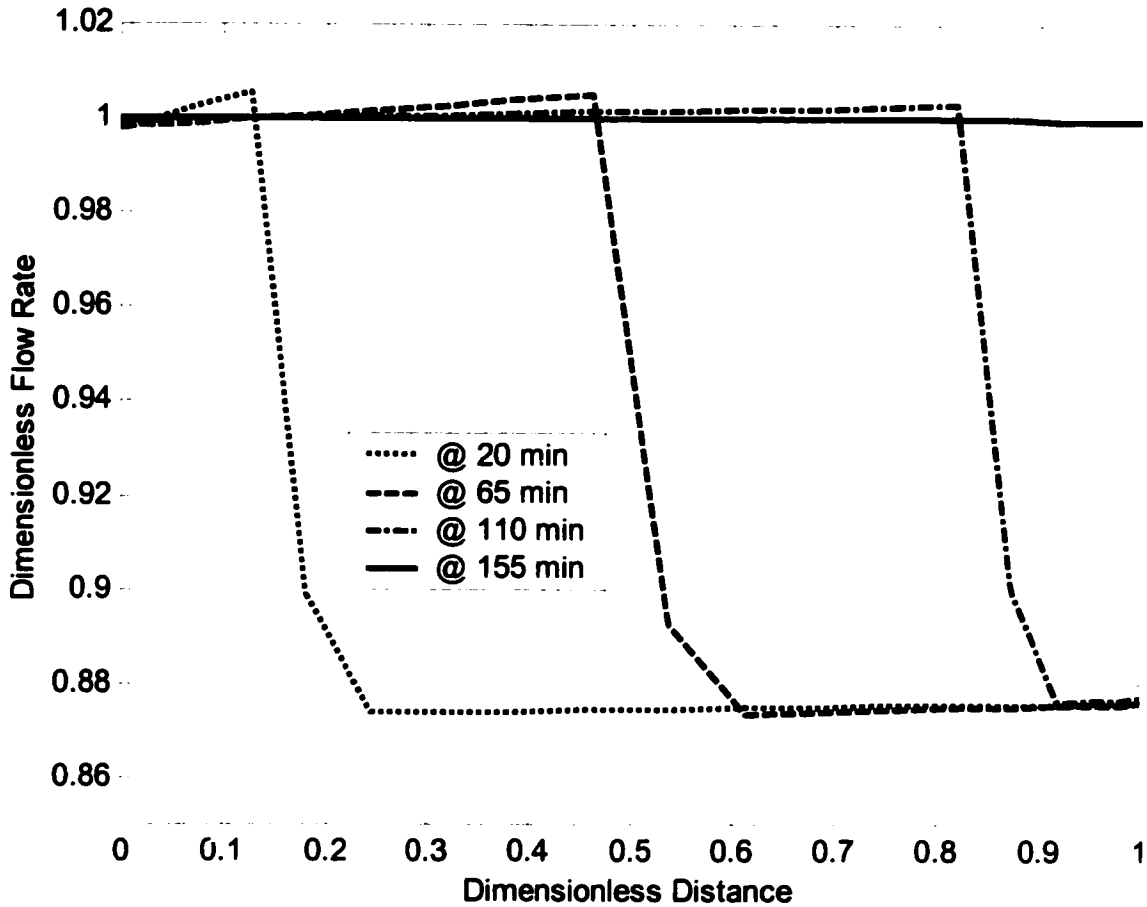

Figure 3.18. Fluid Flow Rate Profiles at Various Times during the Non-Adiabatic Adsorption Step. Parametric values are in Table 3.4.

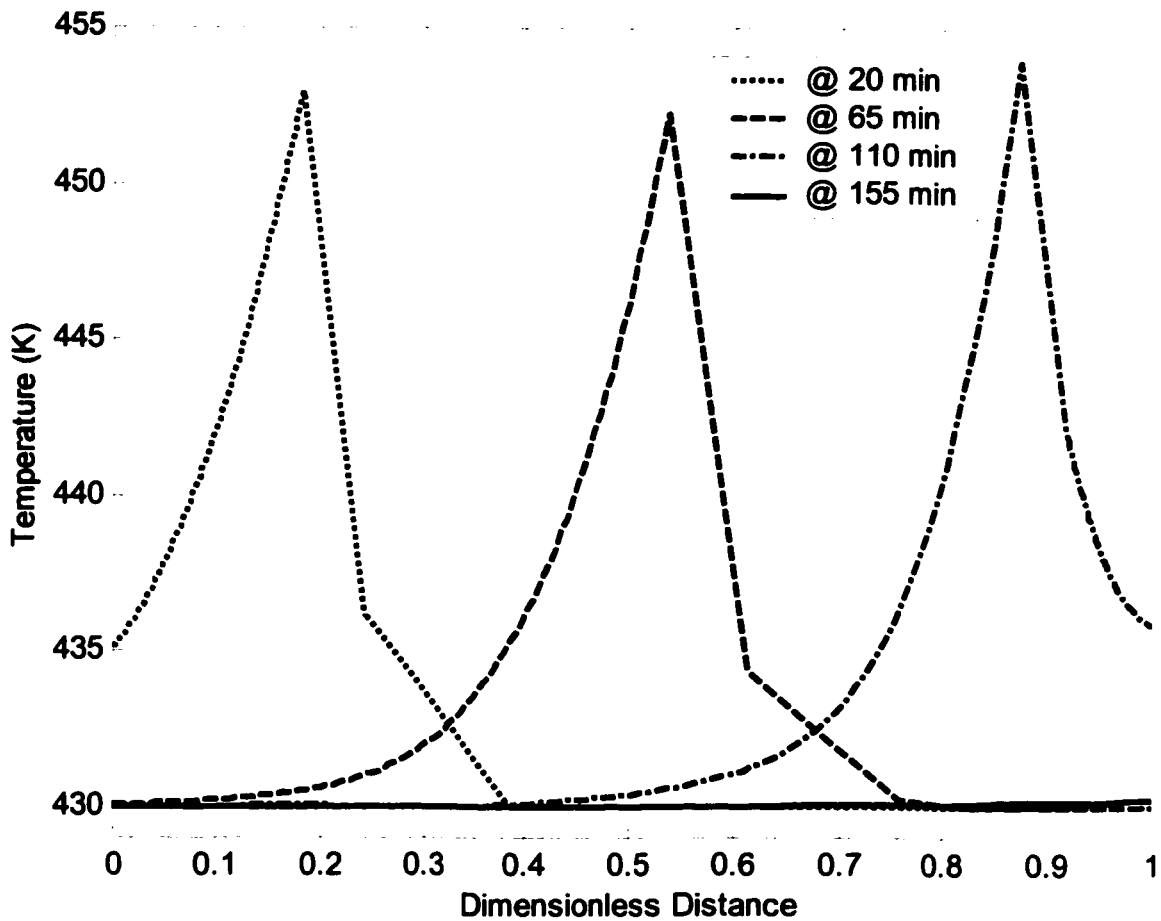

Figure 3.19. Temperature Profiles at Various Times during the Non-Adiabatic Adsorption Step. Parametric values are in Table 3.4.

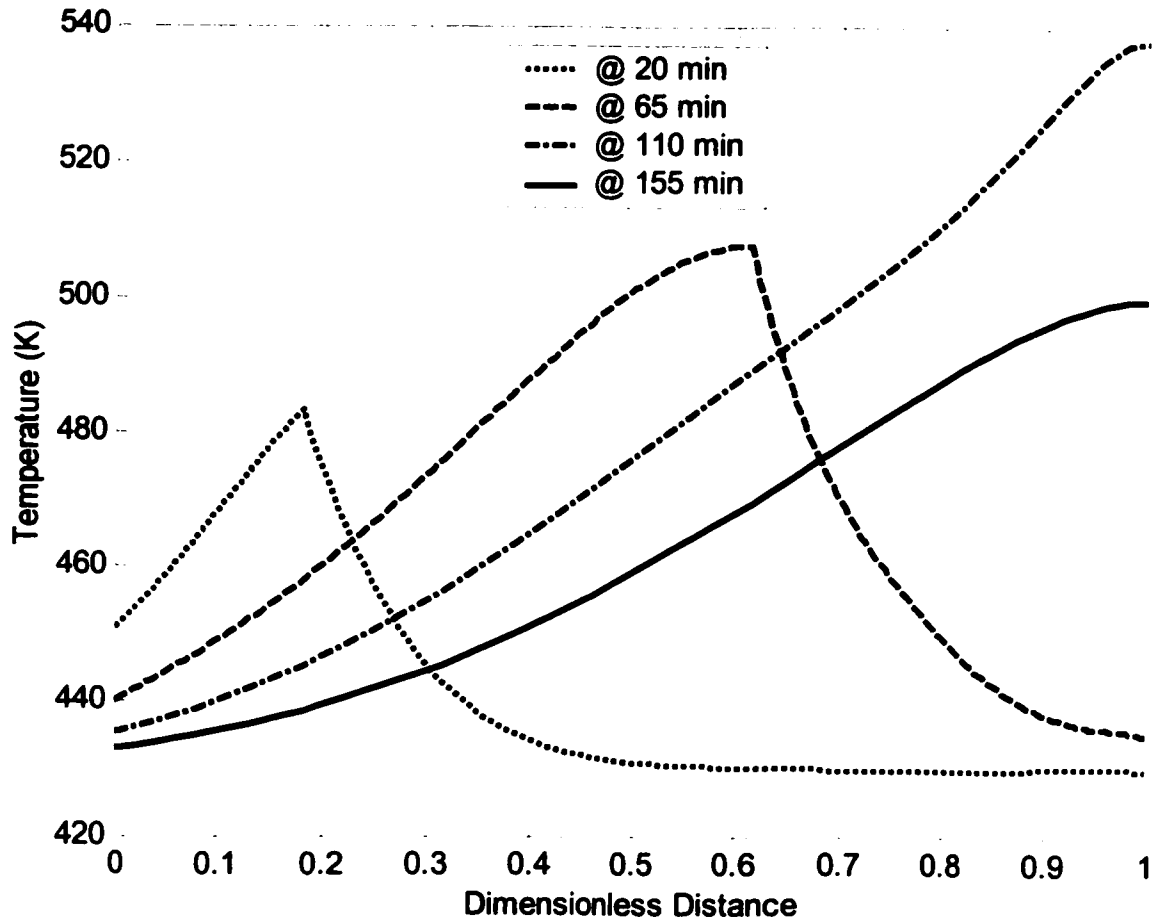

Figure 3.20. Temperature Profiles at Various Times during the Adiabatic Adsorption Step. Parametric values are in Table 3.4.

gases leaving the temperature front heat up the remaining portion of the bed before exiting and there is no mechanism to extract that energy away. In fact, a 110 K rise in temperature is observed.

When the bed is completely filled, it does not make any difference if it is regenerated in the same direction or the reverse. However, it does make a difference if only a portion of the bed is utilized. The desorbed *n*-pentane re-adsorbs in the remaining portion of the bed before exiting when purge flows in the same direction (Figure 3.21). This is totally unacceptable. On the contrary, the unused portion of the bed remains clean if purge passes in the opposite direction (Figure 3.22). Moreover, the *n*-pentane does not re-adsorb on its way out so that a larger quantity is desorbed by the reverse flow regeneration.

3.7b Catalyst Bed

The objective of this section is to give qualitative analysis of the reaction unit by considering various parameters listed in Table 3.5. The breakthrough curves for the three adiabatic reactor models *A*, *B* and *C* are shown in Figure 3.23. The models differ a lot in their dynamic performance but give the same steady state conversion. In effect, model *C* predicts a delayed breakthrough because of the adsorption capacitance term incorporated in it.

The need to have a reactor of sufficient length to get close to the equilibrium conversion is underlined in Figure 3.24. In theory, equilibrium values can only be attained using an infinitely long reactor. The effect of feed temperature on conversion is illustrated in Figure 3.25. A high temperature increases the rate of reaction to an extent

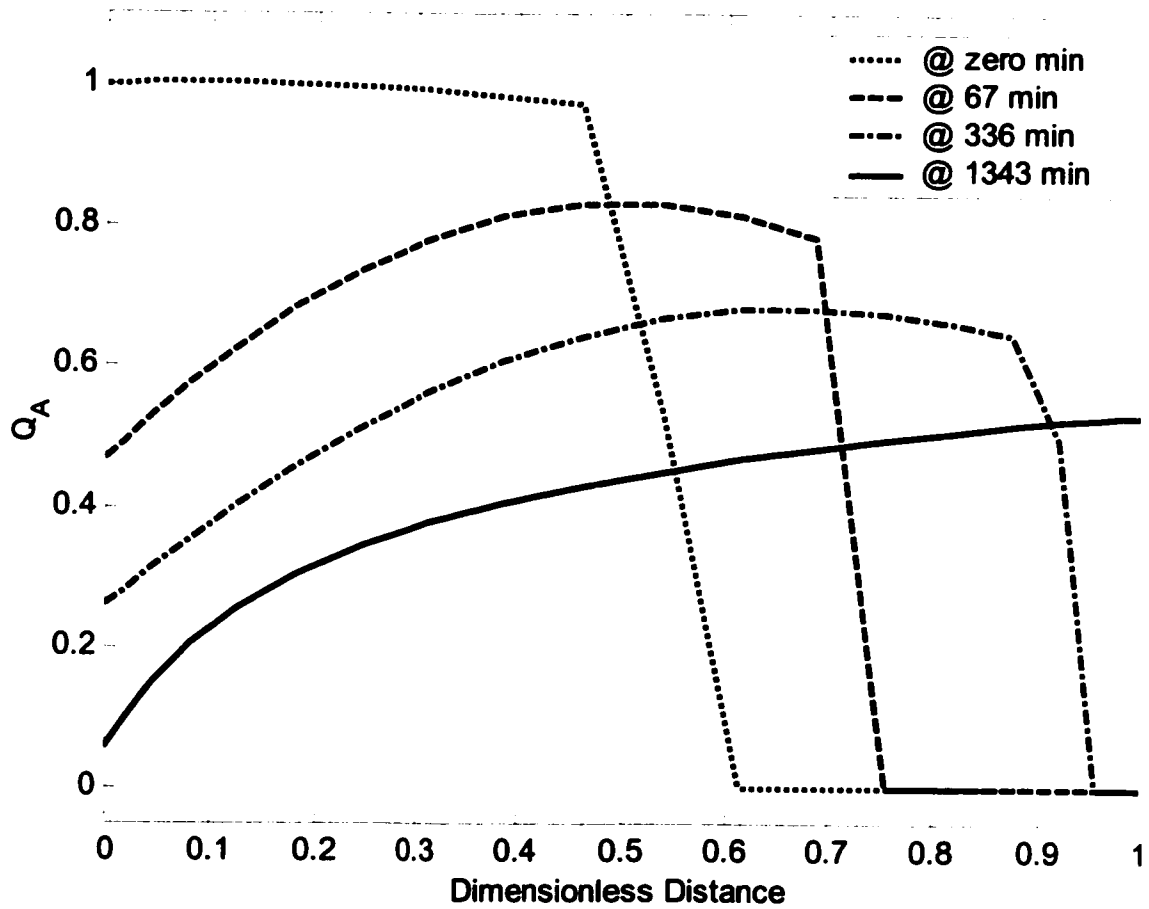

Figure 3.21. Adsorbed Phase Concentration Profiles at Various Times during the Regeneration Step @ 430 K in Forward Direction. Parametric values are in Table 3.4.

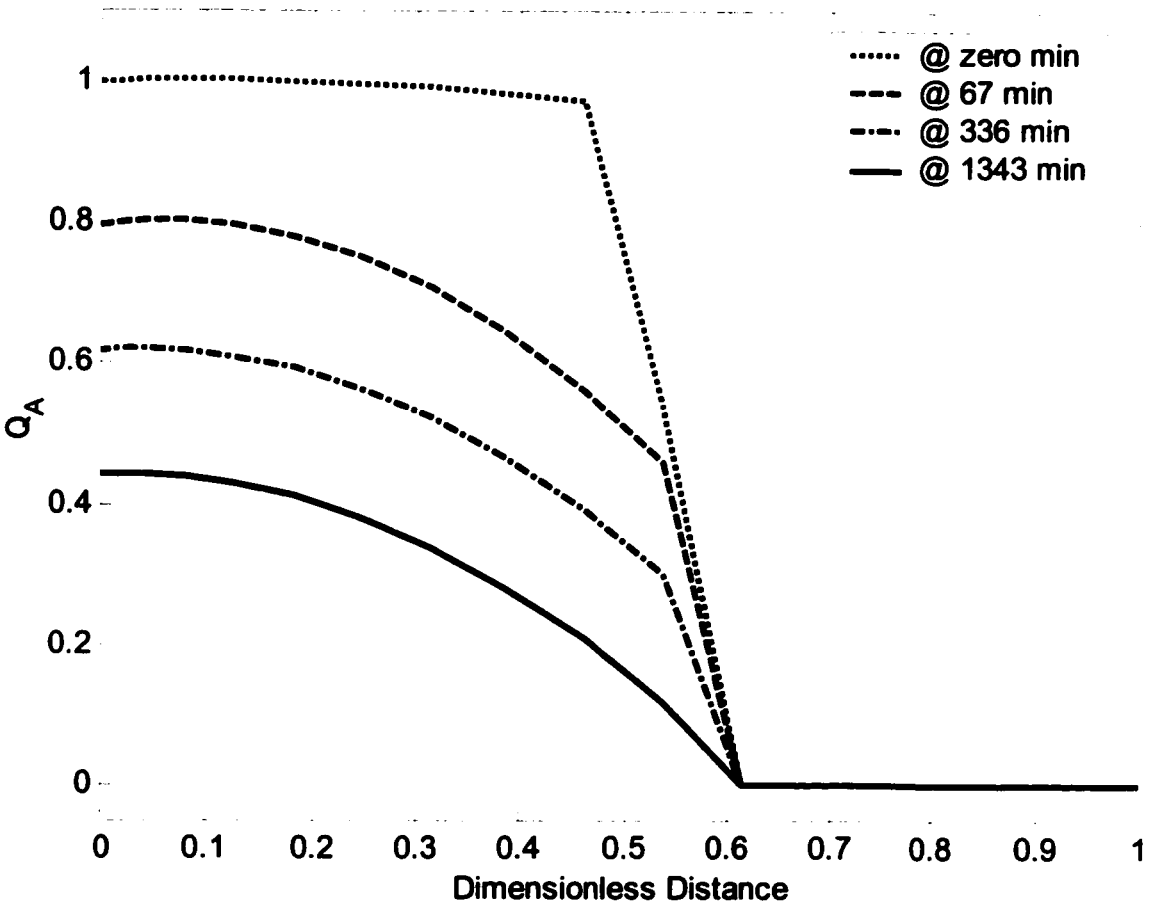

Figure 3.22. Adsorbed Phase Concentration Profiles at Various Times during the Regeneration Step @ 430 K in Reverse Direction. Parametric values are in Table 3.4.

Table 3.5. Parametric Values for Adiabatic Reactor Simulations @ 15 bar

Parameters	**Figure 3.24**	**Figure 3.25**	**Figure 3.26**
Varying parameter	L	T_f	y_{Af}
y_{Af} (y_{If} = 0.75)	0.125*	0.125	0.2475, 0.125, 0.0025
F_f (mol/m^2.s)	0.20*	0.20	0.20
T_f (K)	514*	464, 514, 573	514
$y_{A,eq}$	0.059	0.051, 0.059, 0.068	0.059
L (cm)	1.4, 5.6, 28*	28	28
k_{ref} (cm^3/g.s)	0.046*	9.28×10^{-4}, 0.046, 1.92	0.046
D_L (cm^2/s)	0.059*	0.051, 0.059, 0.070	0.059
K_{gl} (cm/s)^{B,C}	0.41*	0.35, 0.41, 0.48	0.41
K_L (W/m.K)	0.35*	0.35	0.35
C_{pg} (J/mol.K)	68.9*	65.5, 68.9, 72.8	68.9
Da	10.7*	0.24, 10.7, 398.5	10.7
Pe	4.21, 16.8, 84.1*	88.9, 84.1, 79.3	84.1
Pe_H	0.55, 2.21, 11.0*	10.5, 11.0, 11.6	11.0
σ^B	0.74*	0.74	0.74
$\zeta_m{}^C$	5.26*	5.77, 5.26, 4.46	5.83, 5.26, 1.51
$\zeta_H{}^{B,C}$	76.7*	72.9, 76.7, 81.0	76.7
$N_f^{B,C}$	2778*	2629, 2778, 2936	2778
$\gamma_f{}^C$	12.9*	14.3, 12.9, 11.6	12.9
γ_r	36.2*	40.1, 36.2, 32.5	36.2
$\theta_{ref}{}^C$	0.497*	0.604, 0.497, 0.378	0.552, 0.497, 0.143

*Note: Parameters marked with asterisks are also used for simulating plots in Figure 3.23.
B: Reactor Model *B*
C: Reactor Model *C*

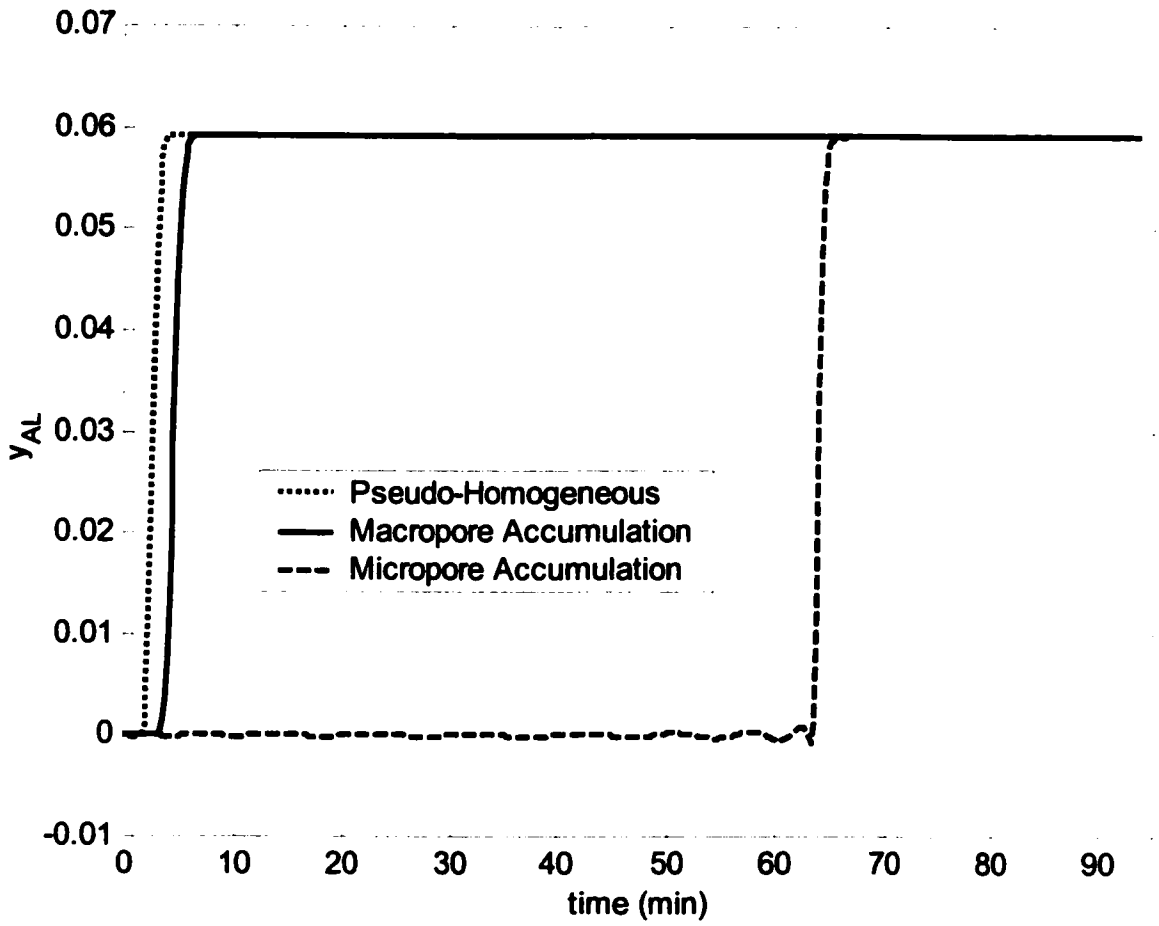

Figure 3.23. Breakthrough Curves for the Three Reactor Models. Parametric values are in Table 3.5.

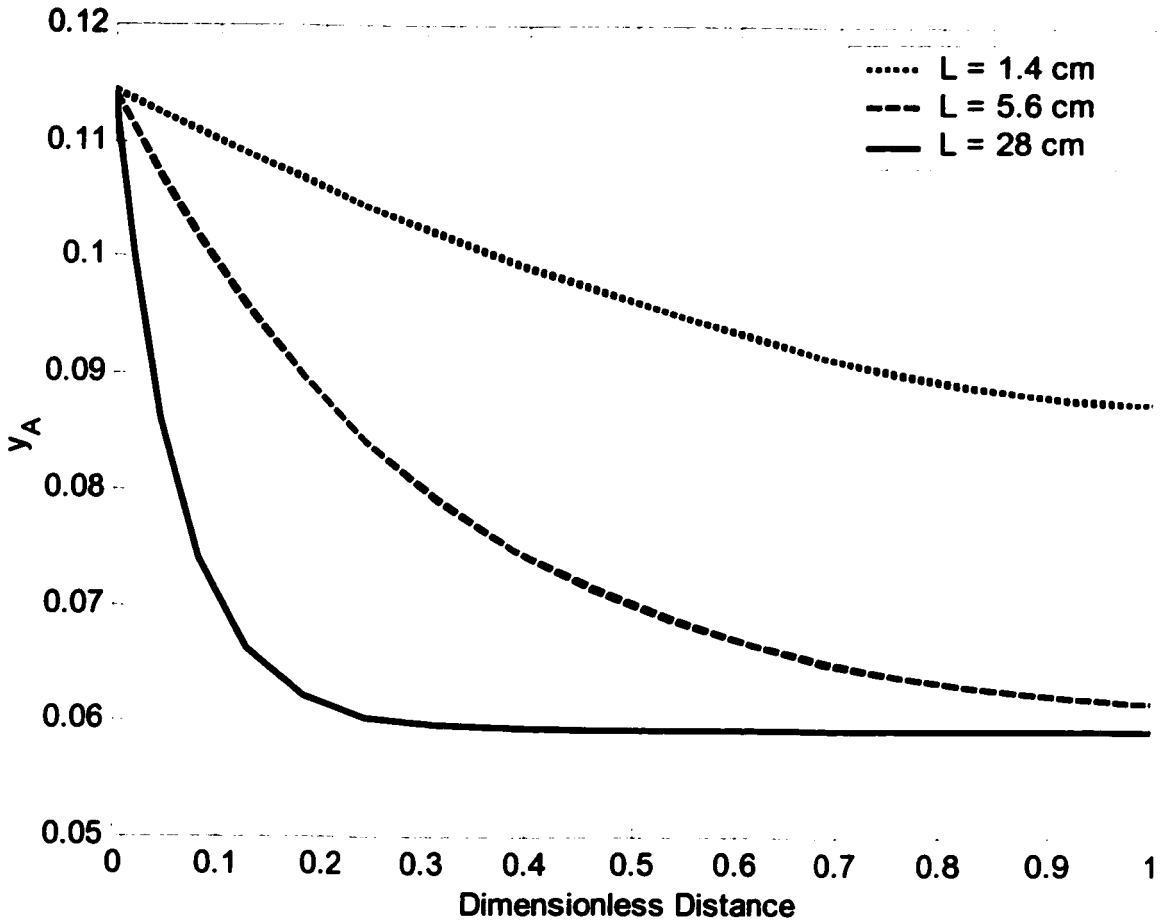

Figure 3.24. Effect of Column Length on Steady State Conversion for the Three Reactor Models (Results Overlap). Parametric values are in Table 3.5.

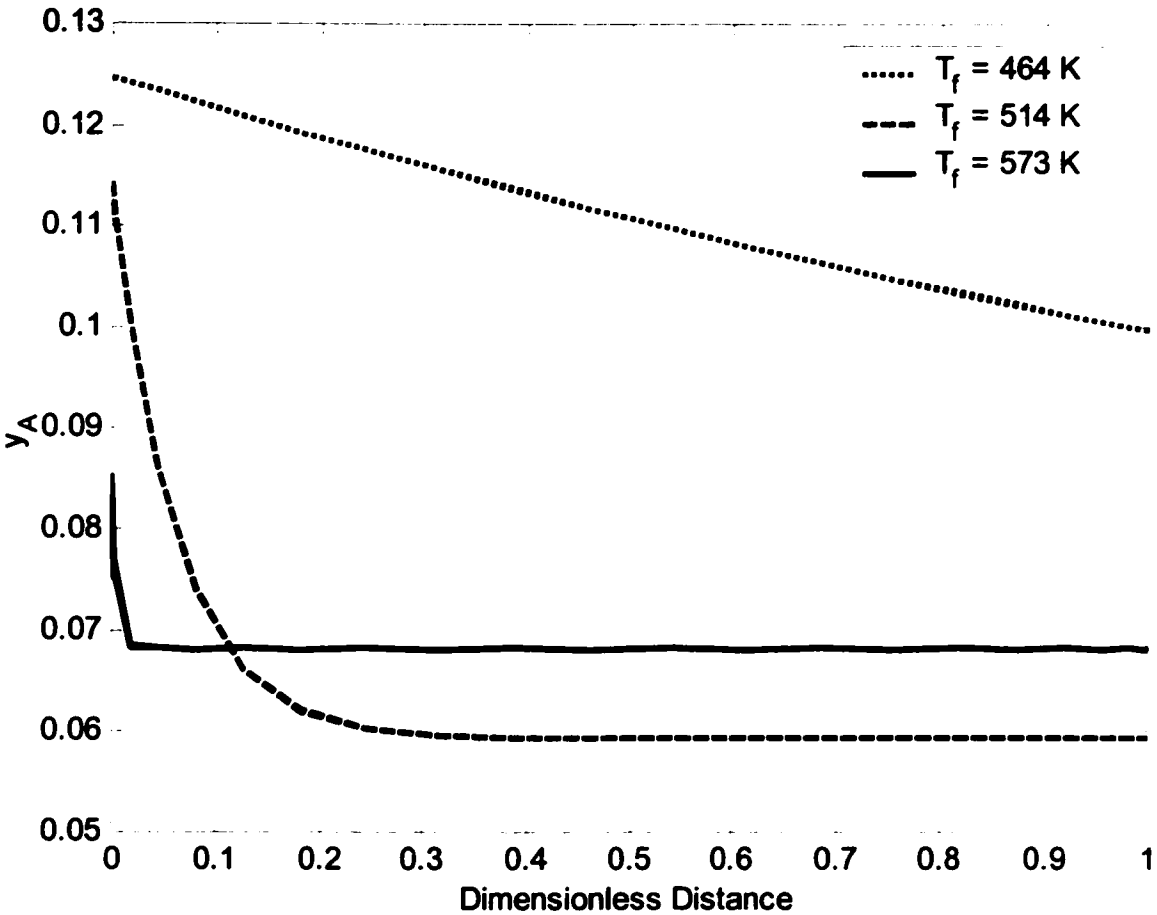

Figure 3.25. Effect of Feed Temperature on Steady State Conversion for the Three Reactor Models (Results Overlap). Parametric values are in Table 3.5.

that it completes near the entrance. At the same time, it reduces the equilibrium conversion. Low temperature, on the other hand, reduces reaction rate tremendously because of the high activation energy, thus lowering the conversion in a given reactor length. There thus exists an optimum temperature at which the conversion is maximum. 514 K appears to be close to that value and is thus preferred as the operating temperature of the reaction section in SMBR. The feed temperature has such a strong effect on conversion because the reactor is operated adiabatically and the heat effects due to reaction and sorption processes over the catalyst are neglected.

The outlet concentration of the reactant is not affected by its inlet concentration (y_{Af}) if the total feed hydrocarbon concentration ($y_{Af} + y_{Bf}$) is kept constant (Figure 3.26). This is because the steady state equilibrium concentration of *n*-pentane is calculated by the relation $(y_{Af} + y_{Bf})/(1+K)$. In fact reverse reaction takes place if reactant concentration is too low in the feed.

It should be noted that at steady state the three reactor models (*A*, *B* and *C*) give exactly the same concentration profiles. Thus, each curve in Figures 3.24 to 3.26 is essentially an overlap of three different curves. This infers an important conclusion that the steady state performance of the reactor depends upon its kinetic parameters and not upon the precise model employed.

3.7c Integrated Reactor-Adsorber

Before incorporating the adsorbent and catalyst beds in the SMBR it is helpful to first study a single reactor in series with an adsorber. Such a simple arrangement was also

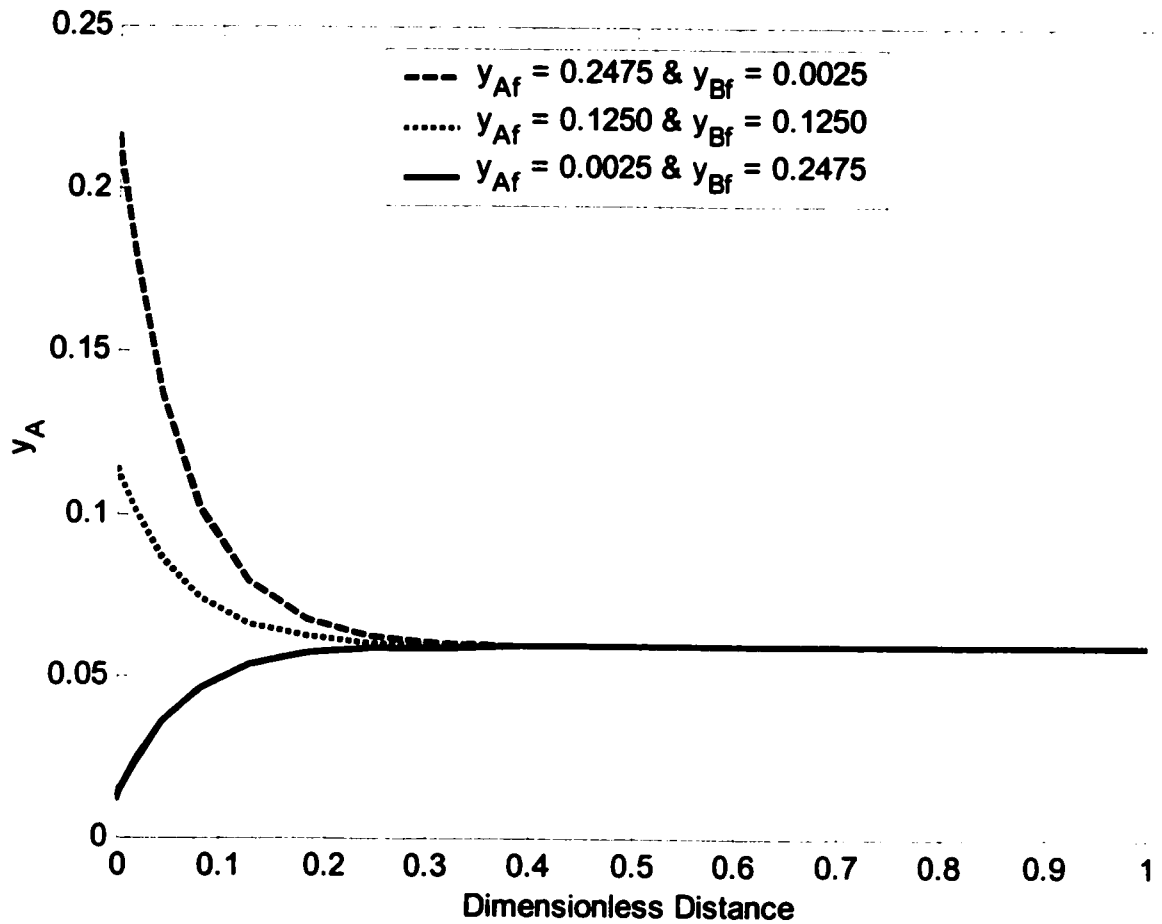

Figure 3.26. Effect of Feed Composition on Steady State Conversion for the Three Reactor Models (Results Overlap). Parametric values are in Table 3.5.

studied in the oxidative coupling of methane [34]. The parametric values for the present assembly are listed in Table 3.6.

The reactor is adiabatic as before and the adsorber has a constant wall temperature applied on it. Fresh feed enters the reaction section and the exit stream passes through the adsorbent bed. The supply of hydrocarbons is cutoff once the reactant breaks through the adsorber (at 324.5 min) but the hydrogen purge supply is retained. The normal and iso-pentanes are expected to breakthrough the reaction section simultaneously because the adsorption equilibrium constant K_{ads} is set equal for both. However, the isomer appears a lot faster in the final exit stream, as it is not adsorbed onto the adsorbent bed (Figure 3.27). Peak tailing takes place during desorption for isopentane as well because it is strongly adsorbed over the catalyst.

Gas phase concentration profiles for *n*-/iso- pentanes at a particular instant during the adsorption step are shown in Figure 3.28. The reaction takes place in the initial portion of the reactor suggesting that it is sufficient for the mixture to attain near equilibrium conditions. The equilibrium mole fraction of *n*-pentane is $y_{A,eq} = (y_{A,feed} + y_{B,feed})/(1+K) = 0.079$ and that of isopentane is $y_{B,eq} = (y_{A,feed} + y_{B,feed})K/(1+K) = 0.254$. The steep adsorption front at midway along the adsorber is also observed. The isopentane mole fraction in exit stream from the adsorbent bed prior to *n*-pentane breakthrough is thus $y_{B,eq}/(y_{B,eq} + y_{I,feed})$ $= 0.254/(0.254+0.667) = 0.276$.

The adsorbed phase concentration profiles are somewhat surprising (Figure 3.29). The gas phase concentration is higher in the reactor than in the adsorber and thus the

Table 3.6. Parametric Values for Integrated Reactor-Adsorber Simulations @ 15 bar (Figures 3.27 to 3.30)

Parameters	**Fresh Feed**	
	Adsorption	**Desorption**
$y_{A,feed} = y_{B,feed}$	0.167	0
F_{feed} (mol/m^2.s)	0.15	0.1
T_{feed} (K)	514	514
	Reference Parameters	
γ_f	12.9	
θ_{ref}	0.520	
	Reactor (Adiabatic, Model *C*)	
L_2 (cm)	28	
k_{ref} (cm^3/g.s)	0.046	
D_L (cm^2/s)	0.056	
K_{gl} (cm/s)	0.41	
K_L (W/m.K)	0.35	
C_{pg} (J/mol.K)	82.1	
Da	14.2	
Pe	67.1	
Pe_H	9.85	
ζ_m	5.50	
ζ_H	64.4	
N_f	3677	
γ_r	36.2	
υ	1.4	

Table 3.6. Parametric Values for Integrated Reactor-Adsorber Simulations @ 15 bar (Figures 3.27 to 3.30, continued)

Parameters	**Adsorber (Non-Adiabatic)**
T_w (K)	430
L_l (cm)	20
D_L (cm^2/s)	0.042
K_{gl} (cm/s)	0.31
K_L (W/m.K)	0.35
C_{pg} (J/mol.K)	74.2
h_w (W/m^2.K)	15
Pe	63.5
Pe_H	6.36
ζ_m	6.40
ζ_H	82.9
N_f	2809
N_w	32.2
B	0.112

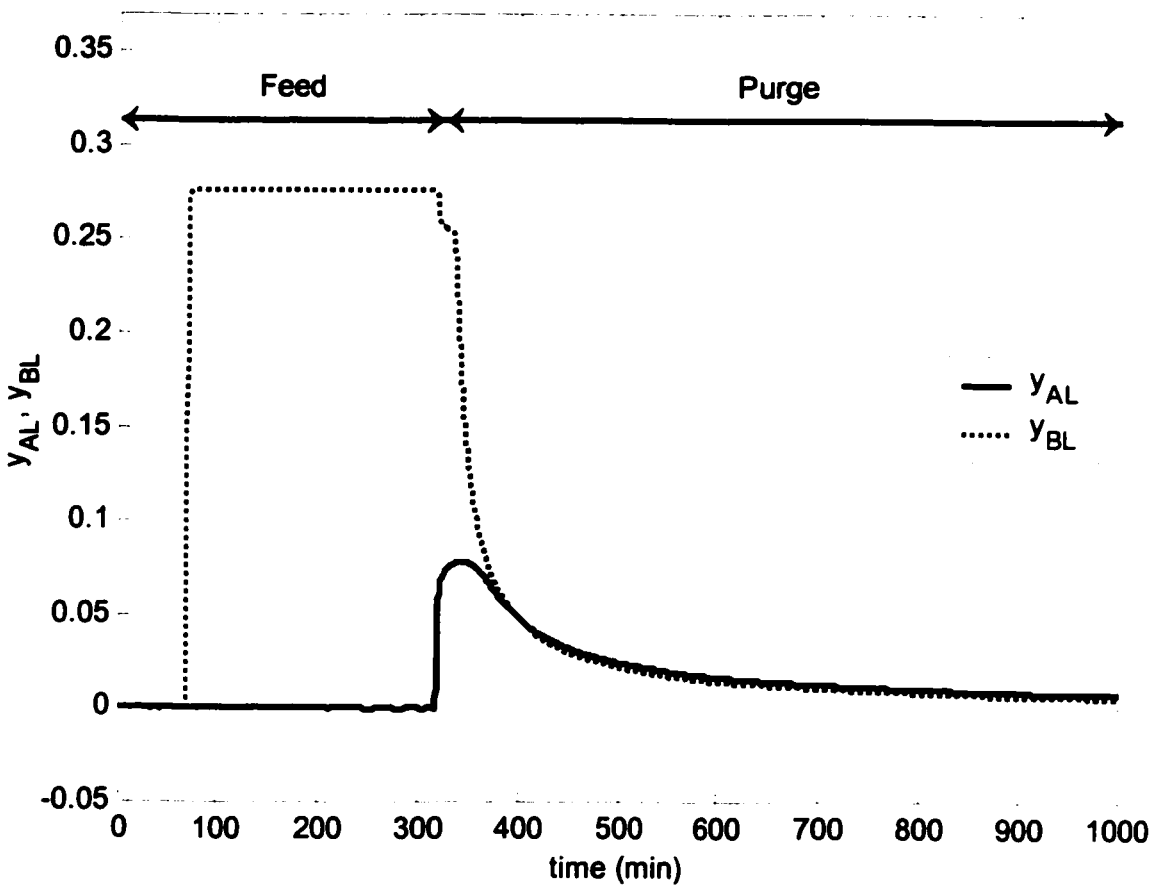

Figure 3.27. Adsorption and Desorption Curves for *n*-/iso- Pentanes in an Integrated Reactor-Adsorber Arrangement. Parametric values are in Table 3.6.

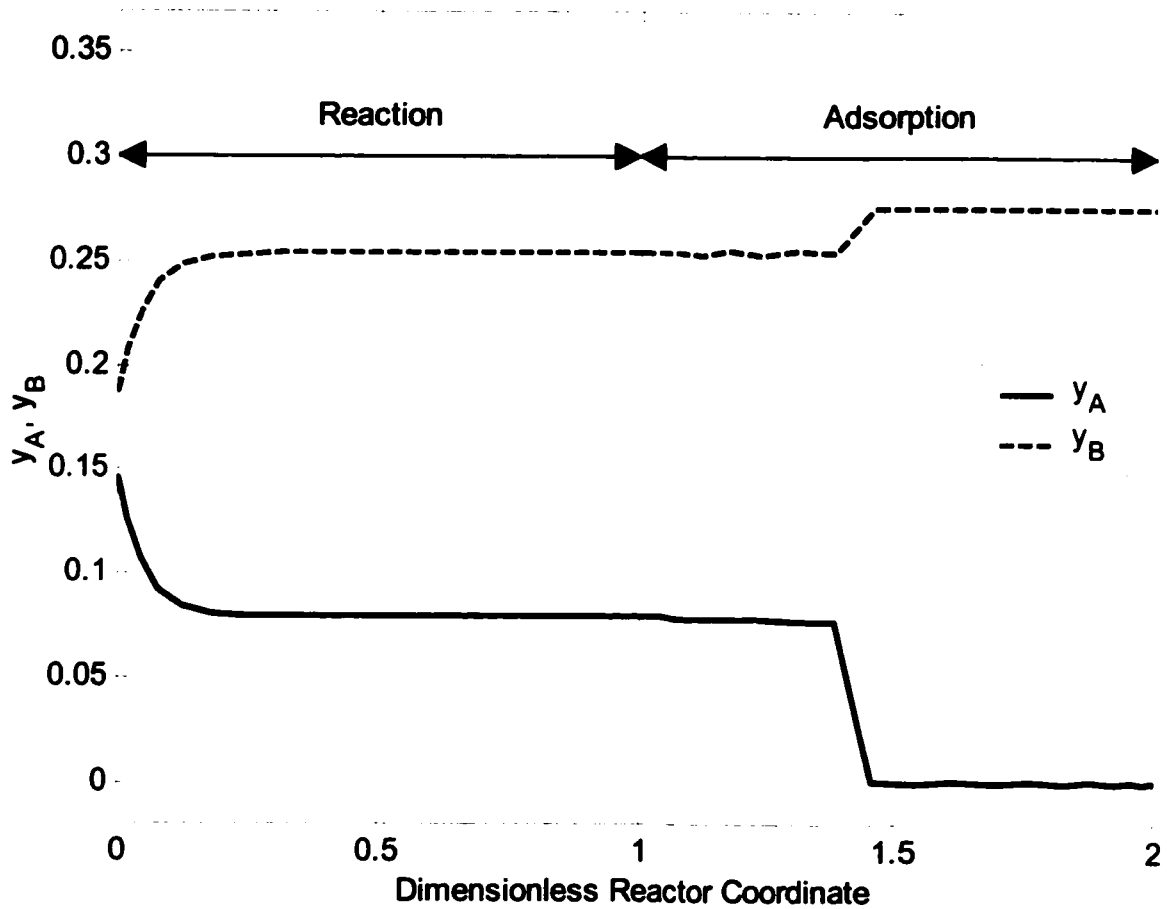

Figure 3.28. Concentration Profiles of *n*-/iso- Pentanes in an Integrated Reactor-Adsorber Arrangement @ 174.5 min. Parametric values are in Table 3.6.

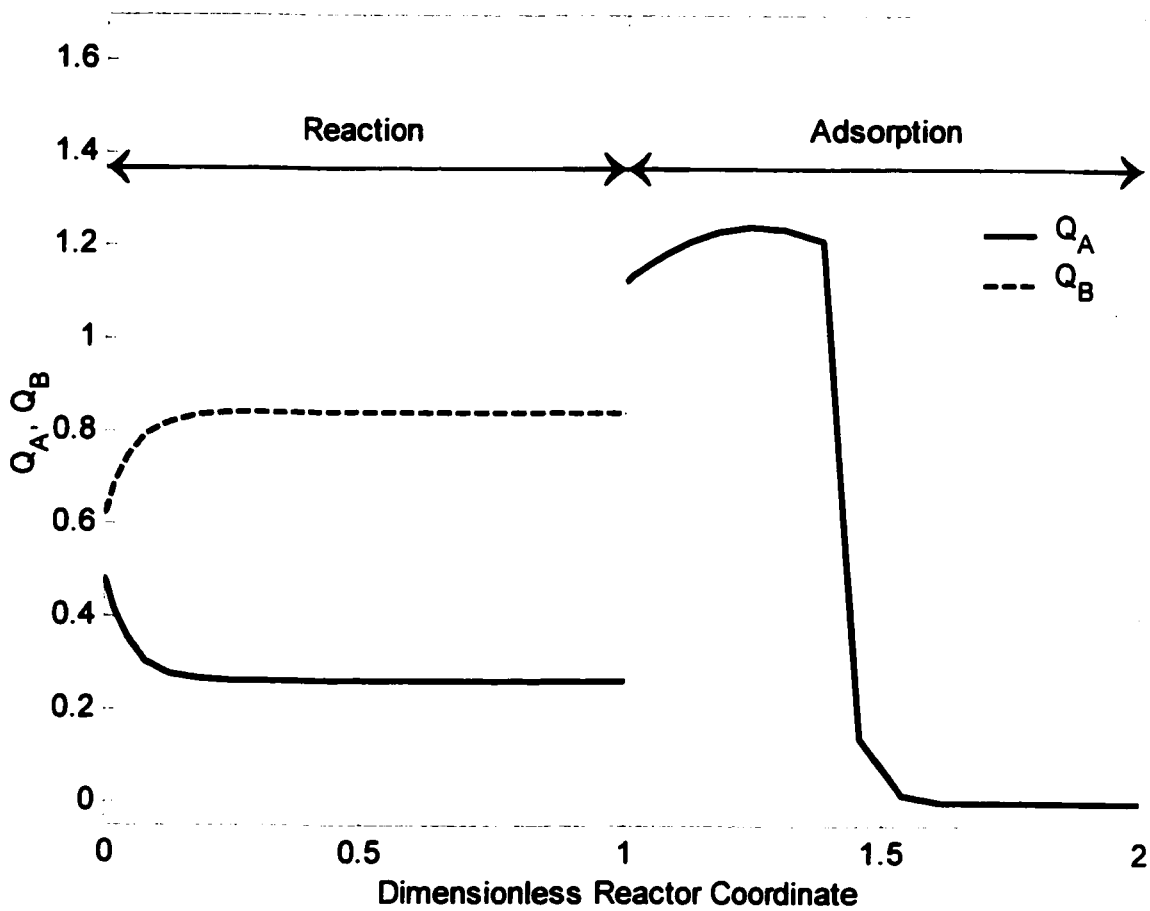

Figure 3.29. Adsorbed Phase Concentration Profiles of *n*-/iso- Pentanes in an Integrated Reactor-Adsorber Arrangement @ 174.5 min. Parametric values are in Table 3.6.

adsorbed phase concentration is also expected to behave in the same manner. The lower adsorbed phase concentration in the reactor however is explained by the fact that it undergoes reaction on the catalyst bed whereas it does not over the adsorbent bed. Moreover, both the reactant and the product share the catalyst in the adsorbed phase.

The adsorbed phase concentration is normalized by taking the fresh feed conditions as the reference parameters. However, the adsorber operates at a much lower temperature so that the *n*-pentane adsorbs more strongly in it. Thus, Q_A exceeds unity in the adsorber and this is yet another reason for the higher adsorbed phase concentration in the latter section.

The temperature profile is shown in Figure 3.30. Temperature remains uniform inside the reactor as the heat effects because of reaction and adsorption are neglected in the catalyst bed model. It however falls initially in the adsorber because of the low wall temperature before rising at the adsorption front. The heat transfer rate is not sufficient for the fluid temperature to drop instantaneously upon entrance to the wall temperature and as a result, the adsorbed phase concentration profile is not flat in that region.

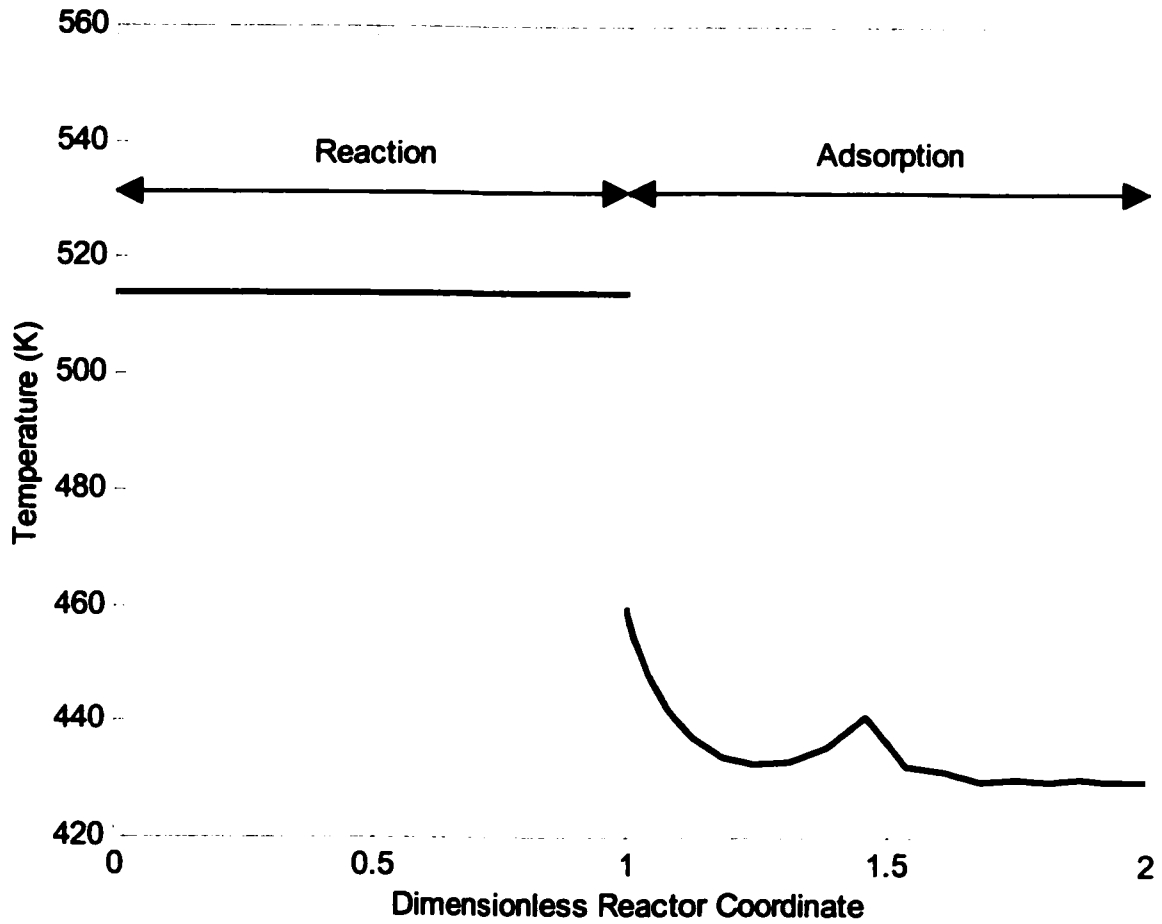

Figure 3.30. Temperature Profile in an Integrated Reactor-Adsorber Arrangement @ 174.5 min. Parametric values are in Table 3.6.

NOMENCLATURE

a_c	specific area of column [m^{-1}]
a_p	specific area of adsorbent or catalyst pellet [m^{-1}]
A	pseudo-homogeneous reactor model
A_{app}	apparent frequency factor [m^3/kg cat. s]
B	adiabatic temperature rise [$=(-\Delta H_{ads})q_{A,ref}/C_{ps}T_{ref}$] or heterogeneous reactor model with macropore accumulation
c_T	total gas concentration [mol/m^3]
c_{Tf}	total gas concentration in inlet stream [mol/m^3]
$c_{T,ref}$	total gas concentration at reference conditions [mol/m^3]
$\langle c_i \rangle$	macropore concentration of species i [mol/m^3]
C	heterogeneous reactor model with micropore accumulation
C_{pg}	heat capacity of gas [J/mol.K]
C_{ps}	heat capacity of solid [J/kg.K]
C_T	dimensionless total gas concentration [-]
d_c	column diameter [m]
d_p	pellet diameter [m]
D_L	axial mass dispersion coefficient [m^2/s]
D_m	molecular diffusivity [m^2/s]
D_p	macropore diffusivity [m^2/s]
Da	Damkohler number [$=(1-\varepsilon)\rho_a k_{ref} L_1/\varepsilon u_{ref}$]
E_{app}	apparent activation energy [J/mol]
F	total molar flux [mol/m^2.s]
F_{Af}	molar flux of component A in the inlet stream [mol/m^2.s]
F_m	molar flux of stream m (see Subscripts) [mol/m^2.s]
F_{ref}	reference total molar flux [mol/m^2.s]
$\bar{F}$	dimensionless total molar flux [-]

$\overline{F}_f$	dimensionless molar flux of the inlet stream [-]
h_w	wall heat transfer coefficient [W/m^2.K]
$-\Delta H_{ads}$	heat of adsorption [J/mol]
k	forward reaction rate constant [m^3/kg cat. s]
k_e	external mass-transfer coefficient [m/s]
k_i	internal mass-transfer coefficient [m/s]
k_{ref}	forward reaction rate constant at reference temperature [m^3/kg cat. s]
K	equilibrium reaction rate constant [-]
K_{ads}	adsorption equilibrium constant [Pa^{-1}]
K_{gl}	global mass-transfer coefficient [m/s]
K_L	effective axial bed thermal conductivity [W/m.K]
K_0	limiting adsorption equilibrium constant [Pa^{-1}]
L	length of vessel [m]
L_j	length of vessel j [m]
n	coefficient of Nitta *et al.* isotherm [-]
N	number of collocation points
N_f	number of film mass-transfer units [$=(1-\varepsilon)a_p K_{gl} L_1/\varepsilon u_{ref}$]
N_w	number of wall heat-transfer units [$=a_c h_w L_1/C_{pg} F_{ref}$]
P	total pressure in column [Pa]
ΔP	pressure drop in bed [Pa]
Pe_{Hj}	thermal Peclet number in vessel j [$=C_{pg} F_{ref} L_j/K_L$]
Pe_j	mass Peclet number in vessel j [$=u_{ref} L_j/D_L$]
$q_{A,ref}$	average adsorbed-phase concentration of component A in equilibrium with $y_{A,ref}$ at T_{ref} [mol/kg]
q_{max}	maximum adsorbed-phase concentration [mol/kg]
$\langle q_i \rangle$	average adsorbed-phase concentration of component i [mol/kg]
Q_i	dimensionless average adsorbed-phase concentration of component i [-]
$-r_A$	rate of reaction [mol/kg cat. s]

R	ideal gas law constant [J/mol.K]
R_p	pellet radius [m]
Re	Reynolds number [$= \rho \varepsilon u d_p / \mu$]
Sc	Schmidt number [$= \mu / \rho D_m$]
Sh	Sherwood number [$= k_e d_p / D_m$]
t	time [s]
T	temperature [K]
T_m	temperature of stream m (see Subscripts) [K]
T_{ref}	reference temperature [K]
T_w	wall temperature [K]
$\bar{T}$	dimensionless temperature [-]
$\bar{T}_f$	dimensionless temperature of inlet stream [-]
$\bar{T}_w$	dimensionless wall temperature [-]
u	interstitial velocity [m/s]
u_f	interstitial velocity of inlet stream [m/s]
u_{ref}	interstitial velocity at reference conditions [m/s]
x_j	dimensionless spatial coordinate in vessel j [-]
$y_{A,ref}$	mole fraction of A at reference conditions [-]
y_i	mole fraction of species i [-]
$y_{i,eq}$	equilibrium mole fraction of species i [-]
y_{im}	mole fraction of species i in stream m (see Subscripts) [-]
$\langle y_i \rangle$	average mole fraction of species i in macropores [-]
z	axial coordinate of column [m]

Greek Letters

ε	bed void fraction [-]
ε_p	particle porosity [-]

γ_f	dimensionless heat of adsorption $[=(-\Delta H_{ads})/RT_{ref}]$
γ_r	dimensionless activation energy $[=E_{app}/RT_{ref}]$
μ	gas viscosity [kg/m.s]
θ_i	fractional coverage of adsorbent with species i [-]
θ_{ref}	nonlinearity parameter of isotherm $[=q_{A,ref}/q_{\max}]$
ρ	gas density [kg/m^3]
ρ_a	apparent density of adsorbent or catalyst pellet [kg/m^3]
ρ_b	bulk density of catalyst bed [kg/m^3]
σ	macropore porosity per unit bed porosity $[=(1-\varepsilon)\varepsilon_p/\varepsilon]$
τ	dimensionless time [-]
τ_R	residence time of gas at steady state [s]
υ	length ratio $[=L_2/L_1]$
ζ_H	thermal capacity factor $[=(1-\varepsilon)\rho_a C_{ps}/\varepsilon c_{T,ref} C_{pg}]$
ζ_m	mass capacity factor $[=(1-\varepsilon)\rho_a q_{A,ref}/\varepsilon c_{T,ref}]$

Subscripts

ads	adsorbent
A	*n*-pentane
B	isopentane
f	inlet stream
feed	fresh feed stream
I	hydrogen
L	outlet stream
1	adsorber
2	reactor

CHAPTER 4

THE SIMULATED MOVING BED REACTOR FOR HYDROCARBON ISOMERIZATION

The simulated moving bed reactor (SMBR) consists of a catalyst bed connected to a cascade of adsorbent beds. Fresh feed containing *n*-/iso- pentanes in equimolar amounts enters the reaction section where *n*-pentane isomerizes into isopentane. The resulting stream passes through the adsorption section containing just one adsorbent bed where the *n*-pentane is retained. The isopentane leaves the system. The supply to the adsorbent bed is cutoff and diverted towards the next bed in series before the reactant breaks through. The filled bed now undergoes regeneration using a hydrogen purge. The exiting extract stream that contains the desorbed reactant and hydrogen is recycled, where it mixes with the fresh feed before entering the reaction section once again.

The adsorbent bed is simulated to travel through the regeneration section (Figure 4.1) until it reaches the end of the series and encounters pure hydrogen purge. It then undergoes maximum regeneration to get ready for the adsorption process in the following step, thus completing a cycle. Hydrogen exits the system via product stream that is partly condensed and flashed. The hydrogen is then recycled to the regeneration section after being heated to the required temperature.

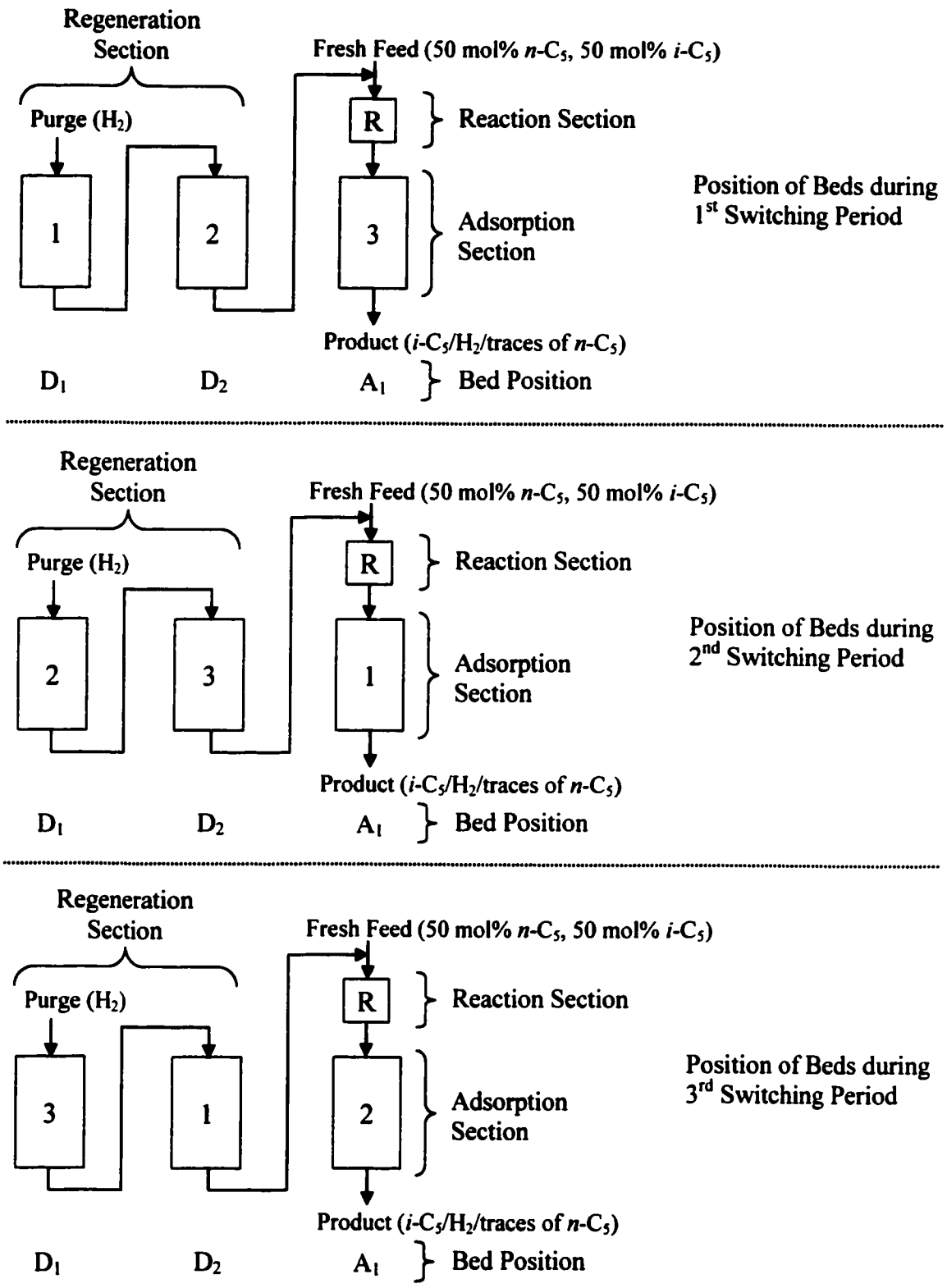

Figure 4.1. SMBR in Operation

4.1 MODEL EQUATIONS

The model equations for catalyst and adsorbent beds are the same as those developed in Chapter 3. However, the inlet quantities are different for each bed and need to be specified.

4.1a Regeneration Section

The adsorbent beds are connected end to end in the regeneration section so that the exit condition of a bed is also the inlet condition for the following bed in series. An assumption implicitly used here is that the tubes connecting the beds are at steady state and that no axial dispersion takes place through them. This is acceptable, as their diameter is small in relation to that of the adsorbers so that the fluid passes relatively fast through them. For regeneration section with n beds:

Bed position D_1:

$$\begin{aligned} y_{Af}^{D_1} &= 0 \\ y_{Bf}^{D_1} &= 0 \\ \overline{T}_f^{D_1} &= \overline{T}_{purge} \\ \overline{F}_f^{D_1} &= \overline{F}_{purge} \end{aligned} \tag{4.1}$$

Bed positions D_2 to D_n:

$$\begin{aligned} y_{Af}^{D_k} &= y_{A,exit}^{D_{k-1}} \\ y_{Bf}^{D_k} &= y_{B,exit}^{D_{k-1}} \\ \overline{T}_f^{D_k} &= \overline{T}_{exit}^{D_{k-1}} \\ \overline{F}_f^{D_k} &= \overline{F}_{exit}^{D_{k-1}} \end{aligned} \qquad k = 2,\ldots,n \tag{4.2}$$

4.1b Reaction Section

Feed to the reaction section is a mixture of fresh feed stream and the extract stream that exits the regeneration section. Assuming no accumulation at the mixing point the total material balance is:

$$F_f^R = F_{feed} + F_{extract} \tag{4.3a}$$

where $F_{extract} = F_{exit}^{D_n}$ (4.3b)

The reference molar flux for SMBR simulations is defined as the mixture of pure hydrogen purge and fresh feed streams, which is in effect the inlet stream to reaction section during the first switching period as pure hydrogen exits the regeneration section during that time:

$$F_{ref} = F_{feed} + F_{purge} \tag{4.4}$$

The dimensionless molar flux of fresh feed is consequently:

$$\overline{F}_{feed} = \frac{F_{feed}}{F_{ref}} = y_{HC}^0 \tag{4.5}$$

where y_{HC}^0 is the total mole fraction of hydrocarbons (normal and isomer) in the reference stream, i.e. the feed to the reaction section during the first switching period. Moreover, the mole fraction of *n*-pentane in this stream is taken as the reference mole fraction $y_{A,ref}$.

Equation 4.3a in the normalized form becomes:

$$\overline{F}_f^R = y_{HC}^0 + \overline{F}_{extract} \tag{4.6}$$

The material balances for normal and iso- pentanes at the mixing point while noting that the fresh feed is hydrogen free and contains equal number of moles of both is:

$$y_{Af}^{R} = \frac{0.5y_{HC}^{0} + \overline{F}_{extract}y_{A,extract}}{\overline{F}_{f}^{R}} \tag{4.7}$$

$$y_{Bf}^{R} = \frac{0.5y_{HC}^{0} + \overline{F}_{extract}y_{B,extract}}{\overline{F}_{f}^{R}} \tag{4.8}$$

Applying energy balance at the mixing point, the temperature of the resultant stream is:

$$T_{f}^{R} = \frac{F_{feed}\widetilde{C}_{p,feed}T_{feed} + F_{extract}\begin{pmatrix}(y_{A,extract} + y_{B,extract})\widetilde{C}_{p,HC_{extract}} \\ +(1 - y_{A,extract} - y_{B,extract})\widetilde{C}_{p,H_{2extract}}\end{pmatrix}T_{extract}}{F_{feed}\widetilde{C}_{p,feed} + F_{extract}\begin{pmatrix}(y_{A,extract} + y_{B,extract})\widetilde{C}_{p,HC_{extract}} \\ +(1 - y_{A,extract} - y_{B,extract})\widetilde{C}_{p,H_{2extract}}\end{pmatrix}} \tag{4.9a}$$

where the mean heat capacities of hydrocarbon and hydrogen in the extract stream are:

$$\widetilde{C}_{p,HC_{extract}} = \frac{\int_{T_f^R}^{T_{extract}} C_{p,HC}dT}{T_{extract} - T_f^R} \tag{4.9b}$$

$$\widetilde{C}_{p,H_{2extract}} = \frac{\int_{T_f^R}^{T_{extract}} C_{p,H_2}dT}{T_{extract} - T_f^R} \tag{4.9c}$$

and that of the fresh feed is:

$$\widetilde{C}_{p,feed} = \frac{\int_{T_{feed}}^{T_f^R} C_{p,HC}dT}{T_f^R - T_{feed}} \tag{4.9d}$$

The expressions for heat capacities of hydrogen and hydrocarbons are taken from Perry and Green [45]. The derivations for the above equations are shown in Appendix A.3.

A calculated fresh feed temperature (T_{feed}) is used so that the resulting temperature of the mixed stream (T_f^R) is exactly 514 K during the first switching period, which is the preferred reaction temperature as pointed out in Chapter 3. Thus unless otherwise stated, temperature of the reference stream (T_{ref}) is taken as 514 K for SMBR simulations. The mixed stream temperature (T_f^R) will however not remain constant at this value during subsequent switches because the extract stream temperature ($T_{extract}$) will drop due to desorption in the regeneration section. The heat capacity is not that sensitive to the changes in temperature and therefore, in order to avoid a trial and error solution for the above system, the mean heat capacities should be evaluated using the approximations $T_f^R \approx T_{ref}$ & $T_{extract} \approx T_{purge}$ before calculating the temperature of the mixed stream (T_f^R) via equation 4.9a. In normalized form, equation 4.9a is:

$$\overline{T}_f^R = \frac{y_{HC}^0 \widetilde{C}_{p,feed} \overline{T}_{feed} + \overline{F}_{extract} \begin{pmatrix} (y_{A,extract} + y_{B,extract}) \widetilde{C}_{p,HC_{extract}} \\ + (1 - y_{A,extract} - y_{B,extract}) \widetilde{C}_{p,H_{2extract}} \end{pmatrix} \overline{T}_{extract}}{y_{HC}^0 \widetilde{C}_{p,feed} + \overline{F}_{extract} \begin{pmatrix} (y_{A,extract} + y_{B,extract}) \widetilde{C}_{p,HC_{extract}} \\ + (1 - y_{A,extract} - y_{B,extract}) \widetilde{C}_{p,H_{2extract}} \end{pmatrix}} \tag{4.10}$$

The temperature of fresh feed stream (T_{feed}) is evaluated by applying an energy balance at the mixing point for the first switching period, i.e. when pure hydrogen exits the regeneration section:

$$F_{purge} \widetilde{C}_{p,purge} (T_{purge} - T_{ref}) = F_{feed} \widetilde{C}_{p,feed} (T_{ref} - T_{feed}) \tag{4.11a}$$

$$\tilde{C}_{p,feed} = \frac{\int_{T_{feed}}^{T_{ref}} C_{p,HC} dT}{T_{ref} - T_{feed}} \tag{4.11b}$$

$$\tilde{C}_{p,purge} = \frac{\int_{T_{ref}}^{T_{purge}} C_{p,H_2} dT}{T_{purge} - T_{ref}} \tag{4.11c}$$

The system is nonlinear but needs to be solved only once, as the fresh feed temperature is held constant during the SMBR simulation. T_{feed} depends upon the inlet flow rates, inlet purge temperature (T_{purge}) and the approximate reaction temperature, i.e. T_{ref}.

One might be eager to examine the performance of the reaction section separately. This can be done by calculating the single pass conversion. Since the process is at unsteady state, the concentrations keep changing with time and therefore only an average value can be measured. The mean concentration during a switching period is defined as the value that would be obtained if the stream were thoroughly mixed in a tank. The single pass conversion of the reactant is therefore:

$$\text{Single Pass Conversion} = 1 - \frac{\int_0^{\tau_s'} \bar{F}_{exit}^R y_{A,exit}^R \, d\tau}{\int_0^{\tau_s'} \bar{F}_f^R y_{Af}^R d\tau} \tag{4.12}$$

4.1c Adsorption Section

The inlet condition to adsorption section is the outlet condition of reaction section:

$$
\begin{aligned}
y_{Af}^{A_1} &= y_{A,exit}^{R} \\
y_{Bf}^{A_1} &= y_{B,exit}^{R} \\
\overline{T}_f^{A_1} &= \overline{T}_{exit}^{R} \\
\overline{F}_f^{A_1} &= \overline{F}_{exit}^{R}
\end{aligned}
\tag{4.13}
$$

During the first switching period, the gas and solid phases are initially clean and hence their initial concentration is zero. Moreover, the initial temperature in the regeneration section is equal to the inlet purge temperature and that of the reaction and adsorption sections depends upon the mode of operation and is stated in the next section.

The adsorbent beds are simulated to move countercurrent to fluid flow during subsequent switches, which is mathematically expressed for the lth switching as:

For bed positions D_1 to D_{n-1}:

$$
\begin{aligned}
y_A^{D_k}\left(x_1, \tau = \left[(l-1)\cdot\tau_s'\right]^+\right) &= y_A^{D_{k+1}}\left(x_1, \tau = \left[(l-1)\cdot\tau_s'\right]^-\right) \\
y_B^{D_k}\left(x_1, \tau = \left[(l-1)\cdot\tau_s'\right]^+\right) &= y_B^{D_{k+1}}\left(x_1, \tau = \left[(l-1)\cdot\tau_s'\right]^-\right) \qquad k = 1,\ldots,n-1 \\
Q_A^{D_k}\left(x_1, \tau = \left[(l-1)\cdot\tau_s'\right]^+\right) &= Q_A^{D_{k+1}}\left(x_1, \tau = \left[(l-1)\cdot\tau_s'\right]^-\right) \qquad l = 2,3,\ldots \\
\overline{T}^{D_k}\left(x_1, \tau = \left[(l-1)\cdot\tau_s'\right]^+\right) &= \overline{T}^{D_{k+1}}\left(x_1, \tau = \left[(l-1)\cdot\tau_s'\right]^-\right)
\end{aligned}
\tag{4.14}
$$

For bed position D_n, when the adsorbent bed is shifted from the adsorption section (position A_1) to the regeneration section:

$$\begin{aligned} y_A^{D_n}\left(x_1,\tau=\left[(l-1)\cdot\tau_s'\right]^+\right) &= y_A^{A_1}\left(x_1,\tau=\left[(l-1)\cdot\tau_s'\right]^-\right) \\ y_B^{D_n}\left(x_1,\tau=\left[(l-1)\cdot\tau_s'\right]^+\right) &= y_B^{A_1}\left(x_1,\tau=\left[(l-1)\cdot\tau_s'\right]^-\right) \\ Q_A^{D_n}\left(x_1,\tau=\left[(l-1)\cdot\tau_s'\right]^+\right) &= Q_A^{A_1}\left(x_1,\tau=\left[(l-1)\cdot\tau_s'\right]^-\right) \\ \bar{T}^{D_n}\left(x_1,\tau=\left[(l-1)\cdot\tau_s'\right]^+\right) &= \bar{T}^{A_1}\left(x_1,\tau=\left[(l-1)\cdot\tau_s'\right]^-\right) \end{aligned} \qquad l=2,3,\ldots \tag{4.15}$$

For bed position A_1, when the adsorbent bed is shifted from the regeneration section (position D_1) to the adsorption section:

$$\begin{aligned} y_A^{A_1}\left(x_1,\tau=\left[(l-1)\cdot\tau_s'\right]^+\right) &= y_A^{D_1}\left(x_1,\tau=\left[(l-1)\cdot\tau_s'\right]^-\right) \\ y_B^{A_1}\left(x_1,\tau=\left[(l-1)\cdot\tau_s'\right]^+\right) &= y_B^{D_1}\left(x_1,\tau=\left[(l-1)\cdot\tau_s'\right]^-\right) \\ Q_A^{A_1}\left(x_1,\tau=\left[(l-1)\cdot\tau_s'\right]^+\right) &= Q_A^{D_1}\left(x_1,\tau=\left[(l-1)\cdot\tau_s'\right]^-\right) \\ \bar{T}^{A_1}\left(x_1,\tau=\left[(l-1)\cdot\tau_s'\right]^+\right) &= \bar{T}^{D_1}\left(x_1,\tau=\left[(l-1)\cdot\tau_s'\right]^-\right) \end{aligned} \qquad l=2,3,\ldots \tag{4.16}$$

When reverse flow regeneration is employed, only one bed is used in the regeneration section (Figure 4.2). Moreover, the adsorbent beds rotate each time they shift from one section to the other, which is mathematically expressed for the lth switching as:

For bed position D_1, when the adsorbent bed is shifted from the adsorption section (position A_1) to the regeneration section:

$$\begin{aligned} y_A^{D_1}\left(x_1,\tau=\left[(l-1)\cdot\tau_s'\right]^+\right) &= y_A^{A_1}\left(x_1',\tau=\left[(l-1)\cdot\tau_s'\right]^-\right) \\ y_B^{D_1}\left(x_1,\tau=\left[(l-1)\cdot\tau_s'\right]^+\right) &= y_B^{A_1}\left(x_1',\tau=\left[(l-1)\cdot\tau_s'\right]^-\right) \\ Q_A^{D_1}\left(x_1,\tau=\left[(l-1)\cdot\tau_s'\right]^+\right) &= Q_A^{A_1}\left(x_1',\tau=\left[(l-1)\cdot\tau_s'\right]^-\right) \\ \bar{T}^{D_1}\left(x_1,\tau=\left[(l-1)\cdot\tau_s'\right]^+\right) &= \bar{T}^{A_1}\left(x_1',\tau=\left[(l-1)\cdot\tau_s'\right]^-\right) \end{aligned} \qquad l=2,3,\ldots \tag{4.17}$$

where $x_1' = 1 - x_1$.

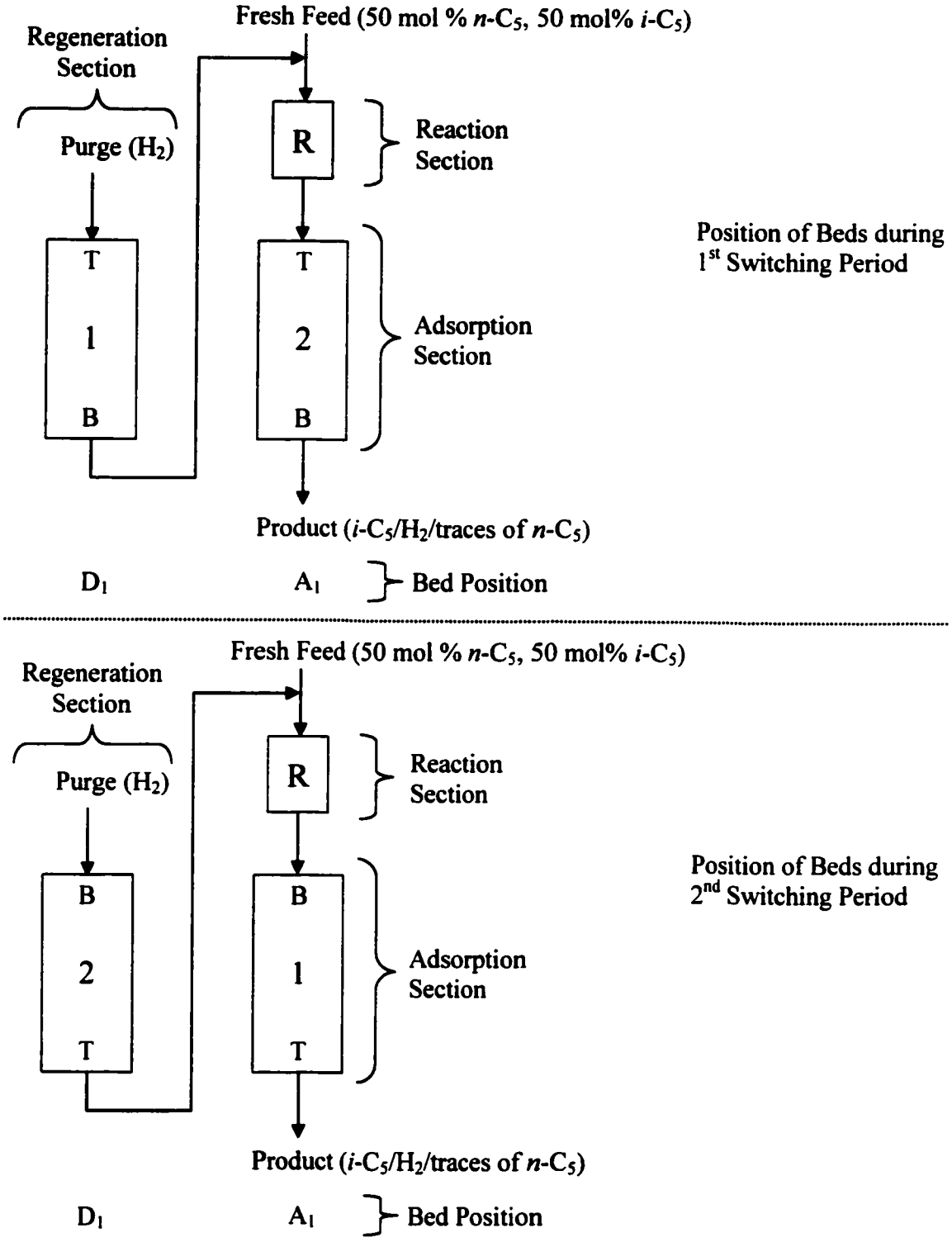

Figure 4.2. SMBR with Reverse Flow Regeneration

For bed position A_1, when the adsorbent bed is shifted from the regeneration section (position D_1) to the adsorption section:

$$\begin{aligned} y_A^{A_1}\left(x_1, \tau = \left[(l-1)\cdot\tau_s'\right]^+\right) &= y_A^{D_1}\left(x_1', \tau = \left[(l-1)\cdot\tau_s'\right]^-\right) \\ y_B^{A_1}\left(x_1, \tau = \left[(l-1)\cdot\tau_s'\right]^+\right) &= y_B^{D_1}\left(x_1', \tau = \left[(l-1)\cdot\tau_s'\right]^-\right) \\ Q_A^{A_1}\left(x_1, \tau = \left[(l-1)\cdot\tau_s'\right]^+\right) &= Q_A^{D_1}\left(x_1', \tau = \left[(l-1)\cdot\tau_s'\right]^-\right) \\ \overline{T}^{A_1}\left(x_1, \tau = \left[(l-1)\cdot\tau_s'\right]^+\right) &= \overline{T}^{D_1}\left(x_1', \tau = \left[(l-1)\cdot\tau_s'\right]^-\right) \end{aligned} \qquad l = 2,3,\ldots \tag{4.18}$$

The only outlet from the system is the raffinate product stream exiting the adsorption section. It mainly consists of the isomer and hydrogen along with small quantities of *n*-pentane that constitutes the impurity. The purity of the product is measured by the amount of isomers present in the hydrocarbon fraction of the stream:

$$\text{Purity} = \frac{\int_0^{\tau_s'} \overline{F}_{exit}^{A_1} y_{B,exit}^{A_1} d\tau}{\int_0^{\tau_s'} \overline{F}_{exit}^{A_1}\left(y_{A,exit}^{A_1} + y_{B,exit}^{A_1}\right) d\tau} \tag{4.19}$$

The overall conversion is calculated as:

$$\begin{aligned} \text{Overall Conversion} &= \frac{F_{feed} y_{A,feed} \tau_s - \int_0^{\tau_s} F_{exit}^{A_1} y_{A,exit}^{A_1} dt}{F_{feed} y_{A,feed} \tau_s} \\ &= 1 - \frac{\int_0^{\tau_s'} \overline{F}_{exit}^{A_1} y_{A,exit}^{A_1} d\tau}{0.5 y_{HC}^0 \tau_s'} \end{aligned} \tag{4.20}$$

The average temperature of a stream during a switching period is defined as the final temperature that would be obtained if it were collected and mixed in an adiabatic tank at constant pressure:

$$T_{mean} = \frac{\int_0^{\tau_s} F \cdot \left((y_A + y_B) \cdot C_{p,HC} + (1 - y_A - y_B) \cdot C_{p,H_2} \right) T dt}{\int_0^{\tau_s} F \cdot \left((y_A + y_B) \cdot C_{p,HC} + (1 - y_A - y_B) \cdot C_{p,H_2} \right) dt} \tag{4.21}$$

The derivation is shown in Appendix A.4. The heat capacities are evaluated at the "arithmetic mean temperature" before calculating the "average temperature" of the stream via the above expression.

4.2 RESULTS AND DISCUSSION

In this section, the simulated moving bed reactor (SMBR) is studied using various parameters. In each case, the objective is to obtain the maximum purity possible. Since the total isomerization process produces a 100% pure product, a target of >99% purity is set for this study. At first, an isothermal process is considered.

4.2a Isothermal Operation

For isothermal process, only the material balance equations need to be solved. Moreover, the adsorption equilibrium constant (K_{ads}), the forward reaction rate constant (k), the equilibrium reaction rate constant (K) and the total gas concentration (c_T) are all constant at the given operating temperature. The various isothermal cases examined are summarized in Table 4.1 and the parametric values used for their simulations in Tables 4.2 to 4.4. The specification of an SMBR is incomplete without mentioning its switch

Table 4.1. Cases for Isothermal and Adiabatic SMBR Simulations

Case	Regeneration Beds	T_{feed} (K)	T_{purge} (K)	Model	Purge Direction	Parametric Values
1	1	514	514	isothermal	forward	Table 4.2
2*	2	514	514	isothermal	forward	Table 4.2
3	3	514	514	isothermal	forward	Table 4.2
4	2	540	540	isothermal	forward	Table 4.3
5	2	573	573	isothermal	forward	Table 4.4
6	1	514	514	isothermal	reverse	Table 4.2
7	2	calc	540	adiabatic	forward	Table 4.6

*Base case for isothermal operations

Note: For all the above cases, equimolar fresh feed and reactor model C are used with P = 15 bar and L_2 = 28 cm.

Table 4.2. Parametric Values for Isothermal SMBR Simulations (Cases 1, 2, 3 & 6)

Run	**1**	**2**	**3**	**4**	**5**	**6**
Parameters	**Inlet Streams**					
F_{feed} (mol/m^2.s)	0.05	0.05	0.05	0.05	0.05	0.05
F_{purge} (mol/m^2.s)	0.15	0.20	0.25	0.30	0.35	0.40
$T_{feed} = T_{purge}$ (K)	514	514	514	514	514	514
	Common Parameters					
$y_{A,ref}$	0.125	0.100	0.083	0.071	0.063	0.056
F_{ref} (mol/m^2.s)	0.20	0.25	0.30	0.35	0.40	0.45
K_{ads} (bar^{-1})	8.24	8.24	8.24	8.24	8.24	8.24
D_L (cm^2/s)	0.059	0.063	0.066	0.070	0.074	0.077
K_{gl} (cm/s)	0.41	0.41	0.42	0.42	0.42	0.42
N_f	2778	2236	1874	1614	1419	1267
θ_{ref}	0.497	0.478	0.462	0.449	0.437	0.426
	Adsorbent Bed					
Pe	60.1	70.9	80.5	89.1	96.9	104
ζ_m	6.12	5.89	5.69	5.53	5.38	5.25
	Catalyst Bed (Model *C*)					
k (cm^3/g.s)	0.046	0.046	0.046	0.046	0.046	0.046
K	3.22	3.22	3.22	3.22	3.22	3.22
Da	10.7	8.53	7.10	6.09	5.33	4.74
Pe	84.1	99.2	112.7	124.7	135.7	145.6
ζ_m	5.26	5.06	4.89	4.75	4.62	4.51
υ	1.4	1.4	1.4	1.4	1.4	1.4

Table 4.3. Parametric Values for Isothermal SMBR Simulations (Case 4)

Run	**1**	**2**	**3**	**4**	**5**	**6**
Parameters	**Inlet Streams**					
F_{feed} (mol/m^2.s)	0.05	0.05	0.05	0.05	0.05	0.05
F_{purge} (mol/m^2.s)	0.15	0.20	0.25	0.30	0.35	0.40
$T_{feed} = T_{purge}$ (K)	540	540	540	540	540	540
	Common Parameters					
$y_{A,ref}$	0.125	0.100	0.083	0.071	0.063	0.056
F_{ref} (mol/m^2.s)	0.20	0.25	0.30	0.35	0.40	0.45
K_{ads} (bar^{-1})	4.42	4.42	4.42	4.42	4.42	4.42
D_L (cm^2/s)	0.064	0.068	0.071	0.075	0.079	0.083
K_{gl} (cm/s)	0.44	0.45	0.45	0.45	0.45	0.46
N_f	2857	2300	1927	1660	1459	1302
θ_{ref}	0.443	0.423	0.407	0.392	0.380	0.369
	Adsorbent Bed					
Pe	58.5	69.1	78.6	87.1	94.8	101.8
ζ_m	5.73	5.47	5.27	5.07	4.92	4.77
	Catalyst Bed (Model *C*)					
k (cm^3/g.s)	0.263	0.263	0.263	0.263	0.263	0.263
K	2.95	2.95	2.95	2.95	2.95	2.95
Da	58.0	46.4	38.7	33.2	29.0	25.8
Pe	81.9	96.7	110	121.9	132.7	142.6
ζ_m	4.92	4.70	4.52	4.36	4.22	4.10
υ	1.4	1.4	1.4	1.4	1.4	1.4

Table 4.4. Parametric Values for Isothermal SMBR Simulations (Case 5)

Run	**1**	**2**	**3**	**4**	**5**	**6**
Parameters	**Inlet Streams**					
F_{feed} (mol/m^2.s)	0.05	0.05	0.05	0.05	0.05	0.05
F_{purge} (mol/m^2.s)	0.15	0.20	0.25	0.30	0.35	0.40
$T_{feed} = T_{purge}$ (K)	573	573	573	573	573	573
	Common Parameters					
$y_{A,ref}$	0.125	0.100	0.083	0.071	0.063	0.056
F_{ref} (mol/m^2.s)	0.20	0.25	0.30	0.35	0.40	0.45
K_{ads} (bar^{-1})	2.18	2.18	2.18	2.18	2.18	2.18
D_L (cm^2/s)	0.070	0.074	0.078	0.082	0.086	0.090
K_{gl} (cm/s)	0.48	0.49	0.49	0.49	0.49	0.50
N_f	2936	2363	1979	1705	1498	1337
θ_{ref}	0.379	0.358	0.340	0.326	0.313	0.302
	Adsorbent Bed					
Pe	56.6	67.0	76.3	84.7	92.4	99.3
ζ_m	5.20	4.91	4.67	4.48	4.30	4.15
	Catalyst Bed (Model *C*)					
k (cm^3/g.s)	1.92	1.92	1.92	1.92	1.92	1.92
K	2.67	2.67	2.67	2.67	2.67	2.67
Da	398.5	318.8	265.6	227.7	199.2	177.1
Pe	79.3	93.8	106.8	118.6	129.3	139
ζ_m	4.47	4.22	4.01	3.84	3.69	3.56
υ	1.4	1.4	1.4	1.4	1.4	1.4

time. There exists an optimal switch time for each run at which the maximum purity is obtained. The switch times used in the simulations are listed in Table 4.5.

In order to get a high purity, adsorbent beds should be thoroughly cleaned by keeping their residence time large in the regeneration section. However, the switch time is restricted by the breakthrough time of *n*-pentane, as separation cannot be achieved subsequently. Higher number of beds thus appears to be the other option left to give a large residence time in the regeneration section and thus a thorough cleaning. However, it is not an effective solution to the problem as illustrated in Figure 4.3. Using two beds in the regeneration section gives a higher purity than that obtained by using just one but it makes no difference by adding any extra bed thereafter. In order to understand this trend the adsorbed phase concentration profiles are examined for the beds in the regeneration section (Figure 4.4).

The profile of the first bed, encountering pure hydrogen, experiences the greatest change. The second bed hardly undergoes any change because the incoming purge gas contains desorbed *n*-pentane from the previous bed thus reducing the driving force. Desorption occurs in an appreciable amount in the last bed as its initial adsorbed phase concentration is high. This is because it has just been switched from the adsorption section into the regeneration section. As stated earlier, reference parameters used for normalizing the variables are defined as the parameters of inlet stream to the reaction section during the first switching period. Clearly, the outlet stream contains a lower amount of *n*-pentane so that the dimensionless adsorbed phase concentration is lesser than unity in the adsorbent beds.

Table 4.5. Switch Times for Isothermal and Adiabatic SMBR Simulations

Run	**1**	**2**	**3**	**4**	**5**	**6**
Case	τ_s **(min)**					
1	69.3	70.7	72.1	72.8	73.8	74.4
2	68.5	71.1	72.6	73.6	74.1	74.5
3	69.3	71.1	72.6	73.6	74.1	74.6
4	63.8	65.6	67.2	66.5	67.3	67.0
5	58.3	58.7	58.8	57.6	57.2	56.6
6	12.2	11.2	11.2	10.2	10.3	10.0
7	50.5	51.5	51.4	51.9	51.5	51.3

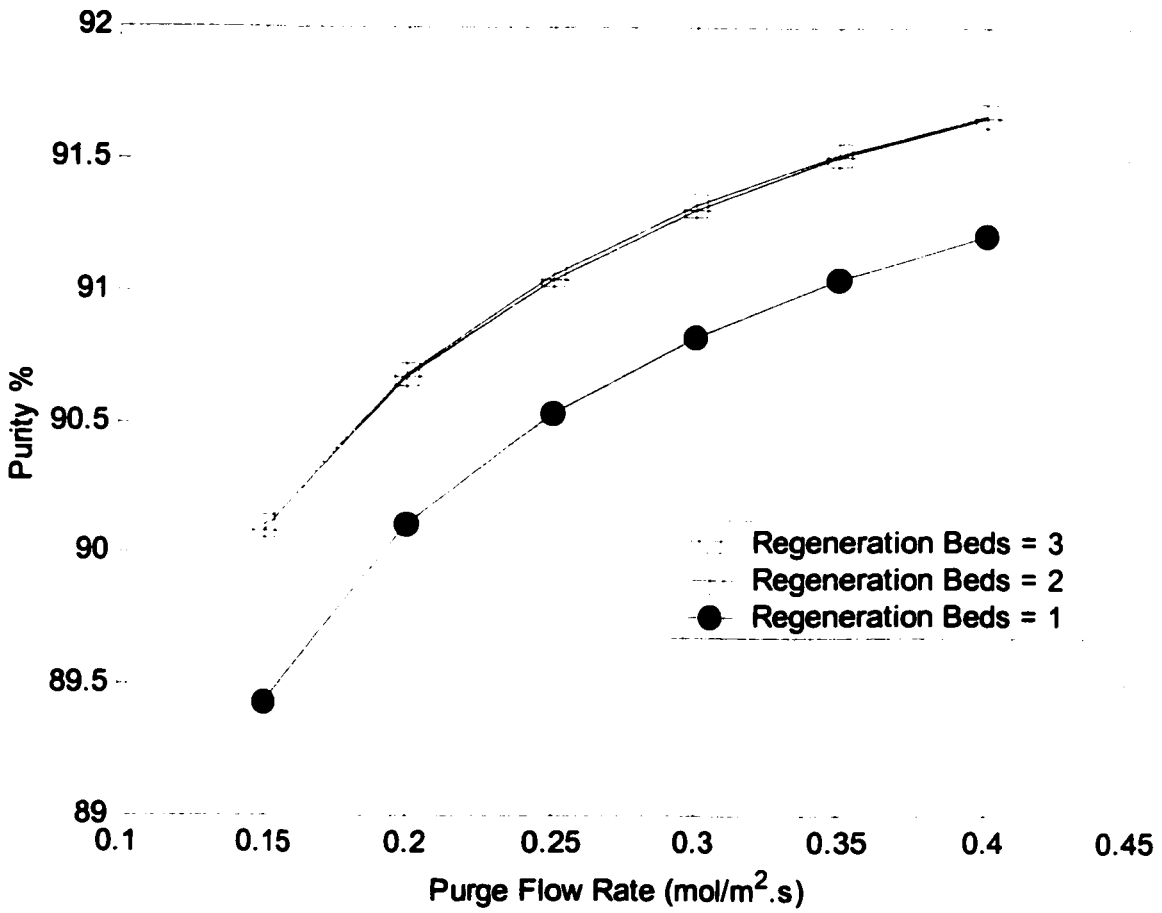

Figure 4.3. Effect of Number of Regeneration Beds on Product Purity (Cases 1, 2 & 3)

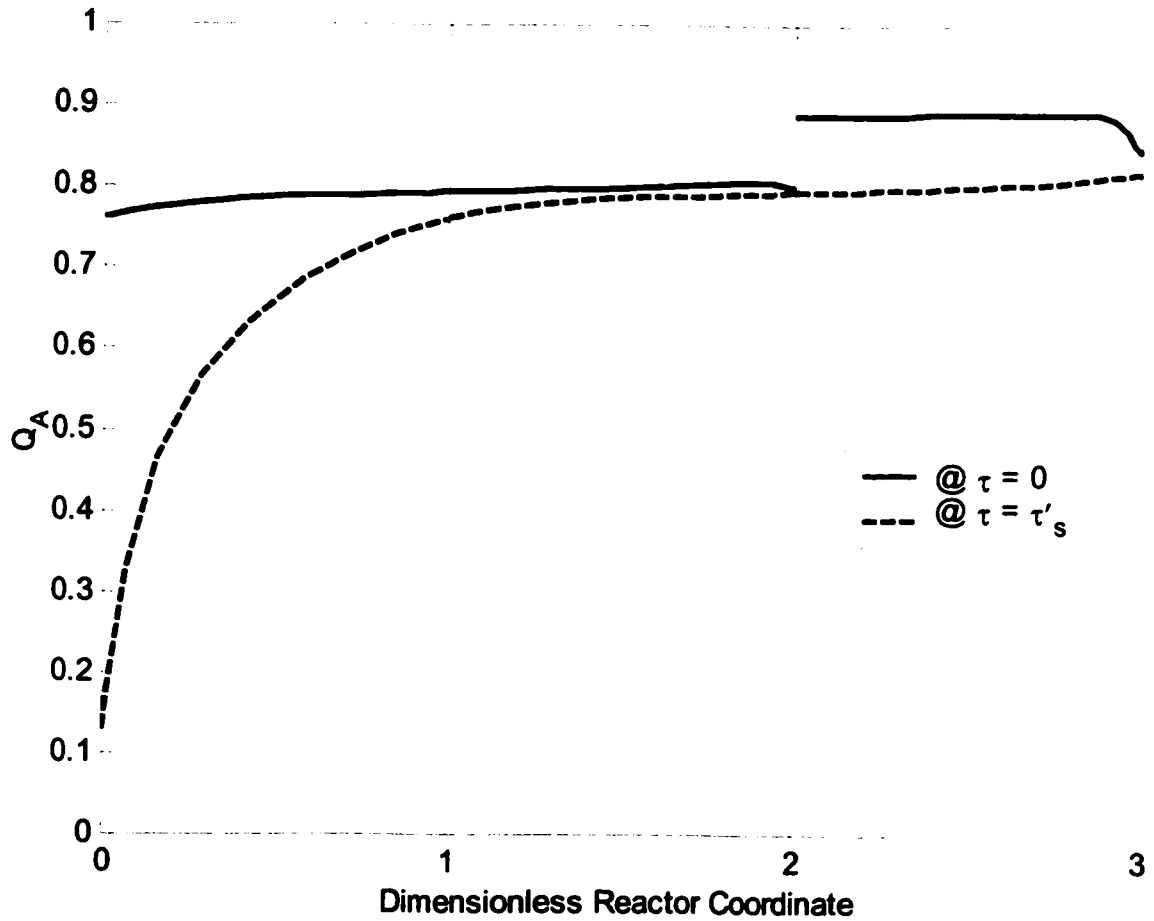

Figure 4.4. Cyclic Steady State Adsorbed Phase Concentration Profiles in the Regeneration Section at the Start and End of Switching Period (Case 3, Run 1)

Increasing purge flow rate by a modest amount also does not solve the problem, as it does not increase purity close to the desired value. Hydrogen is an expensive commodity and cannot be used in excess without justification. Moreover, higher purge rate would lower the hydrocarbon mole fraction in the reaction section and thus the reaction rate. A longer catalyst bed may be required if the mole fraction becomes too low.

Regeneration is faster at higher temperatures and the beds are thus cleaned much more efficiently. However, purity is lowered by operating at temperatures greater than the desired value of 514 K (Figure 4.5). One reason is that adsorption is unfavorable at elevated temperatures, hence reducing the switch time and the cleaning time in regeneration section. This is confirmed by checking the switch times for cases 2, 4 and 5 in Table 4.5. The other explanation, which is verified by observing Figure 4.6, is the lowering of equilibrium conversion and therefore the single pass conversion, which increases the duty of the adsorbent beds. This emphasizes the need to operate the various sections at different temperatures, i.e. to employ a thermal swing operation.

Passing the purge in reverse direction increases the purity significantly but still does not meet the desired standards of >99% (Figure 4.7). The failure of isothermal process should not be taken as a surprise. Regeneration of adsorbent beds using purge gas stripping is applicable only when the adsorbed species is weekly held. More commonly, a combination of purge gas stripping with a modest thermal swing is used [58]. This permits desorption of somewhat more strongly held species while at the same time the temperature change is small enough to avoid most of the disadvantages associated with a standard thermal swing process.

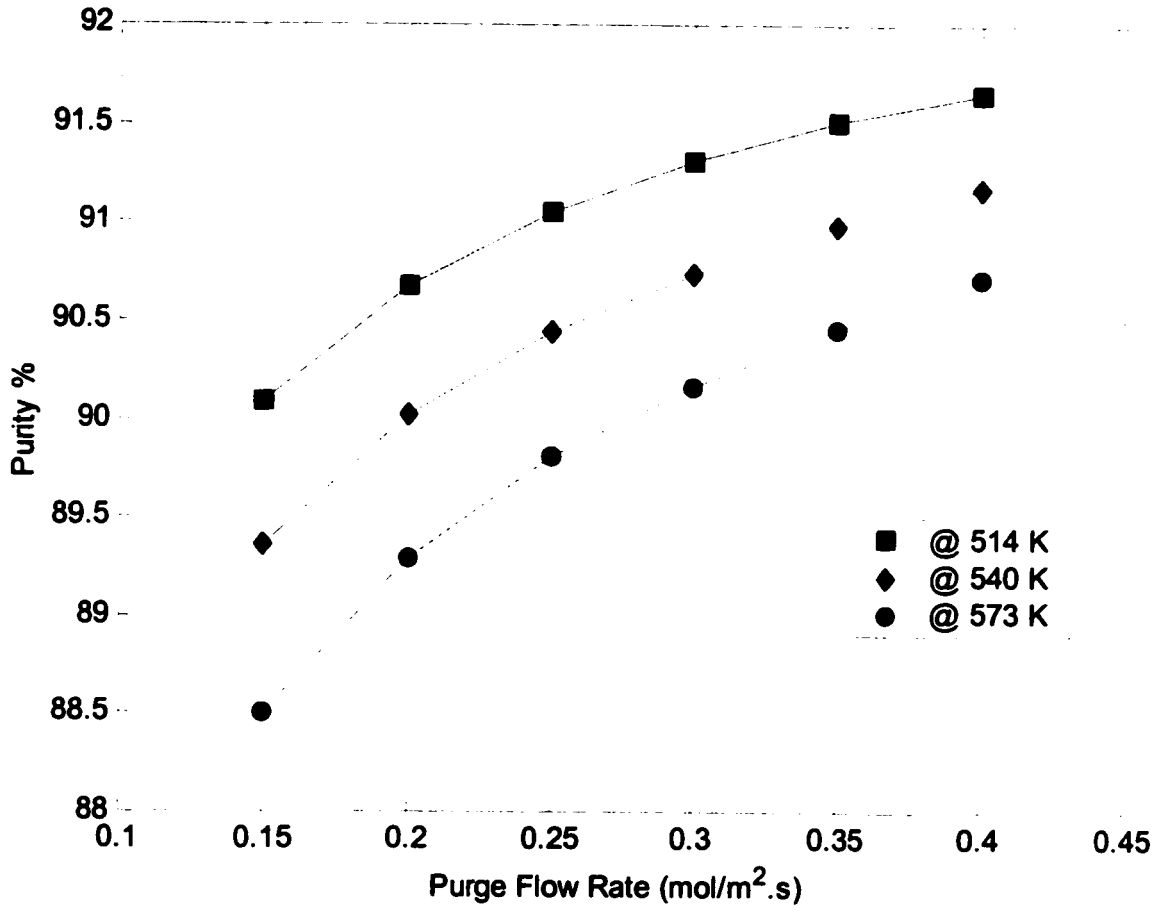

Figure 4.5. Effect of Temperature on Product Purity (Cases 2, 4 & 5)

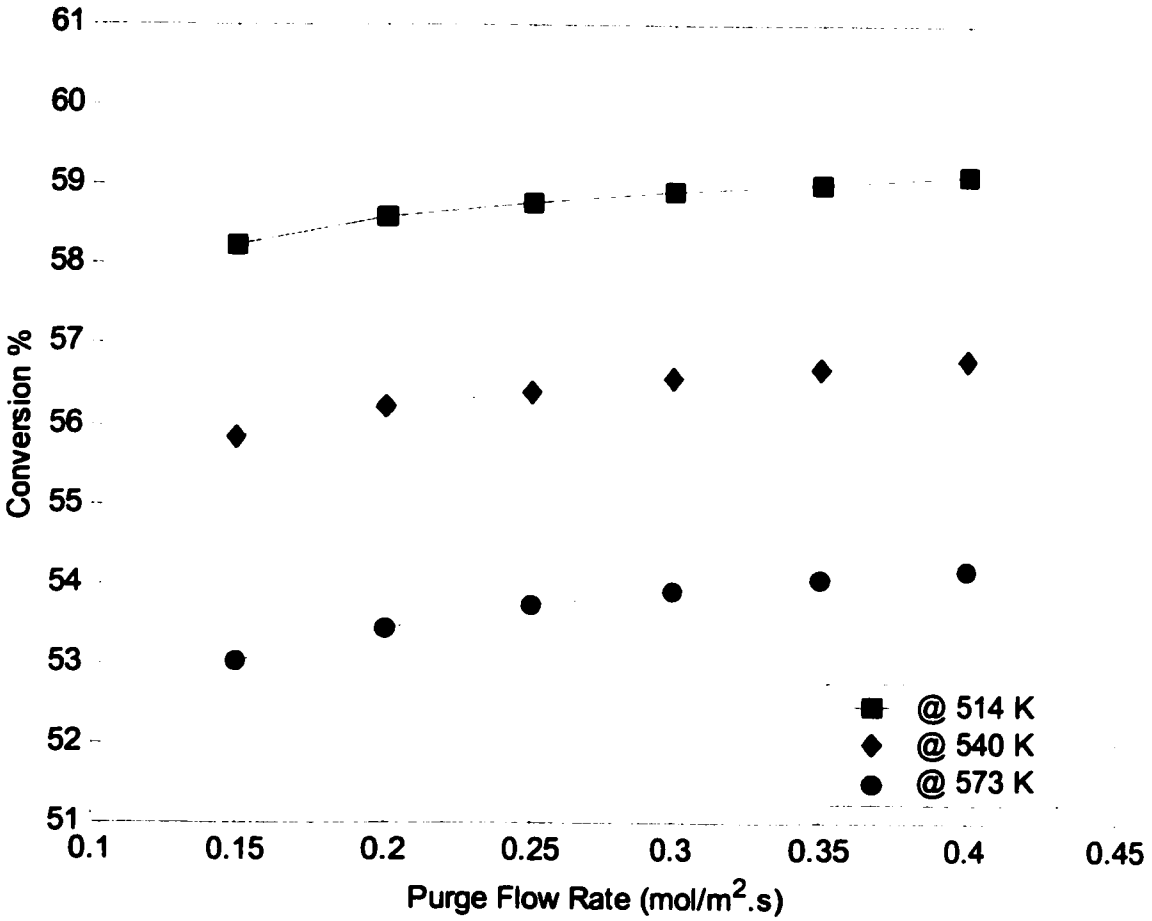

Figure 4.6. Effect of Temperature on Single Pass Conversion (Cases 2, 4 & 5)

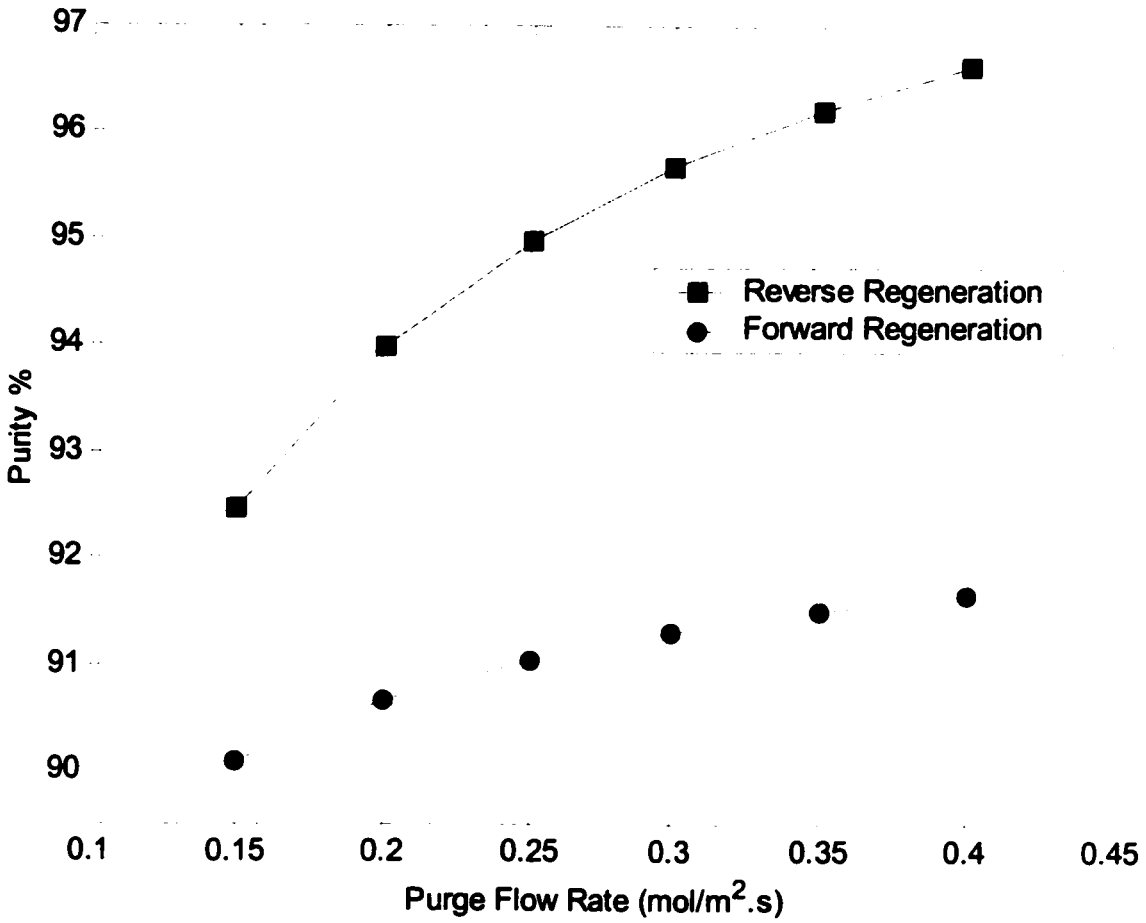

Figure 4.7. Effect of Bed Rotation on Product Purity (Cases 2 & 6)

Mazzotti *et al.* [39] on the other hand achieved a 100% pure isopentane raffinate using the simulated moving bed (SMB) setup although the operation was isothermal. This is because they regenerated the adsorbent by means of displacement chromatography, i.e. using *n*-heptane as a desorbent. However, the *n*-pentane shall have to be separated from the desorbent by distillation before it can be recycled back to the reaction section, otherwise *n*-heptane shall also be consumed thus requiring a fresh desorbent supply at all times. The introduction of a distillation column would require an intermediate storage tank so that it operates independently and is not disrupted by any temporary breakdown in the upstream. Thus, the catalyst bed shall no longer remain integrated with the adsorbent beds and the essence of a simulated moving bed reactor (SMBR) shall be lost.

4.2b Adiabatic Operation

Since desorption is favored at high temperatures and adsorption at low, a thermal swing operation is the next step to follow. Purge is thus supplied at a higher temperature, which mixes with a cold fresh feed after exiting the regeneration section. The adsorption section is therefore expected to operate at a lower temperature and allow a larger switch time, thus giving sufficient time for the beds to be cleaned in the regeneration section. Moreover the fresh feed temperature should not be too low, otherwise the reaction rate and hence the conversion would reduce significantly. In fact, the fresh feed temperature is calculated using equation 4.11 to give a desired value of 514 K in the reaction section.

An adiabatic process with thermal swing (case 7 in Table 4.1) is simulated for the parametric values given in Table 4.6. The switch times used are also listed in Table 4.5 for comparison with the isothermal cases. Initial condition for temperature in the three

Table 4.6. Parametric Values for Adiabatic SMBR Simulations (Case 7)

Run	**1**	**2**	**3**	**4**	**5**	**6**
Parameters	**Inlet Streams**					
F_{feed}	0.05	0.05	0.05	0.05	0.05	0.05
F_{Purge}	0.15	0.20	0.25	0.30	0.35	0.40
T_{feed} (K)	502	497	493	489	485	480
T_{purge} (K)	540	540	540	540	540	540
	Common Parameters					
$y_{A,ref}$	0.125	0.100	0.083	0.071	0.063	0.056
F_{ref} (mol/m^2.s)	0.20	0.25	0.30	0.35	0.40	0.45
T_{ref} (K)	514	514	514	514	514	514
γ_f	12.9	12.9	12.9	12.9	12.9	12.9
θ_{ref}	0.497	0.478	0.462	0.449	0.437	0.426
ζ_m^{Ads}	6.12	5.89	5.69	5.53	5.38	5.25
B^{Ads}	0.107	0.103	0.099	0.097	0.094	0.092
	Adsorption Section					
D_L (cm^2/s)	0.059	0.063	0.066	0.070	0.074	0.077
K_{gl} (cm/s)	0.41	0.41	0.42	0.42	0.42	0.42
K_L (W/m.K)	0.35	0.35	0.35	0.35	0.35	0.35
C_{pg} (J/mol.K)	68.9	61.0	55.8	52.0	49.2	47.0
Pe	60.1	70.9	80.5	89.1	96.9	104
Pe_H	7.88	8.72	9.56	10.4	11.2	12.1
ζ_H	89.3	100.9	110.4	118.4	125.2	131.0
N_f	2778	2236	1874	1614	1419	1267

Table 4.6. Parametric Values for Adiabatic SMBR Simulations (Case 7, continued)

Parameters	**Regeneration Section**					
D_L (cm^2/s)	0.064	0.068	0.071	0.075	0.079	0.083
K_{gl} (cm/s)	0.44	0.45	0.45	0.45	0.45	0.45
K_L (W/m.K)	0.35	0.35	0.35	0.35	0.35	0.35
C_{pg} (J/mol.K)	70.7	62.4	57.0	53.0	50.1	47.8
Pe	55.7	65.8	74.8	82.9	90.2	96.9
Pe_H	8.08	8.92	9.76	10.6	11.5	12.3
ζ_H	87.1	98.6	108.1	116.1	122.9	128.8
N_f	2995	2411	2019	1739	1529	1364
	Reaction Section (Model *C*)					
k_{ref}	0.046	0.046	0.046	0.046	0.046	0.046
D_L (cm^2/s)	0.059	0.063	0.066	0.070	0.074	0.077
K_{gl} (cm/s)	0.41	0.41	0.42	0.42	0.42	0.42
K_L (W/m.K)	0.35	0.35	0.35	0.35	0.35	0.35
C_{pg} (J/mol.K)	68.9	61.0	55.8	52.0	49.2	47.0
Da	10.7	8.53	7.10	6.09	5.33	4.74
Pe	84.1	99.2	112.7	124.7	135.7	145.6
Pe_H	11.0	12.2	13.4	14.6	15.7	16.9
ζ_m	5.26	5.06	4.89	4.75	4.62	4.51
ζ_H	76.7	86.7	94.8	101.7	107.5	112.5
N_f	2778	2236	1874	1614	1419	1267
γ_r	36.2	36.2	36.2	36.2	36.2	36.2
υ	1.4	1.4	1.4	1.4	1.4	1.4

Superscript: Ads: Adsorbent Bed Model

sections, while noting that the reference temperature (T_{ref}) is the initial reaction section temperature, is as follows:

Regeneration section: $$\bar{T}(x_1, \tau = 0) = \bar{T}_{purge} \quad (4.22a)$$

Reaction section: $$\bar{T}(x_2, \tau = 0) = 0 \quad (4.22b)$$

Adsorption section: $$\bar{T}(x_1, \tau = 0) = 0 \quad (4.22c)$$

Unfortunately, the performance is worse than that of the isothermal operation (Figure 4.8). This is because the temperature drops due to the endothermic heat of desorption in the regeneration section and does not remain at the specified value of T_{purge} (Figure 4.9). Moreover, the temperature increases because of the exothermic heat of adsorption in the adsorption section. Thus, both sections operate at similar temperatures and the temperature swing intended does not take place. A mechanism is hence needed that would compensate for any temperature drop in the regeneration section and that would extract the energy released in the adsorption section.

Strictly speaking, the effect of wall temperature must be taken into account for the adiabatic simulations. A cold fluid entering a hot vessel would be heated up by both the packed bed and the wall although the latter is insulated. A simplified method would be to suppose that the wall temperature is in equilibrium with the fluid phase just as the adsorbent bed is assumed to be. However, the adiabatic model is not pursued any further as it gave disappointing results.

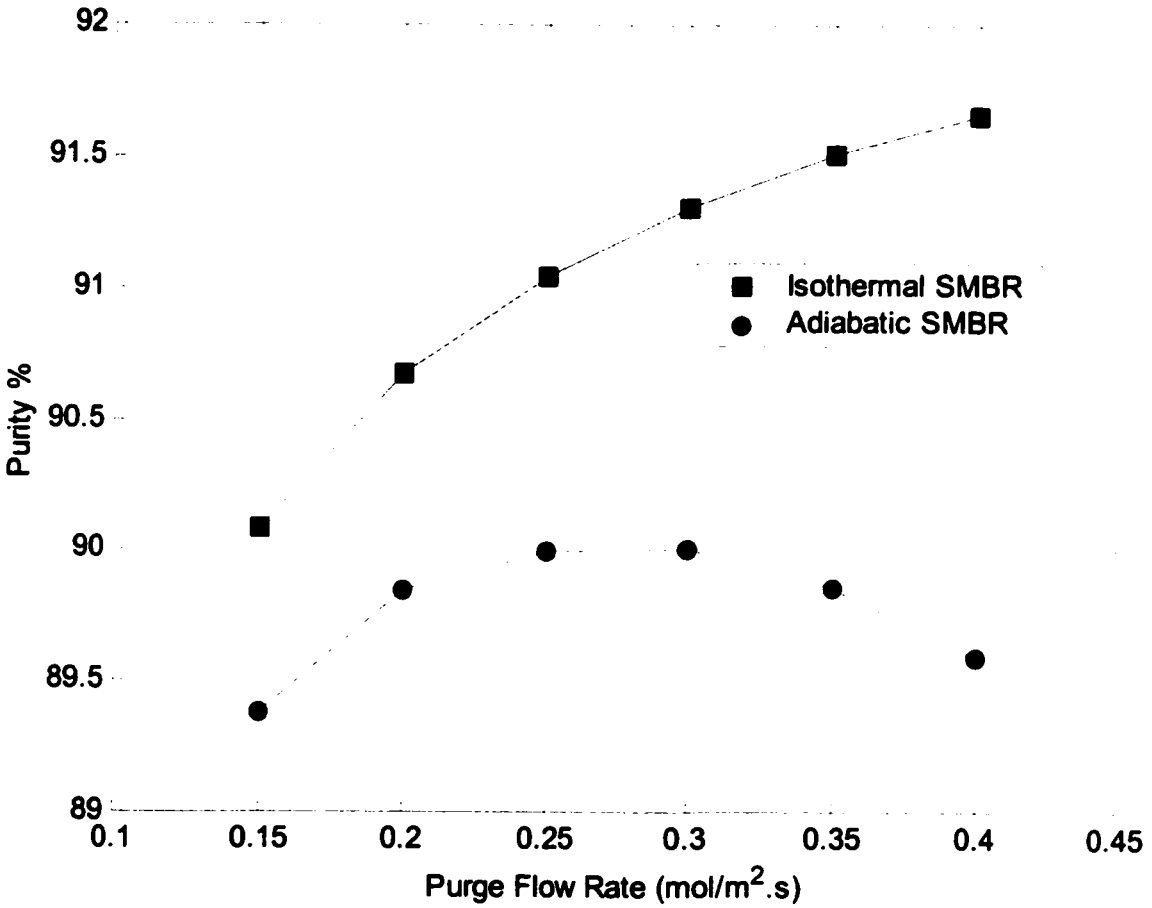

Figure 4.8. Effect of Adiabatic Operation on Product Purity (Cases 2 & 7)

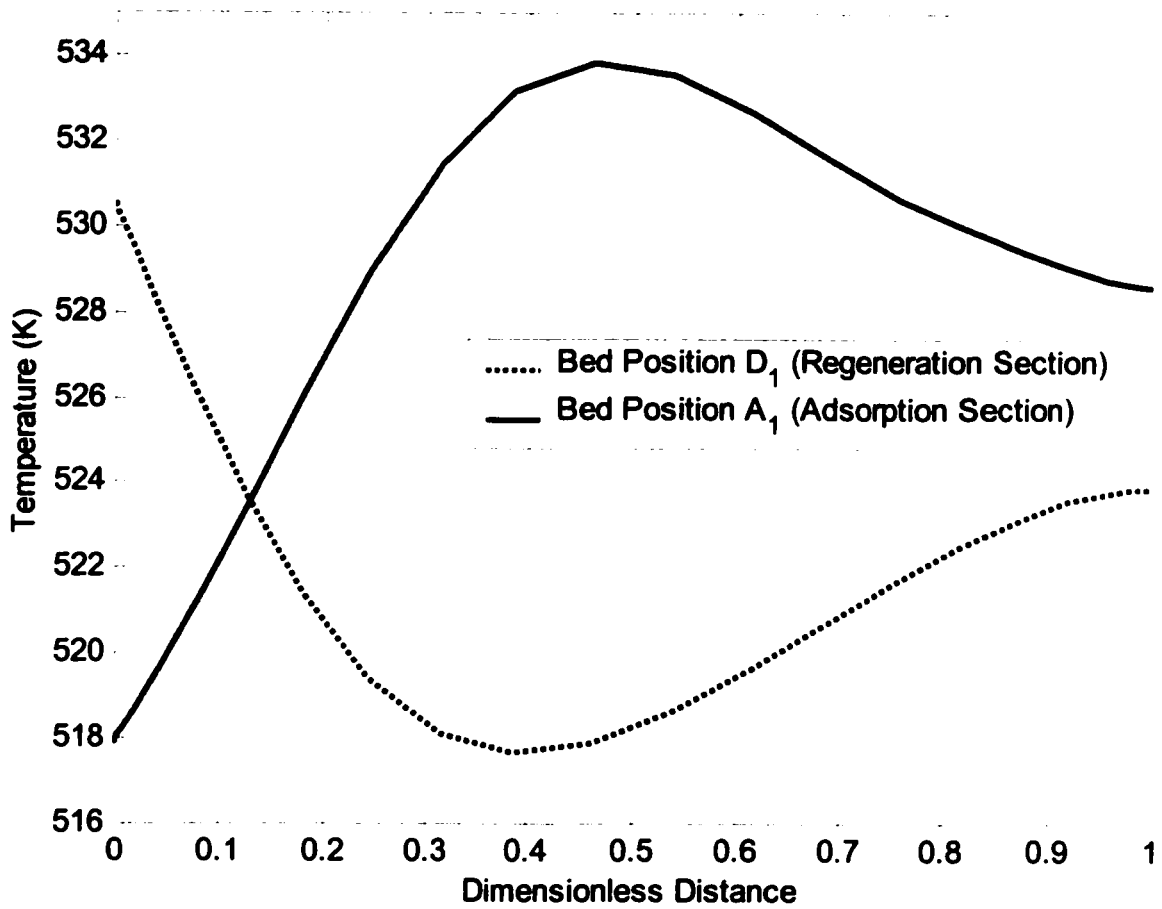

Figure 4.9. Cyclic Steady State Temperature Profiles during Adiabatic Operation at the End of Switching Period (Case 7, Run 1)

4.2c Non-Isothermal Non-Adiabatic Operation

Constant wall temperatures over the adsorbers should be applied to counteract the heats of adsorption/desorption either by condensing saturated steam over the walls or by keeping them in furnaces. In the former case, the adsorber would be a shell-and-tube heat exchanger with adsorbent filled in the tube side and saturated steam passed in the shell side. This method gives much more flexibility as the thermal swing in the adsorption section is now caused by the wall temperature rather than by the fresh feed temperature. Thus, temperatures much below 514 K can be reached in the adsorption section while the reaction section still operates at the desired value. In order to reduce costs, it is advisable to operate the reaction section adiabatically while attaining the operating temperature of around 514 K by using the sensible heat of fresh feed.

The wall temperature of the adsorbers in the regeneration section ($T_{w,des}$) is set equal to the inlet purge temperature (T_{purge}) and that in the adsorption section ($T_{w,ads}$) to the desired temperature necessary to produce an adequate thermal swing. Initial temperatures in the three sections are therefore taken as follows:

Regeneration section: $$\bar{T}(x_1, \tau = 0) = \bar{T}_{w,des} = \bar{T}_{purge} \quad (4.23a)$$

Reaction section: $$\bar{T}(x_2, \tau = 0) = 0 \quad (4.23b)$$

Adsorption section: $$\bar{T}(x_1, \tau = 0) = \bar{T}_{w,ads} \quad (4.23c)$$

The boiling point of pentanes at the operating pressure of 15 bar is 420 K. Moreover, the maximum operating temperature for adsorbent is 573 K as coking takes place beyond that [65]. Thus, the temperature swing is confined in this range with the minimum temperature equal to 430 K in order to give a 10 K margin. A summary of the

various thermal swing operations studied is summarized in Table 4.7 and the parametric values in Tables 4.8 to 4.17. Switch times are listed in Table 4.18.

The effect of number of beds in regeneration section on purity is illustrated in Figure 4.10. A slight increase in purity is observed by increasing the number from one to two but no appreciable increase takes place by using any more beds. Moreover higher purge flow rates also do not increase the purity significantly. Nevertheless, the desired >99% purity is finally reached. The switch time increases with rising purge flow rate (Table 4.18) because the adsorbent beds are cleaned more thoroughly so that they can operate for a longer period in the adsorption section. For the same reason the switch times are higher when either two or three beds are used in the regeneration section (cases 9 and 10 respectively) as compared to those when only one bed is used (case 8).

It was noticed in Chapter 3 that the three reactor models (*A*, *B* and *C*) differed greatly in their dynamic performance but gave exactly the same results after achieving steady state. The SMBR, however, at best reaches cyclic steady state. Thus, the performance of these models when incorporated in an SMBR should be compared. For all practical purposes, they gave the same purity (Figure 4.11).

The single pass conversion in reaction section for the three models is illustrated in Figure 4.12. The performance of the heterogeneous models is alike. The pseudo-homogeneous model deviates somewhat and shows a reverse trend with purge flow rates. It therefore predicts that the length of the catalyst bed is not enough at high purge flow rates to get close to the equilibrium value. It should be noted, however, that the single pass conversion also depends upon the inlet conditions to the reaction section, i.e. the

Table 4.7. Cases for Thermal Swing SMBR Simulations

Case	Regeneration Beds	T_{feed} (K)	$T_{w,ads}$-$T_{w,des}$ (K)	F_{feed} (mol/ m^2.s)	L_2 (cm)	Purge Direction	Reactor Model	Parametric Values
8	1	calc	430-540	0.05	28	forward	*C*	Table 4.8
9*	2	calc	430-540	0.05	28	forward	*C*	Table 4.8
10	3	calc	430-540	0.05	28	forward	*C*	Table 4.8
11	2	calc	430-540	0.05	28	forward	*A*	Table 4.8
12	2	calc	430-540	0.05	28	forward	*B*	Table 4.8
13	2	calc	430-540	0.05	36	forward	*C*	Table 4.9
14	2	calc	430-540	0.05	10	forward	*C*	Table 4.10
15	2	calc	430-520	0.05	28	forward	*C*	Table 4.11
16	2	calc	450-520	0.05	28	forward	*C*	Table 4.12
17	2	calc	450-540	0.05	28	forward	*C*	Table 4.13
18	2	calc	430-540	0.10	28	forward	*C*	Table 4.14
19	2	calc	430-540	0.10	56	forward	*C*	Table 4.15
20	2	460	430-540	0.05	28	forward	*C*	Table 4.16
21	2	430	430-540	0.05	28	forward	*C*	Table 4.17
22	1	calc	430-540	0.05	28	reverse	*C*	Table 4.8

*Base case for thermal swing operations

Note: For all the above cases, equimolar fresh feed is used with P = 15 bar.

Table 4.8. Parametric Values for Thermal Swing SMBR Simulations (Cases 8, 9, 10, 11, 12 & 22)

Run	**1**	**2**	**3**	**4**	**5**	**6**
Parameters	**Inlet Streams**					
F_{feed}	0.05	0.05	0.05	0.05	0.05	0.05
F_{Purge}	0.15	0.20	0.25	0.30	0.35	0.40
T_{feed} (K)	502	497	493	489	485	480
T_{purge} (K)	540	540	540	540	540	540
	Common Parameters					
$y_{A,ref}$	0.125	0.100	0.083	0.071	0.063	0.056
F_{ref} (mol/m^2.s)	0.20	0.25	0.30	0.35	0.40	0.45
T_{ref} (K)	514	514	514	514	514	514
$\gamma_f^{Ads,C}$	12.9	12.9	12.9	12.9	12.9	12.9
$\theta_{ref}^{Ads,C}$	0.497	0.478	0.462	0.449	0.437	0.426
ζ_m^{Ads}	6.12	5.89	5.69	5.53	5.38	5.25
B^{Ads}	0.107	0.103	0.099	0.097	0.094	0.092
	Adsorption Section					
$T_{w,ads}$ (K)	430	430	430	430	430	430
D_L (cm^2/s)	0.045	0.048	0.051	0.054	0.057	0.060
K_{gl} (cm/s)	0.31	0.32	0.32	0.32	0.32	0.32
K_L (W/m.K)	0.35	0.35	0.35	0.35	0.35	0.35
C_{pg} (J/mol.K)	63.0	56.2	51.7	48.5	46.1	44.2
h_w (W/m^2.K)	15	15	15	15	15	15
Pe	79.1	92.8	104.8	115.5	125.1	133.7
Pe_H	7.20	8.03	8.86	9.70	10.5	11.4
ζ_H	97.8	109.5	119.1	127.0	133.7	139.4
N_f	2124	1712	1436	1237	1089	972.4
N_w	28.4	25.5	23.1	21.1	19.4	18.0

Table 4.8. Parametric Values for Thermal Swing SMBR Simulations (Cases 8, 9, 10, 11, 12 & 22, continued)

Parameters	**Regeneration Section**					
$T_{w,des}$ (K)	540	540	540	540	540	540
D_L (cm^2/s)	0.064	0.068	0.071	0.075	0.079	0.083
K_{gl} (cm/s)	0.44	0.45	0.45	0.45	0.45	0.45
K_L (W/m.K)	0.35	0.35	0.35	0.35	0.35	0.35
C_{pg} (J/mol.K)	70.7	62.4	57.0	53.0	50.1	47.8
h_w (W/m^2.K)	15	15	15	15	15	15
Pe	55.7	65.8	74.8	82.9	90.2	96.9
Pe_H	8.08	8.92	9.76	10.6	11.5	12.3
ζ_H	87.1	98.6	108.1	116.1	122.9	128.8
N_f	2995	2411	2019	1739	1529	1364
N_w	25.4	23.0	21.0	19.3	17.9	16.7
	Reaction Section (Adiabatic, Models *A*, *B* & *C*)					
k_{ref}	0.046	0.046	0.046	0.046	0.046	0.046
D_L (cm^2/s)	0.059	0.063	0.066	0.070	0.074	0.077
K_{gl} (cm/s)^{B,C}	0.41	0.41	0.42	0.42	0.42	0.42
K_L (W/m.K)	0.35	0.35	0.35	0.35	0.35	0.35
C_{pg} (J/mol.K)	68.9	61.0	55.8	52.0	49.2	47.0
Da	10.7	8.53	7.10	6.09	5.33	4.74
Pe	84.1	99.2	112.7	124.7	135.7	145.6
Pe_H	11.0	12.2	13.4	14.6	15.7	16.9
σ^B	0.74	0.74	0.74	0.74	0.74	0.74
$\zeta_m{}^C$	5.26	5.06	4.89	4.75	4.62	4.51
$\zeta_H{}^{B,C}$	76.7	86.7	94.8	101.7	107.5	112.5
$N_f^{B,C}$	2778	2236	1874	1614	1419	1267
γ_r	36.2	36.2	36.2	36.2	36.2	36.2
υ	1.4	1.4	1.4	1.4	1.4	1.4

Superscripts: Ads: Adsorbent Bed Model, *B*: Reactor Model *B*, *C*: Reactor Model *C*

Table 4.9. Parametric Values for Thermal Swing SMBR Simulations (Case 13)

Run	**1**	**2**	**3**	**4**	**5**	**6**
Parameters	**Inlet Streams**					
F_{feed}	0.05	0.05	0.05	0.05	0.05	0.05
F_{Purge}	0.15	0.20	0.25	0.30	0.35	0.40
T_{feed} (K)	502	497	493	489	485	480
T_{purge} (K)	540	540	540	540	540	540
	Common Parameters					
$y_{A,ref}$	0.125	0.100	0.083	0.071	0.063	0.056
F_{ref} (mol/m^2.s)	0.20	0.25	0.30	0.35	0.40	0.45
T_{ref} (K)	514	514	514	514	514	514
γ_f	12.9	12.9	12.9	12.9	12.9	12.9
θ_{ref}	0.497	0.478	0.462	0.449	0.437	0.426
ζ_m^{Ads}	6.12	5.89	5.69	5.53	5.38	5.25
B^{Ads}	0.107	0.103	0.099	0.097	0.094	0.092
	Adsorption Section					
$T_{w,ads}$ (K)	430	430	430	430	430	430
D_L (cm^2/s)	0.045	0.048	0.051	0.054	0.057	0.060
K_{gl} (cm/s)	0.31	0.32	0.32	0.32	0.32	0.32
K_L (W/m.K)	0.35	0.35	0.35	0.35	0.35	0.35
C_{pg} (J/mol.K)	63.0	56.2	51.7	48.5	46.1	44.2
h_w (W/m^2.K)	15	15	15	15	15	15
Pe	79.1	92.8	104.8	115.5	125.1	133.7
Pe_H	7.20	8.03	8.86	9.70	10.5	11.4
ζ_H	97.8	109.5	119.1	127.0	133.7	139.4
N_f	2124	1712	1436	1237	1089	972.4
N_w	28.4	25.5	23.1	21.1	19.4	18.0

Table 4.9. Parametric Values for Thermal Swing SMBR Simulations (Case 13, continued)

Parameters	**Regeneration Section**					
$T_{w,des}$ (K)	540	540	540	540	540	540
D_L (cm^2/s)	0.064	0.068	0.071	0.075	0.079	0.083
K_{gl} (cm/s)	0.44	0.45	0.45	0.45	0.45	0.45
K_L (W/m.K)	0.35	0.35	0.35	0.35	0.35	0.35
C_{pg} (J/mol.K)	70.7	62.4	57.0	53.0	50.1	47.8
h_w (W/m^2.K)	15	15	15	15	15	15
Pe	55.7	65.8	74.8	82.9	90.2	96.9
Pe_H	8.08	8.92	9.76	10.6	11.5	12.3
ζ_H	87.1	98.6	108.1	116.1	122.9	128.8
N_f	2995	2411	2019	1739	1529	1364
N_w	25.4	23.0	21.0	19.3	17.9	16.7
	Reaction Section (Adiabatic, Model *C*)					
k_{ref}	0.046	0.046	0.046	0.046	0.046	0.046
D_L (cm^2/s)	0.059	0.063	0.066	0.070	0.074	0.077
K_{gl} (cm/s)	0.41	0.41	0.42	0.42	0.42	0.42
K_L (W/m.K)	0.35	0.35	0.35	0.35	0.35	0.35
C_{pg} (J/mol.K)	68.9	61.0	55.8	52.0	49.2	47.0
Da	10.7	8.53	7.10	6.09	5.33	4.74
Pe	108.2	127.5	144.8	160.4	174.4	187.1
Pe_H	14.2	15.7	17.2	18.7	20.2	21.8
ζ_m	5.26	5.06	4.89	4.75	4.62	4.51
ζ_H	76.7	86.7	94.8	101.7	107.5	112.5
N_f	2778	2236	1874	1614	1419	1267
γ_r	36.2	36.2	36.2	36.2	36.2	36.2
υ	1.8	1.8	1.8	1.8	1.8	1.8

Superscript: Ads: Adsorbent Bed Model

Table 4.10. Parametric Values for Thermal Swing SMBR Simulations (Case 14)

Run	**1**	**2**	**3**	**4**	**5**	**6**
Parameters	**Inlet Streams**					
F_{feed}	0.05	0.05	0.05	0.05	0.05	0.05
F_{Purge}	0.15	0.20	0.25	0.30	0.35	0.40
T_{feed} (K)	502	497	493	489	485	480
T_{purge} (K)	540	540	540	540	540	540
	Common Parameters					
$y_{A,ref}$	0.125	0.100	0.083	0.071	0.063	0.056
F_{ref} (mol/m^2.s)	0.20	0.25	0.30	0.35	0.40	0.45
T_{ref} (K)	514	514	514	514	514	514
γ_f	12.9	12.9	12.9	12.9	12.9	12.9
θ_{ref}	0.497	0.478	0.462	0.449	0.437	0.426
ζ_m^{Ads}	6.12	5.89	5.69	5.53	5.38	5.25
B^{Ads}	0.107	0.103	0.099	0.097	0.094	0.092
	Adsorption Section					
$T_{w,ads}$ (K)	430	430	430	430	430	430
D_L (cm^2/s)	0.045	0.048	0.051	0.054	0.057	0.060
K_{gl} (cm/s)	0.31	0.32	0.32	0.32	0.32	0.32
K_L (W/m.K)	0.35	0.35	0.35	0.35	0.35	0.35
C_{pg} (J/mol.K)	63.0	56.2	51.7	48.5	46.1	44.2
h_w (W/m^2.K)	15	15	15	15	15	15
Pe	79.1	92.8	104.8	115.5	125.1	133.7
Pe_H	7.20	8.03	8.86	9.70	10.5	11.4
ζ_H	97.8	109.5	119.1	127.0	133.7	139.4
N_f	2124	1712	1436	1237	1089	972.4
N_w	28.4	25.5	23.1	21.1	19.4	18.0

Table 4.10. Parametric Values for Thermal Swing SMBR Simulations (Case 14, continued)

Parameters	**Regeneration Section**					
$T_{w,des}$ (K)	540	540	540	540	540	540
D_L (cm^2/s)	0.064	0.068	0.071	0.075	0.079	0.083
K_{gl} (cm/s)	0.44	0.45	0.45	0.45	0.45	0.45
K_L (W/m.K)	0.35	0.35	0.35	0.35	0.35	0.35
C_{pg} (J/mol.K)	70.7	62.4	57.0	53.0	50.1	47.8
h_w (W/m^2.K)	15	15	15	15	15	15
Pe	55.7	65.8	74.8	82.9	90.2	96.9
Pe_H	8.08	8.92	9.76	10.6	11.5	12.3
ζ_H	87.1	98.6	108.1	116.1	122.9	128.8
N_f	2995	2411	2019	1739	1529	1364
N_w	25.4	23.0	21.0	19.3	17.9	16.7
	Reaction Section (Adiabatic, Model *C*)					
k_{ref}	0.046	0.046	0.046	0.046	0.046	0.046
D_L (cm^2/s)	0.059	0.063	0.066	0.070	0.074	0.077
K_{gl} (cm/s)	0.41	0.41	0.42	0.42	0.42	0.42
K_L (W/m.K)	0.35	0.35	0.35	0.35	0.35	0.35
C_{pg} (J/mol.K)	68.9	61.0	55.8	52.0	49.2	47.0
Da	10.7	8.53	7.10	6.09	5.33	4.74
Pe	30.1	35.4	40.2	44.6	48.5	52.0
Pe_H	3.94	4.36	4.78	5.20	5.62	6.04
ζ_m	5.26	5.06	4.89	4.75	4.62	4.51
ζ_H	76.7	86.7	94.8	101.7	107.5	112.5
N_f	2778	2236	1874	1614	1419	1267
γ_r	36.2	36.2	36.2	36.2	36.2	36.2
υ	0.5	0.5	0.5	0.5	0.5	0.5

Superscript: Ads: Adsorbent Bed Model

Table 4.11. Parametric Values for Thermal Swing SMBR Simulations (Case 15)

Run	**1**	**2**	**3**	**4**	**5**	**6**
Parameters	**Inlet Streams**					
F_{feed}	0.05	0.05	0.05	0.05	0.05	0.05
F_{Purge}	0.15	0.20	0.25	0.30	0.35	0.40
T_{feed} (K)	511	510	509	508	507	506
T_{purge} (K)	520	520	520	520	520	520
	Common Parameters					
$y_{A,ref}$	0.125	0.100	0.083	0.071	0.063	0.056
F_{ref} (mol/m^2.s)	0.20	0.25	0.30	0.35	0.40	0.45
T_{ref} (K)	514	514	514	514	514	514
γ_f	12.9	12.9	12.9	12.9	12.9	12.9
θ_{ref}	0.497	0.478	0.462	0.449	0.437	0.426
ζ_m^{Ads}	6.12	5.89	5.69	5.53	5.38	5.25
B^{Ads}	0.107	0.103	0.099	0.097	0.094	0.092
	Adsorption Section					
$T_{w,ads}$ (K)	430	430	430	430	430	430
D_L (cm^2/s)	0.045	0.048	0.051	0.054	0.057	0.060
K_{gl} (cm/s)	0.31	0.32	0.32	0.32	0.32	0.32
K_L (W/m.K)	0.35	0.35	0.35	0.35	0.35	0.35
C_{pg} (J/mol.K)	63.0	56.2	51.7	48.5	46.1	44.2
h_w (W/m^2.K)	15	15	15	15	15	15
Pe	79.1	92.8	104.8	115.5	125.1	133.7
Pe_H	7.20	8.03	8.86	9.70	10.5	11.4
ζ_H	97.8	109.5	119.1	127.0	133.7	139.4
N_f	2124	1712	1436	1237	1089	972.4
N_w	28.4	25.5	23.1	21.1	19.4	18.0

Table 4.11. Parametric Values for Thermal Swing SMBR Simulations (Case 15, continued)

Parameters	**Regeneration Section**					
$T_{w,des}$ (K)	520	520	520	520	520	520
D_L (cm^2/s)	0.060	0.064	0.068	0.071	0.075	0.078
K_{gl} (cm/s)	0.42	0.42	0.42	0.43	0.43	0.43
K_L (W/m.K)	0.35	0.35	0.35	0.35	0.35	0.35
C_{pg} (J/mol.K)	69.3	61.4	56.0	52.3	49.4	47.2
h_w (W/m^2.K)	15	15	15	15	15	15
Pe	59.0	69.6	79.1	87.6	95.3	102.3
Pe_H	7.93	8.77	9.61	10.5	11.3	12.1
ζ_H	88.8	100.3	109.9	117.8	124.6	130.5
N_f	2825	2274	1905	1641	1443	1288
N_w	25.8	23.4	21.3	19.6	18.1	16.9
	Reaction Section (Adiabatic, Model *C*)					
k_{ref}	0.046	0.046	0.046	0.046	0.046	0.046
D_L (cm^2/s)	0.059	0.063	0.066	0.070	0.074	0.077
K_{gl} (cm/s)	0.41	0.41	0.42	0.42	0.42	0.42
K_L (W/m.K)	0.35	0.35	0.35	0.35	0.35	0.35
C_{pg} (J/mol.K)	68.9	61.0	55.8	52.0	49.2	47.0
Da	10.7	8.53	7.10	6.09	5.33	4.74
Pe	84.1	99.2	112.7	124.7	135.7	145.6
Pe_H	11.0	12.2	13.4	14.6	15.7	16.9
ζ_m	5.26	5.06	4.89	4.75	4.62	4.51
ζ_H	76.7	86.7	94.8	101.7	107.5	112.5
N_f	2778	2236	1874	1614	1419	1267
γ_r	36.2	36.2	36.2	36.2	36.2	36.2
υ	1.4	1.4	1.4	1.4	1.4	1.4

Superscript: Ads: Adsorbent Bed Model

Table 4.12. Parametric Values for Thermal Swing SMBR Simulations (Case 16)

Run	**1**	**2**	**3**	**4**	**5**	**6**
Parameters	**Inlet Streams**					
F_{feed}	0.05	0.05	0.05	0.05	0.05	0.05
F_{Purge}	0.15	0.20	0.25	0.30	0.35	0.40
T_{feed} (K)	511	510	509	508	507	506
T_{purge} (K)	520	520	520	520	520	520
	Common Parameters					
$y_{A,ref}$	0.125	0.100	0.083	0.071	0.063	0.056
F_{ref} (mol/m^2.s)	0.20	0.25	0.30	0.35	0.40	0.45
T_{ref} (K)	514	514	514	514	514	514
γ_f	12.9	12.9	12.9	12.9	12.9	12.9
θ_{ref}	0.497	0.478	0.462	0.449	0.437	0.426
ζ_m^{Ads}	6.12	5.89	5.69	5.53	5.38	5.25
B^{Ads}	0.107	0.103	0.099	0.097	0.094	0.092
	Adsorption Section					
$T_{w,ads}$ (K)	450	450	450	450	450	450
D_L (cm^2/s)	0.048	0.051	0.055	0.058	0.061	0.064
K_{gl} (cm/s)	0.34	0.34	0.34	0.34	0.34	0.35
K_L (W/m.K)	0.35	0.35	0.35	0.35	0.35	0.35
C_{pg} (J/mol.K)	64.5	57.4	52.7	49.4	46.8	44.9
h_w (W/m^2.K)	15	15	15	15	15	15
Pe	73.8	86.6	98.0	108.1	117.2	125.4
Pe_H	7.37	8.20	9.03	9.87	10.7	11.5
ζ_H	95.5	107.3	116.8	124.8	131.5	137.2
N_f	2272	1830	1534	1322	1163	1039
N_w	27.8	25.0	22.7	20.7	19.1	17.7

Table 4.12. Parametric Values for Thermal Swing SMBR Simulations (Case 16, continued)

Parameters	**Regeneration Section**					
$T_{w,des}$ (K)	520	520	520	520	520	520
D_L (cm^2/s)	0.060	0.064	0.068	0.071	0.075	0.078
K_{gl} (cm/s)	0.42	0.42	0.42	0.43	0.43	0.43
K_L (W/m.K)	0.35	0.35	0.35	0.35	0.35	0.35
C_{pg} (J/mol.K)	69.3	61.4	56.0	52.3	49.4	47.2
h_w (W/m^2.K)	15	15	15	15	15	15
Pe	59.0	69.6	79.1	87.6	95.3	102.3
Pe_H	7.93	8.77	9.61	10.5	11.3	12.1
ζ_H	88.8	100.3	109.9	117.8	124.6	130.5
N_f	2825	2274	1905	1641	1443	1288
N_w	25.8	23.4	21.3	19.6	18.1	16.9
	Reaction Section (Adiabatic, Model *C*)					
k_{ref}	0.046	0.046	0.046	0.046	0.046	0.046
D_L (cm^2/s)	0.059	0.063	0.066	0.070	0.074	0.077
K_{gl} (cm/s)	0.41	0.41	0.42	0.42	0.42	0.42
K_L (W/m.K)	0.35	0.35	0.35	0.35	0.35	0.35
C_{pg} (J/mol.K)	68.9	61.0	55.8	52.0	49.2	47.0
Da	10.7	8.53	7.10	6.09	5.33	4.74
Pe	84.1	99.2	112.7	124.7	135.7	145.6
Pe_H	11.0	12.2	13.4	14.6	15.7	16.9
ζ_m	5.26	5.06	4.89	4.75	4.62	4.51
ζ_H	76.7	86.7	94.8	101.7	107.5	112.5
N_f	2778	2236	1874	1614	1419	1267
γ_r	36.2	36.2	36.2	36.2	36.2	36.2
υ	1.4	1.4	1.4	1.4	1.4	1.4

Superscript: Ads: Adsorbent Bed Model

Table 4.13. Parametric Values for Thermal Swing SMBR Simulations (Case 17)

Run	**1**	**2**	**3**	**4**	**5**	**6**
Parameters	**Inlet Streams**					
F_{feed}	0.05	0.05	0.05	0.05	0.05	0.05
F_{Purge}	0.15	0.20	0.25	0.30	0.35	0.40
T_{feed} (K)	502	497	493	489	485	480
T_{purge} (K)	540	540	540	540	540	540
	Common Parameters					
$y_{A,ref}$	0.125	0.100	0.083	0.071	0.063	0.056
F_{ref} (mol/m^2.s)	0.20	0.25	0.30	0.35	0.40	0.45
T_{ref} (K)	514	514	514	514	514	514
γ_f	12.9	12.9	12.9	12.9	12.9	12.9
θ_{ref}	0.497	0.478	0.462	0.449	0.437	0.426
ζ_m^{Ads}	6.12	5.89	5.69	5.53	5.38	5.25
B^{Ads}	0.107	0.103	0.099	0.097	0.094	0.092
	Adsorption Section					
$T_{w,ads}$ (K)	450	450	450	450	450	450
D_L (cm^2/s)	0.048	0.051	0.055	0.058	0.061	0.064
K_{gl} (cm/s)	0.34	0.34	0.34	0.34	0.34	0.35
K_L (W/m.K)	0.35	0.35	0.35	0.35	0.35	0.35
C_{pg} (J/mol.K)	64.5	57.4	52.7	49.4	46.8	44.9
h_w (W/m^2.K)	15	15	15	15	15	15
Pe	73.8	86.6	98.0	108.1	117.2	125.4
Pe_H	7.37	8.20	9.03	9.87	10.7	11.5
ζ_H	95.5	107.3	116.8	124.8	131.5	137.2
N_f	2272	1830	1534	1322	1163	1039
N_w	27.8	25.0	22.7	20.7	19.1	17.7

Table 4.13. Parametric Values for Thermal Swing SMBR Simulations (Case 17, continued)

Parameters	**Regeneration Section**					
$T_{w,des}$ (K)	540	540	540	540	540	540
D_L (cm^2/s)	0.064	0.068	0.071	0.075	0.079	0.083
K_{gl} (cm/s)	0.44	0.45	0.45	0.45	0.45	0.45
K_L (W/m.K)	0.35	0.35	0.35	0.35	0.35	0.35
C_{pg} (J/mol.K)	70.7	62.4	57.0	53.0	50.1	47.8
h_w (W/m^2.K)	15	15	15	15	15	15
Pe	55.7	65.8	74.8	82.9	90.2	96.9
Pe_H	8.08	8.92	9.76	10.6	11.5	12.3
ζ_H	87.1	98.6	108.1	116.1	122.9	128.8
N_f	2995	2411	2019	1739	1529	1364
N_w	25.4	23.0	21.0	19.3	17.9	16.7
	Reaction Section (Adiabatic, Model *C*)					
k_{ref}	0.046	0.046	0.046	0.046	0.046	0.046
D_L (cm^2/s)	0.059	0.063	0.066	0.070	0.074	0.077
K_{gl} (cm/s)	0.41	0.41	0.42	0.42	0.42	0.42
K_L (W/m.K)	0.35	0.35	0.35	0.35	0.35	0.35
C_{pg} (J/mol.K)	68.9	61.0	55.8	52.0	49.2	47.0
Da	10.7	8.53	7.10	6.09	5.33	4.74
Pe	84.1	99.2	112.7	124.7	135.7	145.6
Pe_H	11.0	12.2	13.4	14.6	15.7	16.9
ζ_m	5.26	5.06	4.89	4.75	4.62	4.51
ζ_H	76.7	86.7	94.8	101.7	107.5	112.5
N_f	2778	2236	1874	1614	1419	1267
γ_r	36.2	36.2	36.2	36.2	36.2	36.2
υ	1.4	1.4	1.4	1.4	1.4	1.4

Superscript: Ads: Adsorbent Bed Model

Table 4.14. Parametric Values for Thermal Swing SMBR Simulations (Case 18)

Run	**1**	**2**	**3**	**4**	**5**	**6**
Parameters	**Inlet Streams**					
F_{feed}	0.10	0.10	0.10	0.10	0.10	0.10
F_{Purge}	0.30	0.40	0.50	0.60	0.70	0.80
T_{feed} (K)	502	497	493	489	485	480
T_{purge} (K)	540	540	540	540	540	540
	Common Parameters					
$y_{A,ref}$	0.125	0.100	0.083	0.071	0.063	0.056
F_{ref} (mol/m^2.s)	0.40	0.50	0.60	0.70	0.80	0.90
T_{ref} (K)	514	514	514	514	514	514
γ_f	12.9	12.9	12.9	12.9	12.9	12.9
θ_{ref}	0.497	0.478	0.462	0.449	0.437	0.426
ζ_m^{Ads}	6.12	5.89	5.69	5.53	5.38	5.25
B^{Ads}	0.107	0.103	0.099	0.097	0.094	0.092
	Adsorption Section					
$T_{w,ads}$ (K)	430	430	430	430	430	430
D_L (cm^2/s)	0.057	0.063	0.069	0.075	0.081	0.087
K_{gl} (cm/s)	0.33	0.33	0.33	0.34	0.34	0.34
K_L (W/m.K)	0.35	0.35	0.35	0.35	0.35	0.35
C_{pg} (J/mol.K)	63.0	56.2	51.7	48.5	46.1	44.2
h_w (W/m^2.K)	15	15	15	15	15	15
Pe	125.1	141.6	155.2	166.6	176.4	184.8
Pe_H	14.4	16.1	17.7	19.4	21.1	22.7
ζ_H	97.8	109.5	119.1	127.0	133.7	139.4
N_f	1108	894.9	751.8	649.0	571.6	511.1
N_w	14.2	12.8	11.6	10.6	9.72	9.01

Table 4.14. Parametric Values for Thermal Swing SMBR Simulations (Case 18, continued)

Parameters	**Regeneration Section**					
$T_{w,des}$ (K)	540	540	540	540	540	540
D_L (cm^2/s)	0.079	0.086	0.094	0.10	0.11	0.12
K_{gl} (cm/s)	0.46	0.46	0.47	0.47	0.47	0.47
K_L (W/m.K)	0.35	0.35	0.35	0.35	0.35	0.35
C_{pg} (J/mol.K)	70.7	62.4	57.0	53.0	50.1	47.8
h_w (W/m^2.K)	15	15	15	15	15	15
Pe	90.2	103.0	113.8	123.0	130.9	137.7
Pe_H	16.2	17.8	19.5	21.2	22.9	24.6
ζ_H	87.1	98.6	108.1	116.1	122.9	128.8
N_f	1552	1251	1050	905.7	796.9	712.1
N_w	12.7	11.5	10.5	9.65	8.94	8.33
	Reaction Section (Adiabatic, Model *C*)					
k_{ref}	0.046	0.046	0.046	0.046	0.046	0.046
D_L (cm^2/s)	0.074	0.081	0.088	0.095	0.10	0.11
K_{gl} (cm/s)	0.43	0.43	0.43	0.44	0.44	0.44
K_L (W/m.K)	0.35	0.35	0.35	0.35	0.35	0.35
C_{pg} (J/mol.K)	68.9	61.0	55.8	52.0	49.2	47.0
Da	5.33	4.26	3.55	3.05	2.66	2.37
Pe	135.7	154.6	170.4	183.9	195.5	205.6
Pe_H	22.1	24.4	26.8	29.1	31.5	33.8
ζ_m	5.26	5.06	4.89	4.75	4.62	4.51
ζ_H	76.7	86.7	94.8	101.7	107.5	112.5
N_f	1441	1163	975.8	841.8	740.8	662.1
γ_r	36.2	36.2	36.2	36.2	36.2	36.2
υ	1.4	1.4	1.4	1.4	1.4	1.4

Superscript: Ads: Adsorbent Bed Model

Table 4.15. Parametric Values for Thermal Swing SMBR Simulations (Case 19)

Run	**1**	**2**	**3**	**4**	**5**	**6**
Parameters	**Inlet Streams**					
F_{feed}	0.10	0.10	0.10	0.10	0.10	0.10
F_{Purge}	0.30	0.40	0.50	0.60	0.70	0.80
T_{feed} (K)	502	497	493	489	485	480
T_{purge} (K)	540	540	540	540	540	540
	Common Parameters					
$y_{A,ref}$	0.125	0.100	0.083	0.071	0.063	0.056
F_{ref} (mol/m^2.s)	0.40	0.50	0.60	0.70	0.80	0.90
T_{ref} (K)	514	514	514	514	514	514
γ_f	12.9	12.9	12.9	12.9	12.9	12.9
θ_{ref}	0.497	0.478	0.462	0.449	0.437	0.426
ζ_m^{Ads}	6.12	5.89	5.69	5.53	5.38	5.25
B^{Ads}	0.107	0.103	0.099	0.097	0.094	0.092
	Adsorption Section					
$T_{w,ads}$ (K)	430	430	430	430	430	430
D_L (cm^2/s)	0.057	0.063	0.069	0.075	0.081	0.087
K_{gl} (cm/s)	0.33	0.33	0.33	0.34	0.34	0.34
K_L (W/m.K)	0.35	0.35	0.35	0.35	0.35	0.35
C_{pg} (J/mol.K)	63.0	56.2	51.7	48.5	46.1	44.2
h_w (W/m^2.K)	15	15	15	15	15	15
Pe	125.1	141.6	155.2	166.6	176.4	184.8
Pe_H	14.4	16.1	17.7	19.4	21.1	22.7
ζ_H	97.8	109.5	119.1	127.0	133.7	139.4
N_f	1108	894.9	751.8	649.0	571.6	511.1
N_w	14.2	12.8	11.6	10.6	9.72	9.01

Table 4.15. Parametric Values for Thermal Swing SMBR Simulations (Case 19, continued)

Parameters	**Regeneration Section**					
$T_{w,des}$ (K)	540	540	540	540	540	540
D_L (cm^2/s)	0.079	0.086	0.094	0.10	0.11	0.12
K_{gl} (cm/s)	0.46	0.46	0.47	0.47	0.47	0.47
K_L (W/m.K)	0.35	0.35	0.35	0.35	0.35	0.35
C_{pg} (J/mol.K)	70.7	62.4	57.0	53.0	50.1	47.8
h_w (W/m^2.K)	15	15	15	15	15	15
Pe	90.2	103.0	113.8	123.0	130.9	137.7
Pe_H	16.2	17.8	19.5	21.2	22.9	24.6
ζ_H	87.1	98.6	108.1	116.1	122.9	128.8
N_f	1552	1251	1050	905.7	796.9	712.1
N_w	12.7	11.5	10.5	9.65	8.94	8.33
	Reaction Section (Adiabatic, Model *C*)					
k_{ref}	0.046	0.046	0.046	0.046	0.046	0.046
D_L (cm^2/s)	0.074	0.081	0.088	0.095	0.10	0.11
K_{gl} (cm/s)	0.43	0.43	0.43	0.44	0.44	0.44
K_L (W/m.K)	0.35	0.35	0.35	0.35	0.35	0.35
C_{pg} (J/mol.K)	68.9	61.0	55.8	52.0	49.2	47.0
Da	5.33	4.26	3.55	3.05	2.66	2.37
Pe	271.3	309.2	340.9	367.9	391	411.2
Pe_H	44.1	48.8	53.5	58.3	63.0	67.7
ζ_m	5.26	5.06	4.89	4.75	4.62	4.51
ζ_H	76.7	86.7	94.8	101.7	107.5	112.5
N_f	1441	1163	975.8	841.8	740.8	662.1
γ_r	36.2	36.2	36.2	36.2	36.2	36.2
υ	2.8	2.8	2.8	2.8	2.8	2.8

Superscript: Ads: Adsorbent Bed Model

Table 4.16. Parametric Values for Thermal Swing SMBR Simulations (Case 20)

Run	**1**	**2**	**3**	**4**	**5**	**6**
Parameters	**Inlet Streams**					
F_{feed}	0.05	0.05	0.05	0.05	0.05	0.05
F_{Purge}	0.15	0.20	0.25	0.30	0.35	0.40
T_{feed} (K)	460	460	460	460	460	460
T_{purge} (K)	540	540	540	540	540	540
	Common Parameters					
$y_{A,ref}$	0.125	0.100	0.083	0.071	0.063	0.056
F_{ref} (mol/m^2.s)	0.20	0.25	0.30	0.35	0.40	0.45
T_{ref} (K)	486.7	491.9	496.2	499.8	502.9	505.5
γ_f	13.7	13.5	13.4	13.3	13.2	13.1
θ_{ref}	0.555	0.526	0.502	0.481	0.462	0.446
ζ_m^{Ads}	6.47	6.20	5.97	5.76	5.57	5.40
B^{Ads}	0.126	0.118	0.112	0.106	0.102	0.098
	Adsorption Section					
$T_{w,ads}$ (K)	430	430	430	430	430	430
D_L (cm^2/s)	0.045	0.048	0.051	0.054	0.057	0.060
K_{gl} (cm/s)	0.31	0.32	0.32	0.32	0.32	0.32
K_L (W/m.K)	0.35	0.35	0.35	0.35	0.35	0.35
C_{pg} (J/mol.K)	63.0	56.2	51.7	48.5	46.1	44.2
h_w (W/m^2.K)	15	15	15	15	15	15
Pe	74.9	88.8	101.2	112.3	122.4	131.5
Pe_H	7.20	8.03	8.86	9.70	10.5	11.4
ζ_H	92.6	104.8	115	123.5	130.8	137.1
N_f	2237	1784	1484	1271	1111	987.5
N_w	28.4	25.5	23.1	21.1	19.4	18.0

Table 4.16. Parametric Values for Thermal Swing SMBR Simulations (Case 20, continued)

Parameters	**Regeneration Section**					
$T_{w,des}$ (K)	540	540	540	540	540	540
D_L (cm^2/s)	0.064	0.068	0.071	0.075	0.079	0.083
K_{gl} (cm/s)	0.44	0.45	0.45	0.45	0.45	0.45
K_L (W/m.K)	0.35	0.35	0.35	0.35	0.35	0.35
C_{pg} (J/mol.K)	70.7	62.4	57.0	53.0	50.1	47.8
h_w (W/m^2.K)	15	15	15	15	15	15
Pe	52.7	62.9	72.2	80.6	88.3	95.3
Pe_H	8.08	8.92	9.76	10.6	11.5	12.3
ζ_H	82.5	94.4	104.4	112.9	120.3	126.6
N_f	3155	2514	2088	1786	1561	1386
N_w	25.4	23.0	21.0	19.3	17.9	16.7
	Reaction Section (Adiabatic, Model *C*)					
k_{ref}	0.006	0.009	0.013	0.016	0.021	0.025
D_L (cm^2/s)	0.055	0.059	0.063	0.067	0.071	0.075
K_{gl} (cm/s)	0.38	0.39	0.39	0.40	0.41	0.41
K_L (W/m.K)	0.35	0.35	0.35	0.35	0.35	0.35
C_{pg} (J/mol.K)	67.1	59.8	54.9	51.4	48.8	46.7
Da	1.48	1.75	2.01	2.24	2.45	2.62
Pe	86.7	101.4	114.6	126.3	136.9	146.6
Pe_H	10.7	12.0	13.2	14.4	15.6	16.8
ζ_m	5.56	5.32	5.13	4.95	4.78	4.64
ζ_H	74.7	84.6	92.9	100.0	106.0	111.3
N_f	2693	2180	1834	1593	1404	1257
γ_r	38.3	37.9	37.5	37.3	37.0	36.8
υ	1.4	1.4	1.4	1.4	1.4	1.4

Superscript: Ads: Adsorbent Bed Model

Table 4.17. Parametric Values for Thermal Swing SMBR Simulations (Case 21)

Run	**1**	**2**	**3**	**4**	**5**	**6**
Parameters	**Inlet Streams**					
F_{feed}	0.05	0.05	0.05	0.05	0.05	0.05
F_{Purge}	0.15	0.20	0.25	0.30	0.35	0.40
T_{feed} (K)	430	430	430	430	430	430
T_{purge} (K)	540	540	540	540	540	540
	Common Parameters					
$y_{A,ref}$	0.125	0.100	0.083	0.071	0.063	0.056
F_{ref} (mol/m^2.s)	0.20	0.25	0.30	0.35	0.40	0.45
T_{ref} (K)	467.6	474.9	480.8	485.7	489.8	493.4
γ_f	14.2	14.0	13.8	13.7	13.6	13.5
θ_{ref}	0.597	0.564	0.537	0.513	0.492	0.474
ζ_m^{Ads}	6.69	6.42	6.19	5.97	5.77	5.60
B^{Ads}	0.141	0.131	0.123	0.117	0.111	0.106
	Adsorption Section					
$T_{w,ads}$ (K)	430	430	430	430	430	430
D_L (cm^2/s)	0.045	0.048	0.051	0.054	0.057	0.060
K_{gl} (cm/s)	0.31	0.32	0.32	0.32	0.32	0.32
K_L (W/m.K)	0.35	0.35	0.35	0.35	0.35	0.35
C_{pg} (J/mol.K)	63.0	56.2	51.7	48.5	46.1	44.2
h_w (W/m^2.K)	15	15	15	15	15	15
Pe	72.0	85.7	98.0	109.2	119.2	128.4
Pe_H	7.20	8.03	8.86	9.70	10.5	11.4
ζ_H	89.0	101.2	111.4	120.0	127.4	133.8
N_f	2323	1845	1529	1305	1139	1010
N_w	28.4	25.5	23.1	21.1	19.4	18.0

Table 4.17. Parametric Values for Thermal Swing SMBR Simulations (Case 21, continued)

Parameters	**Regeneration Section**					
$T_{w,des}$ (K)	540	540	540	540	540	540
D_L (cm^2/s)	0.064	0.068	0.071	0.075	0.079	0.083
K_{gl} (cm/s)	0.44	0.44	0.45	0.45	0.45	0.45
K_L (W/m.K)	0.35	0.35	0.35	0.35	0.35	0.35
C_{pg} (J/mol.K)	70.7	62.4	57.0	53.0	50.1	47.8
h_w (W/m^2.K)	15	15	15	15	15	15
Pe	50.7	60.8	69.9	78.3	86.0	93.0
Pe_H	8.08	8.92	9.76	10.6	11.5	12.3
ζ_H	79.3	91.1	101.1	109.7	117.1	123.6
N_f	3279	2599	2152	1835	1600	1418
N_w	25.4	23.0	21.0	19.3	17.9	16.7
	Reaction Section (Adiabatic, Model *C*)					
k_{ref}	0.001	0.002	0.004	0.006	0.008	0.010
D_L (cm^2/s)	0.051	0.056	0.060	0.064	0.069	0.073
K_{gl} (cm/s)	0.36	0.37	0.38	0.38	0.39	0.40
K_L (W/m.K)	0.35	0.35	0.35	0.35	0.35	0.35
C_{pg} (J/mol.K)	65.7	58.9	54.2	50.9	48.3	46.3
Da	0.32	0.47	0.62	0.78	0.93	1.09
Pe	88.6	103.3	116.3	128.0	138.5	148
Pe_H	10.5	11.8	13.0	14.2	15.5	16.7
ζ_m	5.74	5.51	5.31	5.13	4.96	4.81
ζ_H	73.2	83.0	91.3	98.3	104.3	109.6
N_f	2639	2142	1806	1564	1380	1237
γ_r	39.8	39.2	38.7	38.3	38.0	37.7
υ	1.4	1.4	1.4	1.4	1.4	1.4

Superscript: Ads: Adsorbent Bed Model

Table 4.18. Switch Times for Thermal Swing SMBR Simulations

Run	**1**	**2**	**3**	**4**	**5**	**6**
Case	τ_s **(min)**					
8	118.3	128.0	132.3	133.7	135.3	136.0
9	129.2	134.8	136.7	139.2	140.8	141.7
10	129.9	134.6	137.3	139.1	140.0	140.6
11	128.2	131.3	132.5	132.3	131.5	130.6
12	129.7	134.8	137.3	138.5	139.8	140.4
13	129.5	134.6	136.8	139.1	140.2	140.8
14	128.0	128.8	126.9	122.3	113.9	107.6
15	115.9	119.8	122.3	125.7	126.6	127.1
16	101.1	104.5	107.2	109.0	109.6	110.2
17	113.3	118.0	120.3	121.7	122.7	123.3
18	64.0	65.8	66.0	64.8	62.7	59.1
19	64.6	65.9	67.3	68.1	68.8	69.1
20	130.9	135.4	137.7	139.2	139.9	139.8
21	58.6	82.7	89.7	97.4	102.5	106.8
22	93.6	104.8	87.4	117.7	112.3	128.1

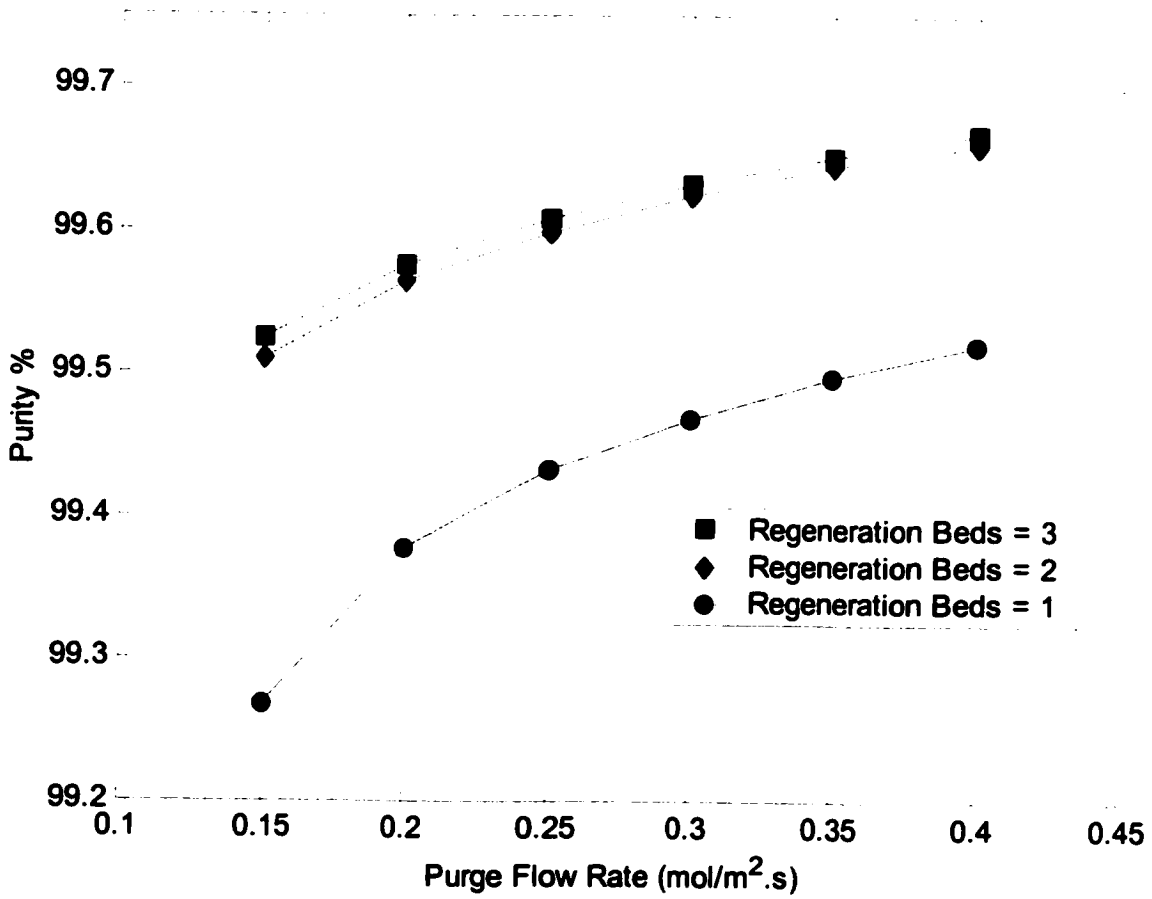

Figure 4.10. Effect of Number of Beds on Product Purity (Cases 8, 9 & 10)

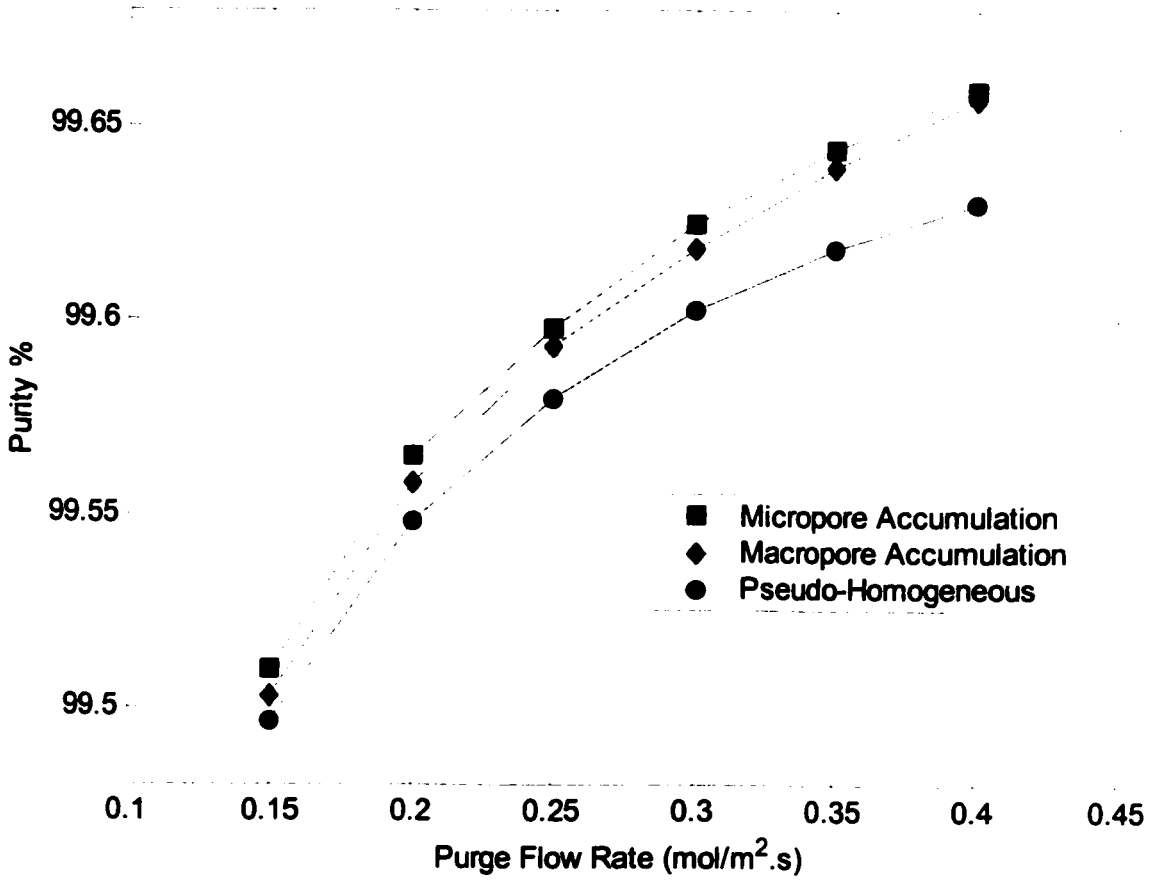

Figure 4.11. Effect of Using Various Reactor Models on Product Purity (Cases 9, 11 & 12)

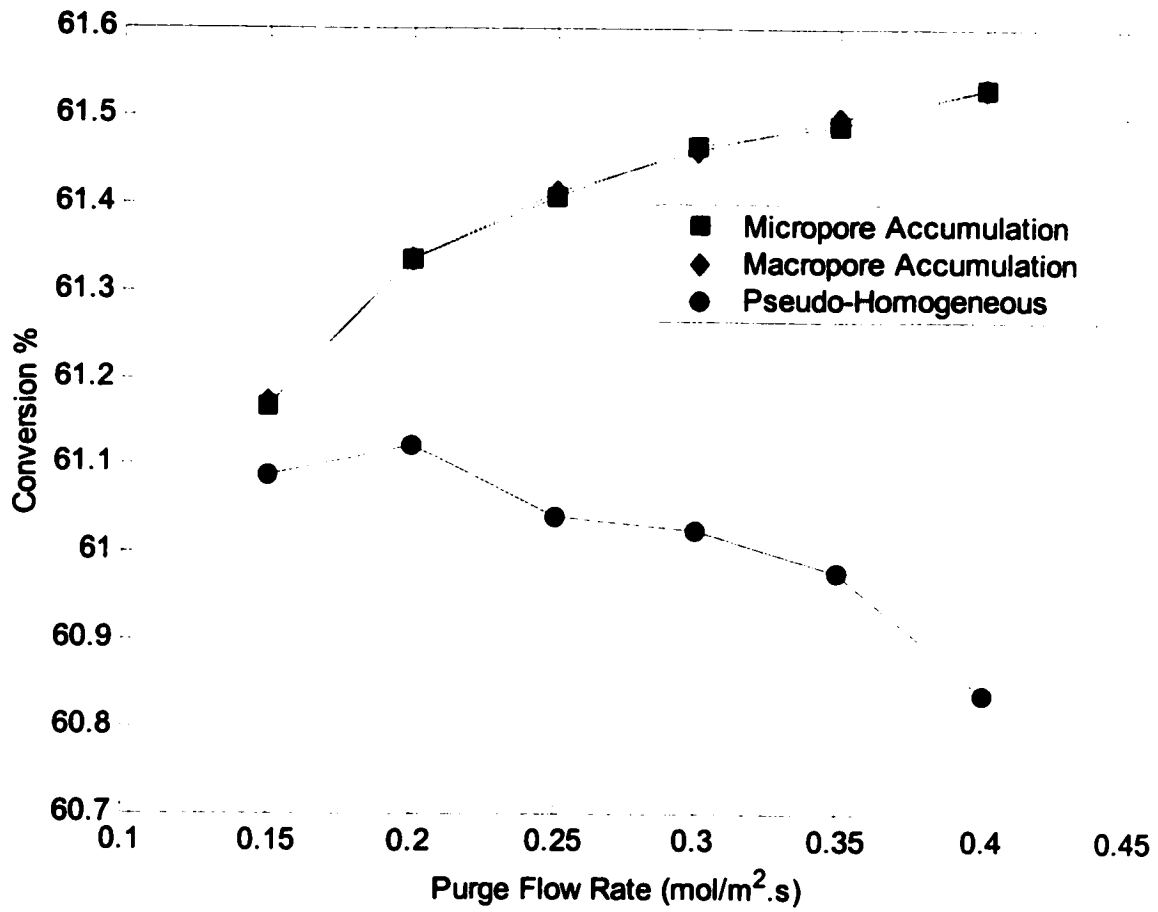

Figure 4.12. Effect of Using Various Reactor Models on Single Pass Conversion (Cases 9, 11 & 12)

performance of the regeneration section. As a result, this method does not measure the performance of the reaction section in an absolute sense.

The switch times for the heterogeneous models (cases 9 & 12) are also similar. The deviation of switch times for the pseudo-homogeneous model (case 11) must be for the same reason mentioned above, i.e. insufficient catalyst bed length. With lesser conversion, the amount of *n*-pentane to be separated increases thus lowering its breakthrough time and correspondingly the switch time.

The effect of changing the catalyst bed length is illustrated in Figures 4.13 and 4.14. Single pass conversion decreases when the length is not sufficient, i.e. L_2 = 10 cm, but the purity is not affected by any considerable amount, perhaps because of the high temperature swing. However, the presence of a maximum in the purity plot is of importance. Increase in purge flow rate cleans the adsorbent beds more efficiently but at the same time lowers the conversion. These two opposing forces produce the maximum. The switch times (case 14) are also lesser than those of the base case (case 9) and a decreasing trend in switch time is observed with increase in purge flow rate, which is characteristic for a system with insufficient catalyst bed length. The regular length used in the simulation runs for this study, i.e. L_2 = 28 cm, is adequate and neither affects the purity nor the conversion because similar results are obtained if it is increased by 30%. The switch times also remain the same (cases 9 and 13).

Having determined the number of beds and the catalyst bed length, concentration profiles are studied next. Cyclic steady state gas phase concentration profiles (case 9, run 1) are shown in Figures 4.15 to 4.17 at various times during a switching period. Reaction

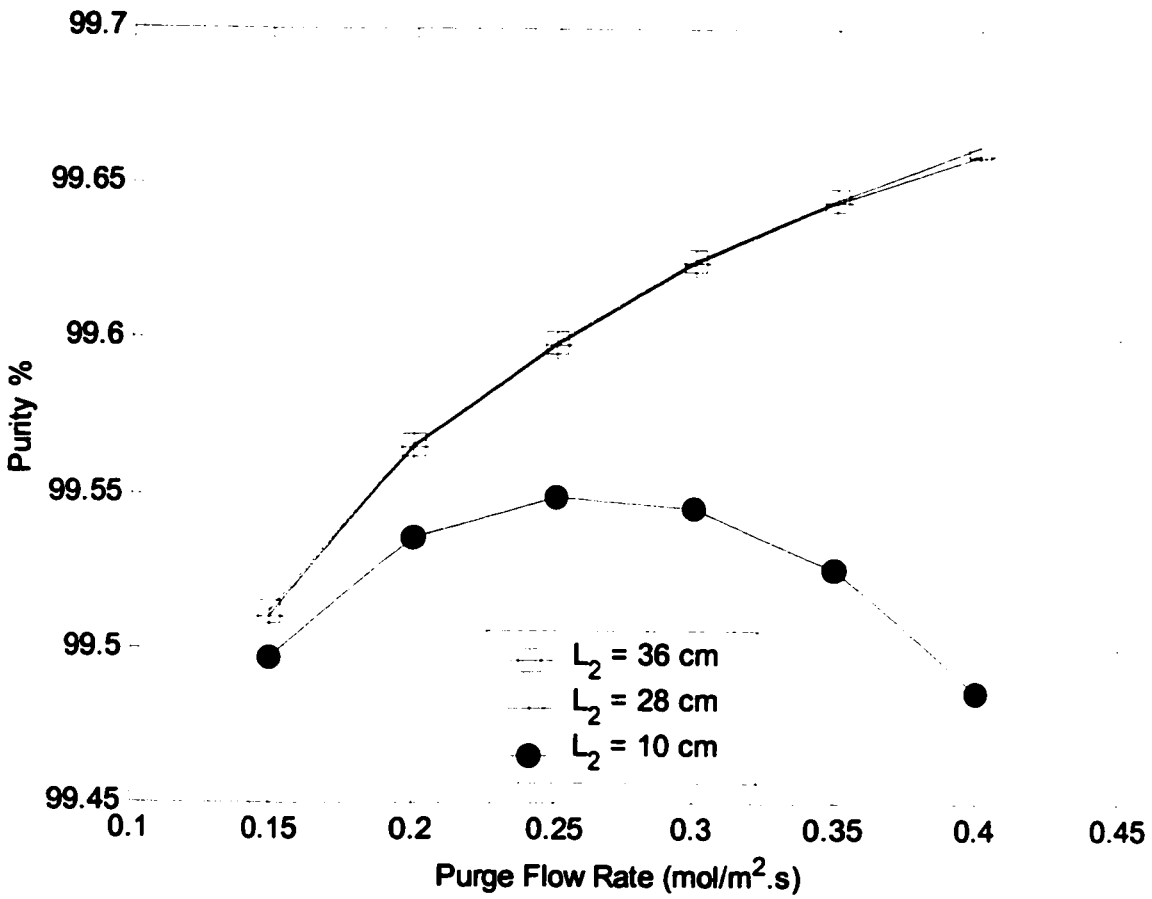

Figure 4.13. Effect of Reaction Section Length on Product Purity (Cases 9, 13 & 14)

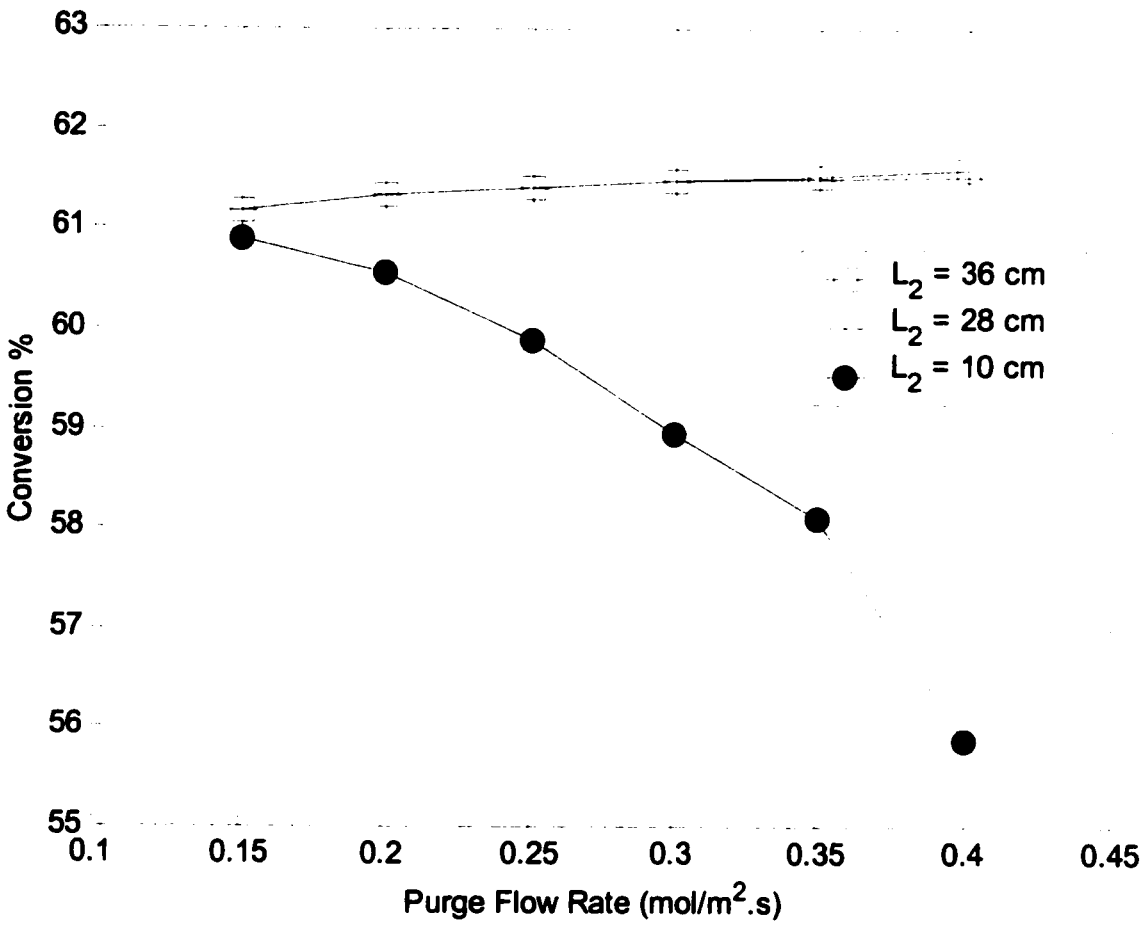

Figure 4.14. Effect of Reaction Section Length on Single Pass Conversion (Cases 9, 13 & 14)

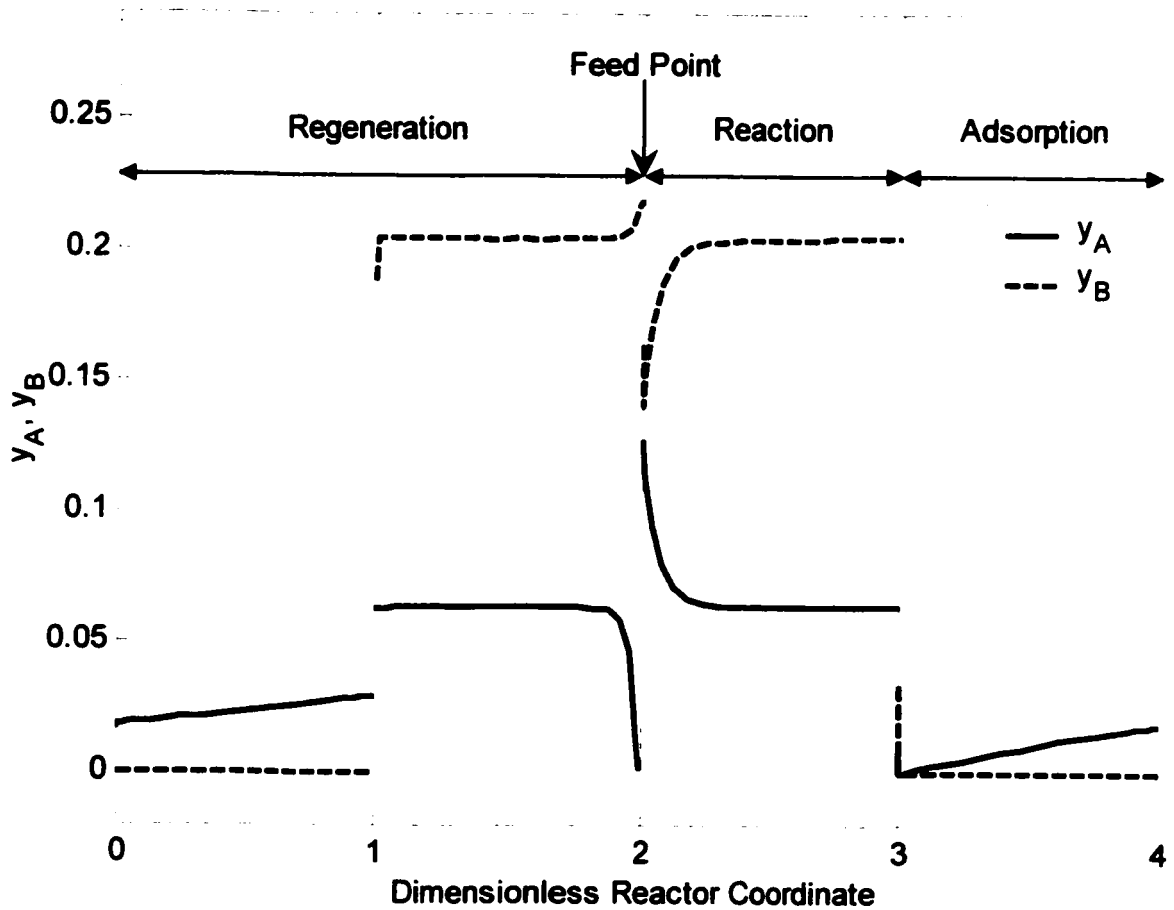

Figure 4.15. Cyclic Steady State Concentration Profiles of *n*-/iso- Pentanes just after Switching Flows (Case 9, Run 1)

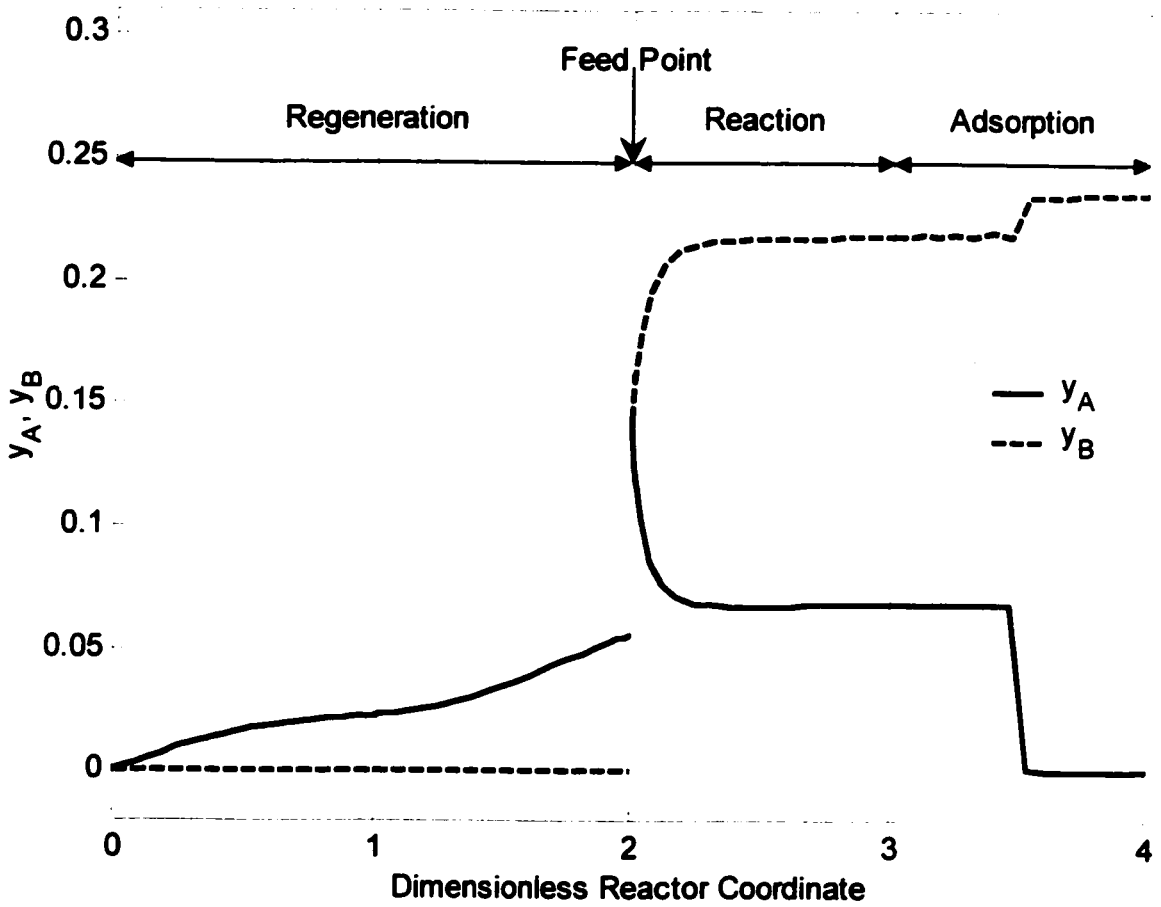

Figure 4.16. Cyclic Steady State Concentration Profiles of *n*-/iso- Pentanes at Half-time Between Switching Flows (Case 9, Run 1)

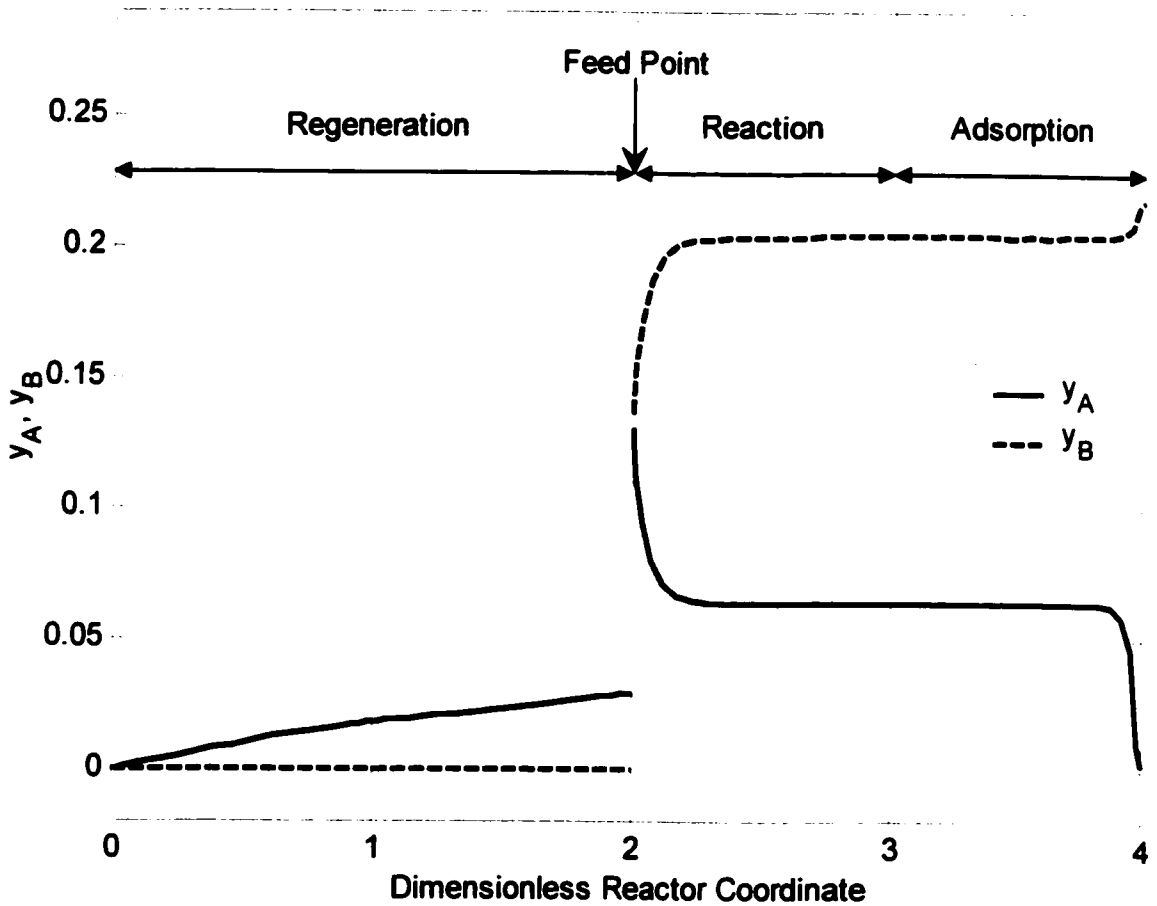

Figure 4.17. Cyclic Steady State Concentration Profiles of *n*-/iso- Pentanes just before Switching Flows (Case 9, Run 1)

takes place in the initial portion of the catalyst bed, which confirms that it is of sufficient length. Moreover, the adsorption front almost reaches the end of the bed when switching takes place. In fact, this is the optimum time to switch flows. The isopentane is flushed very quickly from the regeneration section, as it is not adsorbed over the adsorbent.

The profiles at the beginning of the switching period cannot be understood without first analyzing those at the end of the period. There is no difference between the two because cyclic steady state is reached except that they are shifted by one adsorbent bed. The catalyst bed, however, remains in its original position. When a bed in adsorption section is switched to the regeneration section, it suddenly encounters a zero feed concentration of isopentane. The concentration at the first node becomes different from the rest of the bed because of the Danckwert's boundary conditions thus leading to a slight discontinuity at the entrance (Figure 4.15). The other discontinuities can be explained in a similar manner.

The corresponding adsorbed phase concentration profiles are shown in Figures 4.18 to 4.20. The adsorbed phase concentration in the adsorption section is greater than that in the reaction section because the former operates at a much lower temperature. Moreover, it exceeds unity as the original quantity is normalized using the reference stream parameters at 514 K, i.e. the approximate reaction section temperature. It is surprising that the adsorbed phase concentration of *n*-pentane in the regeneration section is also higher than that in the reaction section, although the former operates at a higher temperature. This is because the adsorbed phase in the catalyst undergoes reaction and is shared by both the *n*-pentane and its isomer.

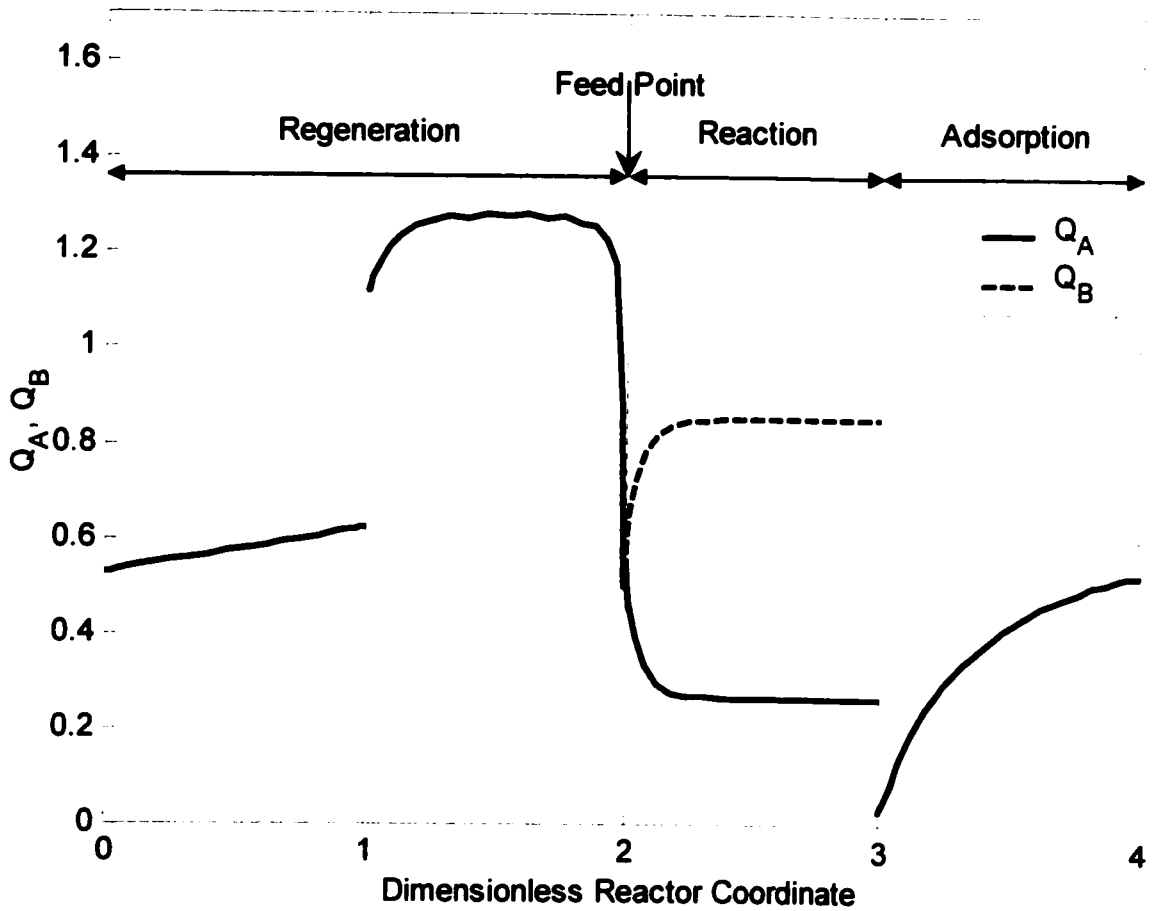

Figure 4.18. Cyclic Steady State Adsorbed Phase Concentration Profiles just after Switching Flows (Case 9, Run 1)

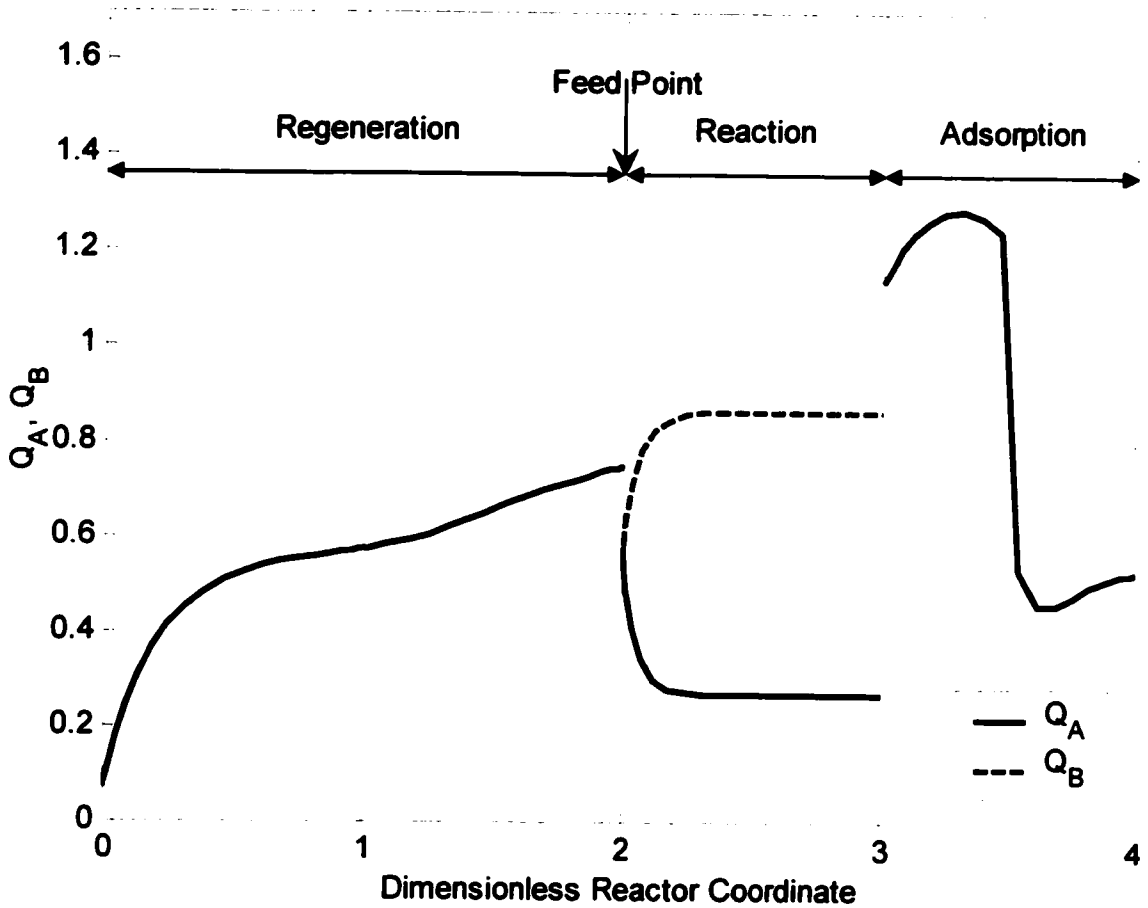

Figure 4.19. Cyclic Steady State Adsorbed Phase Concentration Profiles at Half-time Between Switching Flows (Case 9, Run 1)

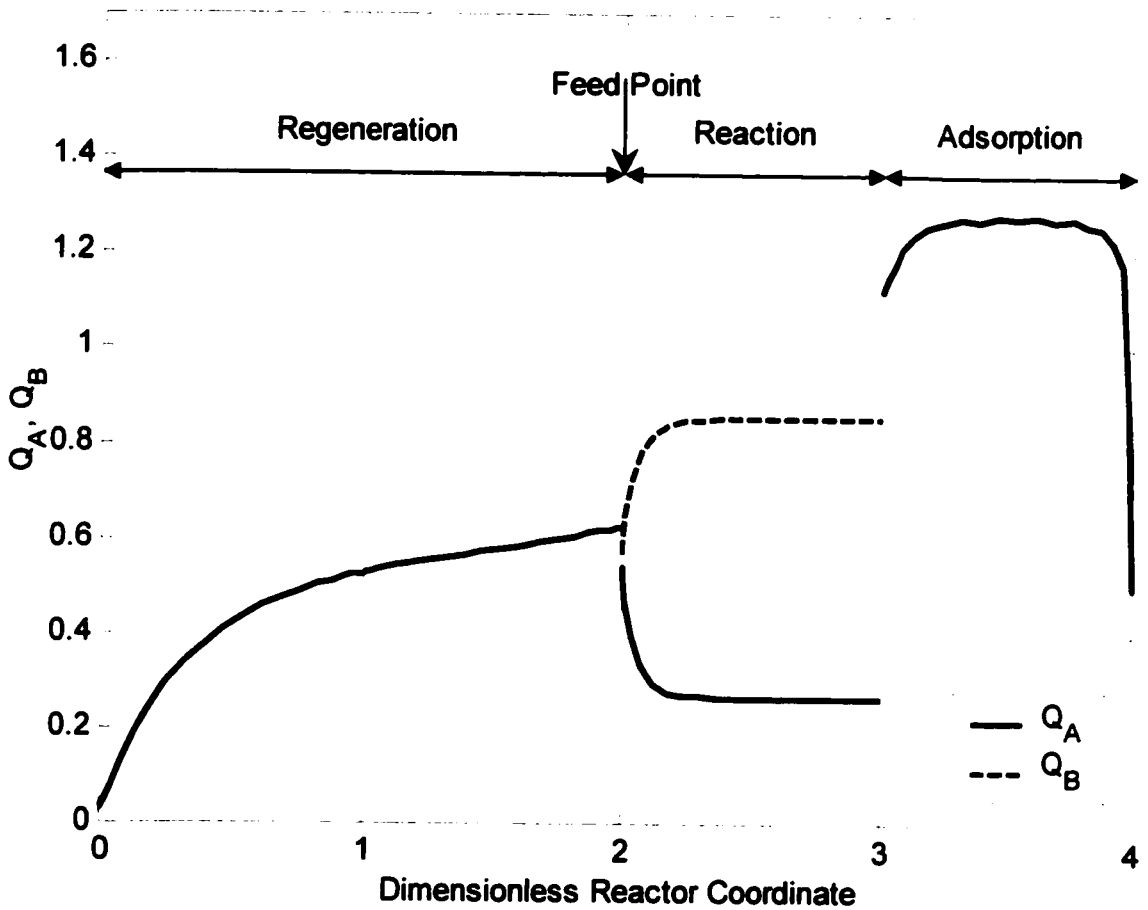

Figure 4.20. Cyclic Steady State Adsorbed Phase Concentration Profiles just before Switching Flows (Case 9, Run 1)

Despite the high regeneration temperature, a significant amount of sorbate remains in the adsorbent bed. This causes impurity in the product stream during subsequent switching. The gas and adsorbed phase concentration profiles during the middle of switching period are worth noticing in this regard. A considerable amount of adsorbed phase *n*-pentane is present at the exit of the adsorption section (Figure 4.19), which is the leftover from the regeneration section. However, the corresponding gas phase concentration is zero (Figure 4.16). In fact, it is not exactly nil but the oscillations are so high in that region that they reach negative values. They are thus filtered off and the final output becomes zero. Moreover, this leftover sorbate is held strongly in the adsorption section because of the lower temperature so that the corresponding gas phase concentration is actually very small. This is the basis for getting the desired >99% purity. It should be noted that the curve fitting is performed only while plotting the profiles and no such manipulation is made in calculating the purity or conversion.

The consequent temperature profiles of the system are illustrated in Figures 4.21 to 4.23. The regeneration section temperature does not change by an appreciable amount and remains almost constant at T_{purge}. This is because desorption is a slow process so that any drop in temperature is immediately compensated by the constant wall temperature. Moreover, that of the reaction section stays uniform at the desired value of 514 K as the vessel is adiabatic and the heat effects over the catalyst are neglected. However, adsorption is favorable so that the temperature front travels through the adsorption section. Furthermore, fluid does not reach the desired operating temperature immediately upon admission and so the adsorbed phase concentration is not maximum at the entrance.

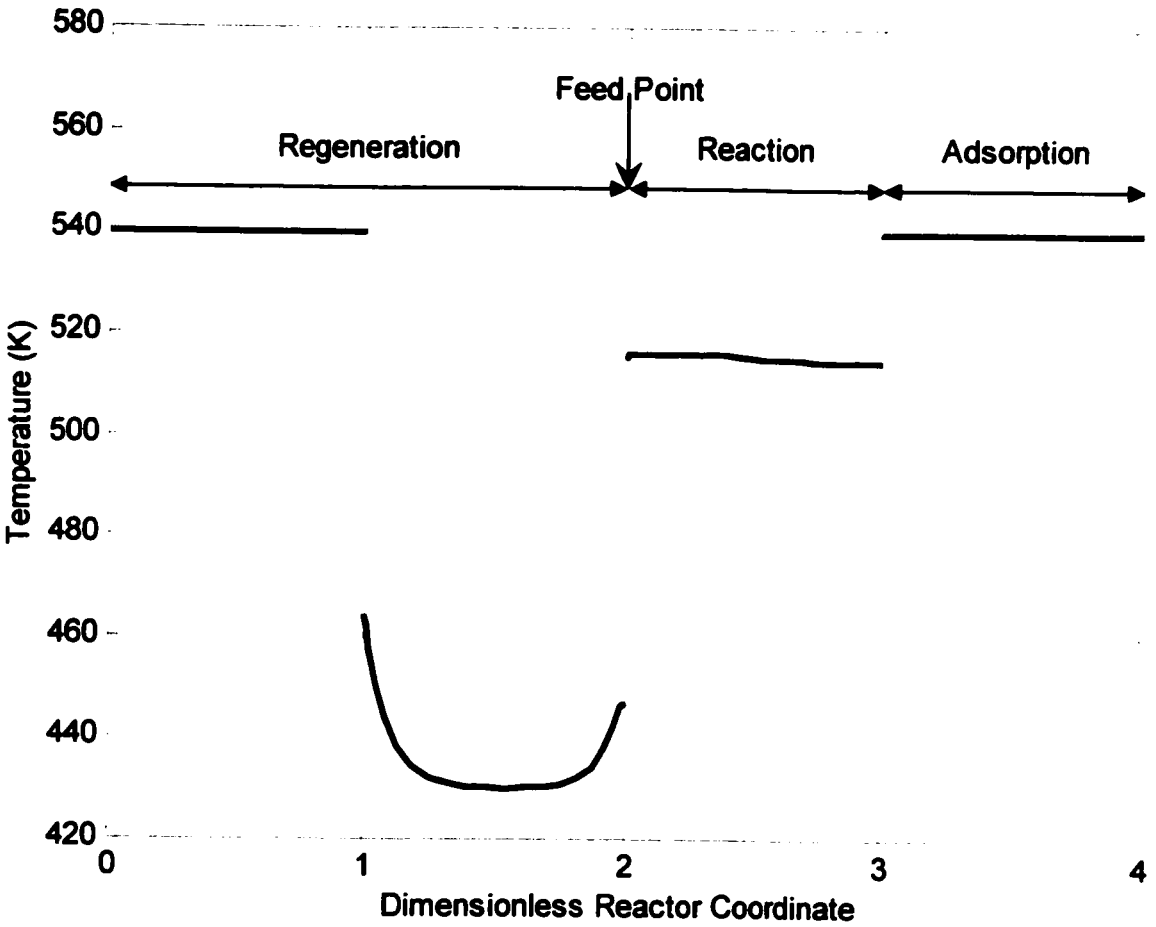

Figure 4.21. Cyclic Steady State Temperature Profile just after Switching Flows (Case 9, Run 1)

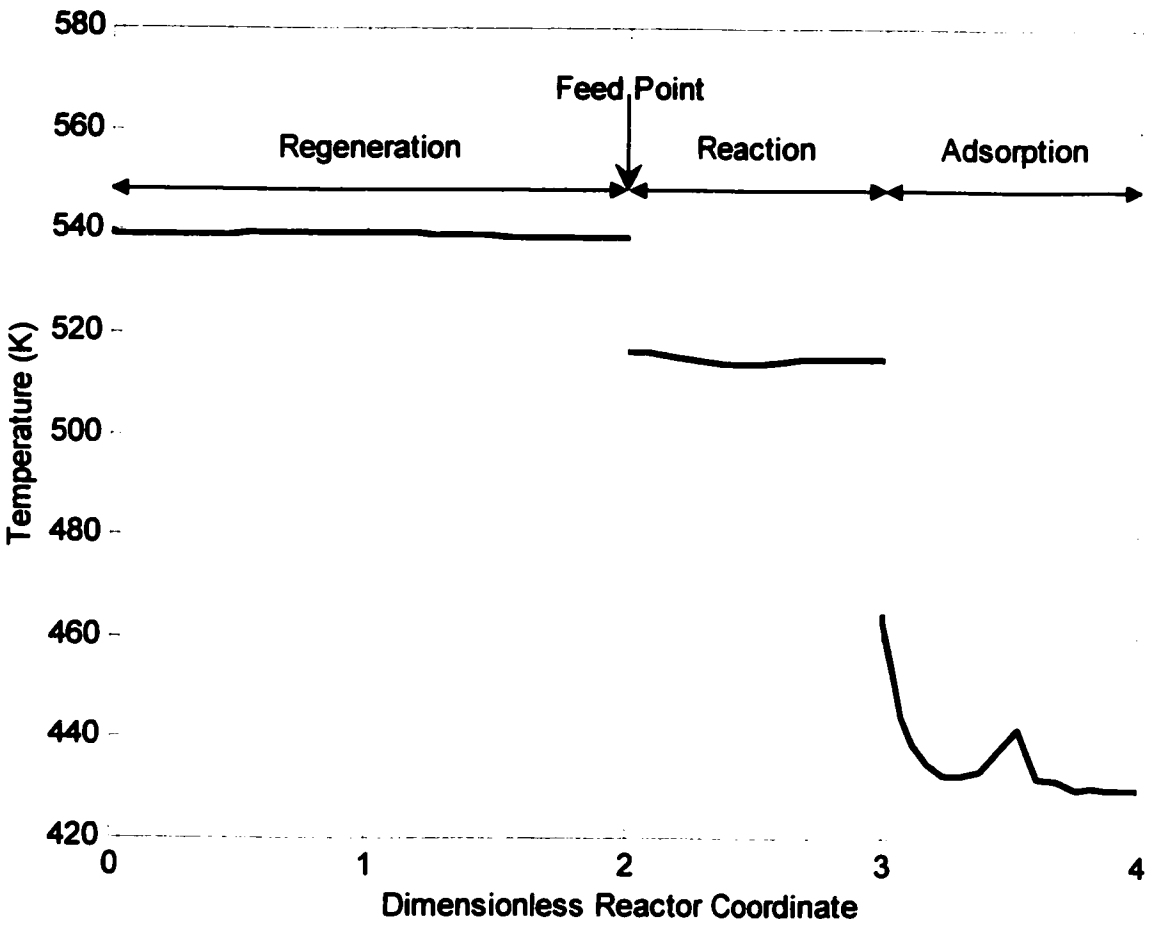

Figure 4.22. Cyclic Steady State Temperature Profile at Half-time Between Switching Flows (Case 9, Run 1)

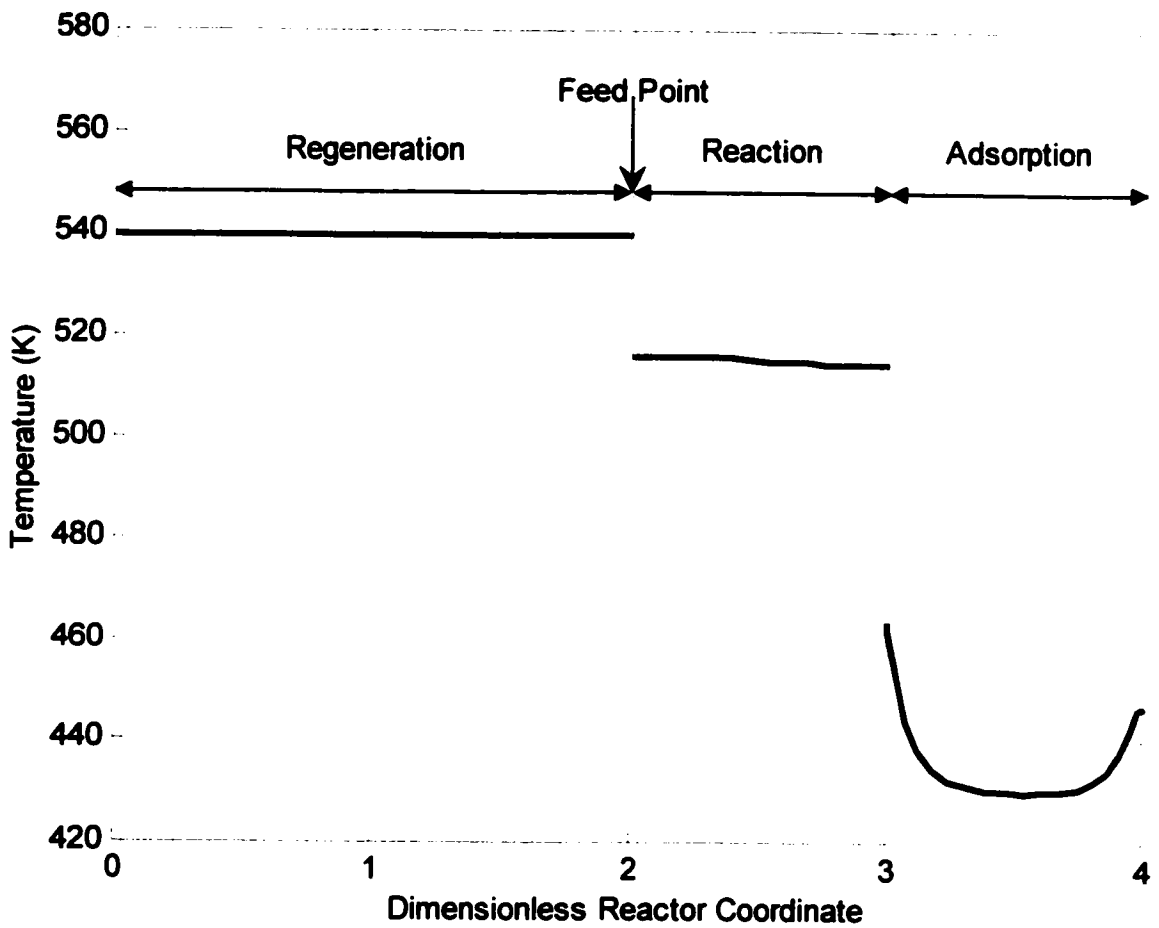

Figure 4.23. Cyclic Steady State Temperature Profile just before Switching Flows (Case 9, Run 1)

The effect of reducing the temperature swing is the lowering of product purity (Figure 4.24), as the beds are cleaned less thoroughly. The switch times also reduce for the same reason (cases 15 and 16). It is important to optimize the amount of temperature swing for two reasons. Firstly, repeated thermal cycling can substantially reduce the life of the adsorbent. Secondly, the saturation pressure for steam over the adsorbers in the regeneration section may be so high that it might not be feasible to produce such a high-pressure steam in the industry. However, the usage of thermal swing in this study is justified because a 100 K rise in temperature usually occurs in a normal adiabatic adsorption process. Besides, the maximum steam saturation pressure needed is 5.2 MPa for the temperatures used in this study.

As mentioned in Chapter 3 the adsorption equilibrium constant K_{ads} is governed by a vant Hoff equation (equation 3.6b). Using a regeneration temperature of 520 K (case 15) instead of 540 K increases K_{ads} from 4.4 bar^{-1} to 7.1 bar^{-1} only. However, employing an adsorption temperature of 450 K (case 17) rather than the regular 430 K reduces K_{ads} tremendously from 102.9 bar^{-1} to 51.8 bar^{-1}. Thus even if the temperature difference is identical, the actual operating temperatures of the two sections determine the system performance (Figure 4.25). Had the dependency of K_{ads} on temperature been linear, the temperature difference alone would have been enough to find out the purity.

Increasing the fresh feed flow rate requires a longer catalyst bed in the SMBR to get the maximum possible purity (Figure 4.26). The purge flow rate is also increased by the same amount to keep the mole fraction of hydrocarbons same. The longer length of reaction section (L_2 = 56 cm) eliminates any effect of single pass conversion on purity

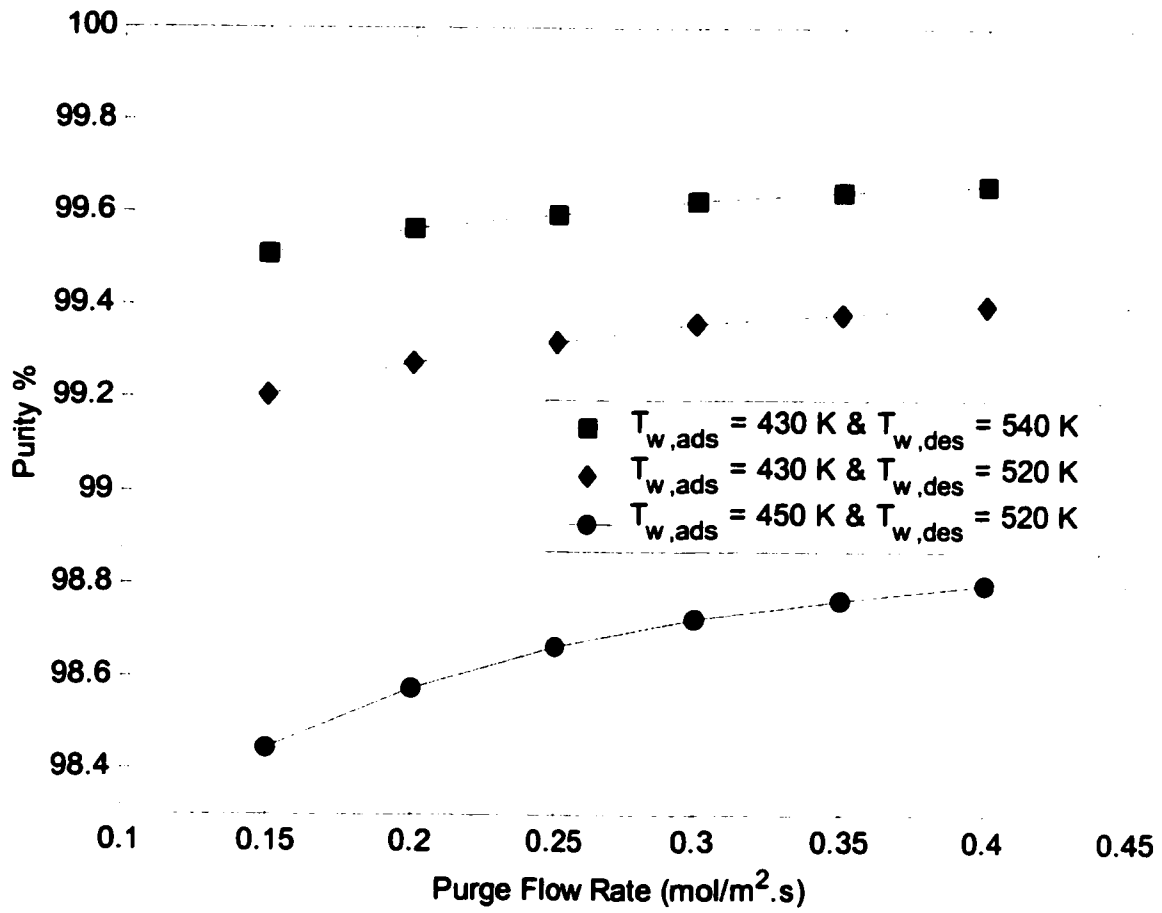

Figure 4.24. Effect of Temperature Difference between Adsorption and Regeneration Sections on Product Purity (Cases 9, 15 & 16)

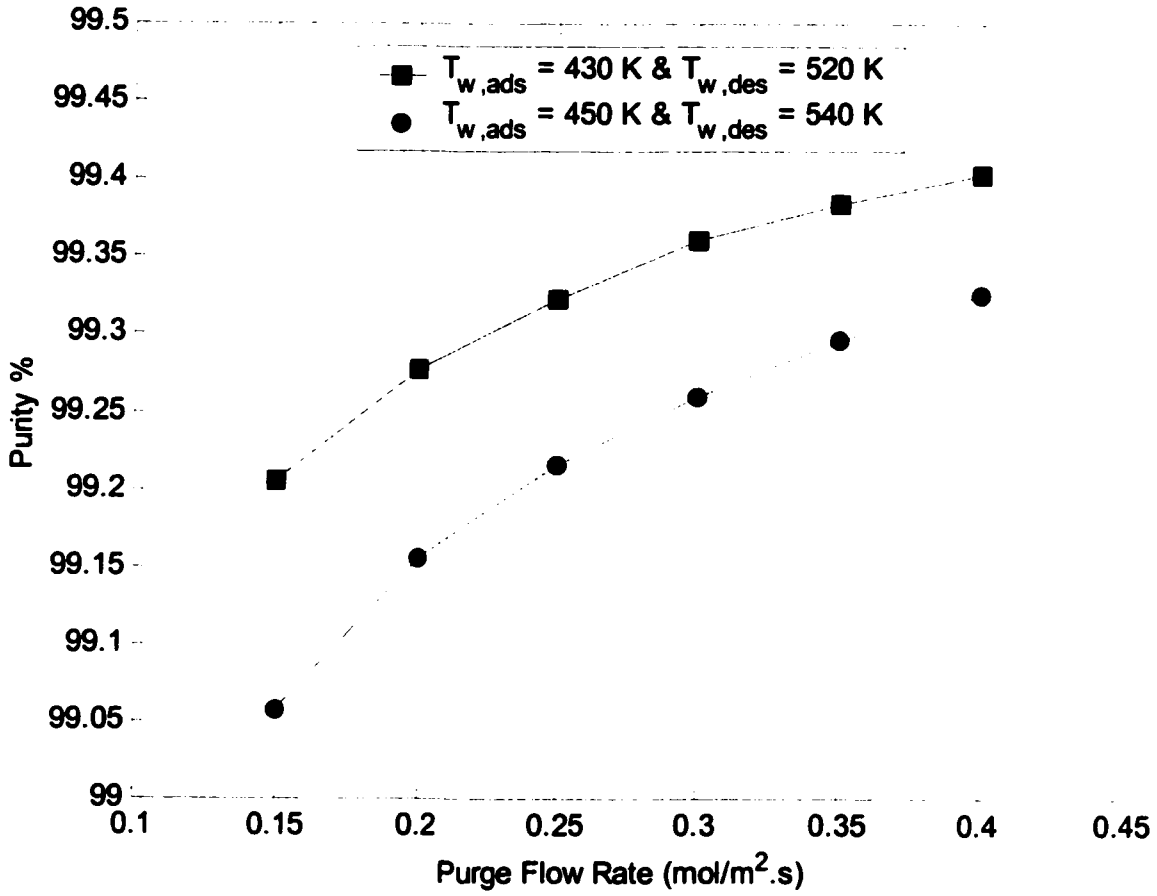

Figure 4.25. Effect of Temperature on Product Purity While Maintaining the Temperature Difference Constant (Cases 15 & 17)

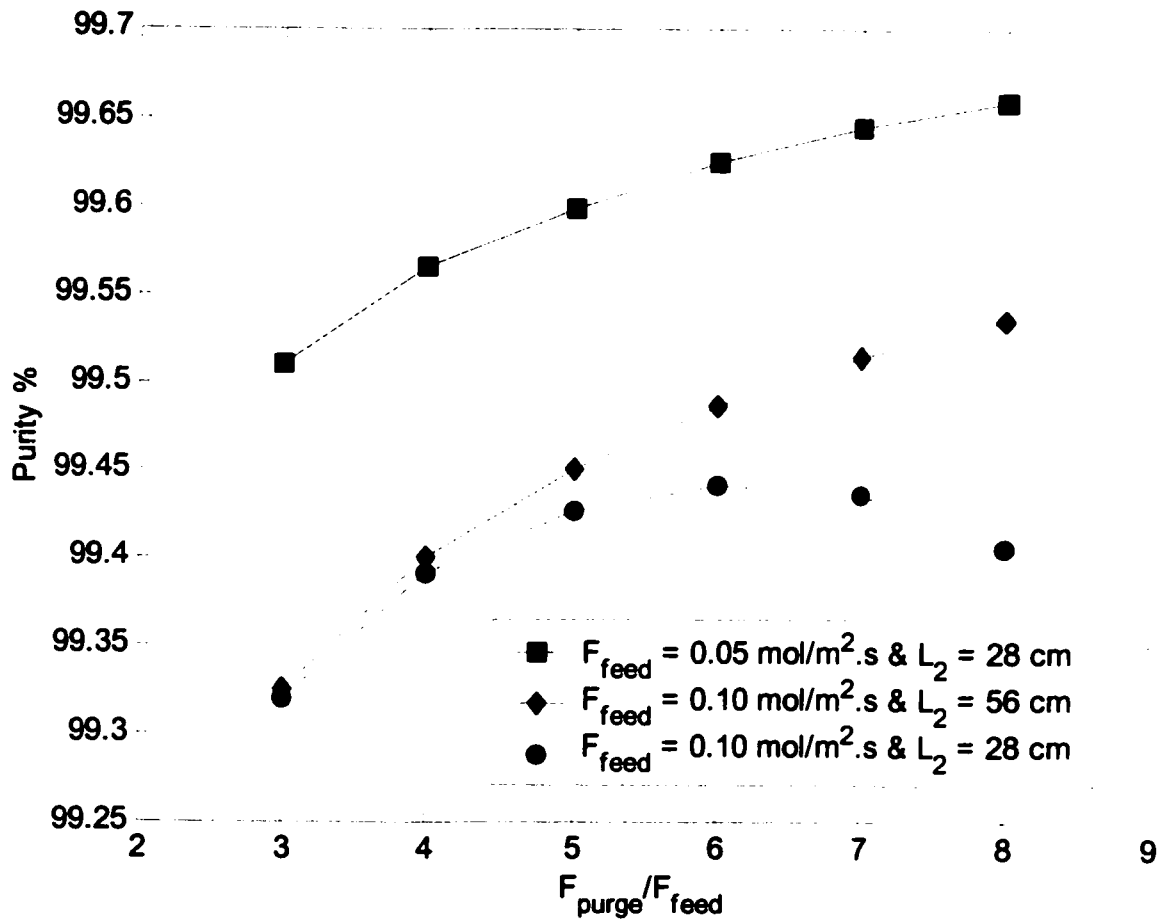

Figure 4.26. Effect of Inlet Flow Rates and Reaction Section Length on Product Purity (Cases 9, 18 & 19)

(Figure 4.27). However, it does not restore the purity to its original value. Thus, a mere knowledge of purge to fresh feed ratio is not sufficient to specify the system performance so that the individual flow rates of the inlet streams must be known. The switch times are halved because of doubling the fluid flow rates (cases 18 and 19). Consequently, the regeneration section is expected to give the same efficiency. Nevertheless, it is unclear at this stage whether the slight reduction in purity is because of the numerical uncertainties involved or because the beds are cleaned less thoroughly.

Until now, the fresh feed temperature was calculated for each simulation run, with the intention that the temperature of the resultant mixed stream was exactly 514 K during the first switching period and close to it during the subsequent switches. In the base case (case 9), the fresh feed temperature varied between 502 K and 480 K (Table 4.8) for the range of purge flow rates used (0.15 mol/m^2.s-0.40 mol/m^2.s). Nevertheless, it is important to study the effect of temperature fluctuations in fresh feed on the performance of the SMBR model. Surprisingly, both the purity and the single pass conversion remain the same if the fresh feed temperature is reduced to 460 K (Figures 4.28 and 4.29). In fact, the resulting mixed stream temperature varied between 487 K and 506 K (Table 4.16). Therefore, a wide range of temperatures exists at which maximum conversion is obtained so that it was not at all necessary to operate the reaction section at precisely 514 K in the previous simulations.

The performance deteriorates significantly if the fresh feed temperature is too low, i.e. 430 K. However, it improves by increasing the hot purge supply as the reaction temperature then becomes favorable to produce the mixture at near equilibrium

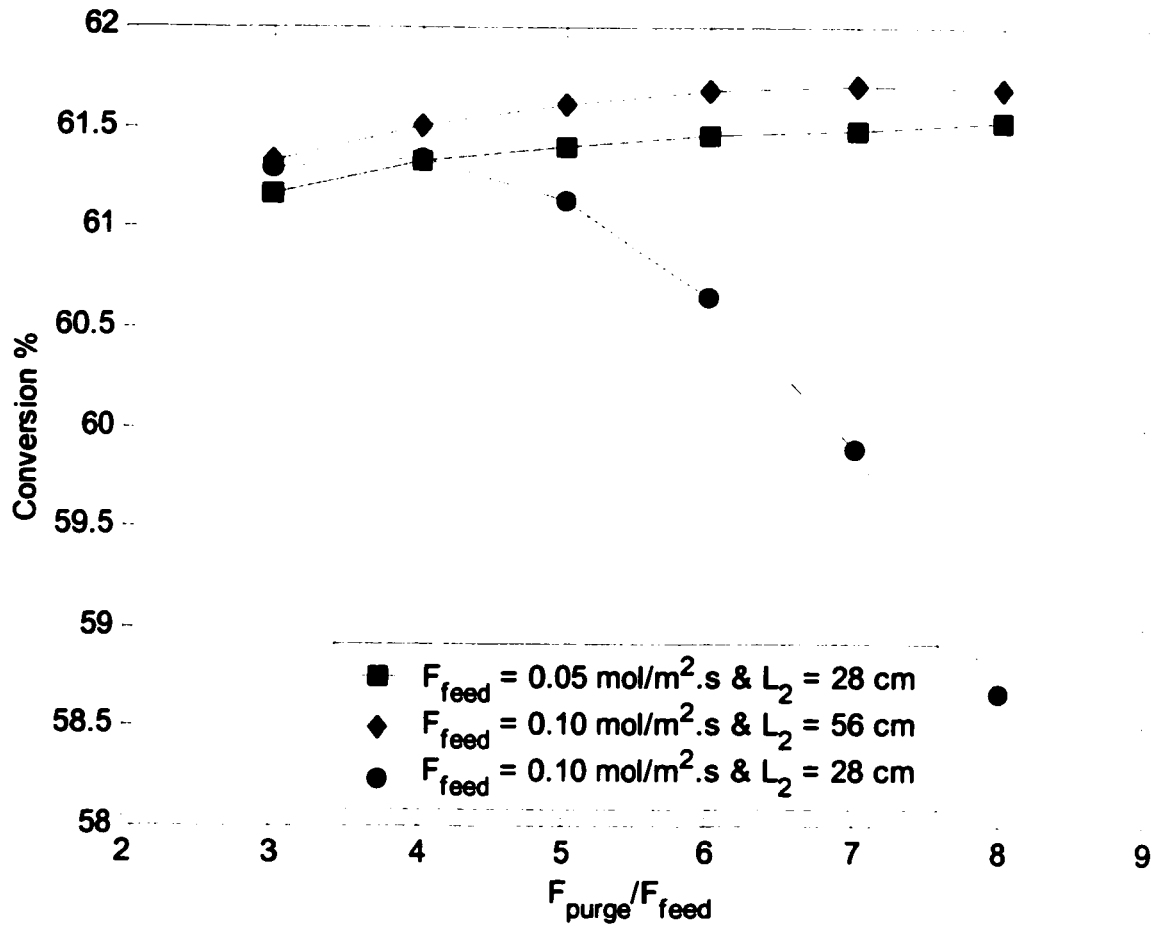

Figure 4.27. Effect of Inlet Flow Rates and Reaction Section Length on Single Pass Conversion (Cases 9, 18 & 19)

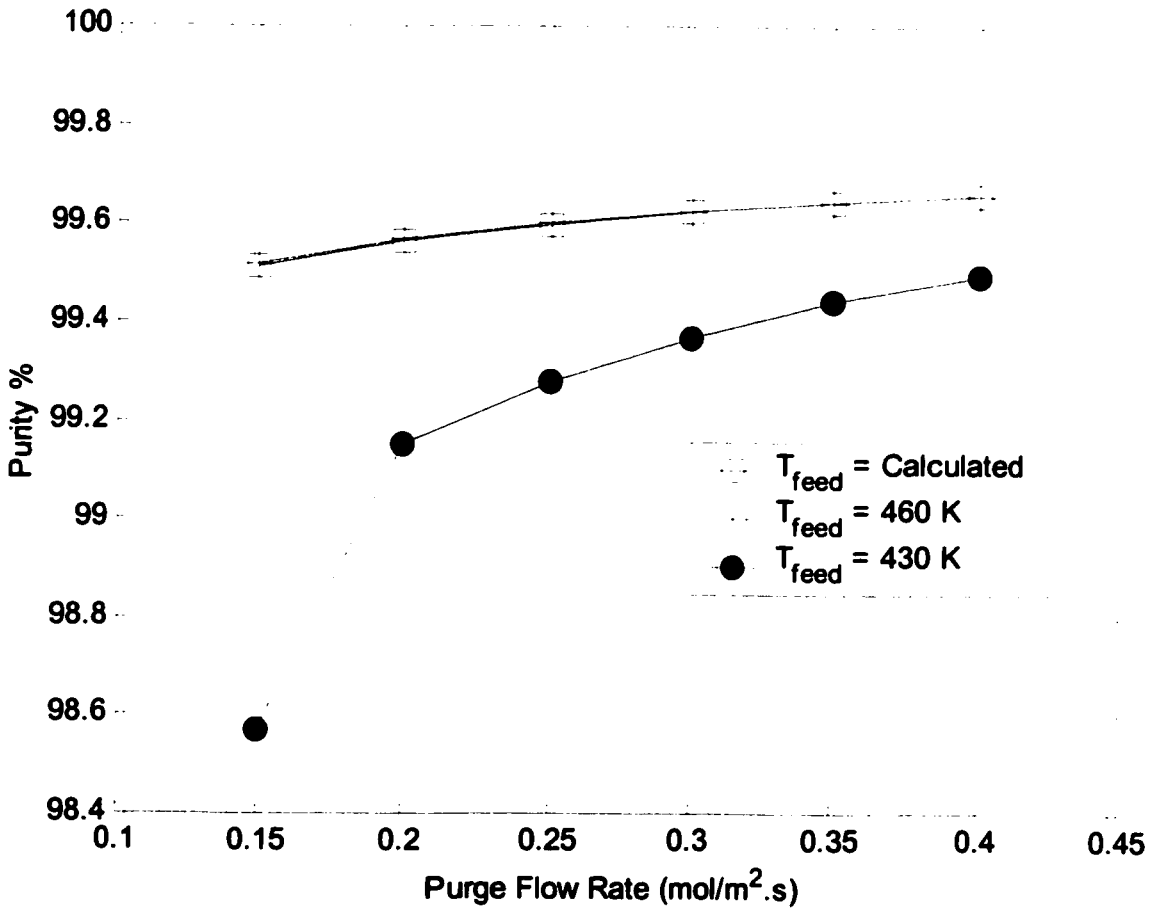

Figure 4.28. Effect of Fresh Feed Temperature on Product Purity (Cases 9, 20 & 21)

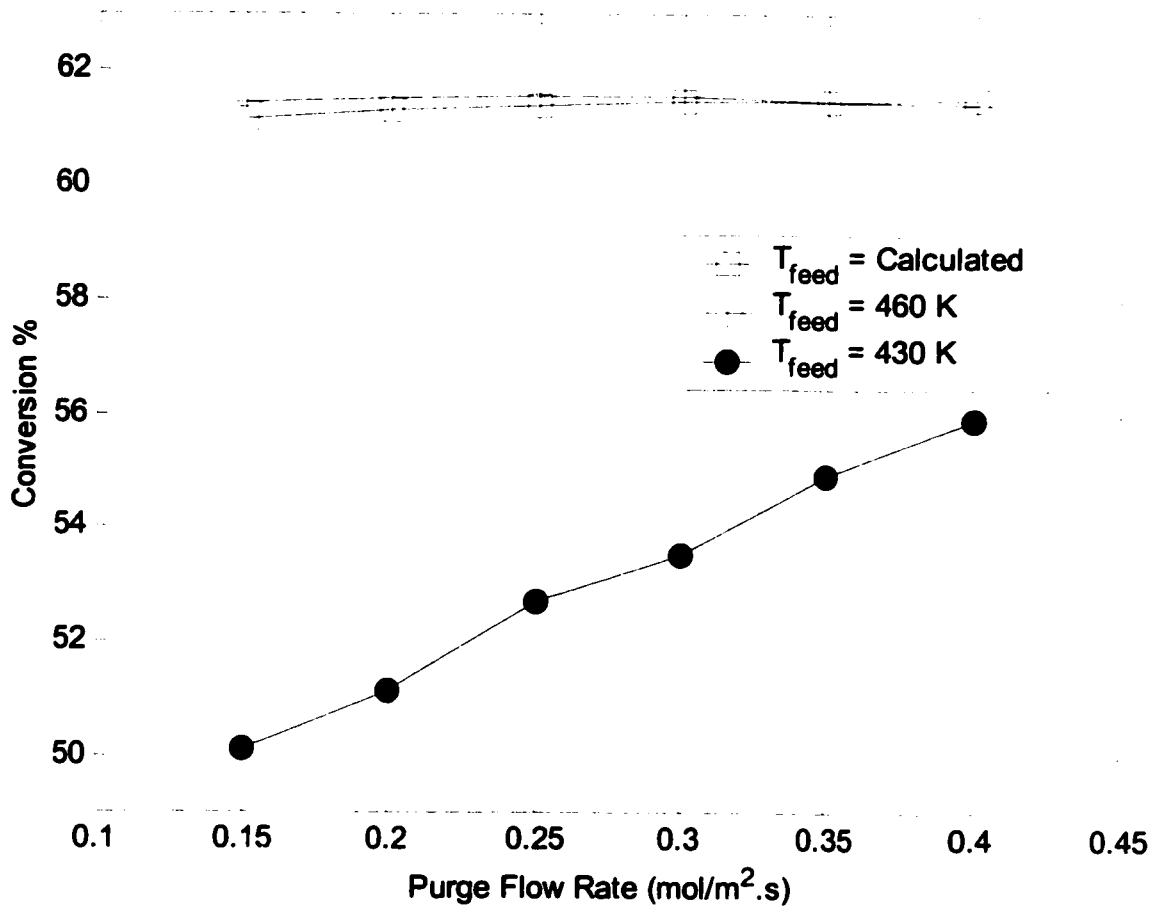

Figure 4.29. Effect of Fresh Feed Temperature on Single Pass Conversion (Cases 9, 20 & 21)

conditions. The switch time increases very fast with increasing purge flow (case 21) as the duty of the adsorbent beds reduces at higher conversions.

As expected a 100% purity is obtained by using reverse flow regeneration (Figure 4.30), which is equivalent to rotating the adsorbent bed each time it is switched from one section to the next. Obviously, the system does not mimic a true countercurrent unit because the equivalent direction of solid flow is no longer the same in the two sections. The disadvantage of forward flow regeneration is that the sorbate accumulates at the bed exit during the desorption step thus contaminating the product in the next adsorption step. The reverse flow regeneration however concentrates the residue at the bed inlet, as a result solving the problem.

The adsorption process is terminated prior to breakthrough in order to ensure the purity of raffinate product. This leaves a region of incompletely saturated adsorbent at the outlet of the bed. Depending upon the length of this region, forward flow regeneration may become very inefficient since the sorbate must first be pushed through the unsaturated region before it can be removed from the outlet. Thus, it is necessary for the adsorption front to reach as close to the bed exit as possible. Such an optimization is not required for the reverse flow regeneration because the sorbate does not pass through the unsaturated region, accordingly producing a wide range of switch times at which the purity is 100%. The switch times thus listed in Table 4.18 are the optimum values except those for the reverse flow operations (case 22).

A switch time greater than the optimum value decreases the purity instantaneously, as the *n*-pentane then breaks through the bed. On the other hand, a lower

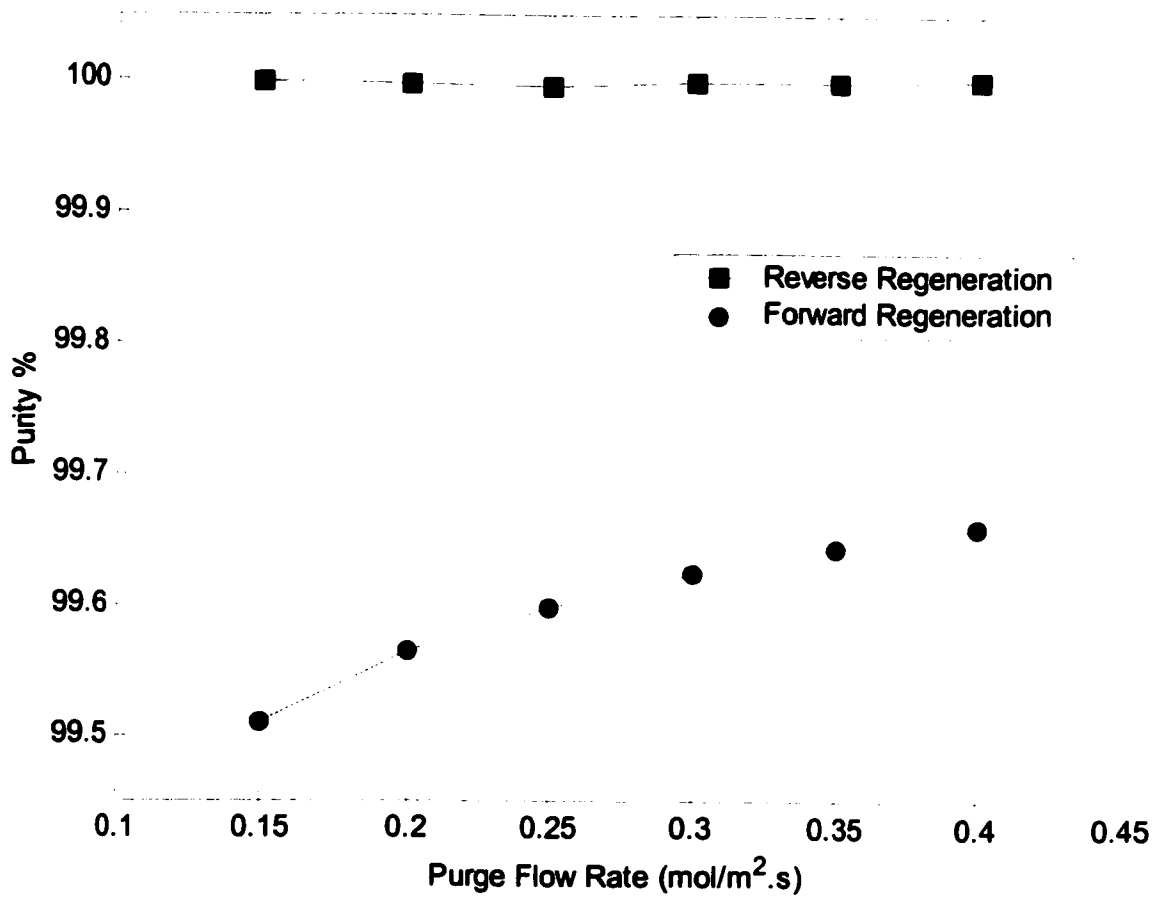

Figure 4.30. Effect of Bed Rotation on Product Purity (Cases 9 & 22)

switch time reduces the regeneration time thus leading to relatively unclean beds at the end of the cycle. This trend is illustrated in Figure 4.31 for the base case (case 9, run 1). Nevertheless, it is important to note that the purity does not fall to any appreciable extent unless the switch time lowers significantly. Thus, desorption takes place mainly during the initial part of switching period, i.e. when the driving force is high and the temperature has just been raised to the higher value. Moreover, if the switch time cannot be controlled accurately because of faulty apparatus, it is appropriate to operate the SMBR at a lower switch time without compromising much on purity.

The gradual change in mean exit concentration of isopentane ($y_{BL,mean}$) and mean exit temperature ($T_{L,mean}$) during startup until the final steady state values are reached is illustrated in Figure 4.32 and that of purity and overall conversion in Figure 4.33. It takes fifteen switches, or five cycles, to reach a cyclic steady state for the base case (case 9, run 1). The overall conversion is directly related to purity, as there is neither a byproduct from the reaction nor a side stream from the system. Initially all the beds are clean because of which 100% purity and overall conversion are recorded. The adsorption front does not reach the bed outlet during early switches so that it takes several switches before the exit temperature reaches its maximum value. The exit concentration of isopentane, on the other hand, should not depend upon the position of the adsorption front, as it is not adsorbed over the adsorbent. However, it is adsorbed over the catalyst, which lowers its exit concentration during the first switch. Moreover, $y_{BL,mean}$ also depends upon the performance of regeneration section because the desorbed *n*-pentane also isomerizes. Hence, it cannot reach a steady state until the rest of the system does.

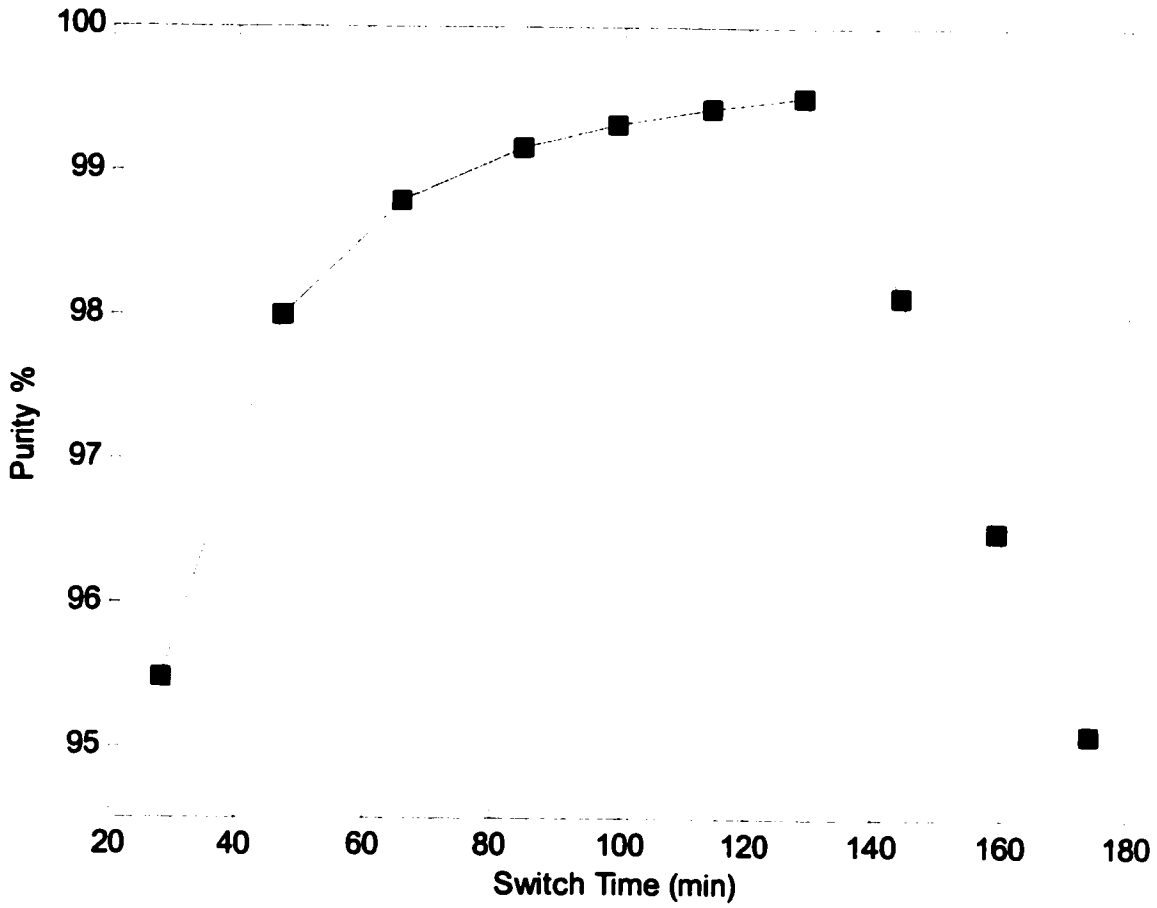

Figure 4.31. Effect of Switch Time on Product Purity (Case 9, Run 1)

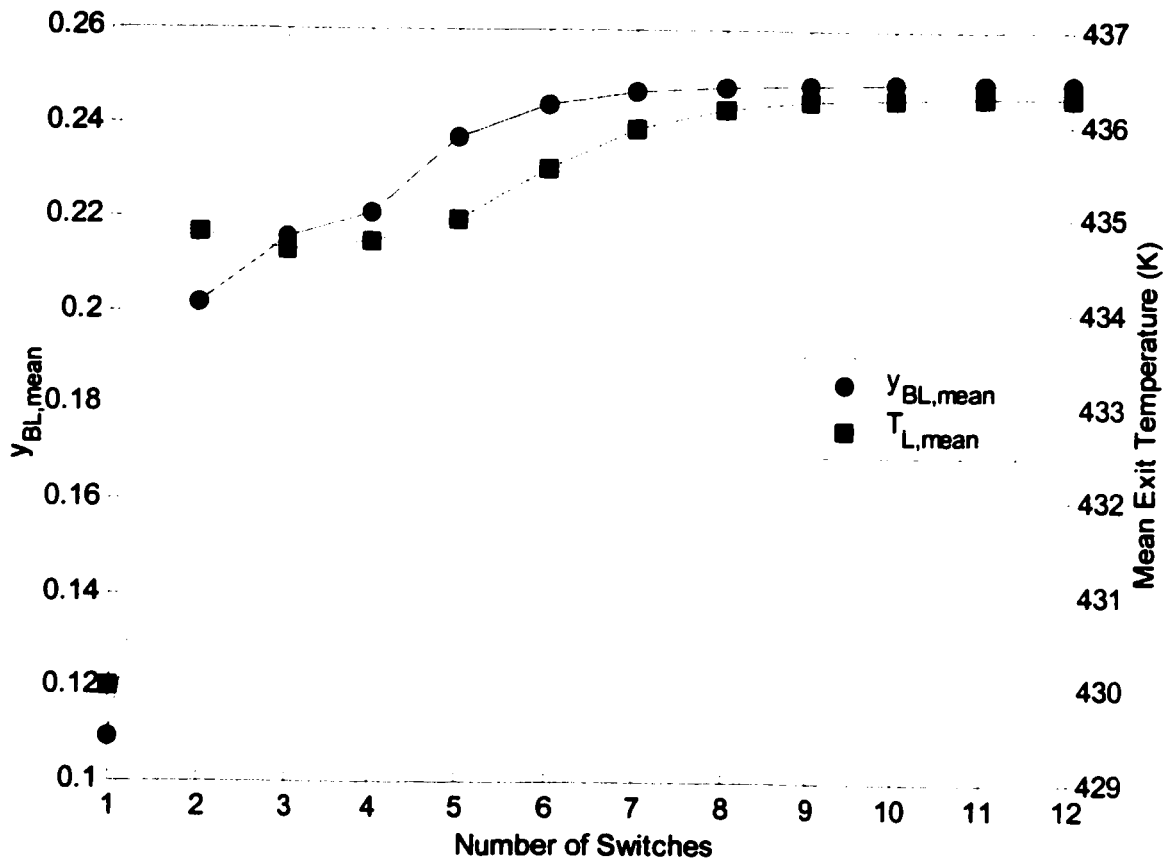

Figure 4.32. Approach to Cyclic Steady State for Mean Exit Concentration of Isopentane and Mean Exit Temperature (Case 9, Run 1)

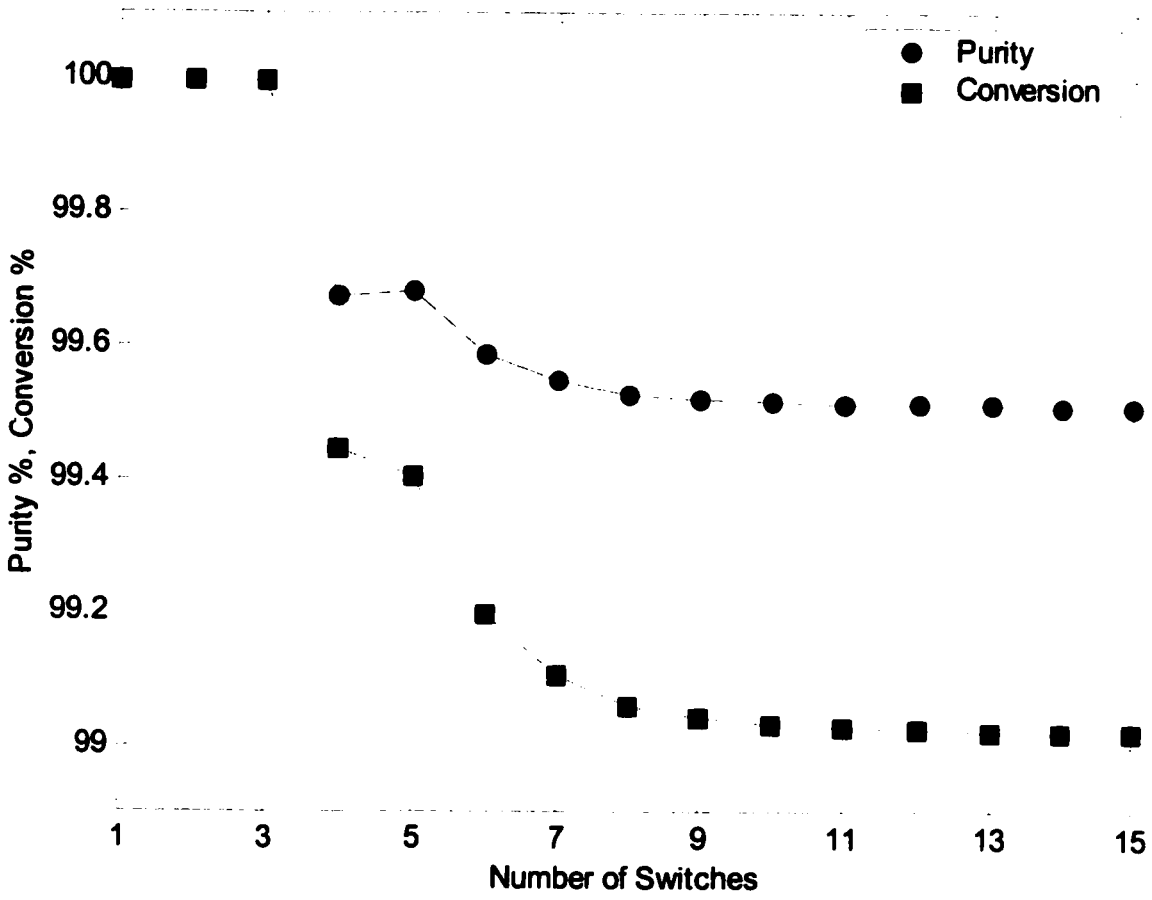

Figure 4.33. Approach to Cyclic Steady State for Purity and Overall Conversion (Case 9, Run 1)

NOMENCLATURE

a_c	specific area of column [m^{-1}]
a_p	specific area of adsorbent or catalyst pellet [m^{-1}]
A	pseudo-homogeneous reactor model
B	adiabatic temperature rise $[=(-\Delta H_{ads})q_{A,ref}/C_{ps}T_{ref}]$ or heterogeneous reactor model with macropore accumulation
c_T	total gas concentration [mol/m^3]
$c_{T,ref}$	total gas concentration at reference conditions [mol/m^3]
C	heterogeneous reactor model with micropore accumulation
C_{pg}	heat capacity of gas [J/mol.K]
$C_{p,i}$	heat capacity of component i [J/mol.K]
C_{ps}	heat capacity of solid [J/kg.K]
$\tilde{C}_{p,feed}$	mean heat capacity of pentanes between T_{feed} and T_{ref} [J/mol.K]
$\tilde{C}_{p,i_{extract}}$	mean heat capacity of species i in extract stream between T_f^R and $T_{extract}$ [J/mol.K]
$\tilde{C}_{p,purge}$	mean heat capacity of purge stream between T_{ref} and T_{purge} [J/mol.K]
D_L	axial mass dispersion coefficient [m^2/s]
Da	Damkohler number $[=(1-\varepsilon)\rho_a k_{ref} L_1/\varepsilon u_{ref}]$
E	total energy [J]
E_{app}	apparent activation energy [J/mol]
E_{sys}	total energy of system [J]
$\tilde{E}_i$	molar energy of species i [J/mol]
F	total molar flux [mol/m^2.s] or molar flow rate of stream [mol/s] (in Appendix A.4)
F_{exit}^s	molar flux of outlet stream from bed position s (see Superscripts) [mol/m^2.s]

F_f^R	molar flux of inlet stream to reaction section [mol/m^2.s]
F_i	molar flow rate of species i [mol/s] (in Appendix A.4)
F_m	molar flux of stream m (see Subscripts) [mol/m^2.s]
$\overline{F}_{exit}^s$	dimensionless molar flux of outlet stream from bed position s (see Superscripts) [-]
$\overline{F}_f^s$	dimensionless molar flux of inlet stream to bed position s (see Superscripts) [-]
$\overline{F}_m$	dimensionless molar flux of stream m (see Subscripts) [-]
h_w	wall heat transfer coefficient [W/m^2.K]
H	enthalpy [J]
$-\Delta H_{ads}$	heat of adsorption [J/mol]
H_{final}	final enthalpy of the system [J]
H_{sys}	enthalpy of the system [J]
$\widetilde{H}_{feed}$	molar enthalpy of fresh feed [J/mol]
$\widetilde{H}_i$	molar enthalpy of species i [J/mol]
$\widetilde{H}_i^0$	molar enthalpy of formation of species i [J/mol]
$\widetilde{H}_{i,m}$	molar enthalpy of species i in stream m (see Subscripts) [J/mol]
k	forward reaction rate constant [m^3/kg cat. s]
k_{ref}	forward reaction rate constant at reference temperature (T_{ref}) [m^3/kg cat. s]
K	equilibrium reaction rate constant [-]
K_{ads}	adsorption equilibrium constant [Pa^{-1}]
K_{gl}	global mass-transfer coefficient [m/s]
K_L	effective axial bed thermal conductivity [W/m.K]
l	switching period
L_j	length of vessel j [m]
n	number of beds in regeneration section or number of components in stream (in Appendix A.4)

N_f	number of film mass-transfer units $[=(1-\varepsilon)a_p K_{gl} L_1/\varepsilon u_{ref}]$
N_i	number of moles of species i in the system [mol]
N_w	number of wall heat-transfer units $[=a_c h_w L_1/C_{pg} F_{ref}]$
P	total pressure of column [Pa]
Pe_{Hj}	thermal Peclet number in vessel j $[=C_{pg} F_{ref} L_j/K_L]$
Pe_j	mass Peclet number in vessel j $[=u_{ref} L_j/D_L]$
$q_{A,ref}$	average adsorbed-phase concentration of component A in equilibrium with $y_{A,ref}$ [mol/kg]
q_{max}	maximum adsorbed-phase concentration [mol/kg]
Q_A^s	dimensionless average adsorbed-phase concentration of component A in bed position s (see Superscripts) [-]
Q_i	dimensionless average adsorbed-phase concentration of component i [-]
$\dot{Q}$	rate of flow of heat to the system [J/s]
R	ideal gas law constant [J/mol.K]
t	time [s]
T	temperature [K]
T_f^R	temperature of inlet stream to reaction section [K]
T_{final}	final temperature of the system [K]
$T_{L,mean}$	mean temperature of product stream [K]
T_m	temperature of stream m (see Subscripts) [K]
T_{mean}	mean temperature of a stream [K]
T_R	reference temperature for enthalpy of formation [K] (in Appendices A.3 & A.4)
$T_{w,z}$	wall temperature of section z [K]
$\overline{T}$	dimensionless temperature [-]
$\overline{T}^s$	dimensionless temperature in bed position s (see Superscripts) [-]

$\overline{T}_{exit}^{s}$	dimensionless temperature of outlet stream from bed position s (see Superscripts) [-]
$\overline{T}_{f}^{s}$	dimensionless temperature of inlet stream to bed position s (see Superscripts) [-]
$\overline{T}_{m}$	dimensionless temperature of stream m (see Subscripts) [-]
$\overline{T}_{w,z}$	dimensionless wall temperature of section z [-]
u_{ref}	interstitial velocity at reference conditions [m/s]
U	internal energy [J]
V	volume [m^3]
V_{sys}	volume of the system [m^3]
$\tilde{V}_i$	molar volume of species i [m^3/mol]
$\dot{W}$	rate of work done by the system [J/s]
$\dot{W}_s$	rate of work done by the system apart from flow work [J/s]
x_j	dimensionless spatial coordinate in vessel j [-]
x_1'	dimensionless spatial coordinate in the rotated adsorbent bed [$=1-x_1$]
$y_{BL,mean}$	mean mole fraction of component B in product stream [-]
y_{HC}^{0}	mole fraction of pentanes at reference conditions [-]
y_i	mole fraction of species i [-]
y_i^s	mole fraction of species i in bed position s (see Superscripts) [-]
$y_{i,exit}^{s}$	mole fraction of species i in outlet stream from bed position s (see Superscripts) [-]
y_{if}^{s}	mole fraction of species i in inlet stream to bed position s (see Superscripts) [-]
$y_{i,m}$	mole fraction of species i in stream m (see Subscripts) [-]

Greek Letters

ε	bed void fraction [-]
ε_p	particle porosity [-]
γ_f	dimensionless heat of adsorption [$= (-\Delta H_{ads})/RT_{ref}$]
γ_r	dimensionless activation energy [$= E_{app}/RT_{ref}$]
θ_{ref}	nonlinearity parameter of isotherm [$= q_{A,ref}/q_{\max}$]
ρ_a	apparent density of adsorbent or catalyst pellet [kg/m^3]
σ	macropore porosity per unit bed porosity [$= (1-\varepsilon)\varepsilon_p/\varepsilon$]
τ	dimensionless time [-]
τ_s	switch time [s]
τ_s'	dimensionless switch time [-]
υ	length ratio [$= L_2/L_1$]
ζ_H	thermal capacity factor [$= (1-\varepsilon)\rho_a C_{ps}/\varepsilon\, c_{T,ref} C_{pg}$]
ζ_m	mass capacity factor [$= (1-\varepsilon)\rho_a q_{A,ref}/\varepsilon\, c_{T,ref}$]

Superscripts

A_1	position of bed in adsorption section
D_k	k^{th} position of bed in regeneration section
R	position of catalyst bed (reaction section)

Subscripts

ads	adsorption section
A	*n*-pentane
B	isopentane
des	regeneration section
extract	extract stream

feed	fresh feed stream
HC	pentanes
mix	inlet stream to reaction section (in Appendix A.3)
purge	purge stream
ref	reference stream
1	adsorbent bed
2	catalyst bed

CHAPTER 5

THE ULTIMATE SANDWICH REACTOR

It was concluded in the previous chapter that a thermal swing operation was inevitable in a simulated moving bed reactor to achieve >99% purity. The operating temperature in the adsorber is maintained by imposing constant wall temperature. The catalyst bed is however operated adiabatically and its temperature controlled by the sensible heat of fresh feed. Moreover reverse flow regeneration yields the ideal performance of 100% purity. This point is further elaborated in this chapter.

Since the lengths of adsorption and regeneration sections are equal in reverse flow operations, it is instructive to combine the entire unit in a single vessel, i.e. the catalyst bed "sandwiched" between the two adsorbent beds, giving rise to a sandwich reactor (Figure 5.1). The adsorbent is packed in the tube sides of shell and tube heat exchangers to provide a high heat transfer area with the condensing steam.

It is tempting to use a conventional shell and tube heat exchanger instead where each tube is packed with adsorbent-catalyst-adsorbent layers and the operating temperature of every layer controlled by dividing the shell side into corresponding sections. However, this would require provision for a separate inlet stream of fresh feed to every tube, which would be very difficult to construct and handle during maintenance operations. Thus, the reactor is divided into separate sections altogether.

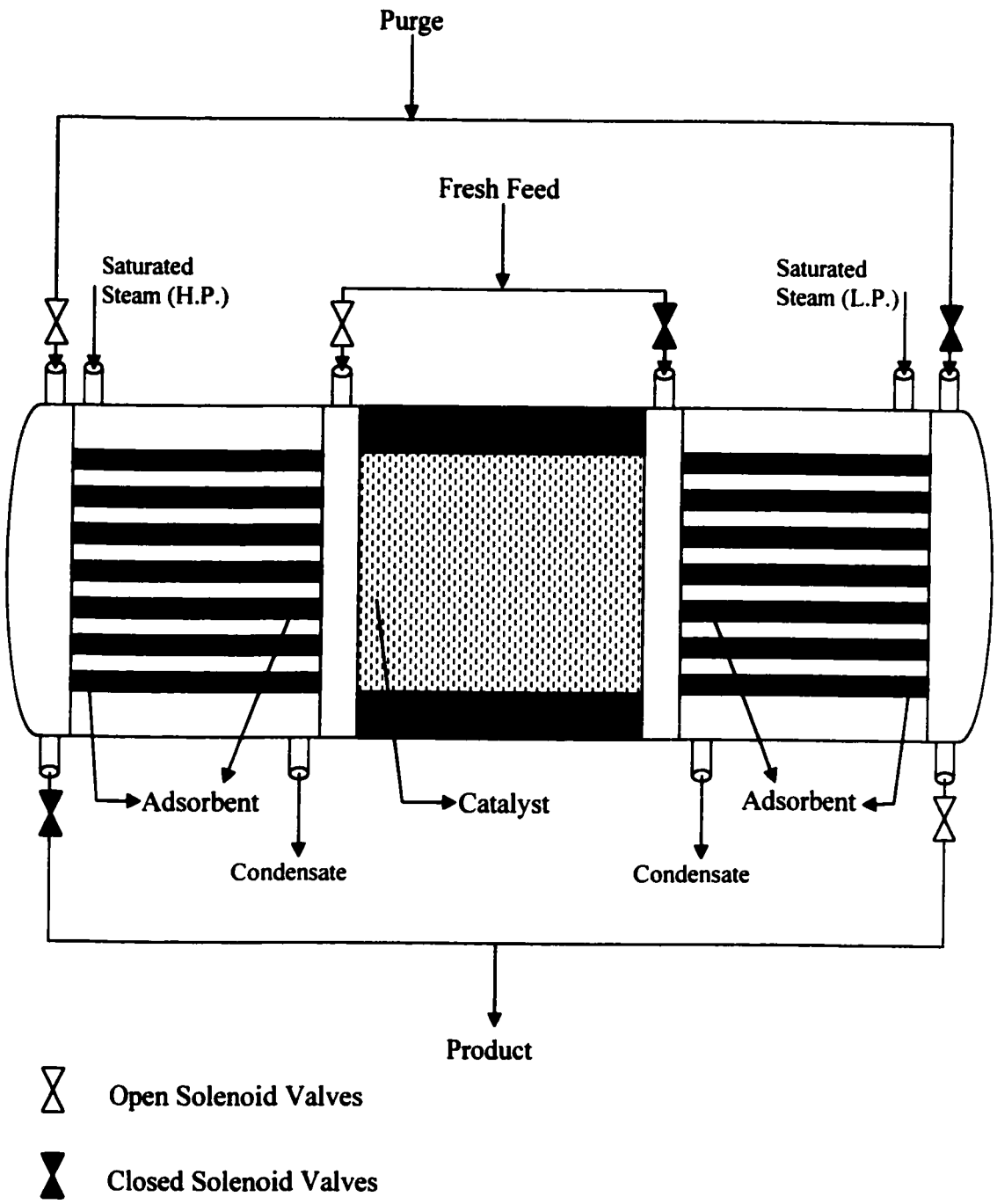

Figure 5.1. Industrial Sandwich Reactor

Since this study is concerned with a laboratory scale reactor, only one tube is required in each section. It thus becomes possible as a substitute to integrate the three beds in a single long cylinder. This necessitates a different type of mathematical model similar to the one proposed by Al-Juhani [1] for the pressure swing adsorption reactor, i.e. the Danckwert's boundary conditions are applied only at the entrance and exit of the vessel. It is not worth the effort because the model is anyhow inapplicable to the industrial sandwich reactor, which is divided into separate sections. The simulated moving bed reactor model with reverse flow regeneration, on the other hand, is valid for the segregated sandwich reactor because the Danckwert's boundary conditions are applied over every section. However, a simple modification still needs to be made which is mentioned later.

Apart from its compact nature, the sandwich reactor also differs from the reverse flow simulated moving bed reactor because of flow reversal in the reaction section. In some cases, reactions are favored in the region of heat front hence making it advantageous to keep the front inside the catalyst bed. This is achieved by operating the conventional fixed bed reactor under forced unsteady state conditions via periodic flow reversal [38]. In this study, however, heat effects over the catalyst are negligible because of which there is no temperature front in the reaction section thus making the flow reversal redundant. However, because of the compact design of sandwich reactor the flow reversal is unavoidable in the reaction section.

The operation of sandwich reactor is illustrated in Figure 5.2. Hot hydrogen purge enters the regeneration section and mixes with cold fresh feed upon exit before entering

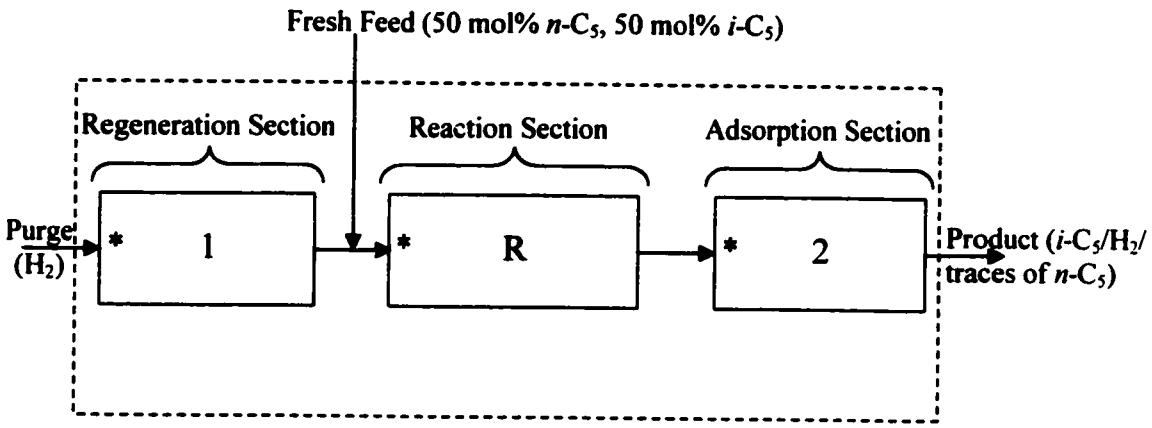

Position of Beds during 1st Switching Period

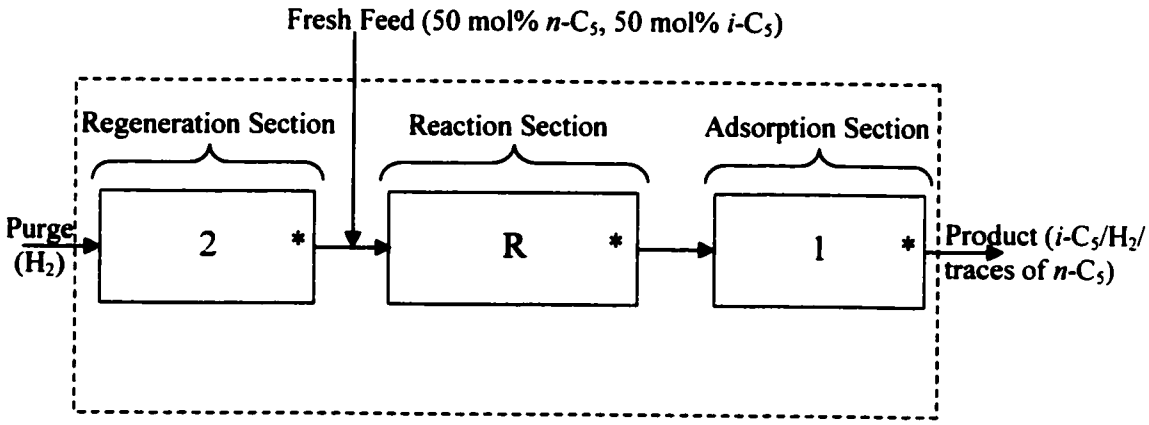

Position of Beds during 2nd Switching Period

Figure 5.2. Simulation of Sandwich Reactor

the reaction section. The hydrogen free fresh feed contains equimolar amounts of normal and iso- pentanes. The *n*-pentane isomerizes over Pd/Y-zeolite catalyst. The reaction is equilibrium limited and the exit stream thus passes into the adsorption section containing 5A zeolite adsorbent that retains the reactant and lets the product pass through. After some definite period, i.e. before *n*-pentane breaks through, flow is reversed. The adsorption section now acts as the regeneration section where the sorbate is desorbed. Fresh feed enters through the other end of reaction section and product is collected at the exit of adsorbent bed that was previously in the regeneration section. This operation is equivalent to periodically rotating the entire reactor about its centre and keeping the flow direction the same.

5.1 MODEL EQUATIONS

The model equations, inlet conditions and initial conditions for the various sections of sandwich reactor are similar to that of the simulated moving bed reactor with reverse flow regeneration except that the reaction section is periodically rotated as well. For the lth switching:

$$\begin{aligned}
y_A^R\left(x_2,\tau=\left[(l-1)\cdot\tau_s'\right]^+\right)&=y_A^R\left(x_2',\tau=\left[(l-1)\cdot\tau_s'\right]^-\right)\\
y_B^R\left(x_2,\tau=\left[(l-1)\cdot\tau_s'\right]^+\right)&=y_B^R\left(x_2',\tau=\left[(l-1)\cdot\tau_s'\right]^-\right)\\
Q_A^R\left(x_2,\tau=\left[(l-1)\cdot\tau_s'\right]^+\right)&=Q_A^R\left(x_2',\tau=\left[(l-1)\cdot\tau_s'\right]^-\right)\qquad l=2,3,\ldots\\
Q_B^R\left(x_2,\tau=\left[(l-1)\cdot\tau_s'\right]^+\right)&=Q_B^R\left(x_2',\tau=\left[(l-1)\cdot\tau_s'\right]^-\right)\\
\bar{T}^R\left(x_2,\tau=\left[(l-1)\cdot\tau_s'\right]^+\right)&=\bar{T}^R\left(x_2',\tau=\left[(l-1)\cdot\tau_s'\right]^-\right)
\end{aligned}\tag{5.1}$$

where $x_2'=1-x_2$.

5.2 RESULTS AND DISCUSSION

Since the simulated moving bed reactor (SMBR) produces a 100% pure product by employing reverse flow regeneration and the sandwich reactor operates in a similar manner, a target of 100% purity is set for the latter as well. It is of no use to operate the reactor under isothermal conditions, as the corresponding SMBR model did not even produce 97% pure product. The operating parameters used for simulation of sandwich reactor are the same as that of SMBR with bed rotation (Table 4.8). The switch times (τ_s) for flow reversal are also similar (case 22, Table 4.18) except for the last run, i.e. for F_{purge} = 0.40 mol/m^2.s, where it was reduced to 119.8 min in order to achieve >99.995% purity. As expected the sandwich reactor also produced 100% pure product (Figure 5.3).

Cyclic steady state gas phase concentration profiles are shown in Figures 5.4 to 5.6 at various times during a switching period. Reaction takes place in the initial portion of the catalyst bed, which confirms that it is of sufficient length. It is not necessary for the adsorption front to reach the exit of the adsorption section before flow reversal is performed. This is because the front is pushed backwards in the following switching period thus giving rise to a wide range of switch times at which 100% purity is obtained. The isopentane is flushed very quickly from the regeneration section, as it is not adsorbed over the adsorbent.

Since cyclic steady state is reached, the profiles at the start of switching period are similar to those at the end except that the entire reactor is rotated. Moreover, discontinuities exist at entrance to various sections initially during the switching period because these sections experience a different concentration at the exit prior to rotation.

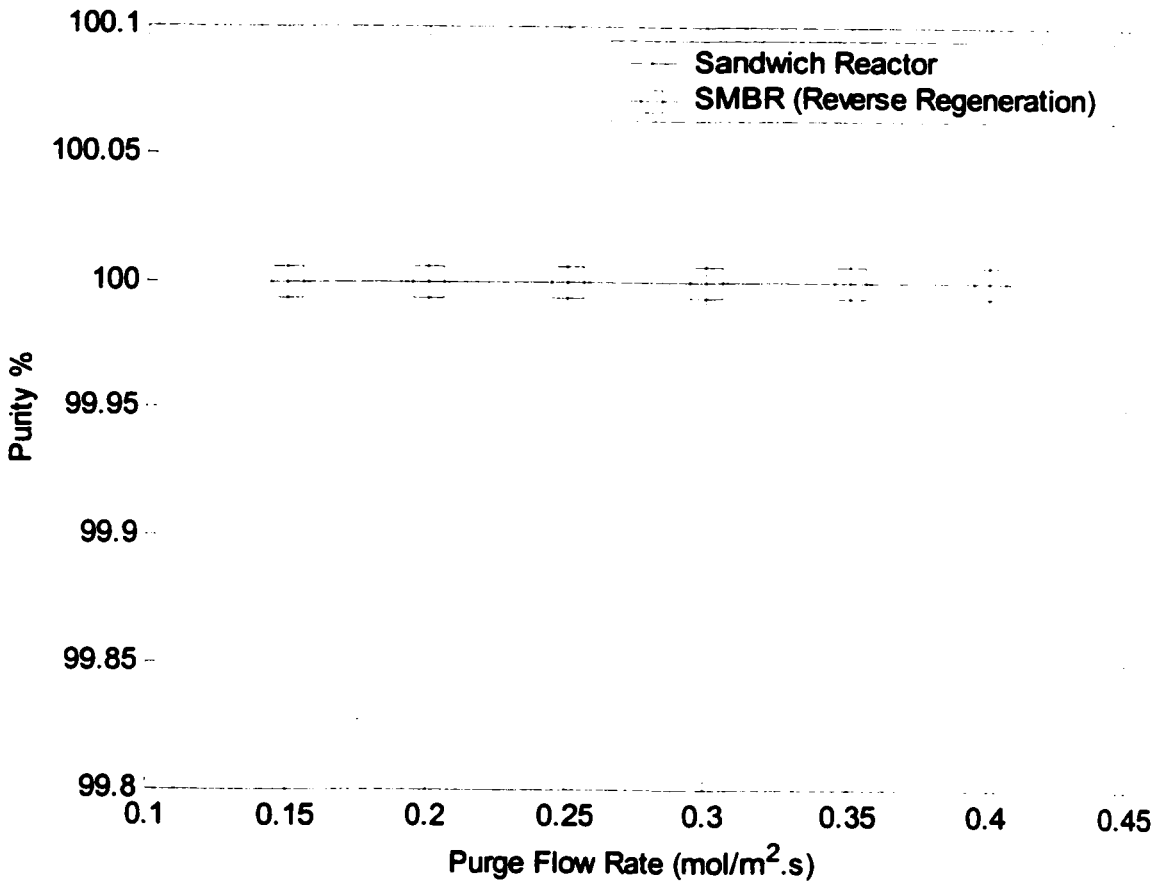

Figure 5.3. Purity Obtained by a Sandwich Reactor

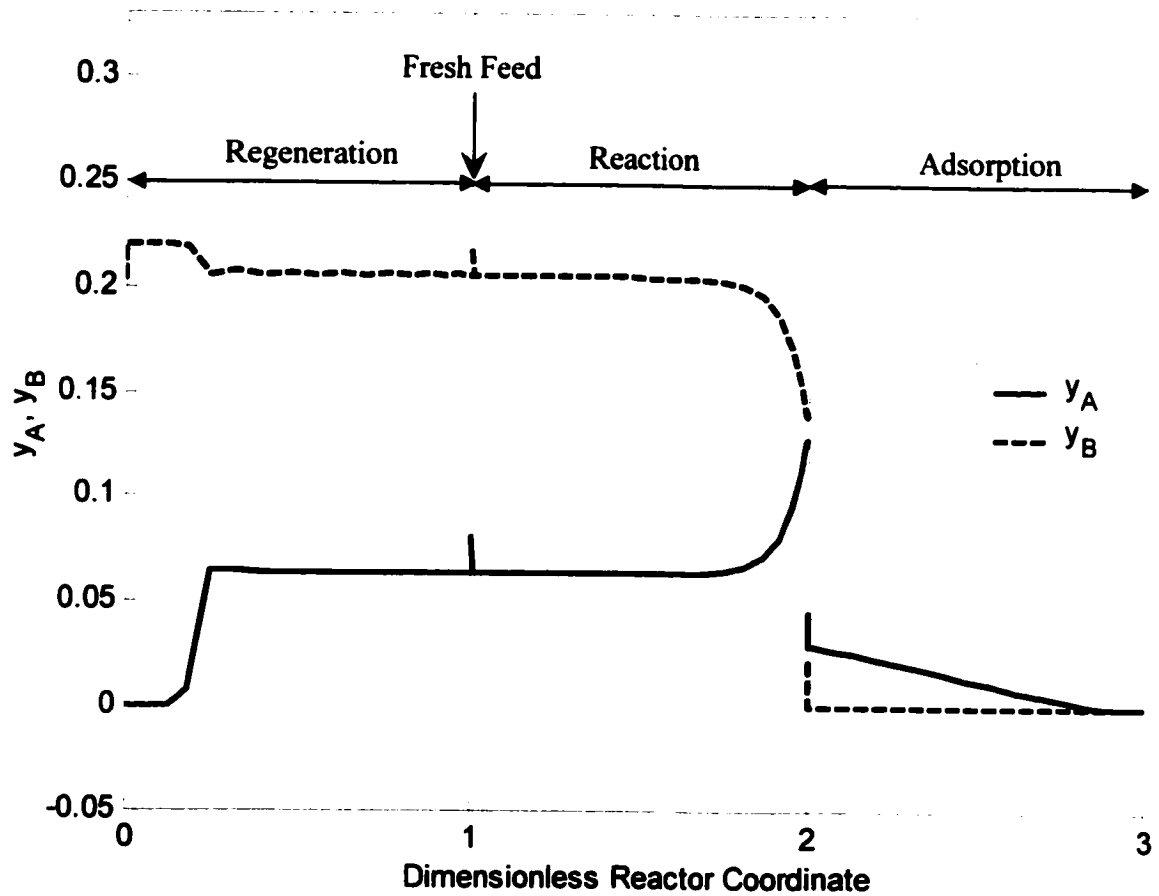

Figure 5.4. Cyclic Steady State Concentration Profiles of *n*-/iso- Pentanes just after Reversing Flow

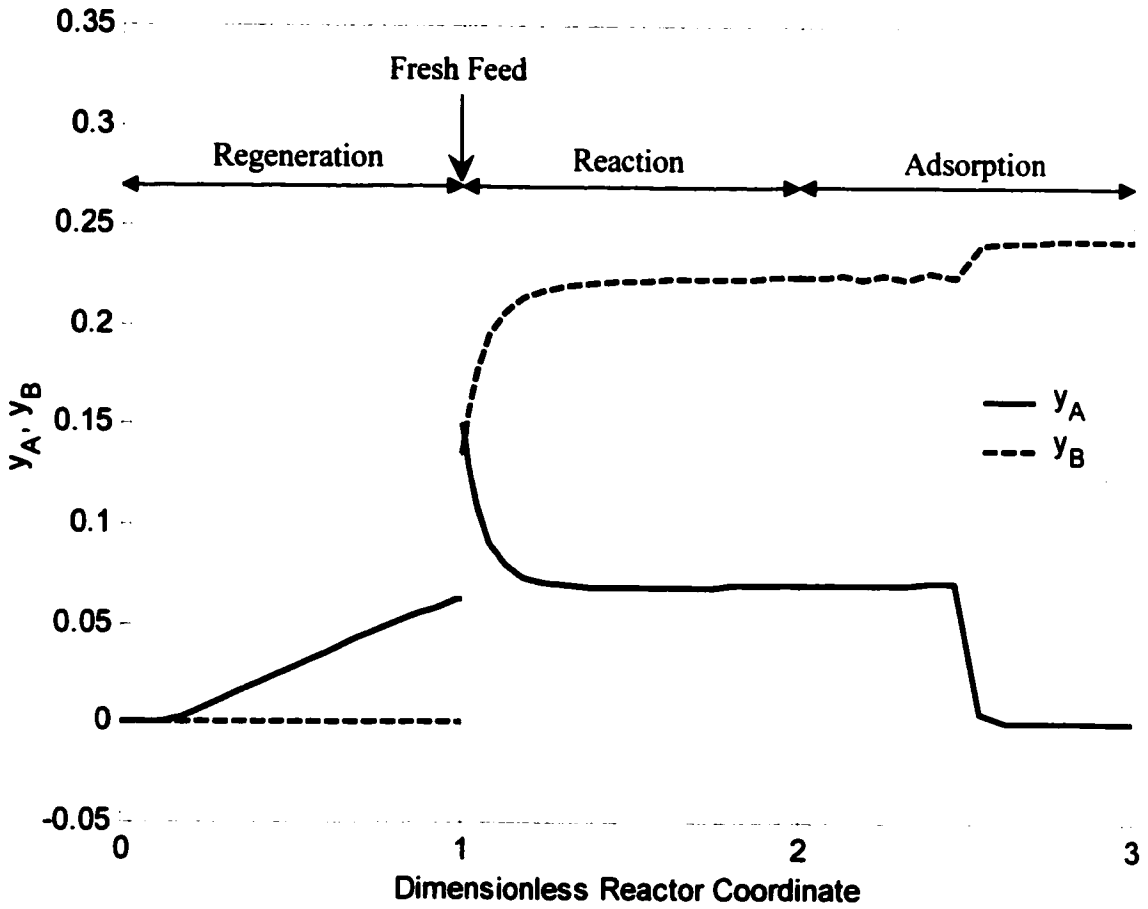

Figure 5.5. Cyclic Steady State Concentration Profiles of *n*-/iso- Pentanes at Half-time Between Reversing Flow

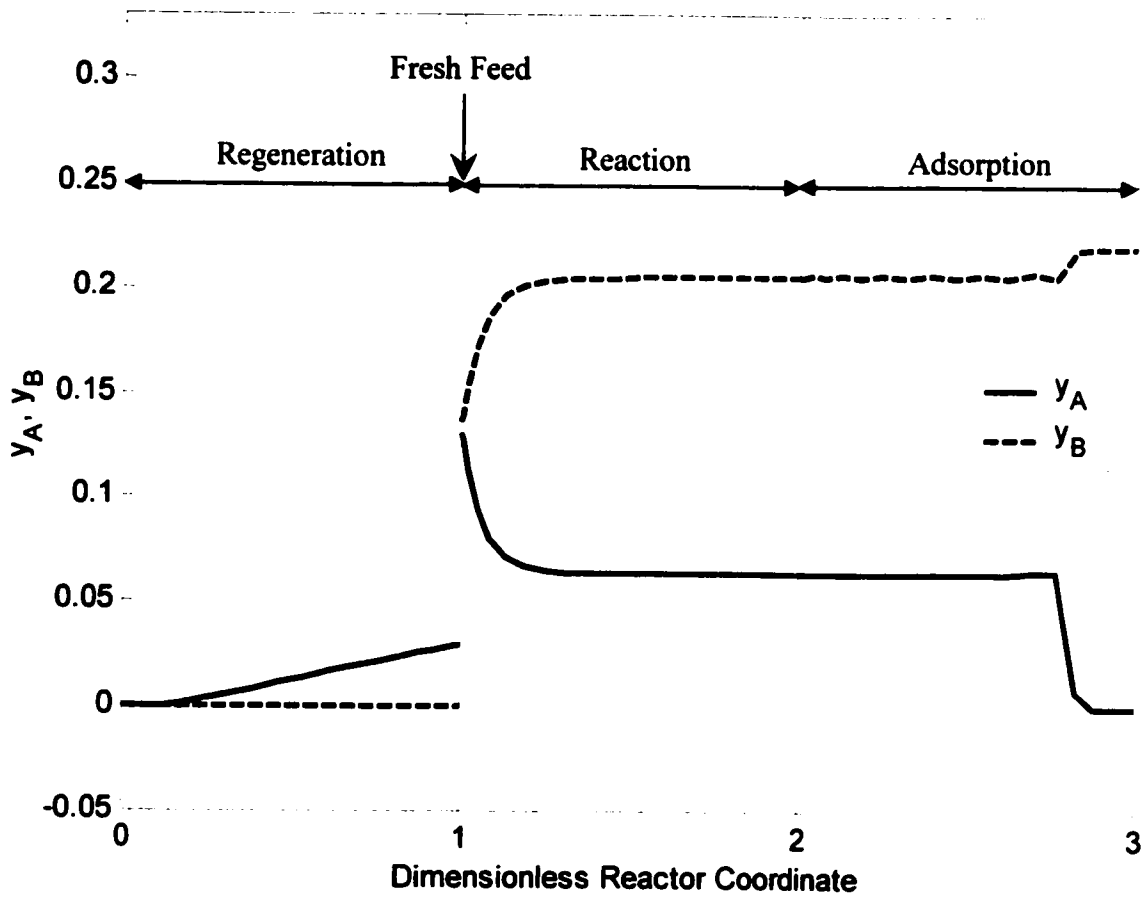

Figure 5.6. Cyclic Steady State Concentration Profiles of *n*-/iso- Pentanes just before Reversing Flow

The corresponding adsorbed phase concentration profiles are shown in Figures 5.7 to 5.9. The adsorbed phase concentration in adsorption section is greater than in the reaction section because it operates at a much lower temperature. Moreover, it exceeds unity as the original quantity is normalized using the reference stream parameters, which is at a higher temperature. The *n*-pentane concentration is also higher in the regeneration section although it operates at a higher temperature. This is because the adsorbed phase in the catalyst undergoes reaction and is shared by both the *n*-pentane and its isomer.

Despite the high regeneration temperature, a significant amount of sorbate remains in the adsorbent bed. However, 100% purity is obtained because the beds are rotated thus maintaining a clean adsorbent at the exit of the adsorption section at all times. Furthermore, the switch time is also chosen to be less than the breakthrough time of sorbate.

The consequent temperature profiles of the system are illustrated in Figures 5.10 to 5.12. The regeneration section temperature does not change by an appreciable amount and remains almost constant at T_{purge}. This is because desorption is a slow process so that any drop in temperature is immediately compensated by the constant wall temperature. Moreover, that of reaction section stays uniform at the desired value of 514 K as it is insulated and the heat effects due to reaction are neglected. However, adsorption is favorable. Thus, the temperature front travels through the adsorption section. Furthermore, fluid does not reach the desired operating temperature immediately upon admission to the adsorption section. Consequently, the adsorbed phase concentration is not maximum at the entrance.

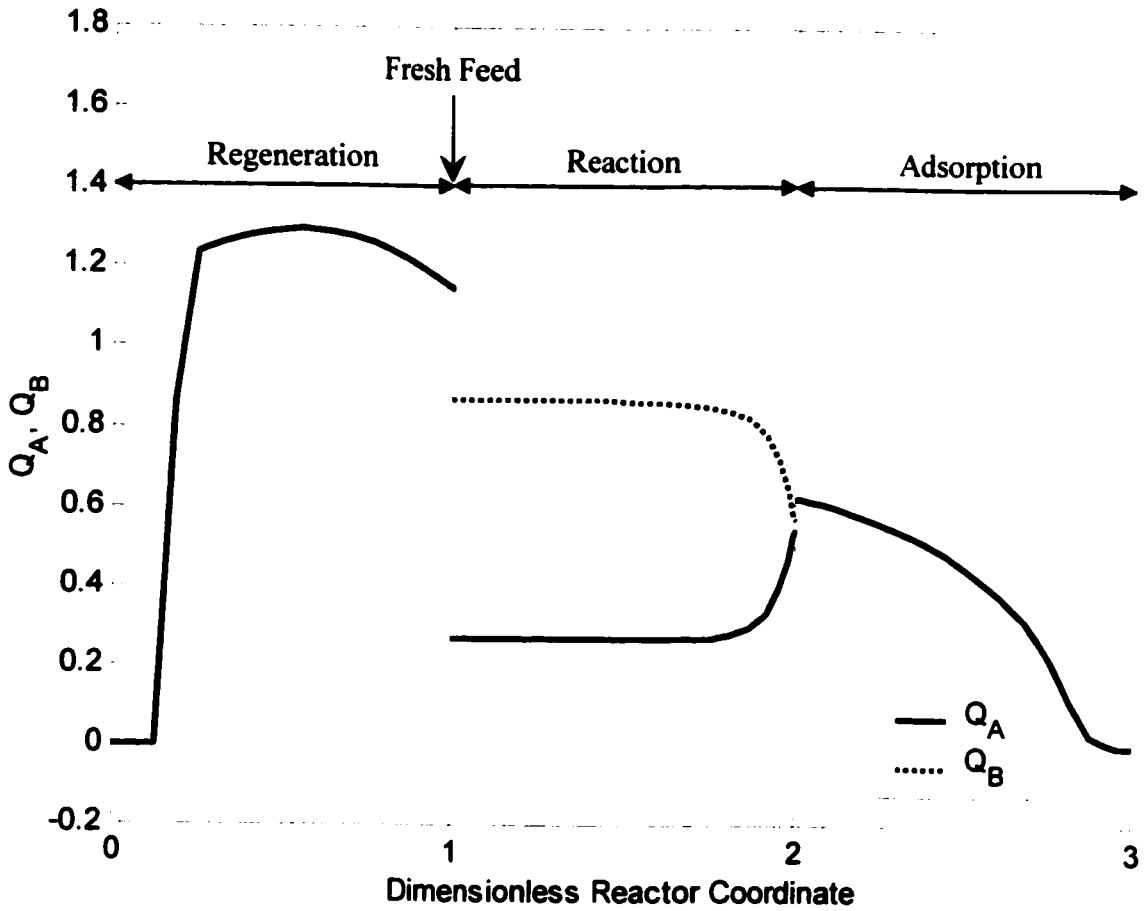

Figure 5.7. Cyclic Steady State Adsorbed Phase Concentration Profiles just after Reversing Flow

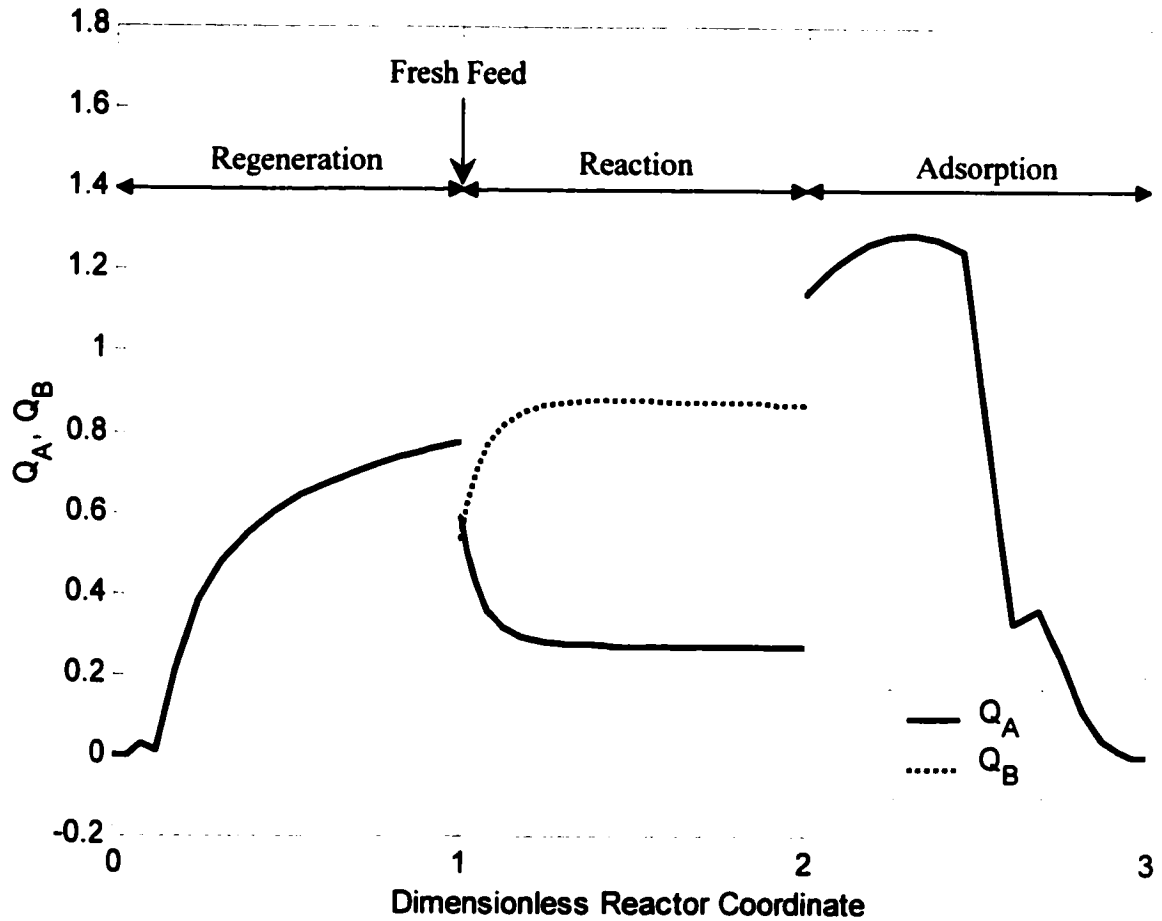

Figure 5.8. Cyclic Steady State Adsorbed Phase Concentration Profiles at Half-time Between Reversing Flow

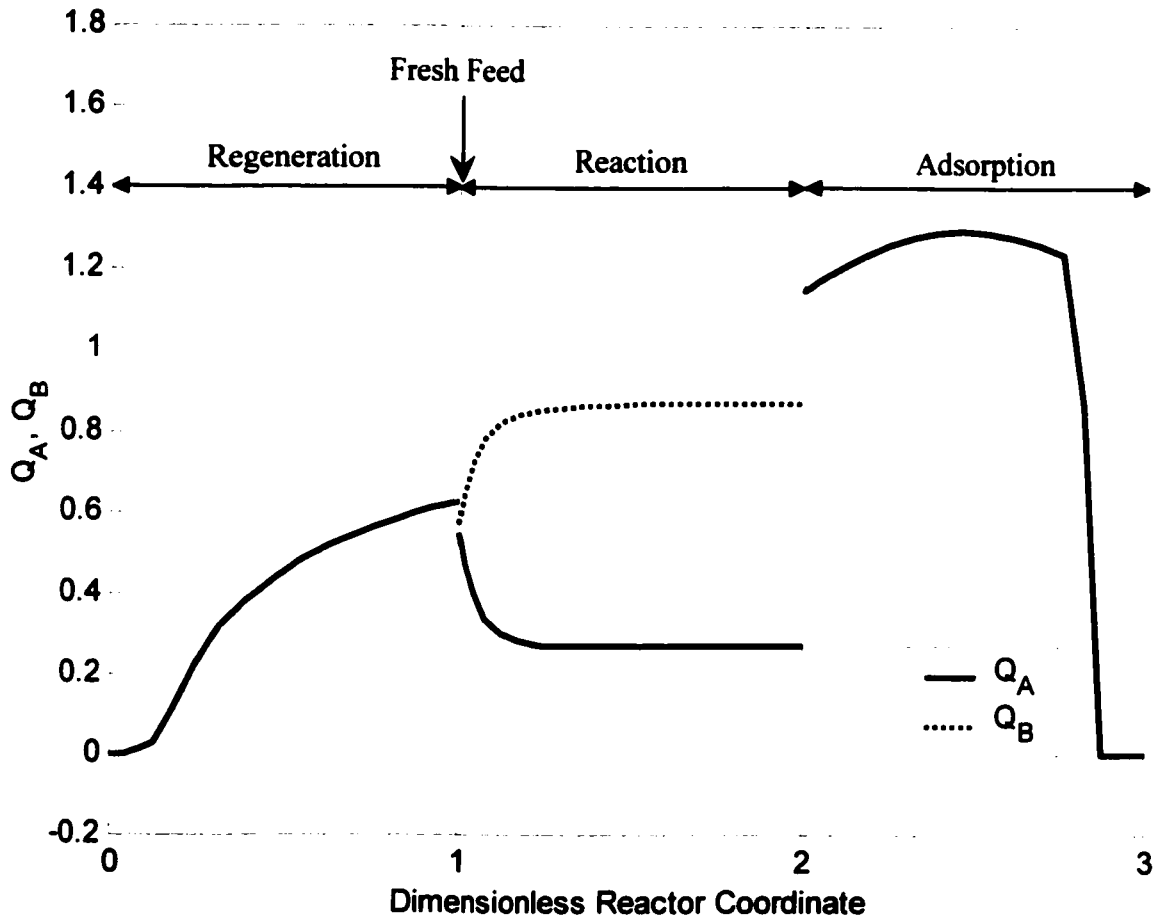

Figure 5.9. Cyclic Steady State Adsorbed Phase Concentration Profiles just before Reversing Flow

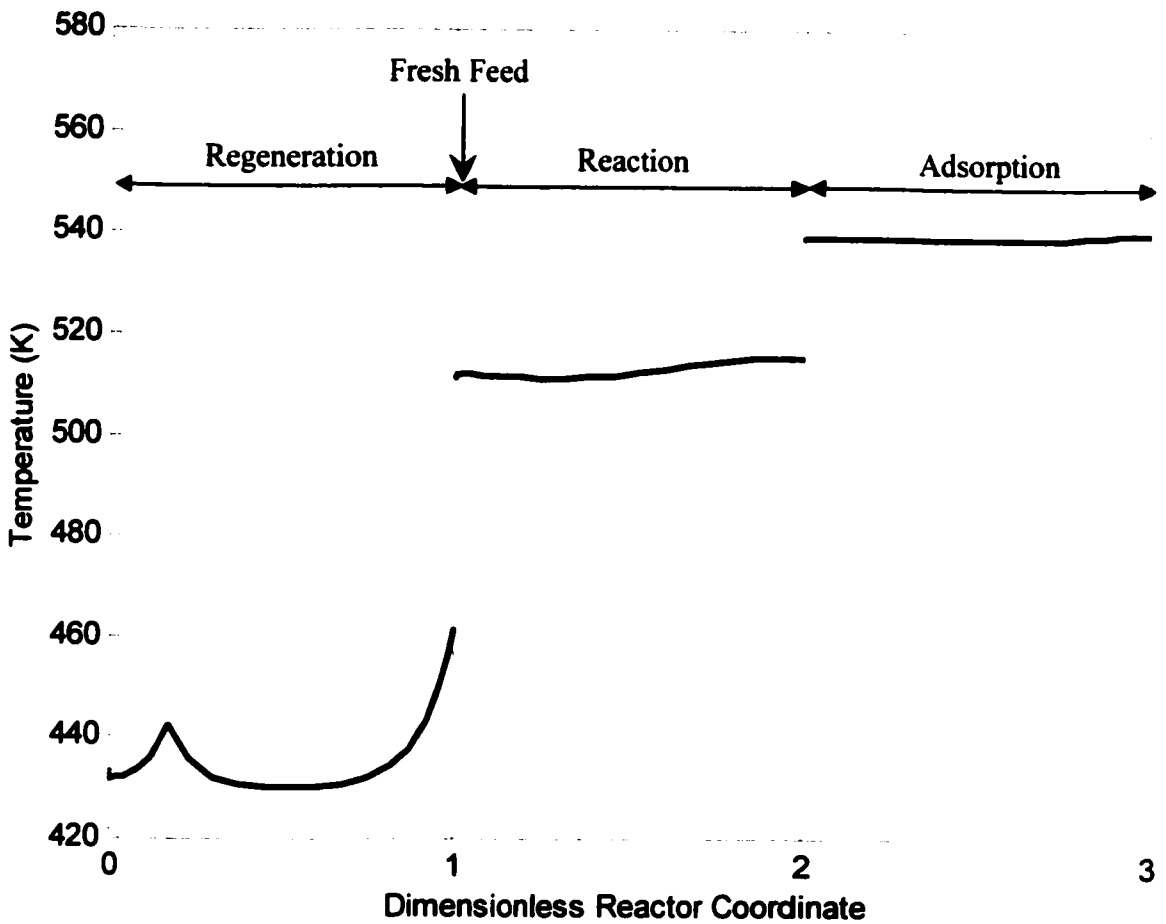

Figure 5.10. Cyclic Steady State Temperature Profile just after Reversing Flow

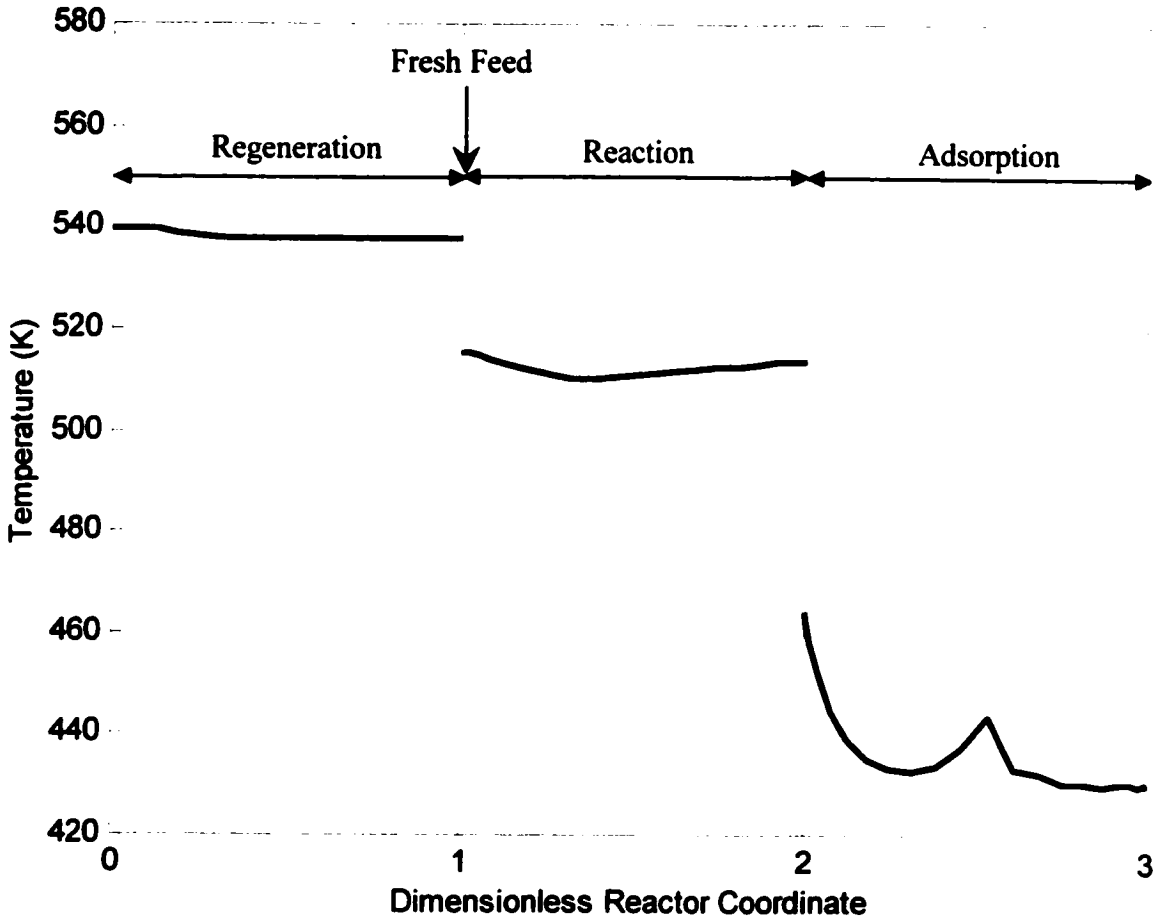

Figure 5.11. Cyclic Steady State Temperature Profile at Half-time Between Reversing Flow

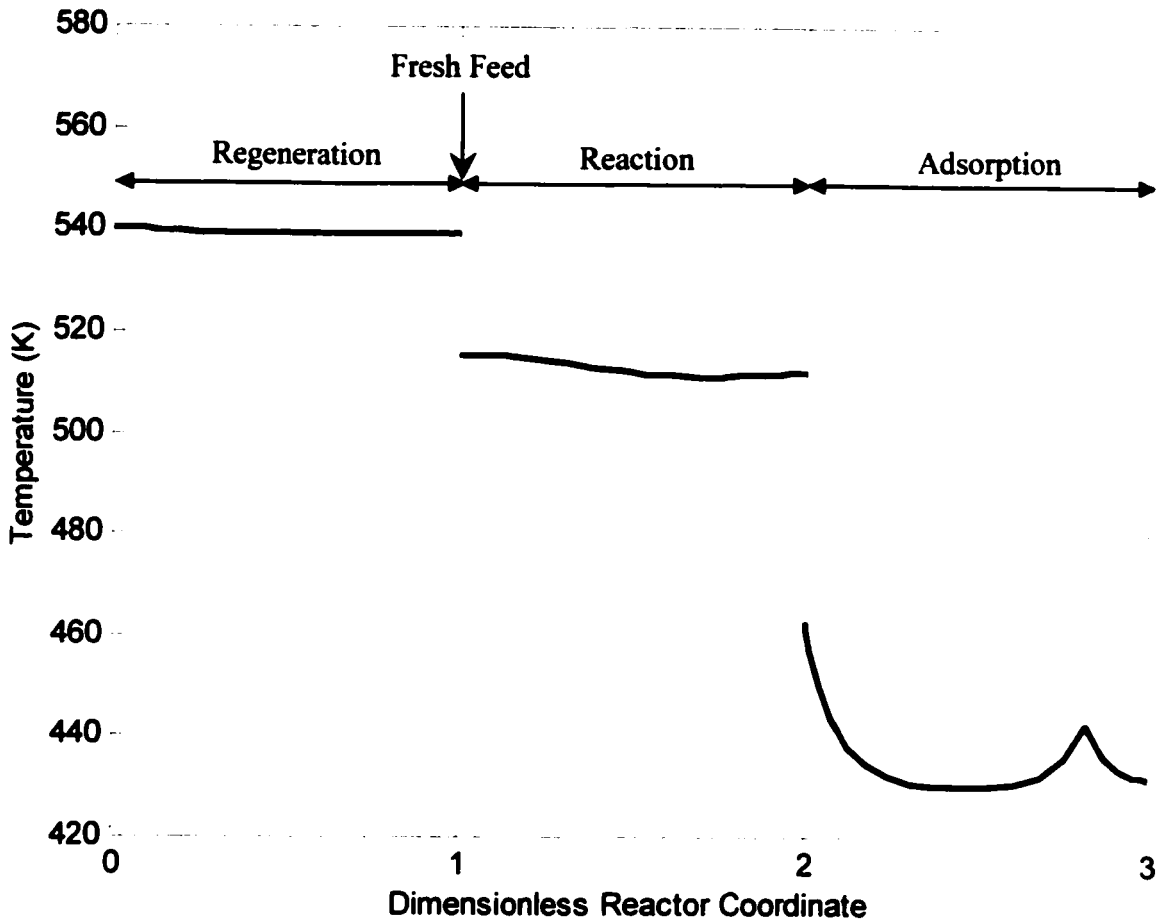

Figure 5.12. Cyclic Steady State Temperature Profile just before Reversing Flow

NOMENCLATURE

F_{purge}	molar flux of purge stream [mol/m^2.s]
l	switching period
Q_i	dimensionless average adsorbed-phase concentration of component i [-]
Q_i^R	dimensionless average adsorbed-phase concentration of component i in reaction section [-]
T_{purge}	temperature of purge stream [K]
$\overline{T}^R$	dimensionless temperature in reaction section [-]
x_2	dimensionless spatial coordinate in catalyst bed [-]
x_2'	dimensionless spatial coordinate in the rotated catalyst bed $[=1-x_2]$
y_i	mole fraction of species i [-]
y_i^R	mole fraction of species i in reaction section [-]

Greek Letters

τ	dimensionless time [-]
τ_s	switch time [s]
τ_s'	dimensionless switch time [-]

Subscripts

A	*n*-pentane
B	isopentane

CHAPTER 6

CONCLUSIONS & RECOMMENDATIONS

6.1 SUMMARY OF CONCLUSIONS

The isomerization of *n*-paraffin is an important process that upgrades light straight-run naphtha to a higher octane number gasoline. This study is concerned with the isomerization of *n*-pentane using a Simulated Moving Bed Reactor (SMBR). The SMBR is one of the several alternative systems available that take an equilibrium-limited reaction to near completion.

Fresh feed, comprising of equimolar amounts of normal and iso- pentanes, mixes with hydrogen purge supplied through the regeneration section before entering the reaction section that consists of a Pd/Y-zeolite catalyst. The resulting effluent mixture is separated in the adsorption section where the *n*-pentane is adsorbed over 5A zeolite and the isomer discarded completely because of steric effects.

The system was first modeled and simulated in an isothermal mode. A target of >99% purity was set which could not be met. Neither rise in purge flow rates by modest amounts nor increase in number of beds in regeneration section proved efficient in increasing the purity significantly. A reverse flow regeneration did increase the purity but not to the desired level.

A thermal swing operation was performed next with the hope of achieving better purity. The scheme failed when operated in an adiabatic manner. However the desired goal of >99% purity was finally accomplished by applying constant wall temperatures over the adsorber vessels. Each adsorber at an industrial level would thus be a shell and tube heat exchanger with the adsorbent packed in the tube side and saturated steam condensing in the shell side to get the desired wall temperature. Moreover, calculations need to be performed for a single tube only, as the entire bundle shall operate under similar conditions.

The effect of various parameters on the arrangement was studied next. A smaller catalyst bed lowered the purity slightly by reducing the conversion thus increasing load over adsorbent beds. The actual operating temperatures must be known in the adsorption and regeneration sections, as knowledge of their difference is not sufficient to determine the system outcome. This is because the dependence of adsorption equilibrium constant is not linear with temperature and instead according to the vant Hoff equation.

Increase in fresh feed flow rate lowers the purity slightly even if the purge flow is increased by a similar amount. Thus, the actual flow rates of inlet streams determine the system's performance rather than the purge to feed ratio. Minor temperature fluctuation in fresh feed does not change the purity but a substantial decrease in temperature does have an effect.

Thermal swing with bed rotation gave the ideal performance of 100% purity. This is because the sorbate is no longer pushed through the remaining part of the unsaturated bed during the regeneration step. There thus exists a wide range of switch times at which

maximum purity is obtained. However, optimization of switch time is required when the usual forward flow regeneration is used. Moreover, SMBR can be operated at slightly lower switch times than the optimum value without compromising much on purity.

The optimum switch times for SMBR operations under forward flow regeneration increased with increasing purge flow rates, as the adsorbent was cleaned more thoroughly thus allowing it to remain in the adsorption section for a greater time period. However, a reverse trend was observed whenever the catalyst bed length was not sufficient to take the reaction to near equilibrium conditions. This is because higher purge rates dilute the feed to reaction section thus requiring a longer catalyst bed.

SMBR with reverse flow regeneration automatically gives rise to a sandwich reactor, which consists of a catalyst bed sandwiched between two adsorbent beds in a single vessel. It also yielded 100% purity because the only difference between the two arrangements is that flow is reversed in the reaction section as well for the latter case.

Desorption is a slow process because of unfavorable isotherm conditions. Thus, wall temperature immediately compensates for any temperature drop in the regeneration section. The adsorption process is however favorable under the conditions studied. Hence, the temperature front is clearly noticeable traveling through the adsorption section.

Three reactor models were simulated in this study. The fixed bed simulations revealed that their dynamic performance differed significantly but the steady state outcome was similar. Besides when incorporated in an SMBR, a similar purity was predicted using anyone of them. Thus, the important conclusion is deduced that the steady state/cyclic steady state results depend only on the kinetic parameters of catalyst.

6.2 RECOMMENDATIONS FOR FUTURE WORK

In this study, many assumptions were made which need to be relaxed in order to get results that are more accurate. The heat effects because of adsorption and desorption wont nullify over the catalyst during unsteady state operations, and therefore should be taken into account. The adsorption equilibrium isotherm and physical properties of Y-zeolite catalyst should be determined separately rather than assuming equal to that of 5A zeolite adsorbent.

Although it is common to assume the fluid and solid to be in thermal equilibrium during fixed bed simulations, the heat transfer resistance between them should be taken into account for the sake of completeness. Moreover, the values of effective axial bed thermal conductivity and wall heat transfer coefficient should be calculated for each run as they have a strong impact on temperature profiles.

There were oscillations in concentration profiles because of the steep adsorption front and were thus filtered off. As an alternative, the collocation points could be concentrated in the regime of adsorption front by dividing the adsorbent bed into several finite elements. However, the adsorption front travels through the bed hence making it necessary to move or deform the finite elements at each time step. Such an approach was adopted by Ray and Carr [53] in the Galerkin finite element formulation [13] and by Kruglov [33] in the finite difference scheme.

It was observed that a higher fresh feed rate reduced the purity even if the reaction section length is increased to counteract any decline in conversion. The adsorbent bed

length should be increased as well to examine whether the purity is then restored or not. This shall give an idea of the performance of the upsized version of the reactor.

The catalyst and adsorbent were not homogeneously mixed in this study because the product would otherwise undergo reverse reaction in the latter part of vessel where the reactant has not yet reached. However, a homogeneous mixture has been used elsewhere for a similar case where the reactant was the more strongly adsorbed species, i.e. in the hydrogenation of mesitylene to 1,3,5-trimethylcyclohexane [52]. This issue should be investigated further and if promising results are obtained, it should be included in the hydrocarbon isomerization as well. This shall allow several beds to be incorporated in regeneration section as the catalyst would constantly lower the reactant concentration in purge stream thus increasing driving force for desorption.

The real life problem is the isomerization of light straight run naphtha, which consists of pentanes and hexanes. Since the adsorption equilibrium isotherm of *n*-hexane is also available in literature [64], the next step is to simulate the reactors for a multicomponent system.

The minimum temperature swing should be determined for the sandwich reactor that would give the same 100% purity. This would be an additional advantage of the sandwich reactor over SMBR. Finally, experimental reactors should be constructed in the laboratory to verify the above results.

REFERENCES

1. Al-Juhani, A. A., "Modeling and Simulation of a Combined Isomerization Reactor/Pressure Swing Adsorption Unit," M.S. Thesis, King Fahd University of Petroleum & Minerals, May 2000.

2. Azevedo, D. C. S., and A. E. Rodrigues, "Design methodology and operation of a simulated moving bed reactor for the inversion of sucrose and glucose-fructose separation," *Chem. Eng. J.*, **82**, 95-107 (2001).

3. Benazzi, E., G. Hotier, J. M. Basset, A. Choplin, A. Theolier, and C. Nedez, "Separation of aliphatic paraffins by adsorption," U.S. Patent No. 5,326,928 (1993).

4. Bhatia, S., and K. Jothimurugesan, "Isomerization of *n*-hexane over nickel-loaded zeolite catalysts," *Can. J. Chem. Eng.*, **62**, 390 (1984).

5. Broughton, D. B., and C. G. Gerhold, "Continuous sorption process employing fixed beds of sorbent and moving inlets and outlets," U.S. Patent No. 2,985,589 (1961).

6. Broughton, D. B., "Molex: case history of a process," *Chem. Eng. Prog.*, **64**, 60 (1968).

7. Broughton, D. B., R. Neuzil, J. Pharls, and C. Brearly, "The Parex process for recovering *para*-xylene" *Chem. Eng. Prog.*, **66**, 70 (1970).

8. Bryant, P. A., "Hydroisomerization of Normal Pentane over a Zeolite Catalyst," Ph.D. Dissertation, Louisiana State University, 1966.

9. Bunimovich, G. A., V. O. Strots, and O. V. Goldman, "Theory and industrial application of SO_2 oxidation reverse-process for sulfuric acid production," in *Unsteady State Processes in Catalysis*, (Y. S. Matros, Ed.), p. 7, VSP, Netherlands, 1990.

10. Chihara, K., and M. Suzuki, "Simulation of nonisothermal pressure swing adsorption," *J. Chem. Eng. Japan*, **16**, 53 (1983).

11. Cho, B. K., R. Aris, and R. W. Carr, "The mathematical theory of a countercurrent catalytic reactor," *Proc. Roy. Soc. London*, **A383**, 147 (1982).

12. Fajula, F., D. McQueen, B. H. Chiche, A. Auroux, C. Guimon, F. Fitoussi, and P. Schulz, "A multitechnique characterization of the acidity of dealuminated mazzite," *J. Catal.*, **161**, 587-596 (1996).

13. Finlayson, B. A., *Nonlinear Analysis in Chemical Engineering*, McGraw-Hill, New York, 1980.

14. Fish, B. B., R. W. Carr, and R. Aris, "The continuous countercurrent moving bed chromatographic reactor," *Chem. Eng. Sci.*, **41**, 661 (1986).

15. Fish, B. B., and R. W. Carr, "An experimental study of the countercurrent moving-bed chromatographic reactor," *Chem. Eng. Sci.*, **44**, 1773 (1989).

16. Fogler, H. S., *Elements of Chemical Reaction Engineering*, Prentice Hall, New Jersey, 1999.

17. Fricke, J., M. Meurer, J. Dreisomer, and H. Schmidt-Traub, "Effect of process parameters on the performance of a simulated moving bed chromatographic reactor," *Chem. Eng. Sci*, **54**, 1487-1492 (1999).

18. Froment, G. F., "Reversed flow operation of fixed bed catalytic reactors," in *Unsteady State Processes in Catalysis*, (Y. S. Matros, Ed.), p. 57, VSP, Netherlands, 1990.

19. Froment, G. F., and K. B. Bischoff, *Chemical Reactor Analysis and Design*, John Wiley & Sons, Singapore, 1990.

20. Fujimoto, K., A. Zhang, I. Nakamura, and K. Aimoto, "Isomerization of *n*-pentane and other light hydrocarbons on hybrid catalyst: Effect of hydrogen spillover," *Ind. Eng. Chem. Res.*, **34**, 1074-1080 (1995).

21. Funk, G. A., C. Stream, H. W. Dandekar, and S. H. Hobbs, "Process for concurrent hydrolysis of esters and separation of products using a simulated moving bed," U.S. patent No. 5,502,248 (1996).

22. Glueckauf, E., "Formulae for diffusion into spheres and their application to chromatography," *J. Chem. Soc.*, **51**, 540 (1955).

23. Gray, R. L., "Total Isomerization Process and Apparatus," U.S. Patent No. 4,709,117 (1987).

24. Hashimoto, K., S. Adachi, H. Noujima, and Y. Ueda, "A new process combining adsorption and enzyme reaction for producing higher-fructose syrup," *Biotechnol. & Bioeng.*, **25**, 2371-2393 (1983).

25. Hopper, J. R., "A Study of the Catalytic Hydroisomerization Reactions of n-Pentane and Cyclohexane over Structurally Modified Mordenites," Ph.D. Dissertation, Louisiana State University, 1969.

26. Hosten, L. H., and G. F. Froment, "Isomerization of n-pentane," *Ind. Eng. Chem. Proc. Des. Dev.*, **10**, 280-287 (1971).

27. Huang, S., and R. W. Carr, "A simple adsorber dynamics approach to simulated countercurrent moving bed reactor performance," *Chem. Eng. J.*, **82**, 87-94 (2001).

28. Johnson, J. A., and R. G. Kabza, "SORBEX: industrial-scale adsorptive separation," in *Preparative and Production Scale Chromatography*, (G. Ganetsos and P. E. Barker, Eds.), p. 257, Marcel Dekker, New York, 1993.

29. Karger, J., and D. M. Ruthven, *Diffusion in Zeolites and Other Microporous Solids*, John Wiley & Sons, Inc., New York, 1992.

30. Kawase, M., T. B. Suzuki, K. Inoue, K. Yoshimoto, and K. Hashimoto, "Increased esterification conversion by application of the simulated moving-bed reactor," *Chem. Eng. Sci.*, **51**, 2971-2976 (1996).

31. Kawase, M., Y. Inoue, T. Araki, and K. Hashimoto, "The simulated-moving-bed reactor for production of Bisphenol A," *Catal. Today*, **48**, 199-209 (1999).

32. Kouwenhoven, H. W., "Isomerization of paraffins," in *Molecular Sieves*, (W. M. Meier and J. B. Uytterhoeven, Eds.), p. 529, Adv. Chem. Ser., 121, ACS, Washington, 1973.

33. Kruglov, A. V., "Methanol synthesis in a simulated countercurrent moving-bed adsorptive catalytic reactor," *Chem. Eng. Sci.*, **49**, 4699-4716 (1994).

34. Kruglov, A. V., M. C. Bjorklund, and R. W. Carr, "Optimization of the simulated countercurrent moving-bed chromatographic reactor for the oxidative coupling of methane," *Chem. Eng. Sci.*, **51**, 2945-2950 (1996).

35. Langmuir, I., "The adsorption of gases on plane surfaces of glass, mica and platinum," *J. Am. Chem. Soc.*, **40**, 163 (1918).

36. Liapis, A. I., and D. W. T. Rippin, "A general model for the simulation of multi-component adsorption from a finite bath," *Chem. Eng. Sci.*, **32**, 619-627 (1977).

37. Lode, F., M. Houmard, C. Migliorini, M. Mazzotti, and M. Morbidelli, "Continuous reactive chromatography," *Chem. Eng. Sci.*, **56**, 269-291 (2001).

38. Matros, Y. S., "Performance of catalytic processes under unsteady-state conditions," in *Unsteady State Processes in Catalysis*, (Y. S. Matros, Ed.), p. 131, VSP, Netherlands, 1990.

39. Mazzotti, M., R. Baciocchi, G. Storti, and M. Morbidelli, "Vapor-phase SMB adsorptive separation of linear/nonlinear paraffins," *Ind. Eng. Chem. Res.*, **35**, 2313-2321 (1996).

40. Mazzotti, M., A. Kruglov, B. Neri, D. Gelosa, and M. Morbidelli, "A continuous chromatographic reactor: SMBR," *Chem. Eng. Sci.*, **51**, 1827-1836 (1996).

41. Meurer, M., U. Altenhoner, J. Strube, and H. Schmidt-Traub, "Dynamic simulation of simulated moving bed chromatographic reactors," *J. Chromatography*, **769**, 71-79 (1997).

42. Migliorini, C., M. Fillinger, M. Mazzotti, and M. Morbidelli, "Analysis of simulated moving-bed reactors," *Chem. Eng. Sci.*, **54**, 2475-2480 (1999).

43. Morbidelli, M., A. Servida, G. Storti, and S. Carra, "Simulation of multicomponent adsorption beds. Model analysis and numerical solution," *Ind. Eng. Chem. Fundam.*, **21**, 123-131 (1982).

44. Nitta, T., T. Shigetomi, M. Kuro-Oka, and T. Katayama, "An adsorption isotherm of multi-site occupancy model for homogeneous surface," *J. Chem. Eng. Jpn.*, **17**, 39-51 (1984).

45. Perry, R. H., and D. W. Green, *Perry's Chemical Engineers' Handbook*, McGraw-Hill, New York, 1997.

46. Petroulas, T., R. Aris, and R. W. Carr, "Analysis of a countercurrent moving-bed chromatographic reactor," *Comput. Math. Appl.*, **11**, 5 (1985).

47. Petroulas, T., R. Aris, and R. W. Carr, "Analysis and performance of a countercurrent moving bed chromatographic reactor," *Chem. Eng. Sci.*, **40**, 2233 (1985).

48. Pines, H., K. Vetinskas, K. Assel, and I. Patieff, "Determination of Equilibrium Constants for Butanes and Pentanes," *J. Am. Chem. Soc.*, **67**, 631 (1945).

49. Ramirez, W. F., *Computational Methods for Process Simulation*, Butterworth Publishers, Boston, 1989.

50. Ray, A. K., "The Simulated Countercurrent Moving Bed Chromatographic Reactor: A Novel Reactor-Separator," Ph.D. Thesis, University of Minnesota, April 1992.

51. Ray, A. K., R. W. Carr, and R. Aris, "The simulated countercurrent moving bed chromatographic reactor: a novel reactor-separator," *Chem. Eng. Sci.*, **49**, 469 (1994).

52. Ray, A. K., and R. W. Carr, "Experimental study of a laboratory-scale simulated countercurrent moving bed chromatographic reactor," *Chem. Eng. Sci.*, **50**, 2195-2202 (1995).

53. Ray, A. K., and R. W. Carr, "Numerical simulation of a simulated countercurrent moving bed chromatographic reactor," *Chem. Eng. Sci.*, **50**, 3033-3041 (1995).

54. Rice, R. G., and D. D. Do, *Applied Mathematics and Modeling for Chemical Engineers*, John Wiley & Sons, Inc., New York, 1995.

55. Runstraat, A., J. Grondelle, and R. A. Santen, "On the temperature dependence of the Arrhenius activation energy for hydroisomerization catalyzed by Pt/mordenite," *J. Catal.*, **167**, 460-463 (1997).

56. Runstraat, A., J. Kamp, P. Stobbelaar, J. Grondelle, S. Krijnen, and R. Santen, "Kinetics of hydroisomerization of *n*-hexane over platinum containing zeolites," *J. Catal.*, **171**, 77-84 (1997).

57. Runstraat, A., J. Grondelle, and R. Santen, "Microkinetics modeling of the hydroisomerization of *n*-hexane," *Ind. Eng. Chem. Res.*, **36**, 3116-3125 (1997).

58. Ruthven, D. M., *Principles of Adsorption and Adsorption Processes*, John Wiley & Sons, New York, 1984.

59. Ruthven, D. M., and N. S. Raghavan, "Numerical simulation of a PSA system-Part III," *AIChE J.*, **31**, 1829 (1985).

60. Ruthven, D. M., and C. B. Ching, "Counter-current and simulated counter-current adsorption separation processes," *Chem. Eng. Sci.*, **44**, 1011 (1989).

61. Shampine, L. F., and M. W. Reichelt, "The MATLAB ODE Suite," *SIAM J. Sci. Comp.*, **18**, 1-22 (1997).

62. Shieh, M. T., and P. Barker, "Combined bioreaction and separation in a simulated counter-current chromatographic bioreactor-separator for the hydrolysis of lactose," *J. Chem. Tech. Biotechnol.*, **66**, 265-278 (1996).

63. Shin, H. S., and K. S. Knaebel, "An experimental study of diffusion-induced separation of gas mixtures by pressure swing adsorption," *AIChE J.*, **33**, 654 (1987).

64. Silva, J. A. C., "Equilibrium and kinetics of *n*-hexane sorption in pellets of 5A zeolite," *AIChE J.*, **43**, 2524 (1997).

65. Silva, J. A. C., and A. E. Rodrigues, "Sorption and diffusion of *n*-pentane in pellets of 5A zeolite," *Ind. Eng. Chem. Res.*, **36**, 493-500 (1997).

66. Silva, J. A. C., and A. E. Rodrigues, "Fixed-bed adsorption of *n*-pentane/isopentane mixtures in pellets of 5A zeolite," *Ind. Eng. Chem. Res.*, **36**, 3769-3777 (1997).

67. Skarstrom, C. W., U.S. Patent No. 2,944,627 (1960).

68. Spivey, J. J., and P. A. Bryant, "Hydroisomerization of n-C_5 and n-C_6 mixtures on zeolite catalysts," *Ind. Eng. Chem. Process Des. Dev.*, **21**, 750-760 (1982).

69. Spry, J. C., and W. H. Sawyer, 68th Annual AICHE Meeting, Los Angeles, 1975.

70. Storti, G., M. Mazzotti, M. Morbidelli, and S. Carra, "Robust design of binary countercurrent separation processes," *AIChE J.*, **39**, 471-492 (1993).

71. Symoniak, M. F., "Upgrade naphtha to... fuels and feedstocks," *Hydrocarbon Process.*, 110 (1980).

72. Takeuchi, K., and Y. Uraguchi, "Separation conditions of the reactant and the product with a chromatographic moving bed reactor," *J. Chem. Eng. Jpn.*, **9**, 164 (1976).

73. Takeuchi, K., and Y. Uraguchi, "Basic design of chromatographic moving bed reactors for product refining," *J. Chem. Eng. Jpn.*, **9**, 246 (1976).

74. Takeuchi, K., and Y. Uraguchi, "The effect of the exhausting section on the performance of a chromatographic moving bed reactor," *J. Chem. Eng. Jpn.*, **10**, 72 (1977).

75. Takeuchi, K., and Y. Uraguchi, "Experimental studies of a chromatographic moving bed reactor," *J. Chem. Eng. Jpn.*, **10**, 455 (1977).

76. Takeuchi, K., T. Miyauchi, and Y. Uraguchi, "Computational studies of a chromatographic moving bed reactor for consecutive and reversible reactions," *J. Chem. Eng. Jpn.*, **11**, 216 (1978).

77. Tonkovich, A. L. Y., and R. W. Carr, "A simulated countercurrent moving-bed chromatographic reactor for the oxidative coupling of methane: Experimental results," *Chem. Eng. Sci.*, **49**, 4647-4656 (1994).

78. Viswanathan, S., and R. Aris, "An analysis of the countercurrent moving bed reactor," *SIAM-AMS Proc.*, **8**, 99 (1974).

79. Viswanathan, S., and R. Aris, "Countercurrent moving bed chromatographic reactors," *Proc. 3rd ISCRE*, Adv. Chem. Ser., **65**, 191 (1974).

80. Voorhies, A. J., and P. A. Bryant, "Hydroisomerization of normal pentane over a zeolite catalyst," *AICHE J.*, **14**, 852-856 (1968).

81. Wakao, N., and T. Funazkri, "Effect of fluid dispersion coefficients on fluid-to-particle mass transfer coefficients in packed beds," *Chem. Eng. Sci.*, **33**, 1375 (1978).

82. Weisz, P. B., "Polyfunctional heterogeneous catalysis," in *Advances in Catalysis and Related Subjects*, Vol. 13, (D. D. Eley, P. W. Selwood, and P. B. Weisz, Eds.), p. 137, Academic Press, London, 1962.

83. Yang, R. T., *Gas Separation by Adsorption Process*, Butterworth, Boston, 1987.

84. Zabransky, R., and R. Anderson, "Simulated moving bed alkylation process," U.S. Patent No. 4,008,291 (1977).

Derivations A

A.1 DERIVATION OF THE LUMPED MODEL

The intraparticle diffusion equation developed in Chapter 2 is:

$$\varepsilon_p \frac{\partial c_{pA}}{\partial t} = \varepsilon_p \frac{D_p}{r^2}\frac{\partial}{\partial r}\left[r^2 \frac{\partial c_{pA}}{\partial r}\right] - \frac{\partial q_A}{\partial t}\rho_s\left(1-\varepsilon_p\right) \tag{A.1}$$

$$\frac{\partial c_{pA}}{\partial r} = 0; \qquad r = 0 \tag{A.2a}$$

$$\varepsilon_p D_p \frac{\partial c_{pA}}{\partial r} = k_e\left(c_A - c_{pA}\right); \qquad r = R_p \tag{A.2b}$$

Integrating both sides of equation A.1 with respect to dV_p, that is, $4\pi r^2 \mathrm{d}r$ for a spherical particle, and dividing by V_p, that is, $\frac{4}{3}\pi R_p^{\,3}$:

$$\begin{aligned}\varepsilon_p \frac{\mathrm{d}}{\mathrm{d}t}\left(\frac{1}{V_p}\int c_{pA}\mathrm{d}V_p\right) = \frac{3\varepsilon_p D_p}{4\pi R_p^{\,3}}\int_0^{R_p}\frac{1}{r^2}\frac{\partial}{\partial r}\left[r^2\frac{\partial c_{pA}}{\partial r}\right]4\pi r^2\mathrm{d}r \\ - \rho_s\left(1-\varepsilon_p\right)\frac{\mathrm{d}}{\mathrm{d}t}\left(\frac{1}{V_p}\int q_A \mathrm{d}V_p\right)\end{aligned} \tag{A.3}$$

$$\varepsilon_p \frac{\mathrm{d}\langle c_A\rangle}{\mathrm{d}t} = \frac{3\varepsilon_p D_p}{R_p^{\,3}}\int_{r=0}^{r=R_p}\partial\left[r^2\frac{\partial c_{pA}}{\partial r}\right] - \frac{\mathrm{d}\langle q_A\rangle}{\mathrm{d}t}\rho_s\left(1-\varepsilon_p\right) \tag{A.4}$$

where $$\langle c_A \rangle = \frac{1}{V_p} \int c_{pA} \mathrm{d}V_p \tag{A.5}$$

and $$\langle q_A \rangle = \frac{1}{V_p} \int q_A \mathrm{d}V_p \tag{A.6}$$

$$\varepsilon_p \frac{\mathrm{d}\langle c_A \rangle}{\mathrm{d}t} = \frac{3\varepsilon_p D_p}{R_p^{\,3}} r^2 \left. \frac{\partial c_{pA}}{\partial r} \right|_{r=0}^{r=R_p} - \frac{\mathrm{d}\langle q_A \rangle}{\mathrm{d}t} \rho_s (1-\varepsilon_p) \tag{A.7}$$

Applying boundary conditions A.2:

$$\varepsilon_p \frac{\mathrm{d}\langle c_A \rangle}{\mathrm{d}t} = k_e \frac{3}{R_p} \left[c_A - c_{pA}(R_p) \right] - \frac{\mathrm{d}\langle q_A \rangle}{\mathrm{d}t} \rho_s (1-\varepsilon_p) \tag{A.8}$$

The above notations are explained in Chapter 2.

A.2 DERIVATION OF THE OVERALL EFFECTIVENESS FACTOR (Ω)

The rate law in terms of the bulk gas phase concentration is:

$$-r_A = k(c_A - c_B/K) \tag{A.9}$$

and that in terms of the average macropore concentration is:

$$-r_A = \frac{k}{\Omega} \left(\langle c_A \rangle - \frac{\langle c_B \rangle}{K} \right) \tag{A.10}$$

The rate of mass transfer of A to the catalyst particle is:

$$\text{rate of mass transfer} = a_p k_e \left(c_A - c_{pA}(R_p) \right) \tag{A.11}$$

Using the linear driving force approximation [43]:

$$k_e \left(c_A - c_{pA}(R_p) \right) = K_{gl} \left(c_A - \langle c_A \rangle \right) \tag{A.12}$$

At steady state conditions, as was the case with Spivey and Bryant [68], rate of mass transfer to the catalyst particle is equal to the rate of reaction:

$$a_p K_{gl}\left(c_A - \langle c_A \rangle\right) = \frac{k\rho_a}{\Omega}\left(\langle c_A \rangle - \frac{\langle c_B \rangle}{K}\right) \tag{A.13}$$

$$a_p K_{gl}\left(c_B - \langle c_B \rangle\right) = -\frac{k\rho_a}{\Omega}\left(\langle c_A \rangle - \frac{\langle c_B \rangle}{K}\right) \tag{A.14}$$

Adding equations A.13 and A.14:

$$\langle c_B \rangle = c_A + c_B - \langle c_A \rangle \tag{A.15}$$

Substituting for $\langle c_B \rangle$ in equation A.13 and solving for $\langle c_A \rangle$:

$$a_p K_{gl}\left(c_A - \langle c_A \rangle\right) = \frac{k\rho_a}{\Omega}\left(\langle c_A \rangle - \frac{c_A + c_B - \langle c_A \rangle}{K}\right) \tag{A.16}$$

$$\langle c_A \rangle = \frac{a_p K_{gl} c_A + \frac{k\rho_a}{\Omega}\frac{c_A + c_B}{K}}{a_p K_{gl} + \frac{k\rho_a}{\Omega}\left(1 + \frac{1}{K}\right)} \tag{A.17}$$

Substituting for $\langle c_A \rangle$ and $\langle c_B \rangle$ in equation A.10:

$$\begin{aligned} -r_A &= \frac{k}{\Omega}\left(\langle c_A \rangle - \frac{c_A + c_B - \langle c_A \rangle}{K}\right) \\ &= \frac{k}{\Omega}\left(\langle c_A \rangle\left(1 + \frac{1}{K}\right) - \frac{c_A + c_B}{K}\right) \\ &= \frac{k}{\Omega}\left(\frac{a_p K_{gl} c_A + \frac{k\rho_a}{\Omega}\frac{c_A + c_B}{K}}{a_p K_{gl} + \frac{k\rho_a}{\Omega}\left(1 + \frac{1}{K}\right)}\left(1 + \frac{1}{K}\right) - \frac{c_A + c_B}{K}\right) \end{aligned} \tag{A.18}$$

$$-r_A = \frac{k}{\Omega}\frac{\left(\begin{array}{l} a_p K_{gl} c_A\left(1+\frac{1}{K}\right)+\frac{k\rho_a}{\Omega}\frac{c_A+c_B}{K}\left(1+\frac{1}{K}\right) \\ \qquad -a_p K_{gl}\frac{c_A}{K}-a_p K_{gl}\frac{c_B}{K}-\frac{k\rho_a}{\Omega}\frac{c_A+c_B}{K}\left(1+\frac{1}{K}\right)\end{array}\right)}{a_p K_{gl}+\frac{k\rho_a}{\Omega}\left(1+\frac{1}{K}\right)} \tag{A.19}$$

Simplifying and dividing the numerator and denominator by the term $(k/\Omega)\cdot a_p K_{gl}$,

$$-r_A = \frac{1}{\frac{1}{k/\Omega}+\frac{\rho_a}{a_p K_{gl}}\left(1+\frac{1}{K}\right)}\left(c_A-\frac{c_B}{K}\right) \tag{A.20}$$

Comparing equations A.9 and A.20:

$$k = \frac{1}{\frac{1}{k/\Omega}+\frac{\rho_a}{a_p K_{gl}}\left(1+\frac{1}{K}\right)} \tag{A.21}$$

Solving for Ω:

$$\Omega = 1-\frac{k\rho_a}{a_p K_{gl}}\left(1+\frac{1}{K}\right) \tag{A.22}$$

The reaction section of SMBR is preferably operated at the following conditions:

T	=	514 K
P_t	=	15 bar
K_{gl}	=	0.41 cm/s
k	=	0.046 cm^3/g.s
K	=	3.22
a_p	=	28.3 cm^{-1}
ρ_a	=	0.97 g/cm^3

Thus, $\Omega = 1 - \frac{0.046 \times 0.97}{28.3 \times 0.41}\left(1 + \frac{1}{3.22}\right) \approx 1$. The notations are explained in Chapter 2.

It should be noted however that the dimensions of the catalyst particle are not known so that the quantity $a_p K_{gl}$ has been approximated to be the same as that of the pellet. In fact $a_p K_{gl}$ is much larger for the catalyst used by Voorhies and Bryant [80] as they report that both the film resistance and the macropore diffusion resistance are not rate limiting. Using a higher value would make Ω even closer to unity. This is understandable because higher the mass transfer coefficient, lesser should be the difference between bulk gas phase and macropore concentrations.

A.3 MATERIAL & ENERGY BALANCES AT THE MIXING POINT

Total material balance at the mixing point is:

$$F_f^R = F_{feed} + F_{extract} \tag{A.23}$$

The material balance for component A is:

$$F_f^R y_{Af}^R = F_{feed} y_{A,feed} + F_{extract} y_{A,extract} \tag{A.24}$$

The material balance for component B is:

$$F_f^R y_{Bf}^R = F_{feed} y_{B,feed} + F_{extract} y_{B,extract} \tag{A.25}$$

The fresh feed contains normal and iso- pentanes only and that too in equimolar amounts, i.e. $y_{A,feed} = y_{B,feed} = 0.5$.

The reference molar flux was defined in Chapter 4 as:

$$F_{ref} = F_{feed} + F_{purge} \tag{A.26}$$

and the dimensionless molar flux of fresh feed as:

$$\overline{F}_{feed} = \frac{F_{feed}}{F_{ref}} = y_{HC}^{0} \tag{A.27}$$

The dimensionless material balance at the mixing point thus becomes:

$$\overline{F}_{f}^{R} = y_{HC}^{0} + \overline{F}_{extract} \tag{A.28}$$

$$y_{Af}^{R} = \frac{0.5y_{HC}^{0} + \overline{F}_{extract}y_{A,extract}}{\overline{F}_{f}^{R}} \tag{A.29}$$

$$y_{Bf}^{R} = \frac{0.5y_{HC}^{0} + \overline{F}_{extract}y_{B,extract}}{\overline{F}_{f}^{R}} \tag{A.30}$$

The thermal properties of normal and iso- pentanes are approximately the same. Hence, they are treated collectively in the energy balance to follow. Summing up equations A.24 and A.25:

$$F_{f}^{R}\left(y_{Af}^{R} + y_{Bf}^{R}\right) = F_{feed} + F_{extract}\left(y_{A,extract} + y_{B,extract}\right) \tag{A.31}$$

Subtracting equation A.31 from A.23 to get a material balance for hydrogen:

$$F_{f}^{R}\left(1 - y_{Af}^{R} - y_{Bf}^{R}\right) = F_{extract}\left(1 - y_{A,extract} - y_{B,extract}\right) \tag{A.32}$$

The energy balance is obtained by summing up the sensible heats of hydrocarbons from fresh feed and extract and that of hydrogen from the extract:

$$\begin{aligned} &F_{feed}\widetilde{H}_{feed} + F_{extract}\left(y_{A,extract} + y_{B,extract}\right)\widetilde{H}_{HC,extract} \\ &\quad + F_{extract}\left(1 - y_{A,extract} - y_{B,extract}\right)\widetilde{H}_{H_2,extract} \\ &= F_{f}^{R}\left(y_{Af}^{R} + y_{Bf}^{R}\right)\widetilde{H}_{HC,mix} + F_{f}^{R}\left(1 - y_{Af}^{R} - y_{Bf}^{R}\right)\widetilde{H}_{H_2,mix} \end{aligned} \tag{A.33a}$$

where molar enthalpies of the various components are as follows:

$$\tilde{H}_{feed} = \tilde{H}^0_{HC}(T_R) + \int_{T_R}^{T_{feed}} C_{p,HC} dT \tag{A.33b}$$

$$\tilde{H}_{HC,extract} = \tilde{H}^0_{HC}(T_R) + \int_{T_R}^{T_{extract}} C_{p,HC} dT \tag{A.33c}$$

$$\tilde{H}_{H_2,extract} = \tilde{H}^0_{H_2}(T_R) + \int_{T_R}^{T_{extract}} C_{p,H_2} dT \tag{A.33d}$$

$$\tilde{H}_{HC,mix} = \tilde{H}^0_{HC}(T_R) + \int_{T_R}^{T_f^R} C_{p,HC} dT \tag{A.33e}$$

$$\tilde{H}_{H_2,mix} = \tilde{H}^0_{H_2}(T_R) + \int_{T_R}^{T_f^R} C_{p,H_2} dT \tag{A.33f}$$

The expressions for the heat capacities of hydrogen and hydrocarbons are taken from Perry and Green [45]. Moreover, the reference temperature (T_R) does not need to be defined, as it will cancel out later in the derivation. Substituting the material balance equations A.31 and A.32 in equation A.33a to express it in terms of the known quantities:

$$\begin{aligned} & F_{feed}\tilde{H}_{feed} + F_{extract}\left(y_{A,extract} + y_{B,extract}\right)\tilde{H}_{HC,extract} \\ & \qquad + F_{extract}\left(1 - y_{A,extract} - y_{B,extract}\right)\tilde{H}_{H_2,extract} \\ & = \left[F_{feed} + F_{extract}\left(y_{A,extract} + y_{B,extract}\right)\right]\tilde{H}_{HC,mix} \\ & \qquad + F_{extract}\left(1 - y_{A,extract} - y_{B,extract}\right)\tilde{H}_{H_2,mix} \end{aligned} \tag{A.34}$$

Substituting the expressions for molar enthalpies from equations A.33b through A.33f into equation A.34:

$$
\begin{aligned}
& F_{feed}\left(\tilde{H}^{0}_{HC}(T_R)+\int_{T_R}^{T_{feed}} C_{p,HC}dT\right) \\
& \quad + F_{extract}\left(y_{A,extract}+y_{B,extract}\right)\left(\tilde{H}^{0}_{HC}(T_R)+\int_{T_R}^{T_{extract}} C_{p,HC}dT\right) \\
& \quad + F_{extract}\left(1-y_{A,extract}-y_{B,extract}\right)\left(\tilde{H}^{0}_{H_2}(T_R)+\int_{T_R}^{T_{extract}} C_{p,H_2}dT\right) \\
& = \left[F_{feed}+F_{extract}\left(y_{A,extract}+y_{B,extract}\right)\right]\left(\tilde{H}^{0}_{HC}(T_R)+\int_{T_R}^{T_f^R} C_{p,HC}dT\right) \\
& \quad + F_{extract}\left(1-y_{A,extract}-y_{B,extract}\right)\left(\tilde{H}^{0}_{H_2}(T_R)+\int_{T_R}^{T_f^R} C_{p,H_2}dT\right)
\end{aligned}
\tag{A.35}
$$

Simplifying and collecting the like terms together:

$$
\begin{aligned}
& F_{feed}\left(\int_{T_R}^{T_{feed}} C_{p,HC}dT-\int_{T_R}^{T_f^R} C_{p,HC}dT\right) \\
& \quad + F_{extract}\left(y_{A,extract}+y_{B,extract}\right)\left(\int_{T_R}^{T_{extract}} C_{p,HC}dT-\int_{T_R}^{T_f^R} C_{p,HC}dT\right) \\
& \quad + F_{extract}\left(1-y_{A,extract}-y_{B,extract}\right)\left(\int_{T_R}^{T_{extract}} C_{p,H_2}dT-\int_{T_R}^{T_f^R} C_{p,H_2}dT\right)=0
\end{aligned}
\tag{A.36}
$$

Applying the rules of integration to simplify the equation further:

$$
\begin{aligned}
& F_{extract}\left(y_{A,extract}+y_{B,extract}\right)\int_{T_f^R}^{T_{extract}} C_{p,HC}dT \\
& \quad + F_{extract}\left(1-y_{A,extract}-y_{B,extract}\right)\int_{T_f^R}^{T_{extract}} C_{p,H_2}dT = F_{feed}\int_{T_{feed}}^{T_f^R} C_{p,HC}dT
\end{aligned}
\tag{A.37}
$$

Using the concept of mean heat capacity:

$$F_{extract}\left(y_{A,extract}+y_{B,extract}\right)\widetilde{C}_{p,HC_{extract}}\left(T_{extract}-T_f^R\right)$$
$$+F_{extract}\left(1-y_{A,extract}-y_{B,extract}\right)\widetilde{C}_{p,H_{2extract}}\left(T_{extract}-T_f^R\right) \tag{A.38a}$$
$$=F_{feed}\widetilde{C}_{p,feed}\left(T_f^R-T_{feed}\right)$$

where the mean heat capacities for the various components are:

$$\widetilde{C}_{p,HC_{extract}}=\frac{\int_{T_f^R}^{T_{extract}}C_{p,HC}dT}{T_{extract}-T_f^R} \tag{A.38b}$$

$$\widetilde{C}_{p,H_{2extract}}=\frac{\int_{T_f^R}^{T_{extract}}C_{p,H_2}dT}{T_{extract}-T_f^R} \tag{A.38c}$$

$$\widetilde{C}_{p,feed}=\frac{\int_{T_{feed}}^{T_f^R}C_{p,HC}dT}{T_f^R-T_{feed}} \tag{A.38d}$$

Collecting the terms for T_f^R together:

$$F_{feed}\widetilde{C}_{p,feed}T_f^R+F_{extract}\left(y_{A,extract}+y_{B,extract}\right)\widetilde{C}_{p,HC_{extract}}T_f^R$$
$$+F_{extract}\left(1-y_{A,extract}-y_{B,extract}\right)\widetilde{C}_{p,H_{2extract}}T_f^R$$
$$=F_{feed}\widetilde{C}_{p,feed}T_{feed}+F_{extract}\left(y_{A,extract}+y_{B,extract}\right)\widetilde{C}_{p,HC_{extract}}T_{extract} \tag{A.39}$$
$$+F_{extract}\left(1-y_{A,extract}-y_{B,extract}\right)\widetilde{C}_{p,H_{2extract}}T_{extract}$$

Solving for T_f^R, the temperature of the mixed stream that enters the reaction section:

$$T_f^R = \frac{F_{feed}\tilde{C}_{p,feed}T_{feed} + F_{extract}\begin{pmatrix}(y_{A,extract} + y_{B,extract})\tilde{C}_{p,HC_{extract}} \\ +(1 - y_{A,extract} - y_{B,extract})\tilde{C}_{p,H_{2extract}}\end{pmatrix}T_{extract}}{F_{feed}\tilde{C}_{p,feed} + F_{extract}\begin{pmatrix}(y_{A,extract} + y_{B,extract})\tilde{C}_{p,HC_{extract}} \\ +(1 - y_{A,extract} - y_{B,extract})\tilde{C}_{p,H_{2extract}}\end{pmatrix}} \tag{A.40}$$

The above notations are explained in Chapter 4.

A.4 EVALUATION OF AVERAGE TEMPERATURE OF A STREAM

For a stream with flow rate $F(t)$, temperature $T(t)$ and components with mole fractions $y_A(t)$ and $y_B(t)$, the average temperature T_{mean} during a switching period is defined as the final temperature that would be obtained if the stream were thoroughly mixed in an adiabatic tank at constant pressure.

Applying energy balance to the tank:

$$\begin{bmatrix}\text{rate of} \\ \text{accumu-} \\ \text{lation of} \\ \text{energy} \\ \text{within} \\ \text{the} \\ \text{system}\end{bmatrix} = \begin{bmatrix}\text{rate of} \\ \text{flow of} \\ \text{heat to} \\ \text{the system} \\ \text{from the} \\ \text{surround-} \\ \text{ings}\end{bmatrix} - \begin{bmatrix}\text{rate of} \\ \text{work done} \\ \text{by the} \\ \text{system} \\ \text{on the} \\ \text{surround-} \\ \text{ings}\end{bmatrix} + \begin{bmatrix}\text{rate of} \\ \text{energy} \\ \text{added to} \\ \text{the system} \\ \text{by mass} \\ \text{flow } \textit{into} \\ \text{the system}\end{bmatrix} - \begin{bmatrix}\text{rate of} \\ \text{energy leav-} \\ \text{ing system} \\ \text{by mass} \\ \text{flow } \textit{out} \\ \text{of the} \\ \text{system}\end{bmatrix} \tag{A.41}$$

$$\frac{dE_{sys}}{dt} = \dot{Q} - \dot{W} + \sum_{i=1}^{n}\tilde{E}_i F_i\Big|_{in} - \sum_{i=1}^{n}\tilde{E}_i F_i\Big|_{out}$$

Work is positive when system does work on surroundings. Moreover, the work term can be separated into:

$$\dot{W} = \overbrace{-\sum_{i=1}^{n} F_i P \tilde{V}_i \Big|_{in} + \sum_{i=1}^{n} F_i P \tilde{V}_i \Big|_{out}}^{[\text{rate of flow work}]} + \dot{W}_s \tag{A.42}$$

Since pressure is held constant, the system expands and does PV work against the surroundings as gas enters the tank during the switching period:

$$\dot{W}_s = P \frac{dV_{sys}}{dt} \tag{A.43}$$

Substituting equations A.42 and A.43 into equation A.41 while noting that the tank is adiabatic and that there is no mass flow out of the system:

$$\frac{dE_{sys}}{dt} = \sum_{i=1}^{n} F_i P \tilde{V}_i \Big|_{in} - P \frac{dV_{sys}}{dt} + \sum_{i=1}^{n} \tilde{E}_i F_i \Big|_{in} \tag{A.44}$$

Collecting the derivative terms together:

$$\frac{d\left(E_{sys} + PV_{sys}\right)}{dt} = \sum_{i=1}^{n} F_i \left(\tilde{E}_i + P\tilde{V}_i\right) \Big|_{in} \tag{A.45}$$

The kinetic, potential and other energy terms are negligible as compared to the internal energy of the system, hence:

$$E = U \tag{A.46}$$

Moreover, the enthalpy is defined as:

$$H = U + PV \tag{A.47}$$

Substituting equations A.46 and A.47 into equation A.45:

$$\frac{dH_{sys}}{dt} = \sum_{i=1}^{n} F_i \tilde{H}_i \Big|_{in} \tag{A.48}$$

Since only the final temperature is required, equation A.48 is integrated over the switching period:

$$\int_0^{H_{final}} dH_{sys} = \sum_{i=1}^{n} \left(\int_0^{\tau_s} F_i \tilde{H}_i dt \right) \tag{A.49}$$

Evaluating the LHS:

$$\begin{aligned} \int_0^{H_{final}} dH_{sys} &= H_{final} \\ &= N_{HC} \cdot \tilde{H}_{HC}(T_{final}) + N_{H_2} \cdot \tilde{H}_{H_2}(T_{final}) \end{aligned} \tag{A.50a}$$

where the molar enthalpies are:

$$\tilde{H}_{HC}(T_{final}) = \tilde{H}^0_{HC}(T_R) + \int_{T_R}^{T_{final}} C_{p,HC} dT \tag{A.50b}$$

$$\tilde{H}_{H_2}(T_{final}) = \tilde{H}^0_{H_2}(T_R) + \int_{T_R}^{T_{final}} C_{p,H_2} dT \tag{A.50c}$$

The number of moles of hydrocarbons (N_{HC}) and hydrogen (N_{H_2}) in the tank at the end of the switching period are:

$$N_{HC} = \int_0^{\tau_s} F \cdot (y_A + y_B) dt \tag{A.51a}$$

$$N_{H_2} = \int_0^{\tau_s} F \cdot (1 - y_A - y_B) dt \tag{A.51b}$$

Substituting equation A.51 into equation A.50a:

$$\int_0^{H_{final}} dH_{sys} = \left(\int_0^{\tau_s} F \cdot (y_A + y_B) dt \right) \cdot \tilde{H}_{HC}(T_{final}) + \left(\int_0^{\tau_s} F \cdot (1 - y_A - y_B) dt \right) \cdot \tilde{H}_{H_2}(T_{final}) \tag{A.52}$$

Since the final enthalpy is a constant value, it can be taken inside the integration:

$$\int_0^{H_{final}} dH_{sys} = \int_0^{\tau_s} F \cdot (y_A + y_B) \cdot \tilde{H}_{HC}(T_{final}) dt + \int_0^{\tau_s} F \cdot (1 - y_A - y_B) \cdot \tilde{H}_{H_2}(T_{final}) dt \tag{A.53}$$

Substituting the molar enthalpies (equations A.50b and A.50c) into equation A.53:

$$\int_0^{H_{final}} dH_{sys} = \int_0^{\tau_s} F \cdot (y_A + y_B) \cdot \left(\tilde{H}^0_{HC}(T_R) + \int_{T_R}^{T_{final}} C_{p,HC} dT \right) dt + \int_0^{\tau_s} F \cdot (1 - y_A - y_B) \cdot \left(\tilde{H}^0_{H_2}(T_R) + \int_{T_R}^{T_{final}} C_{p,H_2} dT \right) dt \tag{A.54}$$

Evaluating the RHS of equation A.49:

$$\sum_{i=1}^{n} \left(\int_0^{\tau_s} F_i \tilde{H}_i dt \right) = \int_0^{\tau_s} F_{HC} \cdot \tilde{H}_{HC}(T) dt + \int_0^{\tau_s} F_{H_2} \cdot \tilde{H}_{H_2}(T) dt \tag{A.55a}$$

where the molar enthalpies are:

$$\tilde{H}_{HC}(T) = \tilde{H}^0_{HC}(T_R) + \int_{T_R}^{T} C_{p,HC} dT \tag{A.55b}$$

$$\tilde{H}_{H_2}(T) = \tilde{H}^0_{H_2}(T_R) + \int_{T_R}^{T} C_{p,H_2} dT \tag{A.55c}$$

The inlet flow rates of the hydrocarbons and hydrogen to the tank are:

$$F_{HC} = F \cdot (y_A + y_B) \tag{A.56a}$$

$$F_{H_2} = F \cdot (1 - y_A - y_B) \tag{A.56b}$$

Substituting the flow rates (equation A.56) and the molar enthalpies (equations A.55b and A.55c) into equation A.55a:

$$\begin{aligned}\sum_{i=1}^{n}\left(\int_0^{\tau_s} F_i \tilde{H}_i dt \right) &= \int_0^{\tau_s} F \cdot (y_A + y_B) \cdot \left(\tilde{H}_{HC}^0(T_R) + \int_{T_R}^{T} C_{p,HC} dT \right) dt \\ &+ \int_0^{\tau_s} F \cdot (1 - y_A - y_B) \cdot \left(\tilde{H}_{H_2}^0(T_R) + \int_{T_R}^{T} C_{p,H_2} dT \right) dt\end{aligned} \tag{A.57}$$

Substituting equations A.54 and A.57 into equation A.49:

$$\begin{aligned}&\int_0^{\tau_s} F \cdot (y_A + y_B) \cdot \left(\tilde{H}_{HC}^0(T_R) + \int_{T_R}^{T_{final}} C_{p,HC} dT \right) dt \\ &\quad + \int_0^{\tau_s} F \cdot (1 - y_A - y_B) \cdot \left(\tilde{H}_{H_2}^0(T_R) + \int_{T_R}^{T_{final}} C_{p,H_2} dT \right) dt \\ &= \int_0^{\tau_s} F \cdot (y_A + y_B) \cdot \left(\tilde{H}_{HC}^0(T_R) + \int_{T_R}^{T} C_{p,HC} dT \right) dt \\ &\quad + \int_0^{\tau_s} F \cdot (1 - y_A - y_B) \cdot \left(\tilde{H}_{H_2}^0(T_R) + \int_{T_R}^{T} C_{p,H_2} dT \right) dt\end{aligned} \tag{A.58}$$

Simplifying and collecting like terms together:

$$\begin{aligned}&\int_0^{\tau_s} F \cdot (y_A + y_B) \cdot \left(\int_{T_R}^{T_{final}} C_{p,HC} dT - \int_{T_R}^{T} C_{p,HC} dT \right) dt \\ &\quad + \int_0^{\tau_s} F \cdot (1 - y_A - y_B) \cdot \left(\int_{T_R}^{T_{final}} C_{p,H_2} dT - \int_{T_R}^{T} C_{p,H_2} dT \right) dt = 0\end{aligned} \tag{A.59}$$

Applying the rules of integration to simplify the equation further:

$$\begin{aligned}&\int_0^{\tau_s} F \cdot (y_A + y_B) \cdot \left(\int_{T}^{T_{final}} C_{p,HC} dT \right) dt \\ &\quad + \int_0^{\tau_s} F \cdot (1 - y_A - y_B) \cdot \left(\int_{T}^{T_{final}} C_{p,H_2} dT \right) dt = 0\end{aligned} \tag{A.60}$$

Assuming that the temperature of the stream does not fluctuate a lot, the heat capacities can be assumed constant and evaluated at the arithmetic mean temperature of the stream:

$$\int_0^{\tau_s} F\cdot(y_A+y_B)\cdot C_{p,HC}\cdot(T_{final}-T)dt + \int_0^{\tau_s} F\cdot(1-y_A-y_B)\cdot C_{p,H_2}\cdot(T_{final}-T)dt = 0 \tag{A.61}$$

As T_{final} is a constant value, it can be taken out of the integration:

$$\left(\int_0^{\tau_s} F\cdot\left[(y_A+y_B)\cdot C_{p,HC}+(1-y_A-y_B)\cdot C_{p,H_2}\right]dt\right)T_{final} = \int_0^{\tau_s} F\cdot\left((y_A+y_B)\cdot C_{p,HC}+(1-y_A-y_B)\cdot C_{p,H_2}\right)Tdt \tag{A.62}$$

Solving for T_{final} while noting that it is the average temperature of the stream:

$$T_{mean} = \frac{\int_0^{\tau_s} F\cdot\left((y_A+y_B)\cdot C_{p,HC}+(1-y_A-y_B)\cdot C_{p,H_2}\right)Tdt}{\int_0^{\tau_s} F\cdot\left((y_A+y_B)\cdot C_{p,HC}+(1-y_A-y_B)\cdot C_{p,H_2}\right)dt} \tag{A.63}$$

The above notations are explained in Chapter 4. Since the flow rate F appears both in the numerator and in the denominator, it can be replaced by the molar flux of the stream instead.

Numerical Solution B

Equations 3.32 through 3.58 in Chapter 3 are written in the orthogonal collocation form below.

B.1 ADSORBENT BED

The fluid phase material balances for components A and B are:

$$\frac{dy_{Ai}}{d\tau} = \frac{1}{Pe_1}\sum_{j=1}^{N+2} B_{i,j} y_{Aj} - \frac{1}{C_T}\sum_{j=1}^{N+2} A_{i,j}\overline{F}_j y_{Aj} - \frac{y_{Ai}}{C_T}\frac{dC_T}{d\tau} - \frac{1}{C_T}\zeta_m \frac{dQ_{Ai}}{d\tau} \qquad i = 2,\ldots,N+1 \tag{B.1a}$$

$$-\frac{1}{Pe_1}\sum_{j=1}^{N+2} A_{1,j} y_{Aj} = \frac{\overline{F}_1}{C_T}\left(y_{Af} - y_{A,1}\right) \tag{B.1b}$$

$$\sum_{j=1}^{N+2} A_{N+2,j} y_{Aj} = 0 \tag{B.1c}$$

$$\frac{dy_{Bi}}{d\tau} = \frac{1}{Pe_1}\sum_{j=1}^{N+2} B_{i,j} y_{Bj} - \frac{1}{C_T}\sum_{j=1}^{N+2} A_{i,j}\overline{F}_j y_{Bj} - \frac{y_{Bi}}{C_T}\frac{dC_T}{d\tau} \qquad i = 2,\ldots,N+1 \tag{B.2a}$$

$$-\frac{1}{Pe_1}\sum_{j=1}^{N+2} A_{1,j} y_{Bj} = \frac{\overline{F}_1}{C_T}\left(y_{Bf} - y_{B,1}\right) \tag{B.2b}$$

$$\sum_{j=1}^{N+2} A_{N+2,j} y_{Bj} = 0 \tag{B.2c}$$

The overall fluid phase material balance is:

$$\sum_{j=1}^{N+2} A_{i,j}\overline{F}_j + \frac{dC_T}{d\tau} + \zeta_m \frac{dQ_{Ai}}{d\tau} = 0 \qquad i = 2,\ldots,N+2 \tag{B.3a}$$

$$\overline{F}_1 = \overline{F}_f \tag{B.3b}$$

The adsorbed phase balance for component A is:

$$\zeta_m \frac{dQ_{Ai}}{d\tau} = N_f C_T\left(y_{Ai} - \langle y_A \rangle_i\right) \qquad i = 1,\ldots,N+2 \tag{B.4}$$

The macropore concentration of component A is calculated by:

$$\langle y_A \rangle_i P = \frac{1}{K_{ads}(\overline{T}_i)} \frac{\theta_{ref} Q_{Ai}}{\left(1 - \theta_{ref} Q_{Ai}\right)^5} \qquad i = 1,\ldots,N+2 \tag{B.5a}$$

$$K_{ads}(\overline{T}_i) = K_0 \exp\left(\frac{\gamma_f}{\overline{T}_i + 1}\right) \qquad i = 1,\ldots,N+2 \tag{B.5b}$$

The energy balance is:

$$\begin{aligned}\frac{d\overline{T}_i}{d\tau} = {} & \frac{1}{Pe_{H1}(C_T + \zeta_H)}\sum_{j=1}^{N+2} B_{i,j}\overline{T}_j - \frac{\overline{F}_i}{(C_T + \zeta_H)}\sum_{j=1}^{N+2} A_{i,j}\overline{T}_j \\ & + \frac{B\zeta_H}{(C_T + \zeta_H)}\frac{dQ_{Ai}}{d\tau} - \frac{N_w}{(C_T + \zeta_H)}\left(\overline{T}_i - \overline{T}_w\right)\end{aligned} \qquad i = 2,\ldots,N+1 \tag{B.6a}$$

$$-\frac{1}{Pe_{H1}}\sum_{j=1}^{N+2} A_{1,j}\overline{T}_j = \overline{F}_1\left(\overline{T}_f - \overline{T}_1\right) \tag{B.6b}$$

$$\sum_{j=1}^{N+2} A_{N+2,j}\overline{T}_j = 0 \tag{B.6c}$$

The initial conditions are:

$$y_{Ai}(\tau = 0) = 0 \qquad i = 2,\ldots,N+1 \tag{B.7a}$$

$$y_{Bi}(\tau = 0) = 0 \qquad i = 2,\ldots,N+1 \tag{B.7b}$$

$$Q_{Ai}(\tau = 0) = 0 \qquad i = 1,\ldots,N+2 \tag{B.7c}$$

$$\overline{T}_i(\tau = 0) = \overline{T}_f \qquad i = 2,\ldots,N+1 \tag{B.7d}$$

B.2 CATALYST BED

The model equations in orthogonal collocation form for both pseudo-homogeneous and heterogeneous models are shown below.

B.2a Pseudo-Homogeneous Model

The material balances for components A and B are:

$$\frac{dy_{Ai}}{d\tau} = \frac{1}{\upsilon \cdot Pe_2}\sum_{j=1}^{N+2} B_{i,j}y_{Aj} - \frac{1}{\upsilon \cdot C_T}\sum_{j=1}^{N+2} A_{i,j}\overline{F}_j y_{Aj} - \frac{y_{Ai}}{C_T}\frac{dC_T}{d\tau} - Da\exp\left(\gamma_r \frac{\overline{T}_i}{\overline{T}_i + 1}\right)\left(y_{Ai} - \frac{y_{Bi}}{K}\right) \qquad i = 2,\ldots,N+1 \tag{B.8a}$$

$$-\frac{1}{Pe_2}\sum_{j=1}^{N+2} A_{1,j}y_{Aj} = \frac{\overline{F}_1}{C_T}\left(y_{Af} - y_{A,1}\right) \tag{B.8b}$$

$$\sum_{j=1}^{N+2} A_{N+2,j}y_{Aj} = 0 \tag{B.8c}$$

$$\frac{dy_{Bi}}{d\tau} = \frac{1}{\upsilon \cdot Pe_2}\sum_{j=1}^{N+2} B_{i,j} y_{Bj} - \frac{1}{\upsilon \cdot C_T}\sum_{j=1}^{N+2} A_{i,j}\overline{F}_j y_{Bj} - \frac{y_{Bi}}{C_T}\frac{dC_T}{d\tau} + Da\exp\left(\gamma_r \frac{\overline{T}_i}{\overline{T}_i + 1}\right)\left(y_{Ai} - \frac{y_{Bi}}{K}\right) \qquad i = 2,\ldots,N+1 \qquad \text{(B.9a)}$$

$$-\frac{1}{Pe_2}\sum_{j=1}^{N+2} A_{1,j} y_{Bj} = \frac{\overline{F}_1}{C_T}\left(y_{Bf} - y_{B,1}\right) \qquad \text{(B.9b)}$$

$$\sum_{j=1}^{N+2} A_{N+2,j} y_{Bj} = 0 \qquad \text{(B.9c)}$$

The overall material balance is:

$$\frac{dC_T}{d\tau} + \frac{1}{\upsilon}\sum_{j=1}^{N+2} A_{i,j}\overline{F}_j = 0 \qquad i = 2,\ldots,N+2 \qquad \text{(B.10a)}$$

$$\overline{F}_1 = \overline{F}_f \qquad \text{(B.10b)}$$

The energy balance for the pseudo-homogeneous model is:

$$\frac{d\overline{T}_i}{d\tau} = \frac{1}{\upsilon \cdot C_T \cdot Pe_{H2}}\sum_{j=1}^{N+2} B_{i,j}\overline{T}_j - \frac{\overline{F}_i}{\upsilon \cdot C_T}\sum_{j=1}^{N+2} A_{i,j}\overline{T}_j \qquad i = 2,\ldots,N+1 \qquad \text{(B.11a)}$$

$$-\frac{1}{Pe_{H2}}\sum_{j=1}^{N+2} A_{1,j}\overline{T}_j = \overline{F}_1\left(\overline{T}_f - \overline{T}_1\right) \qquad \text{(B.11b)}$$

$$\sum_{j=1}^{N+2} A_{N+2,j}\overline{T}_j = 0 \qquad \text{(B.11c)}$$

The initial conditions are:

$$y_{Ai}(\tau = 0) = 0 \qquad i = 2,\ldots,N+1 \qquad \text{(B.12a)}$$

$$y_{Bi}(\tau = 0) = 0 \qquad i = 2,\ldots,N+1 \qquad \text{(B.12b)}$$

$$\overline{T}_i(\tau=0)=\overline{T}_f \qquad i=2,\ldots,N+1 \qquad \text{(B.12c)}$$

B.2b Heterogeneous Model

The fluid phase material balances for components A and B are:

$$\frac{dy_{Ai}}{d\tau}=\frac{1}{\upsilon\cdot Pe_2}\sum_{j=1}^{N+2}B_{i,j}y_{Aj}-\frac{1}{\upsilon\cdot C_T}\sum_{j=1}^{N+2}A_{i,j}\overline{F}_j y_{Aj} -\frac{y_{Ai}}{C_T}\frac{dC_T}{d\tau}-N_f\left(y_{Ai}-\langle y_A\rangle_i\right) \qquad i=2,\ldots,N+1 \qquad \text{(B.13a)}$$

$$-\frac{1}{Pe_2}\sum_{j=1}^{N+2}A_{1,j}y_{Aj}=\frac{\overline{F}_1}{C_T}\left(y_{Af}-y_{A,1}\right) \qquad \text{(B.13b)}$$

$$\sum_{j=1}^{N+2}A_{N+2,j}y_{Aj}=0 \qquad \text{(B.13c)}$$

$$\frac{dy_{Bi}}{d\tau}=\frac{1}{\upsilon\cdot Pe_2}\sum_{j=1}^{N+2}B_{i,j}y_{Bj}-\frac{1}{\upsilon\cdot C_T}\sum_{j=1}^{N+2}A_{i,j}\overline{F}_j y_{Bj} -\frac{y_{Bi}}{C_T}\frac{dC_T}{d\tau}-N_f\left(y_{Bi}-\langle y_B\rangle_i\right) \qquad i=2,\ldots,N+1 \qquad \text{(B.14a)}$$

$$-\frac{1}{Pe_2}\sum_{j=1}^{N+2}A_{1,j}y_{Bj}=\frac{\overline{F}_1}{C_T}\left(y_{Bf}-y_{B,1}\right) \qquad \text{(B.14b)}$$

$$\sum_{j=1}^{N+2}A_{N+2,j}y_{Bj}=0 \qquad \text{(B.14c)}$$

The overall material balance is:

$$\frac{dC_T}{d\tau}+\frac{1}{\upsilon}\sum_{j=1}^{N+2}A_{i,j}\overline{F}_j +N_f C_T\left(y_{Ai}-\langle y_A\rangle_i+y_{Bi}-\langle y_B\rangle_i\right)=0 \qquad i=2,\ldots,N+2 \qquad \text{(B.15a)}$$

$$\overline{F}_1 = \overline{F}_f \tag{B.15b}$$

The initial conditions for fluid phase concentrations are:

$$y_{Ai}(\tau = 0) = 0 \qquad i = 2,\ldots,N+1 \tag{B.16a}$$

$$y_{Bi}(\tau = 0) = 0 \qquad i = 2,\ldots,N+1 \tag{B.16b}$$

The material balances of components A and B over the catalyst while assuming no accumulation in the micropores are:

$$\sigma \frac{d\langle y_A \rangle_i}{d\tau} = N_f\left(y_{Ai} - \langle y_A \rangle_i\right) - Da \exp\left(\gamma_r \frac{\overline{T}_i}{\overline{T}_i + 1}\right)\left(\langle y_A \rangle_i - \frac{\langle y_B \rangle_i}{K}\right) \qquad i = 1,\ldots,N+2 \tag{B.17}$$

$$\sigma \frac{d\langle y_B \rangle_i}{d\tau} = N_f\left(y_{Bi} - \langle y_B \rangle_i\right) + Da \exp\left(\gamma_r \frac{\overline{T}_i}{\overline{T}_i + 1}\right)\left(\langle y_A \rangle_i - \frac{\langle y_B \rangle_i}{K}\right) \qquad i = 1,\ldots,N+2 \tag{B.18}$$

The initial conditions over the catalyst are:

$$\langle y_A \rangle_i (\tau = 0) = 0 \qquad i = 1,\ldots,N+2 \tag{B.19a}$$

$$\langle y_B \rangle_i (\tau = 0) = 0 \qquad i = 1,\ldots,N+2 \tag{B.19b}$$

The adsorbed phase material balances of components A and B while considering the micropore accumulation are:

$$\zeta_m \frac{dQ_{Ai}}{d\tau} = N_f C_T\left(y_{Ai} - \langle y_A \rangle_i\right) - C_T Da \exp\left(\gamma_r \frac{\overline{T}_i}{\overline{T}_i + 1}\right)\left(\langle y_A \rangle_i - \frac{\langle y_B \rangle_i}{K}\right) \qquad i = 1,\ldots,N+2 \tag{B.20}$$

$$\zeta_m \frac{dQ_{Bi}}{d\tau} = N_f C_T \left(y_{Bi} - \langle y_B \rangle_i \right) + C_T Da \exp\left(\gamma_r \frac{\overline{T}_i}{\overline{T}_i + 1} \right) \left(\langle y_A \rangle_i - \frac{\langle y_B \rangle_i}{K} \right) \qquad i = 1, \ldots, N+2 \qquad \text{(B.21)}$$

The macropore concentrations of components A and B are calculated by:

$$\langle y_A \rangle_i P = \frac{1}{K_{ads}(\overline{T}_i)} \frac{\theta_{ref} Q_{Ai}}{\left(1 - \theta_{ref} Q_{Ai} - \theta_{ref} Q_{Bi}\right)^5} \qquad i = 1, \ldots, N+2 \qquad \text{(B.22)}$$

$$\langle y_B \rangle_i P = \frac{1}{K_{ads}(\overline{T}_i)} \frac{\theta_{ref} Q_{Bi}}{\left(1 - \theta_{ref} Q_{Ai} - \theta_{ref} Q_{Bi}\right)^5} \qquad i = 1, \ldots, N+2 \qquad \text{(B.23)}$$

where K_{ads}, the adsorption equilibrium constant, is evaluated as:

$$K_{ads}(\overline{T}_i) = K_0 \exp\left(\frac{\gamma_f}{\overline{T}_i + 1} \right) \qquad i = 1, \ldots, N+2 \qquad \text{(B.24)}$$

The initial conditions in the adsorbed phase are:

$$Q_{Ai}(\tau = 0) = 0 \qquad i = 1, \ldots, N+2 \qquad \text{(B.25a)}$$

$$Q_{Bi}(\tau = 0) = 0 \qquad i = 1, \ldots, N+2 \qquad \text{(B.25b)}$$

The energy balance for the heterogeneous model is:

$$\frac{d\overline{T}_i}{d\tau} = \frac{1}{\upsilon \cdot Pe_{H2} \cdot (C_T + \zeta_H)} \sum_{j=1}^{N+2} B_{i,j} \overline{T}_j - \frac{\overline{F}_i}{\upsilon \cdot (C_T + \zeta_H)} \sum_{j=1}^{N+2} A_{i,j} \overline{T}_j \qquad i = 2, \ldots, N+1 \qquad \text{(B.26a)}$$

$$-\frac{1}{Pe_{H2}} \sum_{j=1}^{N+2} A_{1,j} \overline{T}_j = \overline{F}_1 \left(\overline{T}_f - \overline{T}_1 \right) \qquad \text{(B.26b)}$$

$$\sum_{j=1}^{N+2} A_{N+2,j}\overline{T}_j = 0 \tag{B.26c}$$

The initial reactor temperature is:

$$\overline{T}_i(\tau = 0) = \overline{T}_f \qquad i = 2,\ldots,N+1 \tag{B.27}$$

The Danckwert's Boundary conditions need to be solved simultaneously in order to get explicit expressions for the quantities y_A, y_B and $\overline{T}$ at the boundary nodes. As an example expressions of $y_{A,1}$ and $y_{A,N+2}$ are derived for the adsorbent bed:

$$-\frac{1}{Pe_1}\sum_{j=1}^{N+2} A_{1,j}y_{Aj} = \frac{\overline{F}_1}{C_T}\left(y_{Af} - y_{A,1}\right) \tag{B.1b}$$

$$\sum_{j=1}^{N+2} A_{N+2,j}y_{Aj} = 0 \tag{B.1c}$$

Separating the terms $y_{A,1}$ and $y_{A,N+2}$ from the summation sign in equation B.1c:

$$A_{N+2,1}y_{A,1} + \sum_{j=2}^{N+1} A_{N+2,j}y_{Aj} + A_{N+2,N+2}y_{A,N+2} = 0 \tag{B.1.1}$$

Solving for $y_{A,N+2}$:

$$y_{A,N+2} = \frac{-\sum_{j=2}^{N+1} A_{N+2,j}y_{Aj} - A_{N+2,1}y_{A,1}}{A_{N+2,N+2}} \tag{B.1.2}$$

Separating the terms $y_{A,1}$ and $y_{A,N+2}$ from the summation sign in equation B.1b:

$$-\frac{1}{Pe_1}\left(A_{1,1}y_{A,1} + \sum_{j=2}^{N+1} A_{1,j}y_{Aj} + A_{1,N+2}y_{A,N+2}\right) = \frac{\overline{F}_1}{C_T}\left(y_{Af} - y_{A,1}\right) \tag{B.1.3}$$

Inserting the expression for $y_{A,N+2}$ from equation B.1.2 into B.1.3:

$$-\frac{1}{Pe_1}\left(A_{1,1}y_{A,1}+\sum_{j=2}^{N+1}A_{1,j}y_{Aj}-\frac{A_{1,N+2}}{A_{N+2,N+2}}\sum_{j=2}^{N+1}A_{N+2,j}y_{Aj}-\frac{A_{1,N+2}A_{N+2,1}}{A_{N+2,N+2}}y_{A,1}\right)=\frac{\overline{F}_1}{C_T}\left(y_{Af}-y_{A,1}\right) \tag{B.1.4}$$

Collecting like terms together:

$$\left(-\frac{1}{Pe_1}\left(A_{1,1}-\frac{A_{1,N+2}A_{N+2,1}}{A_{N+2,N+2}}\right)+\frac{\overline{F}_1}{C_T}\right)y_{A,1}-\frac{1}{Pe_1}\sum_{j=2}^{N+1}\left(A_{1,j}-\frac{A_{1,N+2}}{A_{N+2,N+2}}A_{N+2,j}\right)y_{Aj}=\frac{\overline{F}_1}{C_T}y_{Af} \tag{B.1.5}$$

Solving for $y_{A,1}$:

$$y_{A,1}=\frac{\frac{1}{Pe_1}\sum_{j=2}^{N+1}\left(\frac{A_{1,N+2}}{A_{N+2,N+2}}A_{N+2,j}-A_{1,j}\right)y_{Aj}-\frac{\overline{F}_1}{C_T}y_{Af}}{\frac{1}{Pe_1}\left(A_{1,1}-\frac{A_{1,N+2}A_{N+2,1}}{A_{N+2,N+2}}\right)-\frac{\overline{F}_1}{C_T}} \tag{B.1.6}$$

Thus expressions B.1.6 and B.1.2 are the explicit expressions for $y_{A,1}$ and $y_{A,N+2}$ respectively.

C *Simulation Code*

C.1 MAIN PROGRAM

```
global D D1 D2 AD N N1 N2 AN
global R R1 R2 WR AR BR invAR numerR denomR
global Node_des Node_rxr Node_ads NT N_des
global rxr P Tref Tdes Tfeed Fpurge Ffeed Ypurge Yfeed
global K0 thetaref gamma zeta Btemp
global Pe_rxr Pe_temp_rxr zeta_rxr zetah_rxr sigma_rxr Nf_rxr gamma_rxr Da
global T_feed Cpm_C5 Cpm_H2 Cpm_Feed
global Desorb_dataD Desorb_dataN Adsorb_data
global rxr_file D_index DN_index R_index N_index
global a_index ca_index qa_index b_index cb_index qb_index t_index

duration=clock;                                    % Recording Initial Time

adsorber_model='Non-Isothermal';
%adsorber_model='Adiabatic';

%rxr_model='Pseudo Homogeneous';
%rxr_model='Macropore Accumulation';
rxr_model='Solid Accumulation';

regeneration_mode='Forward';
%regeneration_mode='Reverse';
```

```
%regeneration_mode='Sandwich';

%%%%%%%%%%%%%%%%%%% Reaction Section %%%%%%%%%%%%%%%%%%%

R=20;                                          % Number of Collocation Points
R1=R+1;
R2=R+2;

[XR WR AR BR]=feval(['legendre' int2str(R)]);  % Loading Data for Collocation Points
invAR=inv(AR(2:end,2:end));                    % Inverse Matrix

% Coefficients for Equation at Node 1
numerR=AR(1,end)/AR(end)*AR(end,2:R1)-AR(1,2:R1);
denomR=AR(1)-AR(1,end)*AR(end,1)/AR(end);

%%%%%%%%%%%%%%%%%%% Adsorption Section %%%%%%%%%%%%%%%%%%%

N=20;                                          % Number of Collocation Points
N1=N+1;
N2=N+2;

[XN WN AN BN]=feval(['legendre' int2str(N)]);  % Loading Data for Collocation Points
invAN=inv(AN(2:end,2:end));                    % Inverse Matrix

% Coefficients for Equation at Node 1
numerN=AN(1,end)/AN(end)*AN(end,2:N1)-AN(1,2:N1);
denomN=AN(1)-AN(1,end)*AN(end,1)/AN(end);

aN_index=1:N;
qN_index=N1:N+N2;
tN_index=qN_index(end)+1:qN_index(end)+N;
bN_index=tN_index(end)+1:tN_index(end)+N;
Node_ads=bN_index(end);                        % Number of Variables

Node_dataN={N,N1,N2,WN,AN,BN,invAN,numerN,denomN,aN_index,qN_index,...
    tN_index,bN_index};
```

```
%%%%%%%%%%%%%%%%% Regeneration Section %%%%%%%%%%%%%%%%%

N_des=2;                                        % Number of Beds
reverse=0;
sandwich=0;

switch regeneration_mode
case 'Forward'
    if N_des>3
        error('JPattern not available')
    elseif N_des>1
        %D=10;                                  % Number of Collocation Points
        D=20;                                   % Number of Collocation Points
        D1=D+1;
        D2=D+2;

        % Loading Data for Collocation Points
        [XD WD AD BD]=feval(['legendre' int2str(D)]);
        invAD=inv(AD(2:end,2:end));             % Inverse Matrix

        % Coefficients for Equation at Node 1
        numerD=AD(1,end)/AD(end)*AD(end,2:D1)-AD(1,2:D1);
        denomD=AD(1)-AD(1,end)*AD(end,1)/AD(end);

        aD_index=1:D;
        qD_index=D1:D+D2;
        tD_index=qD_index(end)+1:qD_index(end)+D;
        Node_des=tD_index(end);                 % Number of Variables

        Node_dataD={D,D1,D2,WD,AD,BD,invAD,numerD,denomD,aD_index,...
            qD_index,tD_index,[]};
    end
case 'Reverse'
    reverse=1;
    N_des=1;                                    % Number of Beds
```

```
    % Rotation of Adsorbent Beds in SMBR with Reverse Flow Regeneration
    move=[aN_index(end:-1:1),qN_index(end:-1:1),tN_index(end:-1:1),...
        bN_index(end:-1:1)];

case 'Sandwich'
    sandwich=1;
    N_des=1;                                        % Number of Beds

    % Rotation of Adsorbent Beds in Sandwich Reactor
    move=[aN_index(end:-1:1),qN_index(end:-1:1),tN_index(end:-1:1),...
        bN_index(end:-1:1)];

otherwise
    error('Unknown regeneration mode')
end

%%%%%%%%%%%%%%%%%% Vessel Dimensions %%%%%%%%%%%%%%%%%%

L=20;                                               % Length (cm)
dc=3.35;                                            % Diameter (cm)

%%%%%%%%%%%%%%%%%% Dimensionless Length %%%%%%%%%%%%%%%%%%

rxr=1.4;                                            % Reaction Section

%%%%%%%%%%%%%%%%%% Adsorbent Properties %%%%%%%%%%%%%%%%%%

dp=0.16;                                            % Diameter (cm)
ap=28.3;                                            % Specific Area (cm^-1)
pa=1.13;                                            % Apparent Density (g/cm^3)
e=0.32;                                             % Bed Porosity
ep=0.35;                                            % Solid Porosity
Cps=0.9;                                            % Heat Capacity (J/g.K)
```

```
%%%%%%%%%%%%%%%%%% Catalyst Property %%%%%%%%%%%%%%%%%%

pb_rxr=0.66;                          % Bulk Density (g/cm^3)

%%%%%%%%%%%%%%%%%% Operating Parameters %%%%%%%%%%%%%%%%%%

Fpurge=0.15;                          % Purge Flow Rate (mol/m^2.s)
Ffeed=0.05;                           % Fresh Feed Flow Rate (mol/m^2.s)
Fref=Fpurge+Ffeed;                    % Reference Flow Rate (mol/m^2.s)

P=15;                                 % Pressure (bar)
Tdes=540;                             % Regeneration Section Temperature (K)
%Tfeed=460;                           % Feed Temperature (K)

% Reaction Section (Reference Section)
Tref=514;                               % Reference Temperature (K)

%[Tref fvec ifail]=c05nbf('React_temp',500);  % Estimating Reference Temperature (K)
%if ifail~=0|Tref<430|Tref>573
    %Tref
    %fvec
    %error('Try another guess')
%end
%Tref=chop(Tref,4);                   % Reference Temperature (K)

Td=(Tdes-Tref)/Tref;                  % Dimensionless Regeneration Temperature

% Adsorption Section
Tads=430;                             % Temperature (K)
switch adsorber_model
case 'Adiabatic'
    Tads=Tref;                        % Temperature (K)
end
Ta=(Tads-Tref)/Tref;                  % Dimensionless Temperature
```

```
%%%%%%%%%%%%%%%%% Reference Parameters %%%%%%%%%%%%%%%%%

CTref=P/8.314/Tref/10;          % Reference Concentration (mol/cm^3)
uref=Fref*8.314*Tref/P/e/1000;  % Reference Velocity (cm/s)

Ypurge=Fpurge/Fref;             % Dimensionless Purge Velocity
Yfeed=Ffeed/Fref;               % Reference Hydrocarbon Mole Fraction

%%%%%%%%%% Adsorption Equilibrium Isotherm Parameters %%%%%%%%%%

K0=2.01e-5;                     % bar^-1
Hads=13.2*4184;                 % Isosteric Heat of Adsorption (J/mol)
qmax=1.8e-3;                    % Maximum Adsorbed Phase Concentration (mol/g)
gamma=chop(Hads/8.314/Tref,4);  % Dimensionless Heat of Adsorption

% Adsorption Equilibrium Constant at Reference Temperature (bar^-1)
Kads=K0*exp(gamma);

%%%%%%%%%%%%%%%%%% Mass Peclet Numbers %%%%%%%%%%%%%%%%%%

% Regeneration Section
Dm=diffusivity(Tdes,P);                 % Molecular Diffusivity (cm^2/s)
DL=0.7*Dm+0.5*uref*Tdes/Tref*dp;        % Dispersion Coefficient (cm^2/s)
Pe_des=chop(uref*L/DL,4);               % Mass Peclet Number

% Reaction Section
Dm=diffusivity(Tref,P);                 % Molecular Diffusivity (cm^2/s)
DL=0.7*Dm+0.5*uref*dp;                  % Dispersion Coefficient (cm^2/s)
Pe_rxr=chop(uref*rxr*L/DL,4);           % Mass Peclet Number

% Adsorption Section
Dm=diffusivity(Tads,P);                 % Molecular Diffusivity (cm^2/s)
DL=0.7*Dm+0.5*uref*Tads/Tref*dp;        % Dispersion Coefficient (cm^2/s)
Pe_ads=chop(uref*L/DL,4);               % Mass Peclet Number
```

```
%%%%%%%%%%%%%%%%%% Mass Capacity Factors %%%%%%%%%%%%%%%%

% Coverage of Adsorbent at ya,ref
syms theta
theta_vec=double(solve(Yfeed/2*P*Kads-theta./(1-theta).^5));
thetaref=chop(theta_vec(find(imag(theta_vec)==0)),3);
if length(thetaref)~=1
    theta_vec
    error('Thetaref could not be calculated')
end

% Adsorbent Bed
zeta=chop((1-e)/e*pa*thetaref*qmax/CTref,4);                    % Mass Capacity Factor

% Catalyst Bed
switch rxr_model
case 'Pseudo Homogeneous'
    rxr_file='reactor1';

    a_index=1:R;
    b_index=R1:2*R;
    t_index=b_index(end)+1:b_index(end)+R;

    % Rotation of Catalyst Bed in Sandwich Reactor
    move_rxr=[a_index(end:-1:1) b_index(end:-1:1) t_index(end:-1:1)];

case 'Macropore Accumulation'
    rxr_file='reactor2';
    sigma_rxr=chop((1-e)*ep/e,4);            % Macropore Porosity per unit Bed Porosity

    a_index=1:R;
    ca_index=R1:R+R2;
    b_index=ca_index(end)+1:ca_index(end)+R;
    cb_index=b_index(end)+1:b_index(end)+R2;
    t_index=cb_index(end)+1:cb_index(end)+R;
```

```
    % Rotation of Catalyst Bed in Sandwich Reactor
    move_rxr=[a_index(end:-1:1),ca_index(end:-1:1),b_index(end:-1:1),...
        cb_index(end:-1:1),t_index(end:-1:1)];

case 'Solid Accumulation'
    rxr_file='reactor3';
    zeta_rxr=chop(pb_rxr/e*thetaref*qmax/CTref,4);          % Mass Capacity Factor

    a_index=1:R;
    qa_index=R1:R+R2;
    b_index=qa_index(end)+1:qa_index(end)+R;
    qb_index=b_index(end)+1:b_index(end)+R2;
    t_index=qb_index(end)+1:qb_index(end)+R;

    % Rotation of Catalyst Bed in Sandwich Reactor
    move_rxr=[a_index(end:-1:1),qa_index(end:-1:1),b_index(end:-1:1),...
        qb_index(end:-1:1),t_index(end:-1:1)];

otherwise
    error('Unknown reactor model')
end
Node_rxr=t_index(end);                                      % Number of Variables

if ~sandwich
    clear move_rxr
end

%%%%%%%%%%%% Number of Film Mass-Transfer Units %%%%%%%%%%%%

% Regeneration Section
Kgl=global_coeff(Tdes,P,Ypurge,Yfeed,uref);  % Mass Transfer Coefficient (cm/s)
Nf_des=chop((1-e)/e*ap*Kgl*L/uref,4);        % Number of Film Mass-Transfer Units

% Reaction Section
Kgl=global_coeff(Tref,P,Ypurge,Yfeed,uref);  % Mass Transfer Coefficient (cm/s)
Nf_rxr=chop((1-e)/e*ap*Kgl*L/uref,4);        % Number of Film Mass-Transfer Units
```

```
% Adsorption Section
Kgl=global_coeff(Tads,P,Ypurge,Yfeed,uref);  % Mass Transfer Coefficient (cm/s)
Nf_ads=chop((1-e)/e*ap*Kgl*L/uref,4);        % Number of Film Mass-Transfer Units

%%%%%%%%%%%%%%%%% Damkohler Number %%%%%%%%%%%%%%%%%

Eapp=37*4184;                                % Activation Energy (J/mol)

% Reaction Rate Constant at Reference Temperature (cm^3/g.s)
kref=0.046*exp(Eapp/8.314*(1/514-1/Tref));

gamma_rxr=chop(Eapp/8.314/Tref,4);           % Dimensionless Activation Energy
Da=chop(pb_rxr/e*kref*L/uref,4);             % Damkohler Number

%%%%%%%%%%%%%%%%%%%% Heat Capacities %%%%%%%%%%%%%%%%%%%

% Regeneration Section
Cpg_des=heat_capacity(Tdes,[],Ypurge,Yfeed); % Heat Capacity of Gas Phase (J/mol.K)

% Reaction Section
Cpg_rxr=heat_capacity(Tref,[],Ypurge,Yfeed);  % Heat Capacity of Gas Phase (J/mol.K)

% Adsorption Section
Cpg_ads=heat_capacity(Tads,[],Ypurge,Yfeed); % Heat Capacity of Gas Phase (J/mol.K)

% Mixing Point
Cpm_C5=heat_capacity(Tref,Tdes,0,1);    % Mean Heat Capacity of Pentanes (J/mol.K)
Cpm_H2=heat_capacity(Tref,Tdes,1,0);    % Mean Heat Capacity of Hydrogen (J/mol.K)

[Tfeed fvec ifail]=c05nbf('Feed_temp',500);          % Estimating Feed Temperature (K)
if ifail~=0|Tfeed<430
    Tfeed
    fvec
    error('Try another guess')
end
```

```
Tfeed=round(Tfeed);                          % Feed Temperature (K)
T_feed=(Tfeed-Tref)/Tref;                    % Dimensionless Feed Temperature

Cpm_Feed=heat_capacity(Tfeed,Tref,0,1);      % Mean Heat Capacity of Feed (J/mol.K)

%%%%%%%%%%%%%%%% Thermal Peclet Numbers %%%%%%%%%%%%%%%%

KL=0.35;                                     % Axial Bed Thermal Conductivity (W/m.K)
 % Regeneration Section
Pe_temp_des=chop(Cpg_des*Fref*L/KL/100,4);          % Thermal Peclet Number

% Reaction Section
Pe_temp_rxr=chop(Cpg_rxr*Fref*rxr*L/KL/100,4);      % Thermal Peclet Number

% Adsorption Section
Pe_temp_ads=chop(Cpg_ads*Fref*L/KL/100,4);          % Thermal Peclet Number

%%%%%%%%%%%%%%%% Thermal Capacity Factors %%%%%%%%%%%%%%%%

% Regeneration Section
zetah_des=chop((1-e)/e*pa*Cps/Cpg_des/CTref,4);     % Thermal Capacity Factor

% Reaction Section
zetah_rxr=chop(pb_rxr/e*Cps/Cpg_rxr/CTref,4);       % Thermal Capacity Factor

% Adsorption Section
zetah_ads=chop((1-e)/e*pa*Cps/Cpg_ads/CTref,4);     % Thermal Capacity Factor

%%%%%%%%%%%% Number of Wall Heat-Transfer Units %%%%%%%%%%%%

switch adsorber_model
case 'Non-Isothermal'

    hw=15;                                   % Overall Heat Transfer Coefficient (W/m^2.K)
    ac=4/dc;                                 % Specific Area of Column (cm^-1)
```

```
    % Regeneration Section
    Nw_des=chop(ac*hw*L/Cpg_des/Fref,4);      % Number of Wall Heat Transfer Units

    % Adsorption Section
    Nw_ads=chop(ac*hw*L/Cpg_ads/Fref,4);      % Number of Wall Heat Transfer Units

case 'Adiabatic'
    Nw_des=0;
    Nw_ads=0;
otherwise
    error('Unknown adsorber model')
end

% Adiabatic Temperature Rise
Btemp=chop(Hads*thetaref*qmax/Cps/Tref,4);

Desorb_data={Pe_des Pe_temp_des zetah_des Nf_des Nw_des Td};
Desorb_dataN={Node_dataN{:} Desorb_data{:}};

Adsorb_data={Node_dataN{:} Pe_ads Pe_temp_ads zetah_ads Nf_ads Nw_ads Ta};

if N_des==1
    D_index=0;
    AD=0;

    % Initial Conditions
    IC_vec=[zeros(1,N+N2),repmat(Td,1,N),zeros(1,N+Node_rxr+N+N2),...
        repmat(Ta,1,N),zeros(1,N)];
else
    D_index=reshape(1:Node_des*(N_des-1),Node_des,N_des-1)';
    IC_Des=[zeros(1,D+D2) repmat(Td,1,D)];

    % Initial Conditons
    IC_vec=[repmat(IC_Des,1,N_des-1),zeros(1,N+N2),repmat(Td,1,N),...
        zeros(1,N+Node_rxr+N+N2),repmat(Ta,1,N),zeros(1,N)];
```

```
    Desorb_dataD={Node_dataD{:} Desorb_data{:}};
end

DN_index=D_index(end)+1:D_index(end)+Node_ads;
R_index=DN_index(end)+1:DN_index(end)+Node_rxr;
N_index=R_index(end)+1:R_index(end)+Node_ads;

NT=N_index(end);                                    % Total Number of Variables

clear aN_index qN_index tN_index bN_index aD_index qD_index tD_index
clear theta theta_vec Node_dataD Node_dataN Desorb_data

options=odeset('Vectorized','on','JPattern','on','InitialStep',eps);

tswitch=600;                                        % Trial Switch Time
Delta_t=0.1;

pointer=1;
Purity=0;
Setpoint=0.99;

while Purity<Setpoint
    d=IC_vec;
    Tmean_rec=[];
    HCmean_rec=[];
    rxr_inlet_rec=[];
    rxr_outlet_rec=[];
    conversion_rec=[];
    Purity_rec=[];
    conversion_overall_rec=[];
    yb_ads_mean_rec=[];
    T_ads_mean_rec=[];

    for j=1:100
        clear time t c ymat y dydt repAD repAN ybf F1 ya_desD q_desD temp_desD
        clear F_desD Stream ya_desN q_desN yb_desN temp_desN F_desN ya_rxr
```

```
clear qa_rxr yb_rxr qb_rxr temp_rxr F_rxr ya_ads q_ads yb_ads temp_ads F_ads
clear tbreak

yaf=0;                                          % Inlet Purge Concentration
Tf=Td;                                          % Inlet Purge Temperature

Tspan=0:Delta_t:tswitch;
[t,ymat]=ode15s('SMBR_ode',Tspan,d,options,yaf,Tf);   % Solving SMBR Model

T=length(t);
if T~=length(Tspan)
    error('Solution not converged')
end

c=ymat(end,:);                                  % Recording Final Conditions

%%%%%%%%%%%%%% Values at Boundary Nodes %%%%%%%%%%%%%%

y=ymat';
dydt=zeros(NT,T);
F1=repmat(Ypurge,1,T);                          % Inlet Purge Flow Rate

% bed D (Regeneration Section)
repAD=repmat(AD(2:end,1),1,T);
for i=1:N_des-1
    [ya_desD(:,:,i) q_desD(:,:,i) temp_desD(:,:,i) F_desD(:,:,i)]=adsorber('main',...
        y(D_index(i,:),:),dydt(D_index(i,:),:),yaf,[],Tf,F1,repAD,Desorb_dataD);

    % Inlet Conditions for Following Bed
    yaf=ya_desD(end,:,i);
    Tf=temp_desD(end,:,i);
    F1=F_desD(end,:,i);
end

% bed DN (Regeneration Section)
repAN=repmat(AN(2:end,1),1,T);
```

```
[ya_desN q_desN yb_desN temp_desN F_desN]=adsorber('main',...
    y(DN_index,:),dydt(DN_index,:),yaf,0,Tf,F1,repAN,Desorb_dataN);

% Mixing Point
[ya_mix yb_mix T_mix F_mix]=mixing(ya_desN(end,:),yb_desN(end,:),...
    temp_desN(end,:),F_desN(end,:));

% Mean Hydrocarbon Mole Fraction to Reaction Section
HCmean=trapz(t,F_mix.*(ya_mix+yb_mix))/trapz(t,F_mix);
HCmean_rec=[HCmean_rec;HCmean];

Tavg=(mean(T_mix)+1)*Tref;          % Arithmetic Mean Temperature (K)
Cp_C5=heat_capacity(Tavg,[],0,1);   % Heat Capacity of Pentanes (J/mol.K)
Cp_H2=heat_capacity(Tavg,[],1,0);   % Heat Capacity of Hydrogen (J/mol.K)
Stream=F_mix.*(Cp_C5*(ya_mix+yb_mix)+Cp_H2*(1-ya_mix-yb_mix));

% Average Mixed Stream Temperature (K)
Tmean=(trapz(t,T_mix.*Stream)/trapz(t,Stream)+1)*Tref;
Tmean_rec=[Tmean_rec;Tmean];

% Mean Isopentane Mole Fraction @ Inlet of Reaction Section
rxr_inlet=trapz(t,F_mix.*yb_mix)/trapz(t,F_mix.*(ya_mix+yb_mix));
rxr_inlet_rec=[rxr_inlet_rec;rxr_inlet];

% Catalyst Bed
switch rxr_file
case 'reactor1'
    [ya_rxr yb_rxr temp_rxr F_rxr]=reactor1('main',y(R_index,:),T,...
        dydt(R_index,:),ya_mix,yb_mix,T_mix,F_mix);
otherwise
    [ya_rxr qa_rxr yb_rxr qb_rxr temp_rxr F_rxr]=feval(rxr_file,'main',...
        y(R_index,:),T,dydt(R_index,:),ya_mix,yb_mix,T_mix,F_mix);
end
```

```
% Mean Isopentane Mole Fraction @ Outlet of Reaction Section
rxr_outlet=trapz(t,F_rxr(end,:).*yb_rxr(end,:))/...
    trapz(t,F_rxr(end,:).*(ya_rxr(end,:)+yb_rxr(end,:)));
rxr_outlet_rec=[rxr_outlet_rec;rxr_outlet];

% Single Pass Conversion
conversion=trapz(t,F_mix.*ya_mix-F_rxr(end,:).*ya_rxr(end,:))/...
    trapz(t,F_mix.*ya_mix);
conversion_rec=[conversion_rec;conversion];

% bed A (Adsorption Section)
[ya_ads q_ads yb_ads temp_ads F_ads]=adsorber('main',y(N_index,:),...
    dydt(N_index,:),ya_rxr(end,:),yb_rxr(end,:),temp_rxr(end,:),F_rxr(end,:),...
    repAN,Adsorb_data);

% Product Purity
Purity=trapz(t,F_ads(end,:).*yb_ads(end,:))/...
    trapz(t,F_ads(end,:).*(ya_ads(end,:)+yb_ads(end,:)));
Purity_rec=[Purity_rec;Purity];

% Overall Conversion
conversion_overall=1-trapz(t,F_ads(end,:).*ya_ads(end,:))/(Yfeed/2*tswitch);
conversion_overall_rec=[conversion_overall_rec;conversion_overall];

% Mean Mole Fraction of Isopentane in Product Stream
yb_ads_mean=trapz(t,F_ads(end,:).*yb_ads(end,:))/trapz(t,F_ads(end,:));
yb_ads_mean_rec=[yb_ads_mean_rec;yb_ads_mean];

Tavg=(mean(temp_ads(end,:))+1)*Tref; % Arithmetic Mean Temperature (K)
Cp_C5=heat_capacity(Tavg,[],0,1);    % Heat Capacity of Pentanes (J/mol.K)
Cp_H2=heat_capacity(Tavg,[],1,0);    % Heat Capacity of Hydrogen (J/mol.K)
Stream=F_ads(end,:).*(Cp_C5*(ya_ads(end,:)+yb_ads(end,:))+...
    Cp_H2*(1-ya_ads(end,:)-yb_ads(end,:)));

% Average Temperature of Product Stream (K)
T_ads_mean=(trapz(t,temp_ads(end,:).*Stream)/trapz(t,Stream)+1)*Tref;
```

```
T_ads_mean_rec=[T_ads_mean_rec;T_ads_mean];

if Purity<Setpoint
    tbreak=find(ya_ads(end,:)<=0.03*ya_ads(end));
    if pointer
        tswitch1=t(tbreak(end));            % Breakthrough Time for Clean Bed
        pointer=0;
    end
    if ~isempty(tbreak)
        tswitch_new=t(tbreak(end));                    % Breakthrough Time
        if tswitch==tswitch_new
            Setpoint=Setpoint-0.01;                    % Lowering Setpoint
            tswitch=tswitch1;
            Purity=0;
        else
            tswitch=tswitch_new;                       % New Switch Time
        end
    else
        Setpoint=Setpoint-0.01;                        % Lowering Setpoint
        tswitch=tswitch1;
        Purity=0;
    end
    break
end

% Simulating the Movement of Beds
if reverse
    % SMBR with Bed Rotation
    d=[c([N_index(move) R_index move(1:Node_ads-N)]) zeros(1,N)];
elseif sandwich
    % Sandwich Reactor
    d=[c([N_index(move) R_index(move_rxr) move(1:Node_ads-N)]) zeros(1,N)];
elseif N_des==1
    % Forward Flow SMBR (N_des=1)
    d=[c([N_index R_index 1:Node_ads-N]) zeros(1,N)];
```

```
        elseif N==D
            % Forward Flow SMBR (N_des>1 & N=D)
            d=[c([Node_des+1:DN_index(Node_des) N_index R_index 1:Node_des]),...
                zeros(1,N)];
        else
            % Forward Flow SMBR (N_des>1 & N~=D)
            d=[c(Node_des+1:D_index(end)),lagrange(XN,ya_desN(:,end),XD(2:D1)),...
                lagrange(XN,q_desN(:,end),XD),...
                lagrange(XN,temp_desN(:,end),XD(2:D1)),c([N_index R_index]),...
                lagrange(XD,ya_desD(:,end,1),XN(2:N1)),...
                lagrange(XD,q_desD(:,end,1),XN),...
                lagrange(XD,temp_desD(:,end,1),XN(2:N1)),zeros(1,N)];
        end
        time=t*L/uref/60;                    % Converting Switch Time Into Minutes
    end
end

duration=etime(clock,duration)/3600;         % Total Computational Time

save SMBR                                    % Saving the Results
```

C.2 ODE FILE

```
function dydt=SMBR_ode(t,y,flag,yaf,Tf)

global AD AN N_des NT Ypurge D_index DN_index R_index N_index
global Desorb_dataD Desorb_dataN Adsorb_data rxr_file

switch flag
case ''
    Y2=size(y,2);
    dydt=zeros(NT,Y2);                          % Initializing Output Variable
    F1=repmat(Ypurge,1,Y2);                     % Inlet Purge Flow Rate

    % bed D (Regeneration Section)
    repAD=repmat(AD(2:end,1),1,Y2);
    for i=1:N_des-1
    [yaf Tf F1 dydt(D_index(i,:),:)]=adsorber('ode',y(D_index(i,:),:),...
        dydt(D_index(i,:),:),yaf,[],Tf,F1,repAD,Desorb_dataD);
    end

    % bed DN (Regeneration Section)
    repAN=repmat(AN(2:end,1),1,Y2);
    [yaf ybf Tf F1 dydt(DN_index,:)]=adsorber('ode',y(DN_index,:),dydt(DN_index,:),...
        yaf,0,Tf,F1,repAN,Desorb_dataN);

    % Mixing Point
    [yaf ybf Tf F1]=mixing(yaf,ybf,Tf,F1);

    % Catalyst Bed
    [yaf ybf Tf F1 dydt(R_index,:)]=feval(rxr_file,'ode',y(R_index,:),Y2,...
        dydt(R_index,:),yaf,ybf,Tf,F1);

    % bed A (Adsorption Section)
    dydt(N_index,:)=adsorber('ode',y(N_index,:),dydt(N_index,:),yaf,ybf,Tf,F1,repAN,...
        Adsorb_data);
```

```
case 'jpattern'
    dydt=SMBR_JPattern;                          % Sparse Matrix for Jacobian Pattern
end
```

C.2a Ode File for Adsorbent Bed

```
function varargout=adsorber(flag,y,dydt,yaf,ybf,Tf,F1,repA,data)

global K0 P thetaref zeta Btemp gamma

[N,N1,N2,W,A,B,invA,numer,denom,a_index,q_index,t_index,b_index,Pe,Pe_temp,...
    zetah,Nf,Nw,Tw]=deal(data{:});

T1=(numer/Pe_temp*y(t_index,:)-Tf.*F1)./(denom/Pe_temp-F1);          % @ 1st Node
T_end=(-A(end,2:N1)*y(t_index,:)-A(end,1)*T1)/A(end,end);            % @ Last Node
temp=[T1;y(t_index,:);T_end];                                        % Temperature
CT=1./(W*y(t_index,:)+1);                                            % Concentration

U1=F1./CT;                                                           % Inlet Velocity
y_denom=denom/Pe-U1;
ya1=(numer/Pe*y(a_index,:)-yaf.*U1)./y_denom;                        % @ 1st Node
ya_end=(-A(end,2:N1)*y(a_index,:)-A(end,1)*ya1)/A(end,end);          % @ Last Node
ya=[ya1;y(a_index,:);ya_end];                          % Mole Fraction of Species A

% Average Macropore Mole Fraction
ya_avg=thetaref/P/K0./exp(gamma./(temp+1)).*y(q_index,:)./(1-thetaref*...
    y(q_index,:)).^5;

% Material Balance Over Adsorbent
dydt(q_index,:)=Nf/zeta*repmat(CT,N2,1).*(ya-ya_avg);

repC=repmat(CT,N,1);

% Energy Balance
dydt(t_index,:)=(B(2:N1,:)*temp/Pe_temp-A(2:N1,:)*temp.*repmat(F1,N,1)+Btemp*...
    zetah*dydt(q_index(2:N1),:)-Nw*(y(t_index,:)-Tw))./(repC+zetah);
```

```
dCdt=-CT.^2.*(W*dydt(t_index,:));

% Flow Rate
F=[F1;invA*(-zeta*dydt(q_index(2:end),:)-repmat(dCdt,N1,1)-repA.*repmat(F1,N1,1))];
switch flag
case 'ode'
    repdC=repmat(dCdt,N,1);

    % Material Balance of Species A
    dydt(a_index,:)=B(2:N1,:)*ya/Pe-(A(2:N1,:)*(F.*ya)+y(a_index,:).*repdC+...
        zeta*dydt(q_index(2:N1),:))./repC;
    if isempty(ybf)
        varargout={ya_end T_end F(end,:) dydt};          % For Regeneration Section
    else
        yb1=(numer/Pe*y(b_index,:)-ybf.*U1)./y_denom;                  % @ 1st Node
        yb_end=(-A(end,2:N1)*y(b_index,:)-A(end,1)*yb1)/A(end,end);  % @ Last Node
        yb=[yb1;y(b_index,:);yb_end];                    % Mole Fraction of Species B

        % Material Balance of Species B
        dydt(b_index,:)=B(2:N1,:)*yb/Pe-(A(2:N1,:)*(F.*yb)+y(b_index,:).*repdC)./repC;
        if nargout>1
            varargout={ya_end yb_end T_end F(end,:) dydt};
        else
            varargout={dydt};
        end
    end
case 'main'
    if isempty(ybf)
        varargout={ya y(q_index,:) temp F};              % For Regeneration Section
    else
        yb1=(numer/Pe*y(b_index,:)-ybf.*U1)./y_denom;                  % @ 1st Node
        yb_end=(-A(end,2:N1)*y(b_index,:)-A(end,1)*yb1)/A(end,end);  % @ Last Node
        yb=[yb1;y(b_index,:);yb_end];                    % Mole Fraction of Species B
        varargout={ya y(q_index,:) yb temp F};
    end
end
```

C.2b Ode File for Catalyst Bed

```
function varargout=reactor3(flag,y,Y2,dydt,yaf,ybf,Tf,F1)

global R R1 R2 WR AR BR invAR numerR denomR
global rxr K0 P thetaref Tref Pe_rxr Pe_temp_rxr
global zeta_rxr zetah_rxr Nf_rxr gamma gamma_rxr Da
global a_index qa_index b_index qb_index t_index

% @ 1st Node
T1=(numerR/Pe_temp_rxr*y(t_index,:)-Tf.*F1)./(denomR/Pe_temp_rxr-F1);

T_end=(-AR(end,2:R1)*y(t_index,:)-AR(end,1)*T1)/AR(end,end);      % @ Last Node
temp=[T1;y(t_index,:);T_end];                                      % Temperature

CT=1./(WR*y(t_index,:)+1);                                         % Concentration

U1=F1./CT;                                                         % Inlet Velocity
y_denom=denomR/Pe_rxr-U1;
ya1=(numerR/Pe_rxr*y(a_index,:)-yaf.*U1)./y_denom;                 % @ 1st Node
ya_end=(-AR(end,2:R1)*y(a_index,:)-AR(end,1)*ya1)/AR(end,end);     % @ Last Node
ya=[ya1;y(a_index,:);ya_end];                          % Mole Fraction of Species A

yb1=(numerR/Pe_rxr*y(b_index,:)-ybf.*U1)./y_denom;                 % @ 1st Node
yb_end=(-AR(end,2:R1)*y(b_index,:)-AR(end,1)*yb1)/AR(end,end);     % @ Last Node
yb=[yb1;y(b_index,:);yb_end];                          % Mole Fraction of Species B

avg_coeff=thetaref/P/K0./exp(gamma./(temp+1))./(1-thetaref*(y(qa_index,:)+...
    y(qb_index,:))).^5;
ya_avg=y(qa_index,:).*avg_coeff;    % Average Macropore Concentration for Species A
yb_avg=y(qb_index,:).*avg_coeff;    % Average Macropore Concentration for Species B

LDFa=Nf_rxr*(ya-ya_avg);
LDFb=Nf_rxr*(yb-yb_avg);

repC=repmat(CT,R,1);
```

```
% Energy Balance
dydt(t_index,:)=(BR(2:R1,:)*temp/Pe_temp_rxr-AR(2:R1,:)*temp.*repmat(F1,R,1))/...
    rxr./(repC+zetah_rxr);

dCdt=-CT.^2.*(WR*dydt(t_index,:));

% Flow Rate
F=[F1;invAR*(-rxr*(repmat(dCdt,R1,1)+repmat(CT,R1,1).*(LDFa(2:end,:)+...
    LDFb(2:end,:)))-repmat(AR(2:end,1),1,Y2).*repmat(F1,R1,1))];
switch flag
case 'ode'
    repdC=repmat(dCdt,R,1)./repC;

    % Material Balance for Species A
    dydt(a_index,:)=(BR(2:R1,:)*ya/Pe_rxr-AR(2:R1,:)*(F.*ya)./repC)/rxr-...
        y(a_index,:).*repdC-LDFa(2:R1,:);

    % Material Balance for Species B
    dydt(b_index,:)=(BR(2:R1,:)*yb/Pe_rxr-AR(2:R1,:)*(F.*yb)./repC)/rxr-...
        (b_index,:).*repdC-LDFb(2:R1,:);

    K=exp(936.6/Tref./(temp+1)-0.6537);          % Equilibrium Reaction Rate Contanst
    rate=Da*exp(gamma_rxr*temp./(temp+1)).*(ya_avg-yb_avg./K); % Rate of Reaction
    repC2=repmat(CT,R2,1);

    % Material Balance Over The Catalyst
    dydt(qa_index,:)=(LDFa-rate).*repC2/zeta_rxr;                    % For Species A
    dydt(qb_index,:)=(LDFb+rate).*repC2/zeta_rxr;                    % For Species B
    if nargout>1
        varargout={ya_end yb_end T_end F(end,:) dydt};
    else
        varargout={dydt};
    end
case 'main'
    varargout={ya y(qa_index,:) yb y(qb_index,:) temp F};
end
```

VITA

Name	Mohammad Aminuddin
Date & Place of Birth	28-Aug-1975, Abu Dhabi (U.A.E.)
Nationality	Pakistani
Religion	Islam
Educational qualifications	B.S. in Chemical Engineering from Middle East Technical University, Ankara, Turkey (1994-98).